MECHANICAL AND TRANSPORT PROPERTIES OF NAFION® FOR PEM FUEL CELLS; TEMPERATURE AND HYDRATION EFFECTS

Paul William Majsztrik

A DISSERTATION

PRESENTED TO THE FACULTY

OF PRINCETON UNIVERSITY

IN CANDIDACY FOR THE DEGREE

OF DOCTOR OF PHILOSOPHY

RECOMMENDED FOR ACCEPTANCE

BY THE DEPARTMENT OF CHEMISTRY

Advisors: Andrew Bocarsly and Jay Benziger

JANUARY 2008

Abstract

This work investigates the mechanical and water transport properties of Nafion, a fully fluorinated ion conducting polymer used as a membrane material in proton exchange membrane fuel cells (PEMFCs). Both of these properties are extremely important to the short and long term operation of fuel cells.

Nafion is a viscoelastic material, responding to stress in a time-dependant manner. The result is that Nafion flows under stress and responds dynamically to changes in hydration and stress. Stresses applied to the membrane of a PEM fuel cell, both from clamping as well as strain from changing levels of hydration, cause Nafion to flow. This results in thinning in spots and sometimes leads to the development of pinholes or contact problems between membrane and electrode. Temperature and water content strongly affect Nafion's viscoelastic response, of direct importance for operating PEM fuel cells.

The viscoelastic response of Nafion was measured over a range of temperature and hydration using viscoelastic creep. A specially designed creep apparatus with environmental controls was used. It was found that the effects of temperature and hydration on Nafion's viscoelastic response are very complicated. Around room temperature, water acts to plasticize Nafion; elastic modulus and resistance to creep decrease with increasing hydration. As temperature increases, water has the opposite effect on mechanical response; hydration acts to stabilize the material. Mechanical property values are reported over a range of temperature and hydration germane to the operation of PEMFCs. Additionally, the data is used to infer molecular level interactions and the effects of temperature and hydration on microstructure.

Hydration of Nafion and other PEMFC materials is required for the high proton conductivity needed for fuel cell operation. Uptake of water by Nafion results in volumetric swelling. Water transport through Nafion was directly measured by permeation. Both liquid and vapor phase transport was measured as a function of temperature for several membrane thicknesses. Diffusion and interfacial mass transport were considered. Diffusion was found to increase with membrane hydration. Permeation was much greater from liquid than vapor. Interfacial mass transport at the membrane/vapor interface dominated liquid permeation at all temperatures and for all membrane thicknesses. Diffusion dominated for vapor permeation and was found to increase with temperature.

To all the Majsztriks

Acknowledgements

I would like to begin by thanking Prof. Andrew Bocarsly for encouraging me to apply directly to the chemistry department at Princeton, even though my background was in mechanical engineering. Andy gave me the freedom to work on projects which were of interest to me while also teaching me how to think “like a chemist”. I am extremely grateful for having Andy as my advisor. The amount of lab space which I was permitted to use is also gratefully acknowledged.

Prof. Jay Benziger unofficially functioned as my primary advisor and it was under his direction that I conducted research. Jay was an absolutely outstanding advisor. He very generously gave of his time during our often impromptu meetings and was very patient in explaining concepts to me which I was frequently slow to grasp. I am thankful for the freedom Jay allowed me as I spent month long stretches designing and building instruments, giving him updates which included much gesticulation and zero data. Additionally, the speed with which Jay responded to my emails and proof-read my work was astounding. I also gratefully acknowledge the generous financial support from Jay which I received over several semesters.

Next, I would like to acknowledge all the members of the Bocarsly group who not only tolerated the presence of an engineer in the lab, but also befriended me and patiently taught me various aspects of chemistry. Bocarsly members during my tenure here include Brent Kirby, Martina Vondrova, Jonathan Mann, Christine Burgess, Emily Barton, Hitoshi Ota, Carolyn Mordas, Lakshmi Krishnan, Ely Niangar, Kate Keets, and Amanda Tricarico. Several people deserve special mention: Brent has been a great labmate—being an excellent sounding board for ideas, insightful, fun, and offering decisive advice when needed. I thank Martina for her friendship, help with course work, meals at Mathey, and company during long days in the lab. Interesting conversations with Jonathan have made a lasting impression. Christine’s input on bonding and other aspects of chemistry were a huge help.

Members of the Benziger lab are also gratefully acknowledged. Barclay Satterfield worked on related projects and she was very generous with sharing ideas, time, supplies, journal articles, etc. and was overall fun to work with. It was a pleasure to know and work with Erin Kimball, James Nehlsen, and May Jean Cheah.

Thanks go to Ken Andreas of the chemistry machine shop for generously allowing me use of his shop, teaching me much about machining, and giving me welding lessons. Without Ken's generosity and knowledge, my research would have looked significantly different. Thanks also to Prof. Georgia Arbuckle of Rutgers Camden for allowing Barclay and I the use of her DMA.

Thanks to the IV Graduate Christian Fellowship group and Lutheran Campus Ministries for fellowship, support, and helping me keep in mind the things which are most important.

Laura Bennett deserves special mention for listening to me talk about my research more than was healthy. Not only did Laura listen, she also offered intelligent and insightful conversation as well as support.

I am forever grateful of the support and love of my family; mom, dad, Andrew, John, and Vanessa. Thank you for the unfailing support in all that I do.

Most importantly, I give thanks and praise to my rock and my Redeemer, The Lord Jesus Christ, for the gift of Faith and for everything in me that is good.

Table of Contents

List of Figures

List of Tables

1 Introduction

1.1 Motivation: Why fuel cells?

There is increasing worldwide concern about energy sources and supplies. Fossil fuel reserves are limited and are concentrated unequally around the planet, creating political and economic strife. More importantly, there is increasing evidence that anthropogenic CO_2 emissions from burning fossil fuels and non-renewable bio fuels is contributing to rise in average global temperature. This temperature rise is predicted to cause melting of polar ice caps, drastic shifts in weather patterns, mass extinction of species, sea level rise, and other catastrophic results. Reducing CO_2 emissions by replacing fossil fuel use with renewable/carbon neutral technologies offers the hope of mitigating the degree of global warming predicted.

Today, there is a great diversity of carbon-based energy sources (e.g., coal, natural gas, gasoline) and energy conversion technologies (e.g., internal combustion engines, gas turbines, fossil-fuel based electrical power). Undoubtedly, future carbon-free energy sources and technologies will also be varied. The fuel cell is one technology which will likely play an important role in supplying carbon-free energy.

Fuel cells can efficiently generate electricity from many fuels; increased efficiency translates to fuel savings. Additionally, fuel cells can operate on hydrogen, a carbon-neutral energy carrier which will likely play a large role future renewable energy. Presently, fuel cells are finding use in stationary power generation (backup and primary power). The automobile industry is modestly seeking to develop fuel cell powered vehicles which operate using compressed hydrogen as an energy source. Limits in lithium ion batteries are providing hydrogen and methanol based fuel cells with a niche in the portable electronics sector.

To push fuel cells into commercial markets, many engineering challenges must be overcome. Durability, reliability, and performance must increase while price and weight are decreased. This dissertation addresses some of the technical challenges behind improving fuel cells with fundamental studies of a Nafion, a polymer material which is a key component to specific type of fuel cell.

1.2 Fuel cell components and operating principles

A fuel cell is an electrochemical device that directly converts the chemical energy of a fuel into electrical energy. Unlike batteries, which operate on similar principles, fuel cells can be operated continuously since fuel and oxidant are fed in while waste products are removed. There are several types of fuel cells, being grouped according to their ion transport medium. This dissertation focuses solely on proton exchange membrane (PEM)[i] fuel cells.

A schematic of a working PEM fuel cell is shown in Figure 1-1. In this case, the fuel is hydrogen and the oxidant is pure oxygen. PEM fuel cells have been shown to operate on other fuels as well, such as methanol, ethanol, and formic acid. H_2 brought in at the anode is absorbed by a catalyst (typically platinum) at the surface of a membrane which separates the reactants from oxidants. The absorbed H_2 dissociates into protons and electrons. The electrons travel through an external circuit to the cathode due to an electrical potential gradient. It is the flow of electrons which is desired in the fuel cell, as this can be used to do useful work. The protons at the anode travel through the

---

[i] Equally as valid, PEM is also an acronym for “polymer electrolyte membrane”.

membrane to the cathode where they combine with the electrons and oxygen at the cathode catalyst layer to form water. The net reaction of the H_2/O_2 fuel cell is H_2 and O_2 combining to form water. Losses in the system result in the generation of thermal energy.

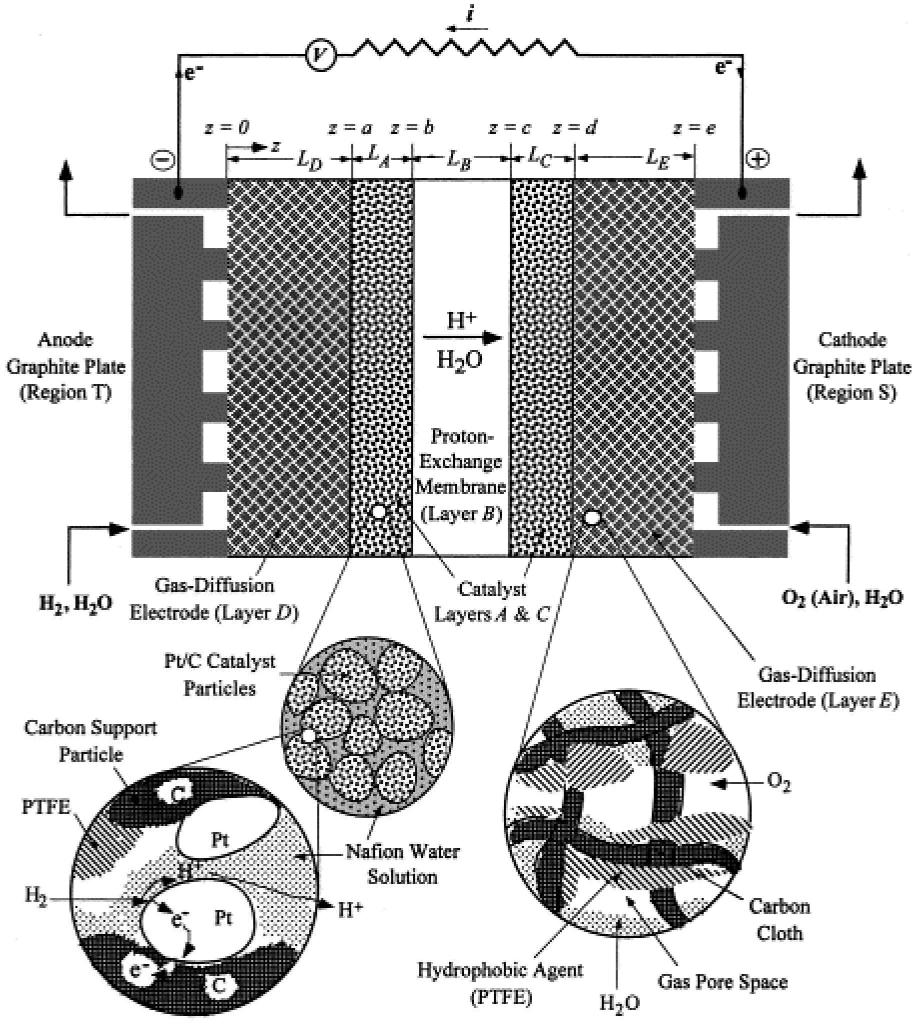

Anode: $H_2 \rightarrow 2H^+ + 2e^-$

Cathode: $1/2O_2 + 2H^+ + 2e^- \rightarrow H_2O$

Overall: $H_2 + 1/2O_2 + \rightarrow H_2O$

Figure 1-1 Schematic representation of a PEM fuel cell operating on H_2 and O_2. Reprinted from reference 1 with permission from Elsevier, © 2001.

At the heart of the PEM fuel cell is a polymer membrane. The membrane must accomplish several tasks. It must 1) physically separate fuel from the oxidant, 2) permit the transport of protons with as little resistance as possible, and 3) be a very poor conductor of electrons. Very few materials are able to do this well. One material which meets these criteria while also being mechanically and chemically stable under a fairly wide range of temperature in the fuel cell environment is Nafion, a polymer developed by DuPont de Nemours in the late 1960s.

A membrane electrode assembly (MEA) is made by pressing together a Nafion membrane with electrodes at both faces with gaskets surrounding. Electrodes are typically made with woven carbon cloth (alternatively, carbon paper can also be used) and have a catalyst layer on one face. The catalyst layer contacts the membrane and is made by having Pt nanoparticles mounted on micron size carbon particles. There is normally a gas diffusion layer (GDL) between the catalyst layer and carbon cloth which is made up of carbon particles. A thin layer of proton conducting polymer (e.g., Nafion) coats the catalyst layer to enable proton conduction between catalyst and membrane. The gas side of the electrode is often coated with PTFE to make it hydrophobic. This reduces water droplet formation which can block gas diffusion to the catalyst.

A schematic of a single cell PEM fuel cell is shown in Figure 1-2. The MEA is clamped between flow plates. Flow plates are electrically conducting and contact the electrodes. They also have flow channels which carry fuel and oxidant to the anode and cathode, respectively. Typically, the flow channels are serpentine. Sufficient clamping pressure is applied with bolts to prevent leaking of gases and provide good electrical contact between flow plates and electrodes. For a brief discussion of estimating clamping pressure from bolt torque, see section 7.1 of the appendix.

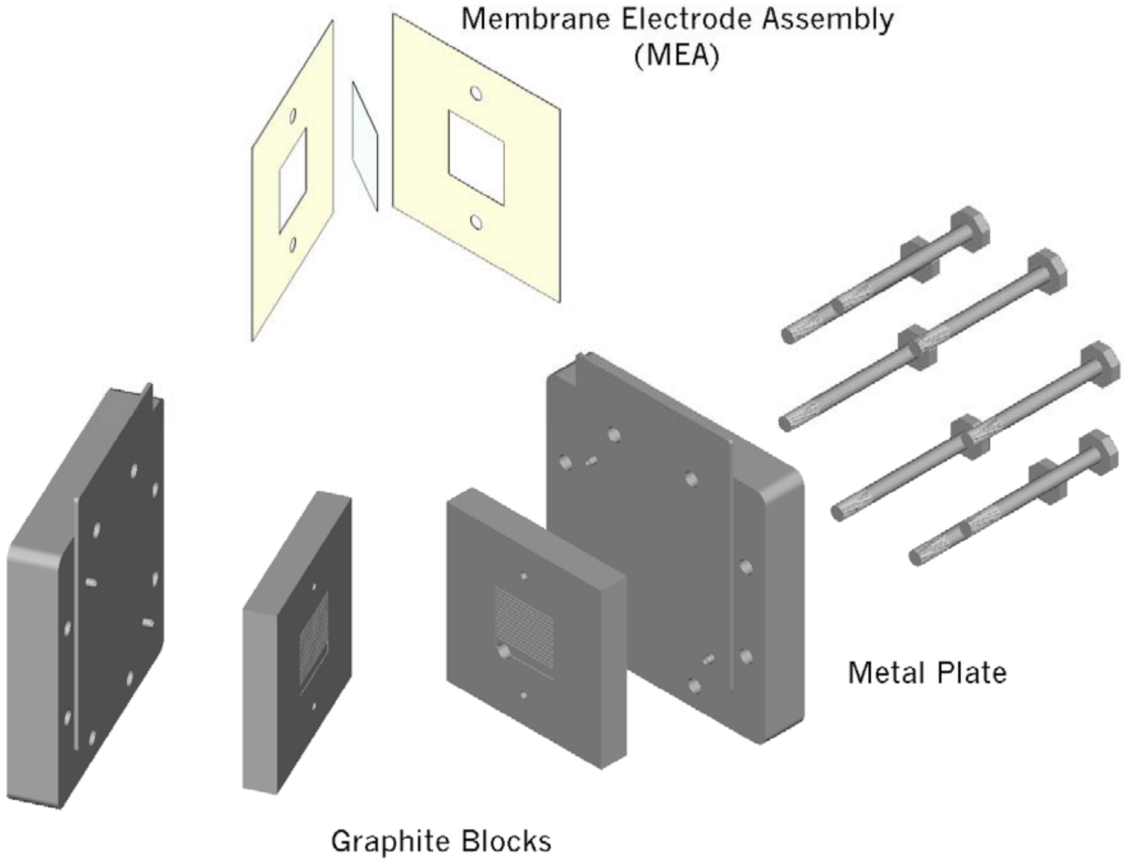

Figure 1-2 An exploded view of a single cell PEM fuel cell showing graphite blocks with serpentine flow channels, MEA, and metal plates which clamp together the graphite blocks and MEA.

1.3 Nafion: a perfluorinated ionomer

1.3.1 Introduction

Nafion is a sulfonated tetrafluorethylene copolymer that was discovered in the late 1960s by Dr.Walther Gustav Grot of DuPont de Nemours. The first of a class of perfluorinated ionomers—a fully fluorinated polymer material terminated at points with ionic groups—it was originally developed as a membrane material for the chlor-alkali process. The material is generated by the copolymerization of a perfluorinated vinyl ether comonomer with tetrafluoroethylene[2].

The chemical structure of Nafion is shown Figure 1-3. The fluorinated backbone of the polymer is essentially polytetrafluoroethylene (PTFE) or Teflon® and gives

Nafion exceptional resistance to harsh chemical environments, good mechanical strength, and a fairly high maximum operating temperature. Fluorinated ether linkages terminate in sulfonate groups.

The ratio of the number of grams of polymer per mole of sulfonic acid groups of the material in the acid form and completely dry is referred to as equivalent weight (EW). Equivalent weight can be varied and strongly affects mechanical and transport properties. Increasing EW (decreasing sulfonic acid group concentration) improves mechanical properties, but decreases proton conductivity. 1,100 EW Nafion is typically used in PEM fuel cell applications since it has a reasonable balance of proton conductivity and mechanical integrity. In 1,100 EW Nafion, the average value of m (the length CF_2 units between side chains) is 14.

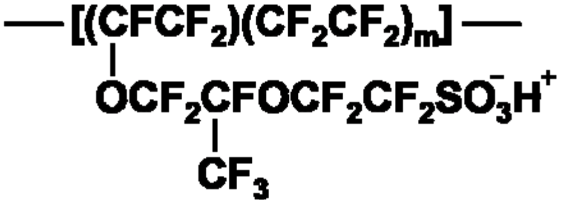

Figure 1-3 Chemical structure of Nafion in the protonated form[2].

Nafion is designated by a system of numbers. The first two numbers denote EW while the third and possible fourth digits denote dry membrane thickness in thousandths of an inch. For Example, Nafion N112 is 1,100 EW and 0.002” (0.0051 cm) thick. In this dissertation, 1,100 EW weight membranes with thickness of 0.002” (0.0051cm), 0.005” (0.0127cm), and 0.010” (0.0254cm) are specifically mentioned. They correspond to N112, N115, and N1110, respectively. The N denotes that the membranes are extruded films.

Various monovalent cations (e.g., Na^+, Li^+) can interact with the sulfonate groups, permitting transport of the ionic species in the presence of a chemical or electrical gradient. Interchange of ionic species can be easily accomplished, converting the Nafion from one form to another. In this dissertation, Nafion is in protonated form unless specifically stated. Na^+ form Nafion is introduced briefly in the chapter on tensile testing.

1.3.2 Morphology

Nafion's morphology has been investigated extensively since the early 1970s and is, to this day, a topic of debate as well as current research. Mauritz and Moore presented an excellent review of our state of understanding of Nafion's morphology as of 2004[2]. They stress in this review that "…a universally accepted morphological model for the solid-state structure of Nafion has yet to be defined". However, the following general statements about Nafion's morphology can be made with reasonable confidence:

1) Nafion phase separates into distinct hydrophobic and hydrophilic regions
2) The hydrophobic region is a continuous semi-crystalline region which is Teflon®-like, being made up of main chain TFE segments.
3) The hydrophilic regions consist of sulfonate groups, swell and change size/shape with water uptake, eventually forming a continuous network, and allow water and proton/ion transport.

Nafion's morphology has been indirectly studied with scattering techniques such as small-angle X-ray scattering (SAXS) and wide-angle X-ray scattering (WAXS) [3-10] as well as small-angle neutron scattering(SANS)[11-13]. Thermal analysis techniques, such as differential scanning calorimetry (DSC) and dynamic mechanical analysis (DMA), have also been used to obtain information about Nafion's transitions and structure[14-19]. Additionally, transmission electron microscopy (TEM) and scanning electron microscopy

(SEM)[9, 20-23] and, more recently, atomic force microscopy (AFM)[24-26] have been used to image Nafion's structure.

Historically, the first morphological model of Nafion was presented by Geirke and co workers and offers an excellent conceptual basis for understanding the structure and properties of Nafion[3-5]. The Geirke model, known as the cluster-network model, assumes that the sulfonate groups form into spherical clusters that resemble inverted micelles. It is also assumed that the clusters are arranged on a regular lattice and interconnected with narrow channels. A schematic representation of the cluster-network model is shown in Figure 1-4. The spacing between clusters for the clusters shown was given as 5.0 nm. The model assumes that cluster size increases with hydration while the number of clusters decreases as clusters grow.

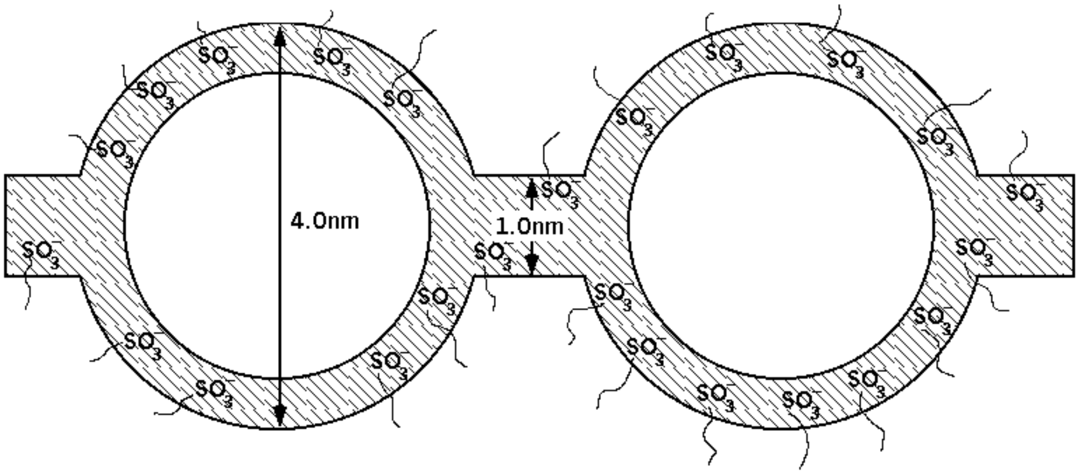

Figure 1-4 Gierke and co workers' cluster-network model of Nafion showing cluster and channel size as well as location of sulfonic acid groups and pendant chains. Reprinted from reference 5 with permission from Elsevier, © 1983.

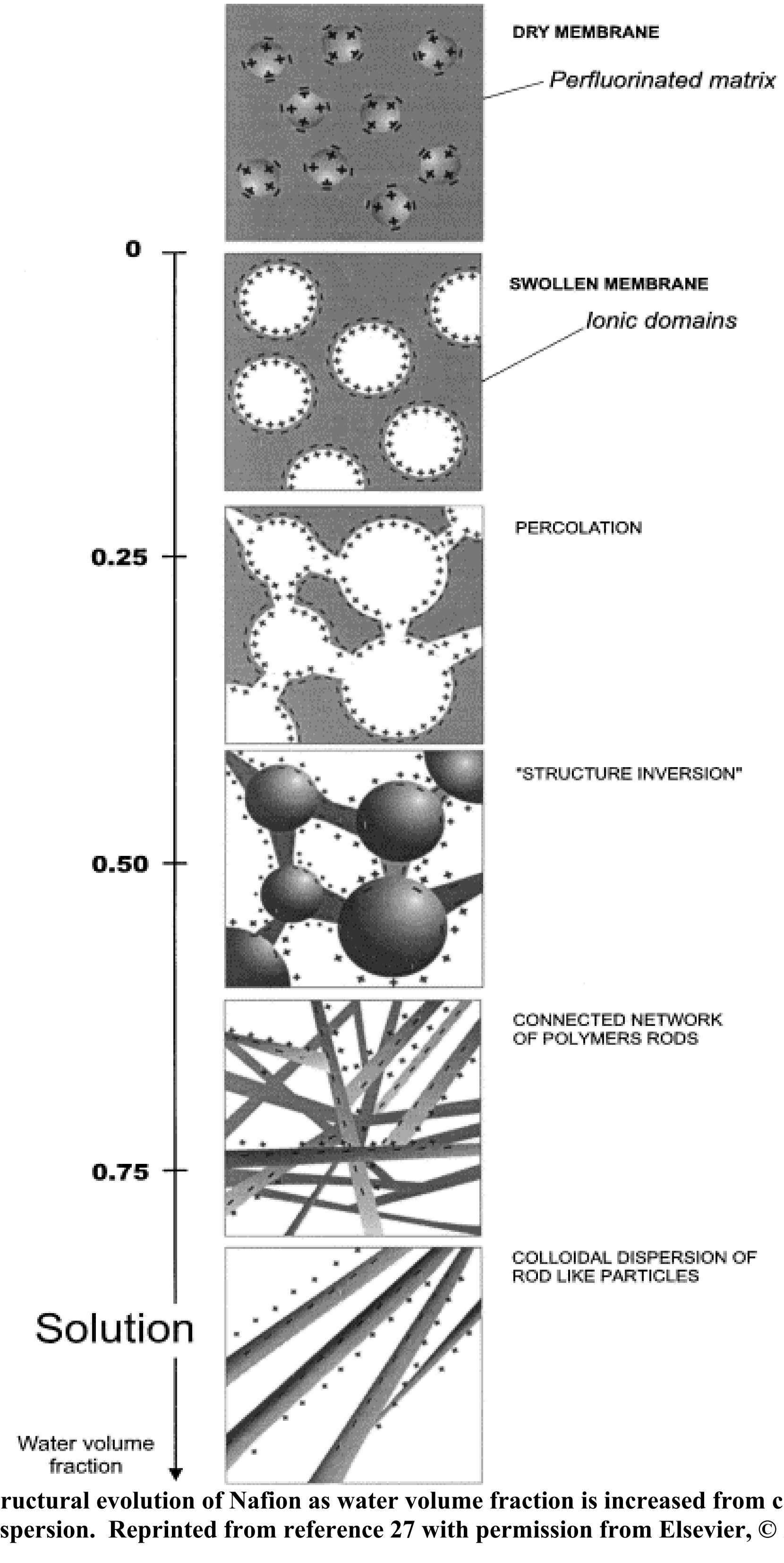

Figure 1-5 Structural evolution of Nafion as water volume fraction is increased from completely dry to colloidal dispersion. Reprinted from reference 27 with permission from Elsevier, © 2000.

Gebel proposed the conceptual model shown in Figure 1-5 for the hydration and dissolution of Nafion with water[27]. This model is based on X-ray scattering data for Nafion over a range of hydration as well as energetics. According to the model, Nafion's structure evolves from isolated sulfonate groups in dry Nafion to spherical ionic clusters that grow in size and become interconnected with hydration. Cylindrical water domains act to interconnected clusters. At water activity of 0.5, an inversion in structure occurs in which the acid groups form a network of interconnected rods. The rod structure is maintained as colloidal particles form upon complete dissolution.

1.4 Importance of water in PEM fuel cells

PEM fuel cells incorporating present day membrane materials require water for operation. This is because water is essential for proton conductivity in the membrane, increasing by nearly 6 orders of magnitude from dry to fully hydrated[28]. Water is usually introduced at the anode and cathode with humidifying the gas feeds. Water is also produced at the cathode as part of the overall reaction.

If liquid water forms at the catalyst surface, so-called "flooding" occurs. This is the result of liquid water at the catalyst surface blocking the transport of fuel/oxidant to the catalyst surface. It is for this reason that electrodes are typically wet-proofed with PTFE. Water management in PEM fuel cells is one of the major engineering hurdles in their commercialization.

1.4.1 Permeation of water through the fuel cell membrane

As already mentioned, membrane hydration is required for proton conduction. How, then, does water enter the membrane?

Water moves by convection and diffusion to the membrane surface where it enters the membrane and travels by diffusion through the membrane. Water can reach the membrane surface in the vapor or liquid phase. Diffusion of water through the membrane is driven by chemical potential gradients, or differences in water activity[ii]. Diffusion is the main process by which differences in water activity in the membrane are equalized[29]. Water uptake by and transport though Nafion are critically important for determining the steady state and dynamic response of fuel cells. To properly understand and model fuel cell behavior in order to optimize operation and design fuel cell systems, water transport must be properly understood.

Prior to this work, water uptake and transport of Nafion has been poorly understood. Little attention has been directed to the interfacial mass transport of the membrane and membrane relaxation during water uptake[30-32]. Additionally, literature values for water diffusivity in Nafion span three orders of magnitude with little discussion of why this has occurred[32].

1.4.2 Mechanical properties of membrane

The mechanical properties of membranes in PEM fuel cells is important to their performance, both in the long and short term. In the short term, uptake of water is partially controlled by polymer relaxation[32, 33]. In the long term, membrane creep caused by clamping pressure and swelling due to water uptake can cause delamination of electrodes from the membrane as well as pin hole formation due to membrane thinning [15, 34, 35]. The mechanical properties of Nafion are strongly dependant on temperature and

---

[ii] Activity is a measure of the concentration of a component in the liquid or vapor phase relative to the saturated concentration of the pure substance at that temperature. In the vapor phase, activity is defined as the ratio of vapor pressure of the component in the mixture to the vapor pressure of the pure substance at that temperature. Relative humidity, which refers specifically to water vapor, is defined as a_w x 100.

hydration. Despite this, little work has been done to measure mechanical properties as a function of hydration and temperature[14, 33, 34, 36-40].

1.4.3 Composite metal oxide/Nafion membranes

Increasing the operating temperature of fuel cells has the advantage of increasing their tolerance to CO poisoning of the catalyst (important if H_2 is produced from hydrocarbon feed stocks) while also making the rejection of waste heat easier. The obstacle to increasing operating temperature of today's PEM fuel cells is that the membrane materials show poor performance and increased degradation at elevated temperature. Additionally, it is desirable to increase membrane performance at reduced relative humidity levels to simplify operating controls and increase performance.

In order to improve Nafion's performance under conditions of elevated temperature and reduced relative humidity, several investigators have taken the approach of making a composite material with Nafion and metal oxide nanoparticles[28, 41-60]. Composite Nafion/metal oxide membranes have shown moderate increases in elevated temperature/reduced relative humidity performance.

1.5 Dissertation overview

This dissertation presents fundamental studies on the transport and mechanical properties of Nafion—namely water permeation and viscoelastic creep. The work is focused on how temperature and hydration affect these properties. Emphasis on discerning microstructure/molecular level interactions in the ionomer and determining how this impacts mechanical and transport properties. Property values, such as elasticity and diffusivity, are also reported.

This dissertation is subdivided into three major areas: 1) water permeation through Nafion, 2) the effects of temperature and hydration on the viscoelastic creep response of Nafion, and 3) composite metal oxide/Nafion membranes.

Water permeation: Transport of water in Nafion was studied by measuring permeation and is presented in Chapter 3. Steady state permeation of water from the liquid and vapor phase through Nafion and into the gas phase was studied for several membrane thicknesses as a function of temperature and water activity. Permeation for plain Nafion membranes is compared to permeation for Nafion with a gas diffusion layer included. Permeation from liquid water and water vapor is compared. Consideration is given to transport phenomena, including interfacial mass transport and diffusion. Permeation of liquid water and vapor is significantly different. It is shown that interfacial mass transport is significant, especially for liquid water permeation. Values are reported for interfacial mass transport coefficient and diffusivity. Diffusivity is shown to depend strongly on membrane hydration

Viscoelastic response: The viscoelastic response of Nafion was studied over a wide range of temperature and hydration using a custom designed creep instrument. These studies are presented in Chapter 2. Elastic modulus and tensile creep are reported as a function of temperature and hydration, representing the most complete set of humidity dependant mechanical property data published to date for Nafion. Discontinuous behavior was observed between the mechanical response of completely dry and hydrated Nafion. Hydration was observed to plasticize Nafion at low temperature. Contrary to the main body of literature, water was observed to stiffen Nafion at temperatures above ca. 50°C (only Satterfield[30] and Bauer[15] report similar findings). Changes in the mechanical response with hydration and temperature are used to explain microstructure and bonding interactions of Nafion. In some respects, these mechanical tests are more sensitive to changes in microstructure and bonding interactions than are microscopy techniques, such as small angle X-ray scattering (SAXS). Additional experiments showing swelling dynamics and equilibrium due to water uptake are summarized in chapter 5.

Composite membranes: Chapter 4 presents techniques developed to fabricate metal oxide/Nafion composite membranes. The process involves suspending metal oxide nanoparticles in solubolized Nafion and removing solvents by evaporation. The process and various physical/chemical considerations for recasting composite membranes with this technique are detailed. Additionally, a study investigating the interaction between particles and polymer is presented. Using thermogravimetric analysis (TGA) and thermogravimetric-mass spectroscopy (TG-MS), it is suggested that bonding interactions occur between particles and polymer, crosslinking the polymer. Mechanical test data are also presented for Nafion composites which give support to the theory that crosslinking occurs between particles and polymer in Nafion/TiO_2 composites.

1.6 References

1. Thampan, T.; Mahotra, S.; Zhang, J.; Datta, R., PEM Fuel Cell as a Membrane Reactor. *Catalysis Today* **2001,** 67, 15-32.
2. Mauritz, K. A.; Moore, R. B., State of Understanding of Nafion. *Chemical Reviews* **2004,** 104, (10), 4535-4585.
3. Gierke, T. D.; Hsu, T. D., *Perfluorinated Ionomer Membranes*. American Chemical Society: Washington D.C., 1982; Vol. 180.
4. Gierke, T. D.; Munn, G. E.; Wilson, F. C., The Morphology in Nafion Perfluorinated Membrane Products, as Determined by Wide-Angle and Small-Angle X-Ray Studies. *Journal of Polymer Science Part B-Polymer Physics* **1981,** 19, (11), 1687-1704.
5. Hsu, W. Y.; Gierke, T. D., Ion-Transport and Clustering in Nafion Perfluorinated Membranes. *Journal of Membrane Science* **1983,** 13, (3), 307-326.

6. Hsu, W. Y.; Gierke, T. D., Elastic Theory for Ionic Clustering in Perfluorinated Ionomers. *Macromolecules* **1982,** 15, (1), 101-105.
7. Gierke, T. D.; Munn, G. E.; Wilson, F. C., Morphology of Perfluorosulfonated Membrane Products - Wide-Angle and Small-Angle X-Ray Studies. *Acs Symposium Series* **1982,** 180, 195-216.
8. Fujimara, M.; Hashimoto, T.; Kawai, H., *Macromolecules* **1981,** 14, (139).
9. Fujimura, M.; Hashimoto, T.; Kawai, H., Small-Angle X-Ray-Scattering Study of Perfluorinated Ionomer Membranes .2. Models for Ionic Scattering Maximum. *Macromolecules* **1982,** 15, (1), 136-144.
10. Roche, E. J.; Pineri, M.; Duplessix, R.; Levelut, A. M., Small-Angle Scattering Studies of Nafion Membranes. *Journal of Polymer Science Part B-Polymer Physics* **1981,** 19, (1), 1-11.
11. Roche, E. J.; Pineri, M.; Duplessix, R., Phase Separation in Perfluorsulfonate Ionomer Membranes. *Journal of Polymer Science* **1982,** 20, 107-116.
12. Lee, E. M.; Thomas, R. K.; Burgess, A. N.; Barnes, D. J.; Soper, A. K.; Rennie, A. R., Local And Long-Range Structure Of Water In A Perfluorinated Ionomer Membrane. *Macromolecules* **1992,** 25, (12), 3106-3109.
13. Dreyfus, B.; Gebel, G.; Aldebert, P.; Pineri, M.; Escoubes, M.; Thomas, M., Distribution of the Micelles in Hydrated Perfluorinated Ionomer Membranes from Sans Experiments. *Journal De Physique* **1990,** 51, (12), 1341-1354.
14. Kyu, T.; Eisenberg, A., Mechanical Relaxations in Perfluorosulfonate-Ionomer Membranes. *Acs Symposium Series* **1982,** 180, 79-110.
15. Bauer, F.; Denneler, S.; Willert-Porada, M., Influence of temperature and humidity on the mechanical properties of Nafion (R) 117 polymer electrolyte membrane. *Journal Of Polymer Science Part B-Polymer Physics* **2005,** 43, (7), 786-795.
16. Uan-Zo-li, J. T. The Effects of Structure, Humidity and Aging on the Mechanical Properties of Polymeric Ionomers for Fuel Cell Applications. Master of Science, Virginia Polytechnic Institute and State University, Blacksburg, Virginia, 2001.
17. Tant, M. R.; Darst, K. P.; Lee, K. D.; Martin, C. W., Structure and Properties of Short-Side-Chain Perfluorosulfonate Ionomers. *Acs Symposium Series* **1989,** 395, 370-400.
18. Miura, Y.; Yoshida, H., Effects of Water and Alcohols on Molecular-Motion of Perfluorinated Ionomer Membranes. *Thermochimica Acta* **1990,** 163, 161-168.
19. Yeo, S. C.; Eisenberg, A., Physical-Properties and Supermolecular Structure of Perfluorinated Ion-Containing (Nafion) Polymers. *Journal of Applied Polymer Science* **1977,** 21, (4), 875-898.
20. Ceynowa, J., Electron-Microscopy Investigation of Ion-Exchange Membranes. *Polymer* **1978,** 19, (1), 73-76.
21. Xue, T.; Trent, J. S.; Osseoasare, K., Characterization of Nafion Membranes by Transmission Electron-Microscopy. *Journal of Membrane Science* **1989,** 45, (3), 261-271.
22. Rieberer, S.; Norian, K. H., Analytical Electron-Microscopy of Nafion Ion-Exchange Membranes. *Ultramicroscopy* **1992,** 41, (1-3), 225-233.
23. Porat, Z.; Fryer, J. R.; Huxham, M.; Rubinstein, I., Electron-Microscopy Investigation Of The Microstructure Of Nafion Films. *Journal Of Physical Chemistry* **1995,** 99, (13), 4667-4671.

24. McLean, R. S.; Doyle, M.; Sauer, B. B., High-resolution imaging of ionic domains and crystal morphology in ionomers using AFM techniques. *Macromolecules* **2000,** 33, (17), 6541-6550.

25. James, P. J.; Antognozzi, M.; Tamayo, J.; McMaster, T. J.; Newton, J. M.; Miles, M. J., Interpretation of Contrast in Tapping Mode AFM and Shear Force Microscopy. A Study of Nafion. *Langmuir* **2001,** 17, 349-360.

26. James, P. J.; Elliott, J. A.; McMaster, T. J.; Newton, J. M.; Elliott, A. M. S.; Hanna, S.; Miles, M. J., Hydration of Nafion (R) studied by AFM and X-ray scattering. *Journal Of Materials Science* **2000,** 35, (20), 5111-5119.

27. Gebel, G., Structural evolution of water swollen perfluorosulfonated ionomers from dry membrane to solution. *Polymer* **2000,** 41, (15), 5829-5838.

28. Yang, C.; Srinivasan, S.; Bocarsly, A. B.; Tulyani, S.; Benziger, J. B., A comparison of physical properties and fuel cell performance of Nafion and zirconium phosphate/Nafion composite membranes. *Journal of Membrane Science* **2004,** 237, (1-2), 145-161.

29. Doyle, M., and Rajendran, G., Perfluorinated Membranes (Ch. 30). In *Handbook of Fuel Cells-Fundamentals, Technology, and Applications*, W. Vielstich, H. G., A Lamm, Ed. 2003; Vol. 3, p 377.

30. Satterfield, M. B. Mechanical and Water Sorption Properties of Nafion and Nafion/Titanium Dioxide Membranes for Polymer Electrolyte membrane Fuel Cells. Princeton University, Princeton, 2007.

31. Satterfield, M. B.; Benziger, J. B., NonFickian Water Sorption Dynamic by Nafion Membranes. **2007,** forthcoming.

32. Majsztrik, P. W.; Satterfield, M. B.; Bocarsly, A. B.; Benziger, J. B., Water Sorption, Desorption and Transport in Nafion Membranes. *Journal of Membrane Science* **2007,** 301, (1-2), 93-106.

33. Satterfield, M. B.; Majsztrik, P. W.; Ota, H.; Benziger, J. B.; Bocarsly, A. B., Mechanical Properties of Nafion and Titania/Nafion Composite Membranes for PEM Fuel Cells. *J. Polymer Science B: Polymer Physics* **2006,** 44, 2327-2345.

34. Tang, Y. L.; Karlsson, A. M.; Santare, M. H.; Gilbert, M.; Cleghorn, S.; Johnson, W. B., An experimental investigation of humidity and temperature effects on the mechanical properties of perfluorosulfonic acid membrane. *Materials Science and Engineering a-Structural Materials Properties Microstructure and Processing* **2006,** 425, (1-2), 297-304.

35. Stanic, V. a. H. M., Mechanism of pinhole formation in membrane electrode assemblies for PEM fuel cells. In NASA Archive 2005.

36. DuPont DuPont Fuel Cells: DuPont Nafion PFSA Membranes N-115, N-117, NE-1110. http://www.dupont.com/fuelcells/pdf/dfc101.pdf

37. Kawano, Y.; Wang, Y. Q.; Palmer, R. A.; Aubuchon, S. R., Stress-Strain Curves of Nafion Membranes in Acid and Salt Forms. *Polimeros* **2002,** 12, (2), 96-101.

38. Kundu, S.; Simon, L. C.; Fowler, M.; Grot, S., Mechanical properties of Nafion (TM) electrolyte membranes under hydrated conditions. *Polymer* **2005,** 46, (25), 11707-11715.

39. Werner, S.; Jorissen, L.; Heider, U., Conductivity and Mechanical Properties of Recast Nafion Films. *Ionics* **1996,** 2, (1), 19-23.

40. Kyriakides, S. A., Mechanical Behavior of Nafion and BPSH Membranes. *Journal of Undergraduate Materials Research* **2005,** 1, 11-14.
41. Yang, C.; Costamagna, P.; Srinivasan, S.; Benziger, J.; Bocarsly, A. B., Approaches and technical challenges to high temperature operation of proton exchange membrane fuel cells. *Journal of Power Sources* **2001,** 103, (1), 1-9.
42. Yang, C.; Srinivasan, S.; Arico, A. S.; Creti, P.; Baglio, V.; Antonucci, V., Composition Nafion/zirconium phosphate membranes for direct methanol fuel cell operation at high temperature. *Electrochemical and Solid State Letters* **2001,** 4, (4), A31-A34.
43. Adjemian, K. T.; Dominey, R.; Krishnan, L.; Ota, H.; Majsztrik, P.; Zhang, T.; Mann, J.; Kirby, B.; Gatto, L.; Velo-Simpson, M.; Leahy, J.; Srinivasant, S.; Benziger, J. B.; Bocarsly, A. B., Function and characterization of metal oxide-naflon composite membranes for elevated-temperature H-2/O-2 PEM fuel cells. *Chemistry of Materials* **2006,** 18, (9), 2238-2248.
44. Watanabe, M.; Uchida, H.; Seki, Y.; Emori, M.; Stonehart, P., Self-humidifying polymer electrolyte membranes for fuel cells. *Journal of the Electrochemical Society* **1996,** 143, (12), 3847-3852.
45. Si, Y. C.; Kunz, H. R.; Fenton, J. M., Nafion-Teflon-Zr(HPO4)(2) composite membranes for high-temperature PEMFCs. *Journal of the Electrochemical Society* **2004,** 151, (4), A623-A631.
46. Park, Y. I.; Kim, J. D.; Nagai, M., Increase of proton conductivity in amorphous phosphate-Nafion membranes. *Journal of Materials Science Letters* **2000,** 19, (18), 1621-1623.
47. Ramani, V.; Kunz, H. R.; Fenton, J. M., Investigation of Nafion (R)/HPA composite membranes for high temperature/low relative humidity PEMFC operation. *Journal of Membrane Science* **2004,** 232, (1-2), 31-44.
48. Jalani, N. H.; Dunn, K.; Datta, R., Synthesis and characterization of Nafion (R)-MO2 (M = Zr, Si, Ti) nanocomposite membranes for higher temperature PEM fuel cells. *Electrochimica Acta* **2005,** 51, (3), 553-560.
49. Baglio, V.; Arico, A. S.; Di Blasi, A.; Antonucci, V.; Antonucci, P. L.; Licoccia, S.; Traversa, E.; Fiory, F. S., Nafion-TiO2 composite DMFC membranes: physico-chemical properties of the filler versus electrochemical performance. *Electrochimica Acta* **2005,** 50, (5), 1241-1246.
50. Baglio, V.; Di Blasi, A.; Arico, A. S.; Antonucci, V.; Antonucci, P. L.; Fiory, F. S.; Licoccia, S.; Traversa, E., Influence of TiO2 nanometric filler on the behaviour of a composite membrane for applications in Direct Methanol Fuel Cells. *Journal of New Materials for Electrochemical Systems* **2004,** 7, (4), 275-280.
51. Thampan, T. M.; Jalani, N. H.; Choi, P.; Datta, R., Systematic approach to design higher temperature composite PEMs. *Journal Of The Electrochemical Society* **2005,** 152, (2), A316-A325.
52. Yuan, S.; Hu, S. S., Characterization and electrochemical studies of Nafion/nano-TiO2 film modified electrodes. *Electrochimica Acta* **2004,** 49, (25), 4287-4293.
53. Klein, L. C.; Daiko, Y.; Aparicio, M.; Damay, F., Methods for modifying proton exchange membranes using the sol-gel process. *Polymer* **2005,** 46, (12), 4504-4509.

54. Mauritz, K. A.; Stefanithis, I. D.; Huang, H. H., Microstructural Evolution of a Silicon-Oxide Phase in Nafion Membranes by an Insitu Sol-Gel Reaction. *Abstracts of Papers of the American Chemical Society* **1991,** 202, 285-POLY.
55. Alberti, G.; Casciola, M., Composite membranes for medium-temperature PEM fuel cells. *Annual Review of Materials Research* **2003,** 33, 129-154.
56. Arico, A. S.; Baglio, V.; Di Blasi, A.; Creti, P.; Antonucci, P. L.; Antonucci, V., Influence of the acid-base characteristics of inorganic fillers on the high temperature performance of composite membranes in direct methanol fuel cells. *Solid State Ionics* **2003,** 161, (3-4), 251-265.
57. Mauritz, K. A., Storey, R.F., amd Jones, C. K., Multiphase Polymer Materials: Blends, Ionomers, and Interpenetrating Networks. In *ACS Symp. Ser. no. 395*, American Chemical Society: Washington, DC, 1989.
58. Mauritz, K. A.; Warren, R. M., Microstructural Evolution of a Silicon-Oxide Phase in a Perfluorosulfonic Acid Ionomer by an Insitu Sol-Gel Reaction .1. Infrared Spectroscopic Studies. *Macromolecules* **1989,** 22, (4), 1730-1734.
59. Mauritz, K. A.; Stefanithis, I. D., Microstructural Evolution of a Silicon-Oxide Phase in a Perfluorosulfonic Acid Ionomer by an Insitu Sol-Gel Reaction .2. Dielectric-Relaxation Studies. *Macromolecules* **1990,** 23, (5), 1380-1388.
60. Stefanithis, I. D.; Mauritz, K. A., Microstructural Evolution of a Silicon-Oxide Phase in a Perfluorosulfonic Acid Ionomer by an Insitu Sol-Gel Reaction .3. Thermal-Analysis Studies. *Macromolecules* **1990,** 23, (8), 2397-2402.

2 Viscoelastic Response of Nafion; Effects of Temperature and Hydration on Tensile Creep

2.1 Introduction and literature review

Nafion is a viscoelastic material, responding to stress in a time-dependant manner. The result is that Nafion flows under stress and responds dynamically to changes in hydration and stress. Stresses applied to the membrane of a PEM fuel cell, both from clamping as well as strain from changing levels of hydration, cause Nafion to flow, resulting in thinning in spots and sometimes leads to the development of pinholes or contact problems between membrane and electrode[1, 2]. Pinhole formation is believed to be one of the leading failure modes in PEM fuel cells which are based on Nafion or similar polymers[3]. Furthermore, the dynamics of fuel cell power response is partially governed by hydration dynamics of the membrane; water adsorption depends on the viscoelastic properties[4, 5]. As such, accurately knowing the mechanical properties of Nafion can lead to better modeling of fuel cell performance, increased understanding of failure mechanisms, as well as improved designs of the overall fuel cell system and next-generation materials.

The mechanical properties of Nafion have been the subject of several studies since its development in the 1960s[1, 4, 6-11]. However, further research in this area is still needed. In their 2004 review "The State of Understanding of Nafion", Mauritz and Moore assert that studies of the mechanical properties of Nafion have been secondary to studies on transport and structure. They also stress the importance of further studies in this area[12]:

> *To be sure, the mechanical integrity of membranes as mounted in cells, and under the perturbation of pressure gradients, swelling-dehydration cycles, mechanical creep, extreme temperatures, and the onset of brittleness and tear resistance, is important and must be taken into consideration.*

The goal of studies investigating the mechanical properties of Nafion has been twofold. The first and most obvious goal of the studies has been to measure mechanical properties of the material in order to obtain values which can be used to predict the material's behavior in a wide range of applications. A small minority of mechanical studies have had this goal, though interest in this area has been increasing of late[1, 4, 6-11]. The second goal of the mechanical studies on Nafion has been to gain a better understanding of what interactions are occurring in the material, on a molecular and microstructural level, which affect mechanical properties. To accomplish this, researchers have largely relied on Dynamic Mechanical Analysis (DMA) which gives information on the thermomechanical transitions attributed to morphological considerations[2, 11, 13-16]. The majority of studies have been focused on the latter.

This chapter presents work related to the viscoelastic response of Nafion over a range of temperature and hydration. Both mechanical property data as well as interpretation of mechanical behavior on molecular and morphological interactions are included. Viscoelastic response was measured by tensile creep utilizing a creep instrument with environmental control designed and built by the author specifically for this purpose. The major areas of study are as follows:

1) Tensile creep of dry Nafion over a range of temperature
2) Effects of hydration and temperature on creep response

3) Instantaneous elastic response over a range of temperature and hydration

4) Solvent effects on swelling and viscoelastic response

5) Thermal history effects

6) Effects of altering membrane composition (Na form, composite (ch. 4))

7) Swelling due to water uptake (ch. 5)

8) Dynamic effects of water uptake and swelling (ch. 5)

2.1.1 Bonding interactions in polymers

In order to understand the mechanical response of Nafion and what effects temperature and hydration have, an understanding of what interactions occur in polymers and how these can impact mechanical properties must first be obtained. Once a general understanding of these interactions is established, results from mechanical studies can be used to infer bonding interactions in the polymer and how temperature and hydration act to affect them.

Five major types of interactions can occur in a polymer: (1) primary covalent bonds, (2) hydrogen bonds, (3) dipole interactions, (4) van der Waals interactions, and (5) ionic bonds[17]. Approximate bond strength, along with average interatomic spacing, are given in Table 2-1 for the different bonding interactions.

Table 2-1 Typical ranges of dissociative energy and interatomic distance for different types of bonding interactions[17].

Bond type	Interatomic Distance (nm)	Dissociative Energy (kJ/mol)
Primary covalent	0.1-0.2	200 - 800
Hydrogen bond	0.2-0.3	12 - 30
Dipole interaction	0.2-0.3	6 - 12
Van der Waals interaction	0.3-0.5	2 - 8
Ionic bond	0.2-0.3	40 - 80

A distinction must be drawn between chemical bonds and other bonding interactions occurring in polymers. Covalent and ionic bonds are true chemical bonds. A covalent bond is the sharing of an electron pair by two atoms. Ionic bonding occurs between oppositely charged ions and is a result of electrons being donated from an atom (or atoms) to another atom (or atoms). Dipole-dipole attraction or dipole interaction occurs between molecules, a result of electrostatic interaction. Typically, dipole-dipole forces are about 1% of covalent or ionic bonds[18]. Hydrogen bonding, a special case of dipole attraction, occurs between molecules which have an O—H, F—H, or N—H group and is significantly stronger than other dipole interactions making it the strongest type of intermolecular force[19]. Van der Waals interactions (London dispersion forces) occur between non-polar molecules as a result of temporary induced dipoles. These interactions are the weakest and have the longest range.

Primary bonding occurs between atoms in molecular chains which make up polymers. These bonds are very strong and if broken, due to thermal excitation, the material degrades. Primary bonds are either covalent or ionic bonds.

Hydrogen bonds, van der Waals interactions, and dipole interactions—referred to collectively as "secondary bonds"—all occur *between* polymer chains, acting to hold the chains together[17]. These bonds are weaker than primary covalent and ionic bonds and can normally be overcome by thermal excitation which does not destroy bonds holding molecular chains together. Strictly speaking, these interactions which are referred to as secondary bonds are not actually considered chemical bonds—only covalent and ionic bonds are true chemical bonds. For linear or branched polymers, only secondary bonds, along with less significant chain entanglements, hold chains together.

Polymers with only secondary bonding between chains are known as thermoplastics and can be shaped and reshaped by heating above the glass transition temperature. Thermal excitation of the polymer, brought about by raising the temperature, decreases secondary bond strength due to molecular vibration. As temperature is increased, an applied stress more easily deforms or breaks bonds, giving rise to increased strain in the material.

If primary bonding occurs between polymer chains, the material is referred to as a thermoset. Primary bonds between chains, known as crosslinks, give thermosets resistance to deformation since chains are unable to slip past one another. Crosslink bonds are usually as strong as the bonding between atoms in chains. Because of this, thermosets cannot be thermally processed; once a thermoset polymer has a certain shape, it cannot be changed by thermal processing. Thermal excitation sufficient to overcome crosslink bonds is also sufficient to overcome intermolecular interactions and bring about degradation of the material.

2.1.2 Temperature and Humidity Effects

Like most polymers, Nafion's mechanical properties are strongly dependant on temperature. This is due to the strength of interactions between polymer chains becoming insignificant with increasing temperature. As temperature increases, the thermal energy of polymer molecules exceeds that of secondary bonds and chains are able to move past one another when a force is applied. For Nafion, this includes van der Waals interactions between the main chains and weak crosslinking interactions between sulfonic acid groups (hydrogen bonding/dipole interactions).

Hydration, however, also strongly affects Nafion's mechanical properties. This is because the ionic regions can absorb water, altering the interactions between chains which occur through sulfonic acid terminated side chains. A majority of the studies investigating the mechanical properties of Nafion either neglect hydration's effect or restrict their study to the conditions most easily attained by commercially available instruments: mostly dry, exposed to liquid water, and ambient humidity ratio.

Indeed, maintaining stable hydration levels between dry and liquid states for the duration of a mechanical test at temperatures of interest is an engineering challenge. Rapid changes in temperature bring about fluctuations in relative humidity. Any area exposed to water vapor which falls below the dew point temperature of the mixture result in condensation. The time required for equilibration of the test material with surrounding solvent activity can be considerable. Instrument parts exposed to water vapor or liquid water at elevated temperatures can degrade unless properly designed. Not only does instrumentation need to be modified or specially designed, but testing procedures must be specifically tailored to account for material and instrument responses.

Recently, several investigators have begun to address the challenges of conducting mechanical tests on Nafion at elevated temperatures over a range of hydration from the vapor phase. These investigators have attempted to modify existing mechanical testing instrumentation to achieve control of humidity over a narrow temperature range. Some examples of this work include tensile instruments (Instron) which include either bubbler controlled feeds[1] or using a plastic Ziploc® bag with water or saturated salt solution in the bottom to create a humidified envelope around the test sample[4]. Another example is the work of Bauer *et al*. which involved modifying a DMA with a bubbler and heated block[2] to provide control over water activity during testing. Other investigators have created a humidified creep apparatus by flowing humidified gas through a tube containing the sample in order to study effects of hydration cycling[20].

2.1.3 Dynamic Mechanical Tests

As mentioned previously, dynamic mechanical analysis has been used to determine thermomechanical transitions in Nafion films in order to better understand the morphology of the material. DMA is employed primarily for characterizing viscoelastic materials. There are two methods by which DMA is performed; free oscillation and forced oscillation[21]. In free oscillation, an initial force is applied to the sample which induces natural oscillations. The amplitude and period are recorded as the oscillations decay due to viscous losses. The torsional pendulum is an example of this method. Forced oscillation involves applying an oscillating force with varying frequency while observing the resulting displacement in the sample. A shift in phase between applied force and resulting oscillations arises from viscous and elastic components of the material's response to stress. Forced oscillation DMA is the most common form of DMA presently used. Examples of this method include the vibrating reed and the tensile extension mode commonly found on modern DMA instruments. Forced oscillation is a sensitive technique that allows for quick scans through a range of applied frequencies. Free oscillation techniques were more popular during the initial DMA studies of Nafion. Since the free oscillation method results in oscillations at the systems natural frequency, it tends to be more sensitive than the forced oscillation method.

Eisenberg and coworkers were the first to report on the thermomechanical properties of Nafion using DMA (torsional pendulum and vibrating reed)[11, 16]. They investigated Nafion films with 1135 EW and its precursor under dry conditions. They also looked at the effect of ionic species on dynamic response. Torsional pendulum and vibrating reed were the two DMA methods which were used. Stress relaxation (dry and underwater) and differential scanning calorimetry (DSC) were also used to obtain information about the thermomechanical transitions occurring in Nafion and their relationship to morphology. They reported three separate tan δ peaks appearing at -120, 20 and 110°C which they referred to as the γ, β, and α transitions, respectively. The α transition was assigned to the relaxation of the ionic groups because of its sensitivity to water and ionic species. Changing the ionic species from H^+ to other alkali ions caused significant increase in the α transition. The β transition was assigned to the relaxation of the teflonic matrix. The authors pointed out that the small size of the phase separated regions caused their relaxations to be closely linked. The γ transition was assigned to short range motion in the teflonic phase. A similar transition is seen in PTFE. Other investigators[14, 15] also have performed DMA analysis on Nafion of different EW, reporting a relaxation around 100-120°C that they ascribe to relaxation of the ionic region.

More recently, Uan-Zo-Li[13] and Bauer *et al.*[2] performed DMA studies on Nafion in both the dry and hydrated states. They report that storage modulus decreases with increasing hydration at room temperature and as temperature increases. The sensitivity of modulus to changes in temperature increased as membranes became drier. For the fully dry case, the storage modulus crosses all of the other curves as temperature is increased from room temperature to 90°C.

The work of and Bauer *et al.*[2] involved modifying a commercially available DMA instrument to allow for good control of vapor phase water activity during mechanical testing. They report installing a custom built sleeve which surrounded the sample and controlled the humidity. Water activity was controlled by mixing two feeds; a dry feed and a hydrated feed which was established by having a bubbler maintained in a water bath, the temperature of which controlled the vapor pressure of the feed.

It should be noted that the approach of modifying a commercially available DMA instrument by installing a custom designed sleeve around the sample was taken by the author of this dissertation in 2004 and was reported during his General Examination. The work was abandoned due to unavailability of a working DMA instrument.

2.1.4 Tensile Creep

Tensile creep provides information about a material's response to a static load at stress and deformation levels which are encountered by materials in actual applications. To date, a limited number of studies have investigated the viscoelastic response of Nafion using the technique of tensile creep[4, 10, 22]. Recent work by Satterfield[4, 22] has been aimed at determining the affects of temperature and hydration on viscoelastic creep of Nafion and Nafion composites while Kyriakides[10] reports on only the affect of temperature.

The work of Kyriakides [10] used a Dynamic Mechanical Analyzer (TA Instruments 2980) to measure the tensile creep of Nafion N117 films in the acid form. Curves were taken over a temperature range of 10 to 130°C. No indication as to the water content of the Nafion during testing or the thermal history of samples was given. A preload force of 0.1N and a creep stress of 1.0MPa is specified for samples which measure 6.5mm by 26mm. Both creep compliance and creep recovery endured for two hours each. From the creep experiments, the author presents a master curve for Nafion which has large amounts of error (i.e., individual curves do not line up well and the resulting master curve is not smooth). The reason why the master curve is of poor quality is likely primarily that hydration levels were not constant during or between runs. If samples were placed in the instrument at ambient conditions and runs started as soon as the instrument reached temperature, partial drying of the sample during the runs would have occurred. Support for this conclusion is partially based on the following sentence taken from reference [10]:

> *Though creep tests on N117 ran from 10 to 130°C, thermal contraction at lower temperatures tended to overwhelm the small stress used in the test, causing the sample to slowly contract instead of expand.*

The "thermal contraction" the author speaks of is more likely shrinkage due to water loss. Whether the samples were undergoing thermal contraction or were shrinking as they dried, runs should not have been started until equilibration was reached. As a result, the author only presented data for 70°C and above. Using similar stresses and careful control of water content, the current work provides a continuous master curve from 23 – 140°C.

A more thorough investigation of the viscoelastic creep response of Nafion is presented the work of Satterfield, Majsztrik and coworkers[4]. In this early work, the author's used a creep setup designed by Satterfield to measure tensile creep of polymers under controlled environments of temperature and hydration. The investigation makes a comparison of Nafion and Nafion TiO_2 composite membranes, suggesting that the addition of TiO_2 nanoparticles to Nafion reduces creep at 23°C for both dry and fully hydrated states. Creep runs were done for Nafion from 23 – 70°C and over a range of hydration. The rate of creep compliance at long times (~100 minutes) is given as

$$\text{Creep Rate} = \frac{\mathrm{d}\left[\dfrac{\sigma}{\varepsilon}\right]}{\mathrm{d}\left[\log(\text{time})\right]}, \qquad \text{Equation 2-1}$$

where ε is strain and σ is stress. The reported trend is that creep rate at 23°C decreases with hydration and creep rate at $\lambda \sim 8$ increases with temperature. Additional tensile creep experiments are reported by Satterfield in [22].

2.1.5 Elastic Response

Stress-strain tests performed on Nafion have been used to obtain values for elastic modulus and other mechanical property data. Investigators have been concerned with the affects of temperature and, to a lesser degree, hydration during these studies. An excellent review of studies in the literature on the stress-strain response of Nafion is presented by M. B. Satterfield[22]. A summary of the values reported in the literature as recently as 2006 prepared by Satterfield is shown in Table 2-2. In general, values are reported over a range of temperature, but only a narrow range of hydration. A comparison of some of the values listed in Table 2-2 for elastic modulus of Nafion ca. 25°C is shown in Figure 2-1. Data obtained by the author are included for comparison. A spread in values exists for the selected points. Good agreement exists between the values reported by the author and DuPont (points *a* and *b*). The spread in values is probably due to a combination of thermal history effects and poor control of hydration.

More recent work expands the range of temperature and hydration over which stress-strain of Nafion was measured. Tang *et al.* reported the stress strain response of Nafion N112 from 25-85°C over a range of humidity of 30-90%. To do this, the authors modified a commercially available tensile elongation instrument to include a humidity chamber and vapor feed system[1]. They report that Young's modulus decreases with both temperature and hydration over the range they investigated. Also reported were the proportional limit and break stress as well as break strain.

Choi, Jalani, and coworkers report the elastic modulus of Nafion from 20- 90°C over the full range of water activity using optoelectronic holography[23-25]. From these data, they proposed the following expression to describe the elastic modulus E of Nafion as a function of membrane hydration:

$$E = E_0 \exp(-2.1753\varepsilon_i), \quad \text{Equation 2-2}$$

where E_o is the elastic modulus of dry Nafion at a given temperature and ε_i is the volume fraction of water sorbed by the polymer. As will be shown later in this chapter, this expression does not accurately describe the effect of hydration and temperature on dry Nafion. At 40°C and above, it will be show that elastic modulus does not simply decrease with hydration from the dry state. The expression does a reasonable job of describing the elastic modulus if only the hydrated states are considered and if E_o is replaced with elastic modulus at water activity $a_w \sim 0.05$.

A comparison of elastic moduli values reported for hydrated Nafion in the literature is made in Figure 2-2. Values reported by Tang *et al.*[1] and Choi *et al.*[23] are compared to values presented by the author in this chapter. Excellent agreement exists between the values obtained by the author at 90°C and those of Tang et al. at 85°C over the range of hydration shown. However, the data presented by Choi *et al.* fails to follow part of the trend established by the data reported by the author.

Satterfield, Majsztrik, and coworkers have recently reported on the effects of temperature and hydration on the elastic modulus of Nafion[4, 22]. In this work, Satterfield developed a clever technique to control the activity of water vapor surrounding a sample during testing in a standard Instron 1122 equipped with an environmental chamber (thermal control only). The technique involved enclosing the test sample with a plastic Ziploc® bag into which was added either water or a saturated salt solution. Care was taken to ensure that the sample remained out of contact with the liquid and was equilibrated with the vapor. To run a stress-strain test, samples were loaded in the jaws of the machine while still in the plastic bag. The difference in dry and wet weight for each sample was obtained to estimate hydration level during the tensile test. Results are reported over a range of temperature (23 – 90°C) and hydration (100% and 33%RH as well as ambient humidity ratio, ω). Room temperature runs were done over a more complete range of water activity. The main findings presented by Satterfield were that 1) elastic modulus decreases with increasing hydration and increasing temperature 2) as hydration increased, temperature had less of an affect on elastic modulus, 3) beyond the yield point, mechanical properties are not affected by changes in hydration.

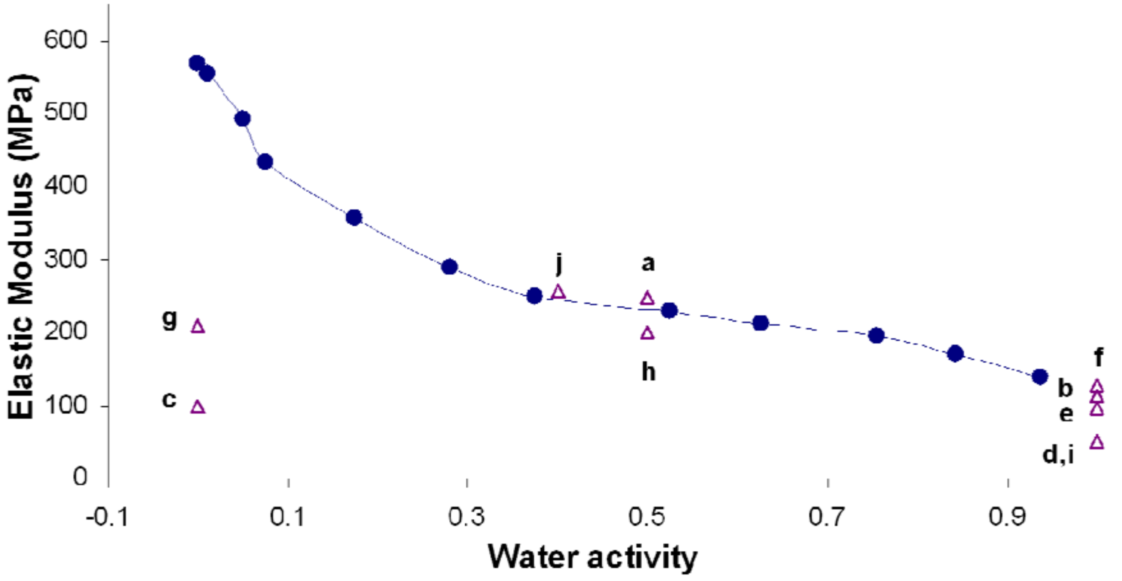

Figure 2-1 Comparison of elastic moduli reported in the literature for Nafion at ~25°C. Values were obtained from references [7, 9, 10, 26-28]. Labels correspond to those given in Table 2-2. Blue dots are for data obtained by the author.

Table 2-2: Summary of values for the elastic modulus of Nafion reported in the literature. Table prepared by and used with the kind permission of M. B. Satterfield[22].

Researcher, Year	**Material**	**Method**	**Water Content**	**Temp**	**Elastic Modulus [MPa]**	**Label**
DuPont Product Info. [6]	Nafion PFSA Membranes, N-112, NE-1135, N-115, N-117, NE-1110	ASTM D 882	50% RH	23°C	249	a
			water soaked	23°C	114	b
				100°C	64	
Werner, Jorissen et al. 1996 [9]	Nafion 117, 50 mm length	Strain rate: 20%/min in machine direction	Dry	25°C	~100	c
			"completely humidified"	25°C	~50	d
			Unspecified	200°C	~1	
Kawano, Wang et al. 2002 [29]	Nafion 117, Aldrich, acid form, 25 mm length x 6mm	Preload force: 0.005N, soak time: 1 min, force ramp rate: 0.500 N/min, upper force: 18.00N	water soaked, 24h	27°C	95	e
			boiling water soaked, 1h	27°C	128	f
			as-received	27°C	200	
				60°C	147	
				90°C	44	
				120°C	5	
				150°C	3	
				180°C	2	
			dry: vacuum oven 70°C, 24h	27°C	210	g
				60°C	176	
				90°C	80	
				120°C	13	
				150°C	4	
				180°C	2	
Kundu, Simon et al. 2005 [30]	Solution Cast Nafion 117, 5mm gauge length x 6mm	Preload force: 0.1N, strain rate: 0.1%/min, max strain: 1.5-2.4%.	water soaked	80°C	~45	
	Solution Cast Nafion 112				~35	
Fujimoto, Hickner et al. 2005 [27]	Nafion 117, 30mm gauge x 9mm	Strain rate: 17%/min	Ambient	RT	200	h
			soaked in water until tested	RT	52	i
Kyriakides 2005 [10]; Liu, Kyriakides et al. 2006 [28]	Nafion 117; pretreated boiling 0.5 M H_2SO_4 2h & boiling DI water 2h, dried 70 °C vacuum, 40 mm gauge length x 12mm	Strain rate: 0.7/min	equilibrated at 23°C, 40%RH 72h, water concentration: 5.3+/-1.5%	23°C	270 ± 4	
		Strain rate: 0.3/min			253 ± 7	
		Strain rate: 0.12/min			256 ± 18	j
		Strain rate: 0.07/min			263 ± 10	
		Strain rate: 0.025/min			250 ± 5	

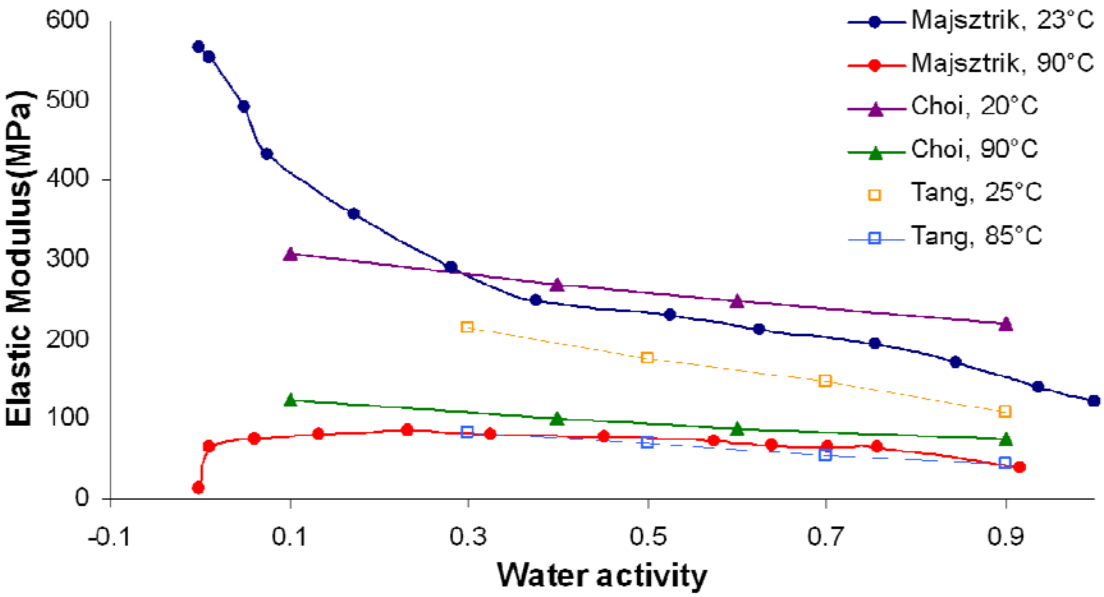

Figure 2-2 Comparison of elastic moduli reported in the literature for Nafion at ~25°C and ~90°C (actual reported temperatures are indicated). Data was obtained from the following sources: Majsztrik = this dissertation, Choi = reference 23, and Tang = reference 1.

2.1.6 Stress Relaxation

Stress relaxation is an experimental technique which measures the viscoelastic response of a material. The technique involves instantly applying a constant tensile strain to a material and recording the stress on the material as a function of time. Due to the delayed elastic and viscous flow components, the stress decays over time. Stress relaxation and tensile creep are related. An expression describing the tensile creep response of a material can be converted into an expression describing its stress relaxation response, and *vice versa*. This is done by obtaining a 4th order tensorial creep constitutive equation $F_{ijkl}(t)$ which is related to the stress relaxation constitutive equation $R_{ijkl}(t)$ by the following expression:

$$[\overline{F}_{ijkl}(s)] = [\overline{R}_{ijkl}(s)]^{-1}, \qquad \text{Equation 2-3}$$

where s is the Laplace transformation variable[31]. The interested reader is directed to reference [31] for a detailed discussion and mathematical derivation.

Several investigators have used stress relaxation to measure the viscoelastic response of Nafion[10, 11, 16, 22, 32]. The effects of hydration were considered in some of the studies by comparing “dry” runs to runs under ambient humidity ratio or under liquid water. The general findings from stress relaxation studies of Nafion are that 1) there are a large distribution of relaxation times giving rise to a broad master curve for dry Nafion[16], 2) hydration increases the stress relaxation rate[16], and 3) the ionic interactions which normally cross-link dry Nafion are reduced with the introduction of water[11] which plasticizes Nafion. Uan-Zo-Li[33] proposed that the glass transition temperature of Nafion increases with hydration based on stress relaxation results.

2.2 Tensile Creep Instrument

Commercially available instrumentation is readily available to assess mechanical properties of materials over a wide range of temperature. However, these instruments offer only limited control of water activity[iii] over a range of temperature and this is usually a secondary feature. Thus, to obtain the desired mechanical property data, the creep instrument described here was designed specifically to test the creep response of Nafion under a controlled environment of temperature and water activity[34, 35].

Referring to Figures 3-5, the test sample is clamped to an upper stationary clamp and a lower moveable clamp. Stress is applied uniaxially to the sample through the bottom clamp by hanging a weight from the bottom of the rod connected to the bottom clamp. The weight hung from the rod is an open container which can be filled with lead shot to give a mass range of 200 – 1,300g. Lower mass values are obtained by

---

[iii] Activity is a measure of the concentration of a component in the liquid or vapor phase relative to the saturated concentration of the pure substance at that temperature. In the vapor phase, activity is defined as the ratio of vapor pressure of the component in the mixture to the vapor pressure of the pure substance at that temperature. Relative humidity, which refers specifically to water vapor, is defined as a_w x 100.

substituting the large open container with smaller brass disks having centered holes through which the rod passes. Strain is measured with a Linear Variable Displacement Transducer (LVDT) (Macro Sensors, HSAR 750-2000) by monitoring the position of a segment of the rod (the LVDT core) connecting the hanging mass to the sample with the moveable clamp. The LVDT provides a measurement of strain without contact. PTFE guides are in place to axially align the rod and prevent it from swinging while introducing only a small amount of friction. A universal joint at the bottom of the rod connects to the mass without transmitting torque due to misalignment. The lower clamp has a total travel of 8.25cm between the upper clamp and base of the environmental chamber. This translates into a maximum strain of 2.25 for a typical 2.54cm long initial sample length.

Components of the creep instrument are aligned and held vertically by mounting on an aluminum plate held vertically on a frame with leveling feet. A sliding stage, mounted on a guide rail parallel to the axial direction of creep, is used to apply and remove the mass from the sample. A pneumatic linear motion piston is in place to provide automation of this action. In order to reduce the collective mass (~90g) of the lower sample clamp, LVDT core, and connecting rod which is carried by the sample to the desired mass (~10g), an adjustable counterweight is used. This is achieved by attaching a balanced (zero torque) cantilevered bar to the sample rod and applying a force opposite in direction to gravity to it by means of the pulley and rope system shown in Figure 2-4.

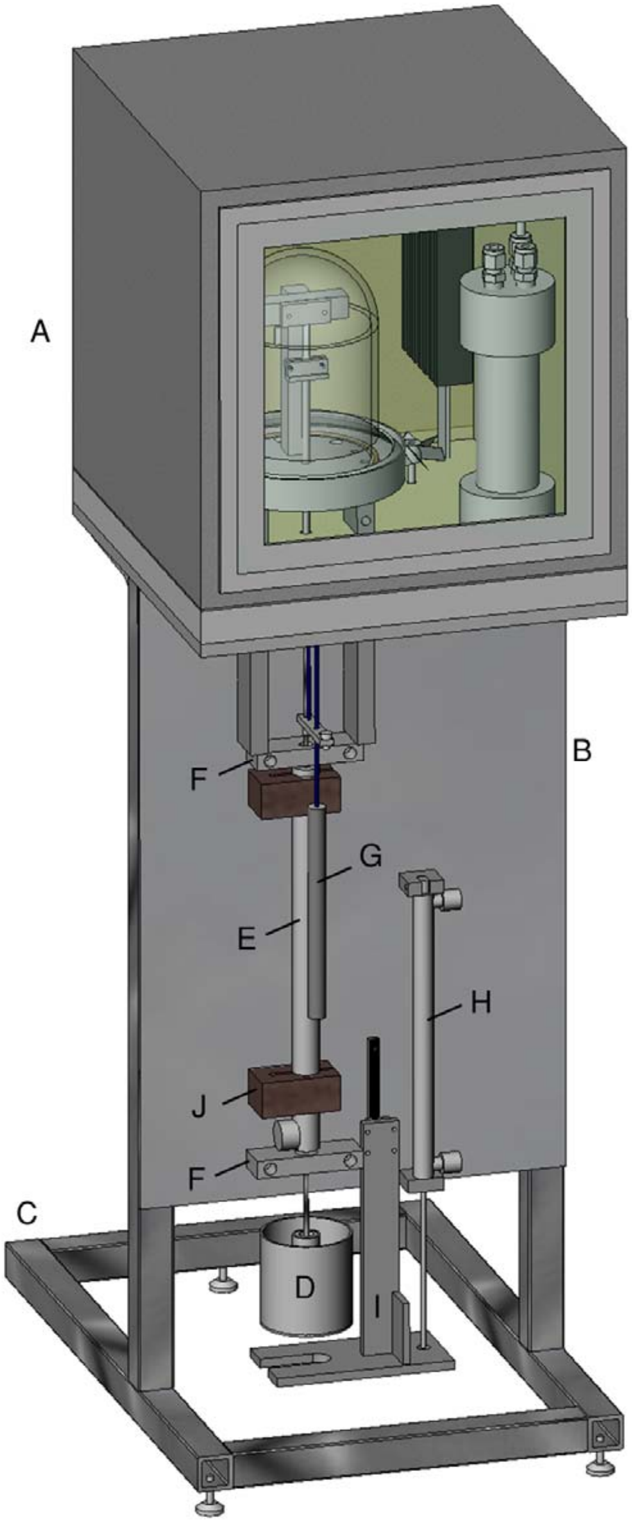

Figure 2-3 Schematic of creep instrument with environmental control; (A) environmental chamber, (B) vertical mounting plate, (C) frame, (D) variable weight, (E) LVDT, (F) rod guide blocks with PTFE bushing, (G) counterweight, (H) linear pneumatic actuator, (I) stage for applying and removing weight from sample, and (J) phenolic LVDT mounts. Photographs of the working prototype used for the experiments described in this chapter can be found in the online archive associated with reference [35].

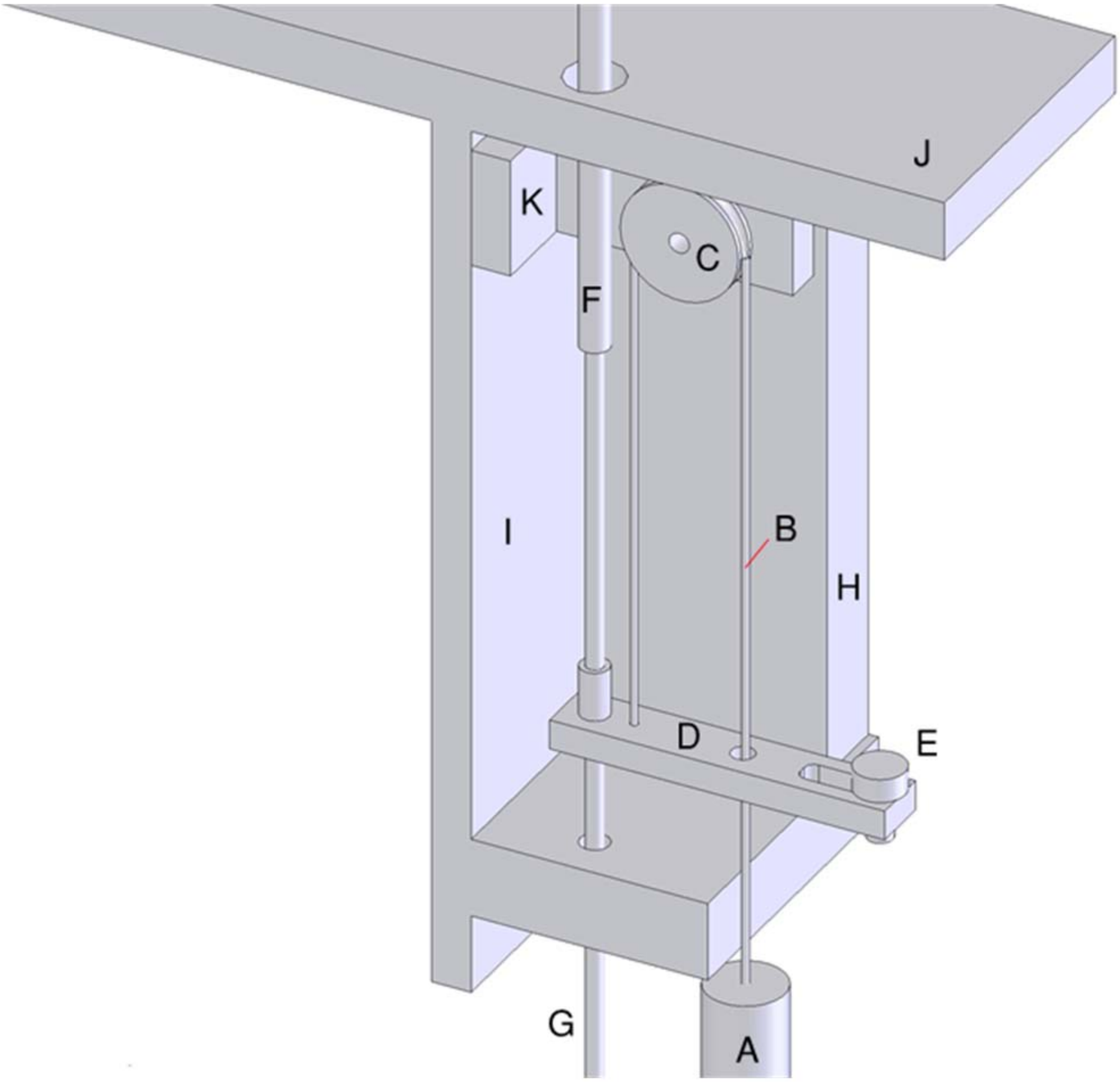

Figure 2-4 Schematic showing a section view of the counterbalance system used to reduce the minimum tensile force applied to the sample due to the weight of the clamp, LVDT core, and rod. Visible are the (A) adjustable counterbalance mass , (B) nylon rope, (C) nylon pulley, (D) torque zeroing bar, (E) adjustable mass (bolt), (F) 3/16" 304 SS rod (to sample clamp), (G) 4-40 threaded SS rod (to LVDT core), (H) SS humidity chamber support bar, (I) fixed aluminum mounting plate, (J) environmental chamber fixed base, and (K) pulley mounting bracket.

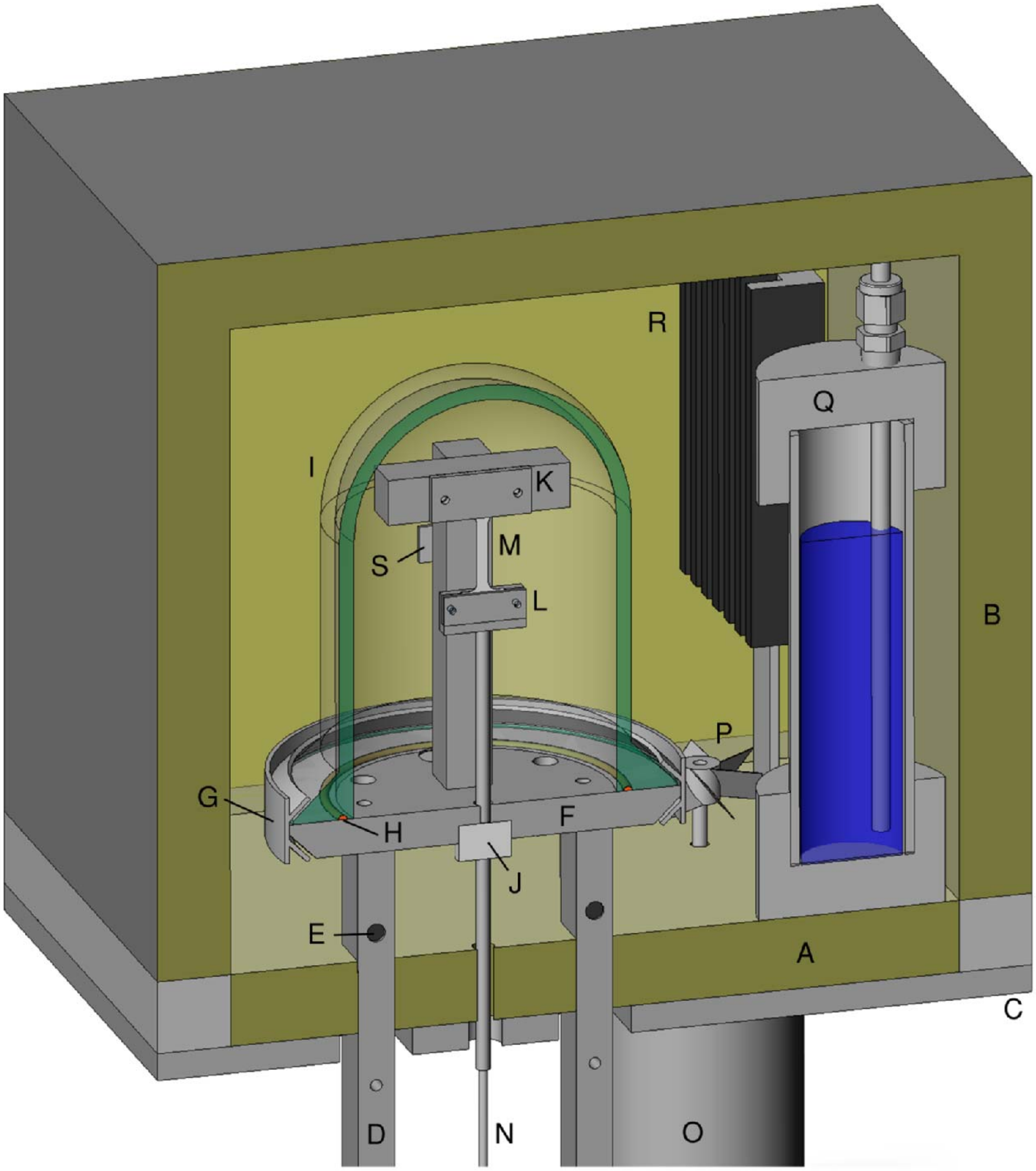

Figure 2-5: Cross-section of the environmental chamber: (A) bottom insulation, (B) removable insulated top, (C) fixed aluminum mounting plate, (D) SS humidity chamber support bars, (E) cartridge heater, (F) SS humidity chamber base, (G) SS Duran clamp, (H) silicone O-ring, (I) glass reaction vessel, (J) PTFE guide bushing, (K) fixed upper clamp, (L) moveable lower clamp, (M) polymer sample, (N) 4-40 threaded SS rod (to LVDT core), (O) high temperature fan motor (P) fan blade, (Q) SS bubbler, (R) finned heater, and (S) dual temperature and relative humidity sensor.

An environmental chamber (Figure 2-5) surrounding the sample consists of an insulated outer shell and a humidified inner chamber. The insulated outer shell consists of a stationary base of 3/8” aluminum plate and a removable upper box with a double paned glass window on one face and aluminum sheet on the remaining four faces. Both the base and upper box are insulated with 1” fiberglass insulation board. The base serves as a fixed mount for sensors and other components needed to maintain an isothermal and isohumid environment. A finned heater and fan together with a PID temperature controller create an isothermal environment around the humidity chamber. A temperature range of 25 – 250°C is possible[iv].

The humidity chamber is made entirely of stainless steel, glass, and PTFE in order to resist corrosion and deterioration from water and other solvents (such as alcohols), even at elevated temperature. These materials were also selected to operate up to 250°C. The humidity sensor, which has a temperature range of -40 – 124°C, is replaced by a ¼” diameter stainless steel sheathed thermocouple when this range is exceeded. A stainless steel compression fitting with NPT adapter mechanically supports the thermocouple and forms a leak-free seal.

The base of the humidity chamber is made from a circular 304 stainless steel plate with a tapered edge machined to mate with a Duran clamp and a 500mL Pyrex reaction vessel (Chemglass) which encloses the sample. The rod connected to the moveable sample clamp passes through the base with a PTFE bushing in place providing a low friction guide and minimal vapor transport. Alternatively, one could use a stainless steel linear guide bearing or magnetic bearings to further reduce friction. The rod passes

---

[iv] Temperatures lower than ambient can be achieved by replacing the heater element with a liquid to air heat exchanger. Flowing a cooled liquid from a chiller or using liquid nitrogen will allow access to stable low temperatures. However, controlling relative humidity at low temperatures becomes difficult.

through a stainless steel tube spanning the gap between humidity chamber base and the fixed base of the oven to provide a quiescent environment, shielding the rod from convection. Also attached to the base is the cantilevered fixed upper clamp. Pipe to tubing adaptors for gas inlet and outlet as well as a male 3/8" NPT plug style feed-thru for a dual humidity and temperature sensor (Sensirion, SHT75) are also included in the base. The silicone O-ring between the reaction vessel and the base forms a good seal when clamped and can withstand temperatures up to 250°C. The base is supported by two 304 stainless steel bars bolted to the face of the mounting plate. Composite (G-11) spacers insulate the base of the humidity chamber from the support bars. ¼" diameter cartridge heaters placed in holes in the bars are used to heat the bars to the temperature of the chamber to avoid condensation if very high (> 90%RH) relative humidity is required.

Humidity is established in the chamber either by introducing open vials of various salt solutions to the chamber or by flowing humidified N_2 gas from a bubbler. Dry N_2 gas is purged through the chamber when a water-free environment is desired. Vapors other than water, such as alcohols and other volatile organic compounds, can also be introduced to the chamber by either bubbler or liquid-vapor equilibrium. A schematic showing humidity control with a bubbler is shown in Figure 2-6. The bubbler is housed within the insulated box and heated by convection. This ensures humidified gas at the same temperature as the humidity chamber and forestalls condensation in lines leading to the chamber. For runs above the solvent's boiling point, the bubbler must be removed from the chamber (to prevent boiling) and heated separately.

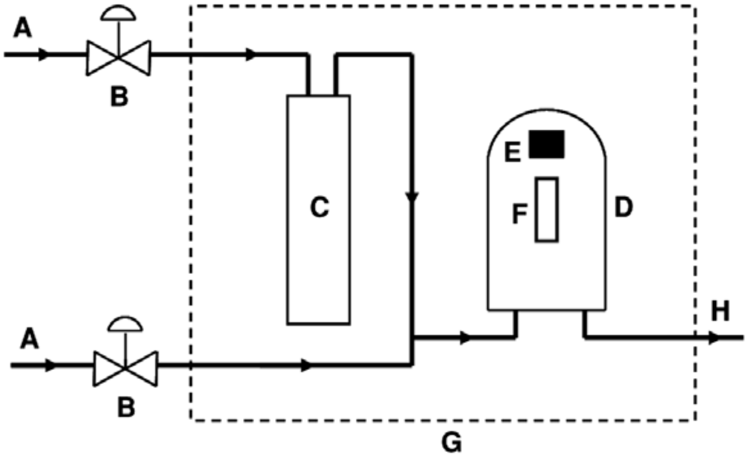

Figure 2-6 Schematic of components used to control the water activity in the test chamber surrounding the test sample. The main components are (A) dry N_2 source, (B) mass flow controller, (C) humidifier (bubbler), (D) humidity chamber, (E) dual temperature and relative humidity sensor, (F) test sample, (G) isothermal oven enclosure (dashed line), and (H) gas outlet.

Using the bubbler system for humidification has several advantages over saturated salt solutions. Firstly, saturated salt solutions provide only a small number of water activity values over the range of 6- 97% RH whereas the bubbler can give a continuous range of humidity from 0 – 100% RH. Secondly, vapor pressure above salt solutions is temperature dependant, so different relative humidities will result for a given salt as temperature changes. Finally, the time required for vapor pressure above the salt solutions to reach equilibrium in the chamber is lengthy (hours) while the bubbler system can very quickly (tens of seconds) reach steady-state once at temperature.

A Labview program is used to record the length of the sample along with the relative humidity and temperature of the humidity chamber in real time. Data is acquired every second for the first 20 minutes of a creep experiment, and then once every minute thereafter. During creep recovery, data capture rate is again increased to 1 Hz for the first 20 minutes. An LVDT indicator equipped with an RS-232 connection (Macro Sensors, DMI-A1-101) provides a conditioned excitation voltage for the LVDT, converts the resulting voltage into a position measurement, and interfaces with a computer for data acquisition. The LVDT together with controller give a position reading over a range of 4” to within ±0.0003” (±8μm).

2.3 Testing Procedures

Test procedures developed for investigating the creep response of Nafion under a range of conditions are outlined. Control of temperature as well as water and other solvent activity during testing is included. Test procedures are also outlined in ref. [35].

2.3.1 Materials

Nafion was purchased from Ion Power as an extruded film and as a solution. Most tests were performed on extruded Nafion N1110 film, which has an equivalent weight of 1,100(g/mol-SO_3) and a nominal dry thickness of 0.0010”. The 1,000 g/mol equivalent weight films were made by solvent recasting a 15 wt% solution of 1,000EW Nafion solution mixed with 2-propanol in a 3:4 ratio. Solvents were removed in an oven at 60-70°C and the resulting film was annealed at 165°C for 1 hr. The dry thickness of the recast films was 0.010”. A more detailed explanation of recasting procedures for plain Nafion and Nafion TiO_2 composites is given in chapter 4.

Both recast and as received extruded Nafion films were treated following the standard cleaning procedure: boil 1 hr in 3% H_2O_2 solution, boil 1hr in deionized (DI) water, boil 1hr in 0.5 M sulfuric acid, boil 1hr in DI water twice. To obtain the Na form of the film, extruded Nafion was prepared according the above procedure, but with the acid washing step replaced by washing in a concentrated NaCl solution. The resulting clean and fully hydrated polymer was then dried flat on the lab bench by placing between several sheets of filter paper with a book placed upon all to ensure a wrinkle-free material. Once dried to ambient conditions, the polymer was cut into strips of uniform width[v] using a template of the correct width (0.25 or 0.5”) and an Exacto® knife.

2.3.2 Sample mounting

Nafion samples, cleaned, dried flat, and cut to the desired width, were mounted in the clamps of the creep instrument at ambient conditions. To assist in ensuring that samples were centered in the clamps and mounted axially, a mounting jig was used. The jig consisted of two rectangular pieces of ¼” acrylic which were exactly 1.000” high, corresponding to the standard gauge length of the sample at the start of creep testing. Two pins aligned the rectangles face to face. Lines were scored on the inside of one of the acrylic pieces to index the alignment of 0.250 or 0.500” wide samples in the jig. The samples were placed between the two pieces of the jig and squeezed in place during mounting.

2.3.3 Tensile creep

Tensile creep was performed on dry and hydrated Nafion from 25 – 150°C. Nafion N1110 in the protonated form was used for these tests and comparison runs for N1110 in the sodium form as well as recast 1000 EW Nafion were made. Humidification was provided either by introducing vials of saturated salt solutions to the humidity chamber or by using the humidified feed described in section 4.3. Air dried polymer samples, prepared according to the procedure given above, were clamped in the jaws of the creep instrument and dried *in situ* at 85°C for at least 2 hours for all runs. During drying, dry N_2 was continuously flushed through the chamber. A flow rate of ~ 250mL/min was found to be sufficient to maintain the sample at the activity of dry N_2

---

[v] The typical dog-bone shape was not necessary since samples did not undergo necking during creep and slipping within the clamps was not a problem.

during creep tests. After drying at 85°C, the temperature of the environmental chamber was changed to the desired test temperature. Once at or below the test temperature, water vapor was introduced unless a water activity of 0.00 was desired. For the dry runs, N_2 was continuously bled into the chamber during the test.

The procedural points of drying at 85°C and then introducing water vapor only after cooling to the test temperature were developed to ensure that history effects were consistent between runs. This is important since drying temperature and the temperature at which water vapor is introduced can affect microstructure and/or hydration levels which give rise to differences in mechanical properties for Nafion. The results of runs designed specifically to test for the effects of thermal history on viscoelastic response illustrate this.

Sample length during the drying procedure is plotted in Figure 2-7 as a function of time. The initial decrease in sample length is attributed to the shrinking of Nafion as it dries. The increase in length following the initial shrinking is thought to be due to compressive creep caused by pressure exerted by the clamping action of the jaws which hold the sample. As Nafion is heated and dried, its resistance to creep decreases. This results in the sample flowing under the pressure of the clamps, causing a slight increase in gauge length. Inspection of samples after drying has indicated that samples are thinned and widened where clamping occurs. Drying cycles performed after the initial drying step resulted only in a decrease in sample length. A small fraction of sample elongation during the initial drying is attributed to tensile creep induced by the small stress used to pull the sample taut.

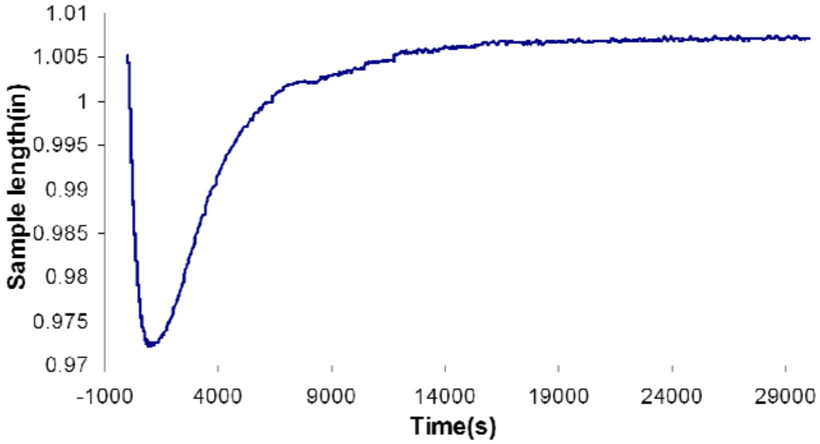

Figure 2-7 Length of Nafion N1110 sample during drying procedure. Initial length is at ambient temperature and water activity. Sample length first decreases, then increases. Decrease is due to water removal. The increase in sample length is due to polymer flow resulting from compressive pressure of clamping.

After the sample reached an equilibrium length while being held at the desired temperature and water activity, force was applied to the sample. In calculating the stress applied to the sample, 10.0g were added to the mass of the test weight being used to account for the constant force of the rod and core assembly along with the influence of the counterbalance. The runs were initiated by quickly and smoothly[vi] lowering the mass onto the rod connected to the bottom clamp. Sample length was monitored and recorded as a function of time along with the temperature and humidity of the chamber. Creep recovery was initiated at the desired time by removing the stress from the sample. Sample length was monitored and recorded during creep recovery. Typically, creep

---

[vi] Application of the weight at the start of a creep run must be done slowly enough to avoid a spike in stress (beyond the desired static stress) caused by impact of the weight with the rod. It also must be done with sufficient speed to be completed in less than 2 seconds so that 1) instantaneous elastic response can be separated from the delayed elastic and viscous components and 2) creep strain is occurring under the full static stress equal to the force applied by the entire mass divided by the cross sectional area of the sample. The initial strain rate of the sample under the applied stress dictates the slowest acceptable speed for lowering of the weight. A reasonably wide range of lowering speeds gave repeatable results. Only when initial creep rate was very large (> 20% per second) did repeatability become an issue, a point beyond the region of linear response of most materials. We found that lowering the mass by hand provided the most flexibility.

recovery was allowed to occur until strain recovery rate was less than 3% of the total strain per hour. This normally occurred within 3 times the active creep time.

A series of creep runs lasting for exactly 1 hr, followed by creep recovery, was done to compare the components of viscous loss and delayed elastic strain at different temperatures and water activities. These runs were done at 25, 50, 80, and 90°C over a range of 6 water activities; 0.00, 0.01, 0.08, 0.35, 0.65, and ~0.95. A bubbler was used to provide humidification for all but the highest water activity level. Open vials of water were placed in the chamber to achieve these high levels of humidification. Water activity of 1 was not achieved because of condensation occurring at certain areas of the chamber due to temperature gradients[vii]. It was observed that condensation did not occur on the sample surface.

2.3.4 Instantaneous Elastic Response

The instantaneous elastic response of Nafion N1110 was also measured as a function of water activity and temperature using the creep instrument. Clean protonated Nafion N1110 films were air dried, cut to a width of 0.25", mounted in the clamps of the creep instrument, and dried *in situ* at 85°C for over 2 hrs. Measurements were made over a wide range of water activity, from 0 - 0.95, at the following temperatures; 23, 40, 50, 60, 70, 80, and 90°C. At a given temperature, measurements were started with the film completely dry and water activity was increased by increments of ~0.1 using a humidified feed from the bubbler mixed with a dry N_2 feed. For dry Nafion, measurements down to -5°C were made by cooling the environmental chamber with dry ice.

[vii] At 80°C, a temperature gradient of 1°C will limit maximum water activity to 0.96 due to condensation at dew point.

With the film in equilibrium with the surrounding vapor, instantaneous elastic response was measured. This was done by lowering a weight to apply a constant stress to the film and removing the weight after 30 seconds. In this manner, stress was cycled on and off at 30 second intervals for four cycles for every temperature and activity setting. Stress was adjusted to give an instantaneous elastic response between 1 and 2% strain. Strain was recorded over time at a frequency of 1 Hz.

2.3.5 Thermal History Effects

The effects of thermal history on the viscoelastic response of Nafion were briefly investigated. Creep runs were carried out with the procedure listed above except that of the drying step. To make a comparison of the drying temperature on viscoelastic response, the drying temperature was increased from 85°C to 150°C. Drying at 150°C was done *in situ* for 2 hours (including ramping time). After drying at 150°C under a purge of dry N_2, the chamber was cooled to the desired test temperature at which point water vapor was introduced (if desired). The remainder of the procedure was identical to that given previously.

2.3.6 Solvent Effects

The effects of different solvents on the creep response of Nafion was measured at 23°C. The effects of five solvents were investigated; acetonitrile, ethanol, isopropanol, methanol, and water. Clean Nafion films were air dried, cut to a width of 0.25”, and clamped in the jaws of the creep instrument. Dry N_2 was flowed into the environmental chamber at room temperature for 30 minutes to partially dry the samples before introducing the solvents[viii]. Six open vials (15mL) of a given solvent were placed in the environmental chamber and at least 12 hrs was allowed to elapse for solvent activity to approach a value of unity in the Nafions. Swelling strain due to solvent uptake was monitored and recorded. Nafion N1110 films were compared to Na form N1110 as well as protonated 1,000 EW recast Nafion 0.010" thick.

Tensile creep was initiated by applying a 150g weight to give a total constant engineering stress of 0.975 MPa. The samples were held under constant stress for exactly 1 hour, after which the stress was removed and the samples underwent creep recovery for at least 3 hrs. Active creep time was kept constant between samples to allow for a comparison of creep components.

2.4 Viscoelastic Response

This section gives an introduction to the fundamentals of viscoelastic materials.

2.4.1 Tensile Creep Response

Tensile creep is an excellent technique when used to measure the viscoelastic response of a material and is achieved by simply applying a constant[ix] stress σ *to* the material. The applied stress results in strain ε which increases with time. Stress and strain are defined as follows:

$$\sigma \equiv \frac{F}{A}, \qquad \text{Equation 2-4}$$

$$\varepsilon \equiv \frac{\Delta\ell}{\ell_0}, \qquad \text{Equation 2-5}$$

[viii] It was assumed that the effect of the presence of small amounts of water in the presence of high concentrations of other solvents on creep response was negligible. This assumption is based on unreported experiments done by the author in which the creep response of Nafion in the presence of pure ethanol and ethanol water mixtures was measured at 50°C. The work of Elliott and coworkers[36] suggests that water and ethanol interact synergistically, but only when a significant volume fraction of both solvent is present.

[ix] Due to changes in the cross sectional area of the test sample resulting from strain, true stress actually changes with time. Engineering stress, the stress calculated using the cross sectional area of the unstrained material, is constant.

where F is the applied force, A is the cross sectional area normal to the applied force, ℓ_0 is the initial length, and $\Delta\ell$ is the change in length (Figure 2-8b). Representative creep strain response for Nafion N1110 is shown in Figure 2-8. Contributions from the different creep response components — instantaneous elastic ε_e, delayed elastic ε_d, and viscous flow ε_v — are indicated. Table 2-3 provides a summary of the three components of creep response along with their characteristics and underlying molecular contributions.

As can be seen in Figure 2-8a, application of stress in a step-wise fashion produces an immediate strain ε_e, which is purely elastic and completely recoverable. Following this, strain increases with time due to the combined components of delayed elastic strain and viscous flow. The contribution from the different components can be separated by allowing the sample to undergo recovery under a state of zero stress, as shown.

The simplest spring and dashpot model able to produce a three component response is shown in Figure 2-8c. This model is made by combining a parallel and series arrangement of a spring and dashpot referred to as the Kelvin (Voigt) and Maxwell models, respectively. Here, η represents non-recoverable viscous flow, E represents instantaneous elastic response, while delayed elastic response is represented by the parallel spring and dashpot combination, E' and η'. Nafion's response to stress is non-linear, however, and is only fit semi-qualitatively by the four component model.

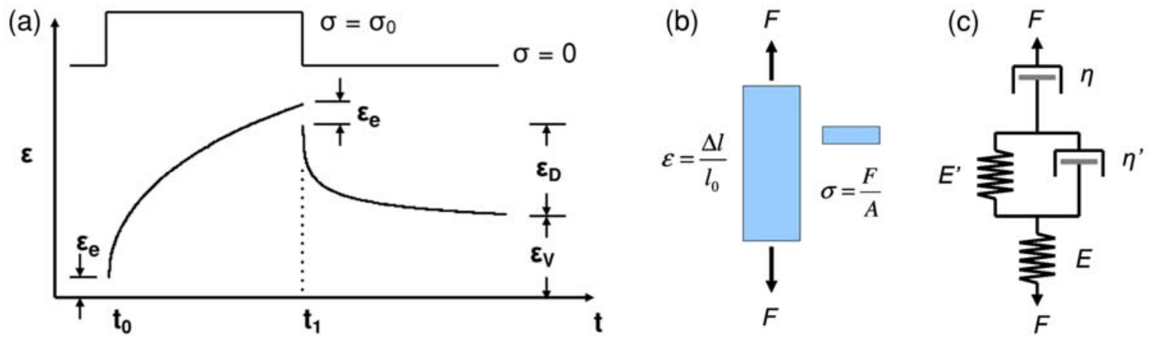

Figure 2-8 (a) Representative tensile creep response of the ionomer Nafion (N1110) at 80°C and 67%RH subjected to a stress of 2.31 MPa. Creep strain components are labeled according to Table I. The loading program is shown at the top of the plot. Sample dimensions are shown at (b) and a spring and dashpot model at (c) is used as a model of the viscoelastic response of the material.

Table 2-3 Ideal creep response components[31].

Component	Characteristic	Molecular Contribution
Instantaneous elastic (ε_e)	Occurs immediately, completely recoverable	Bond stretching/bending, bonds between chains
Delayed elastic (ε_d)	Rate decreases with time, completely recoverable	Chain uncoiling
Viscous flow (ε_v)	Irrecoverable	Chain slipping

The theory of *time-temperature superposition* allows one to predict the response of a material at a given temperature over long periods of time by combining short duration curves over a range of temperature. This principle can also be applied to changes in frequency (for DMA studies) as well as changes in humidity, strain, etc. for some materials[21, 37]. It is based on the fact that the time constant for molecular movement decreases with temperature. By plotting separate tensile creep curves (or stress relaxation or other time-dependant curves) vs. log time, a single master curve is obtained, reduced to a given reference temperature. This is done by separately shifting curves at different temperatures in time by a shift factor a_T, bringing them into alignment with the curve at the reference temperature T_o. The shift factor is less than one for temperatures above the reference temperature because less time is required for a material to reach a given state as temperature increases due to increased molecular motion. The shift factor is defined as

$$a_T = \frac{t_T}{t_{To}}, \qquad \text{Equation 2-6}$$

where t_T is the time required for a given response to be reached at the measured temperature T and t_{To} is the time for the same response to be reached when reduced to the reference temperature T_o[17]. Shift factors determined by tensile creep are applicable to responses obtained from stress relaxation and DMA for a given material[17].

2.4.2 Instantaneous Elastic Response

Before discussing the actual effects of temperature and hydration on the instantaneous elastic response of Nafion, some detail about the method used to measure elastic response and how this relates to elastic modulus obtained from a typical tensile test will be given. Figure 2-9 shows the strain response of Nafion obtained at 50°C and 59%RH, a representative response to cyclical loading obtained from these experiments. Looking at the strain response, one notices an instantaneous jump in length within about a second of applying and removing stress. Between cycles, this jump is repeatable and represents the instantaneous elastic strain. From this strain, an instantaneous elastic modulus can be calculated. The value for the elastic modulus obtained using this method approaches Young's Modulus when determined by tensile test with a fast strain rate. Tensile tests on viscoelastic materials combine the instantaneous elastic response along with viscous and delayed elastic strain. As the strain rate of a tensile test in increased, less contribution from the components of viscous and delayed elastic strain is seen. This is because the viscous and delayed elastic components are time dependant whereas instantaneous elastic strain is, ideally, completely independent of time. In some cases, good agreement exists between values for elastic modulus previously reported in the literature and what the author obtained under similar conditions (Figures 2-1 and 2-2). In cases where large differences exist between data points, poor control of hydration and history effects are likely explanations.

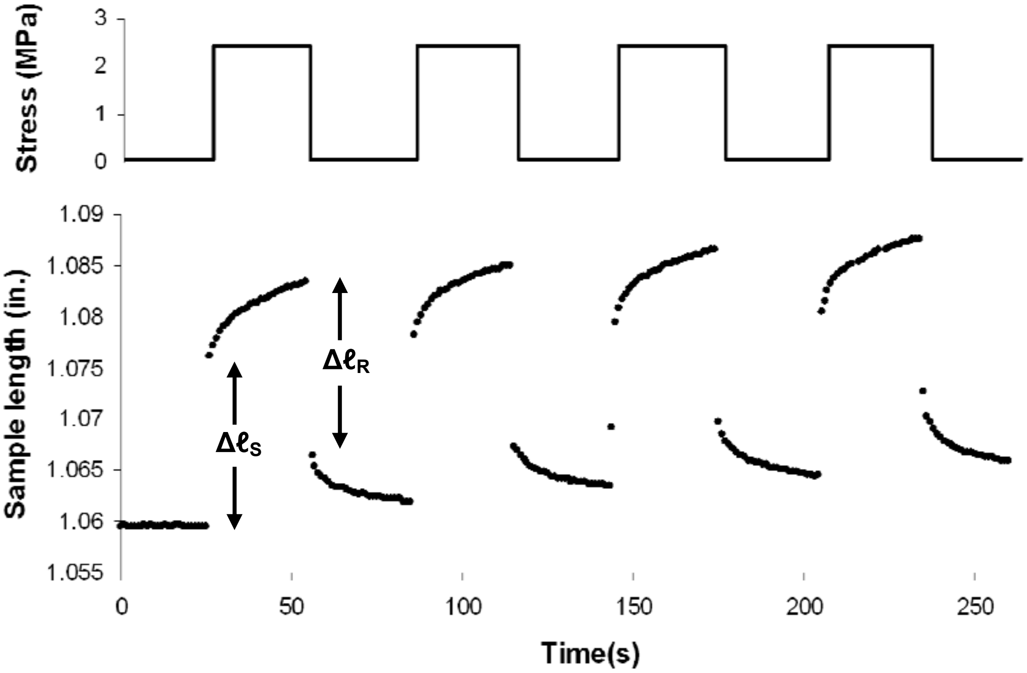

Figure 2-9 Response of sample length (bottom) to cyclical stress indicated at top. Data shown is for N1110 at 59%RH and 50°C. Instantaneous length change at the application and removal of stress, $\Delta\ell_S$ and $\Delta\ell_R$, respectively, are shown for the first cycle. Notice that each curve is higher than the previous, a result of viscous loss and incomplete recovery of delayed elastic strain. Data points are acquired at frequency of 1Hz.

2.5 Results

Results from the various studies related to the viscoelastic response of Nafion are presented here. They are divided by experimental technique.

2.5.1 Creep Response of Dry Nafion

Tensile creep strain for dry Nafion from 23-110°C is shown in Figure 2-10. Samples were all dried *in situ* for at least 2 hrs at 85°C, resulting in very dry films. N1110 samples which were 1.27cm wide and had an initial gauge length of 2.54cm were used for all of the runs in Figure 2-10, with an applied stress of 1.55MPa. Looking at the curves, it is evident that creep strain is strongly dependant on temperature over the given range, increasing with temperature.

Using the principle of Time Temperature Superposition allows us to predict the creep response of dry Nafion at a given temperature over a timescale much longer than the individual creep runs. Figure 2-11 is a master curve for dry Nafion reduced to a reference temperature of 25°C. Also shown are the individual creep curves before they are shifted to form the master curve. Time temperature superposition appears to be valid for tensile creep of dry Nafion over the temperatures investigated, giving a fairly continuous curve.

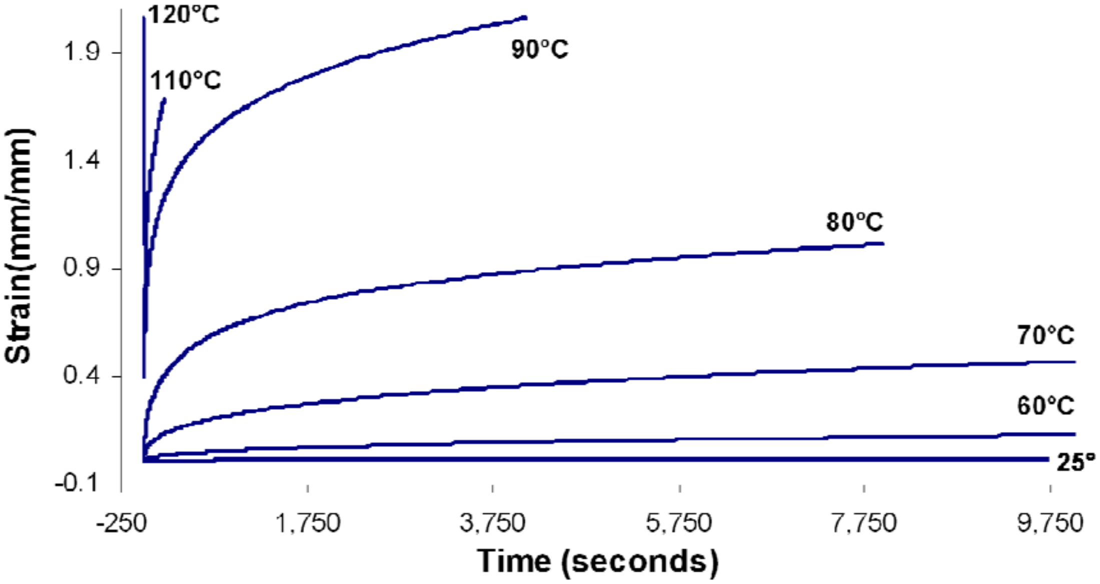

Figure 2-10 Tensile creep response of dry Nafion from 25 – 110°C with an applied stress of 1.55MPa.

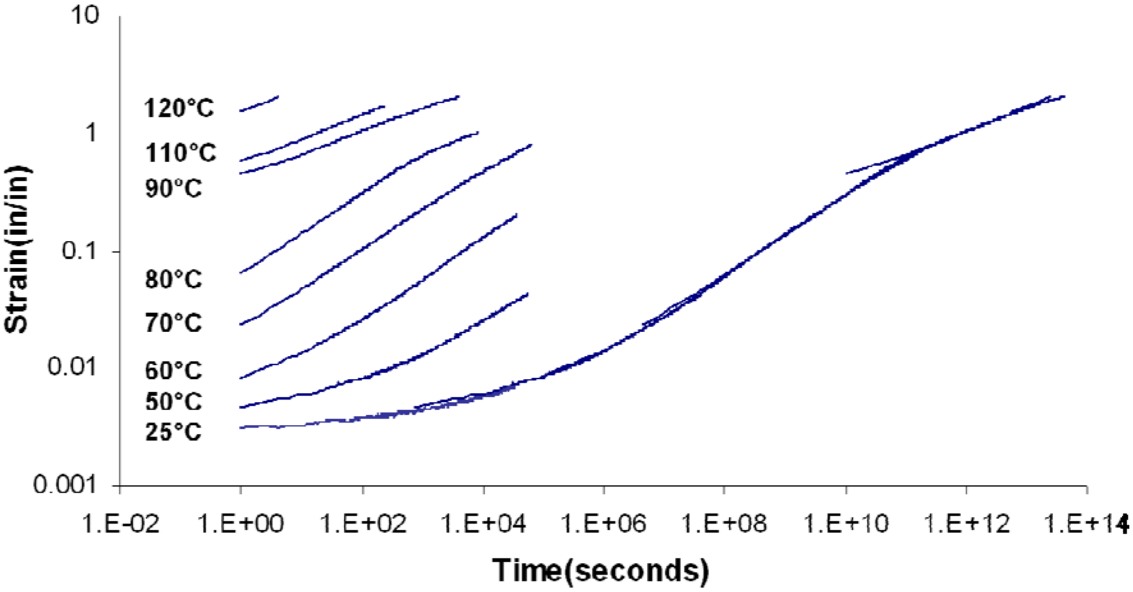

Figure 2-11 Individual creep strain curves and master curve for dry Nafion reduced to a temperature of 25°C, σ = 1.55MPa. A plot of shift factor vs. temperature is show in Figure 2-14.

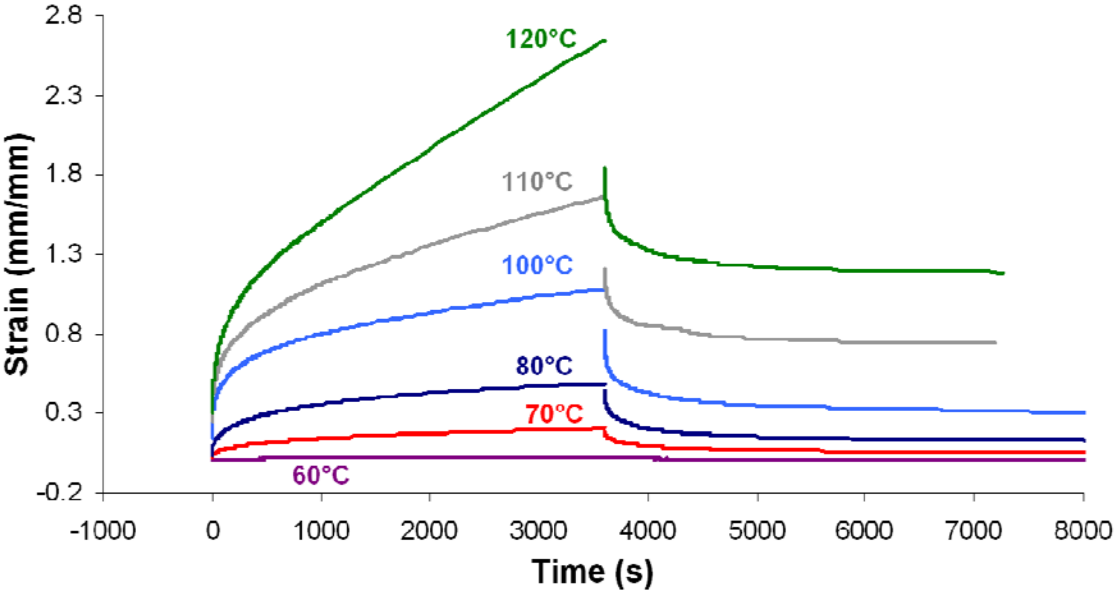

Figure 2-12 Creep response and recovery of dry Nafion N1110 from 60 – 120°C with σ = 0.975MPa.

An additional series of tensile creep curves from 23-140°C (Figure 2-14) for dry Nafion were also collected. For these curves, tensile creep occurred for exactly 1 hr before creep recovery was initiated. The dimensions of the N1110 films used for these curves were 0.635cm wide by 2.54cm initial gauge length[x]. Applied stress for all films was 0.975MPa.

A shift factor plot for the master curve is presented in Figure 2-14. Clearly, there is a linear relationship between 50 and 90°C. The deviation ca. 90°C from linearity strongly suggests that there is a transition occurring between 90 and 120°C. Most likely, this transition is what others have referred to as the glass transition temperature of Nafions with different EW[11, 13-16], as determined by DMA on films which were mostly dry. Eisenberg and co workers suggest that this transition is the glass transition temperature of the ionic groups[11].

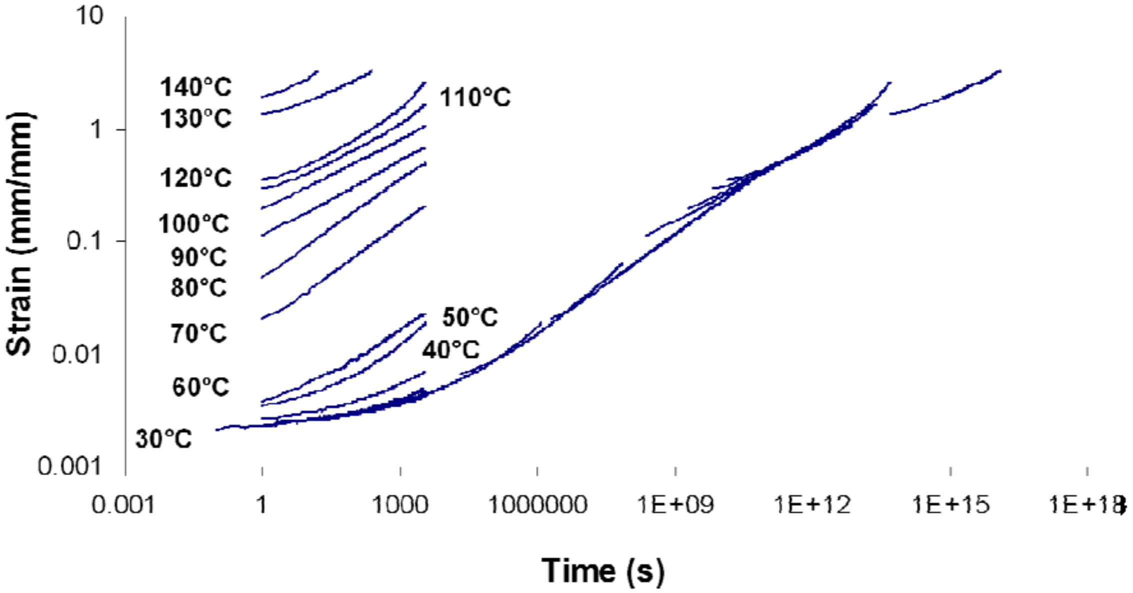

Figure 2-13 Individual creep strain curves and master curve for dry Nafion reduced to a temperature of 30°C, σ = 0.975MPa.

---

[x] For runs above 100°C, initial gauge length was reduced to 0.7" to compensate for the maximum allowable gauge length of the instrument. Comparing runs with the different gauge lengths indicated nearly identical creep response for the dimensions used.

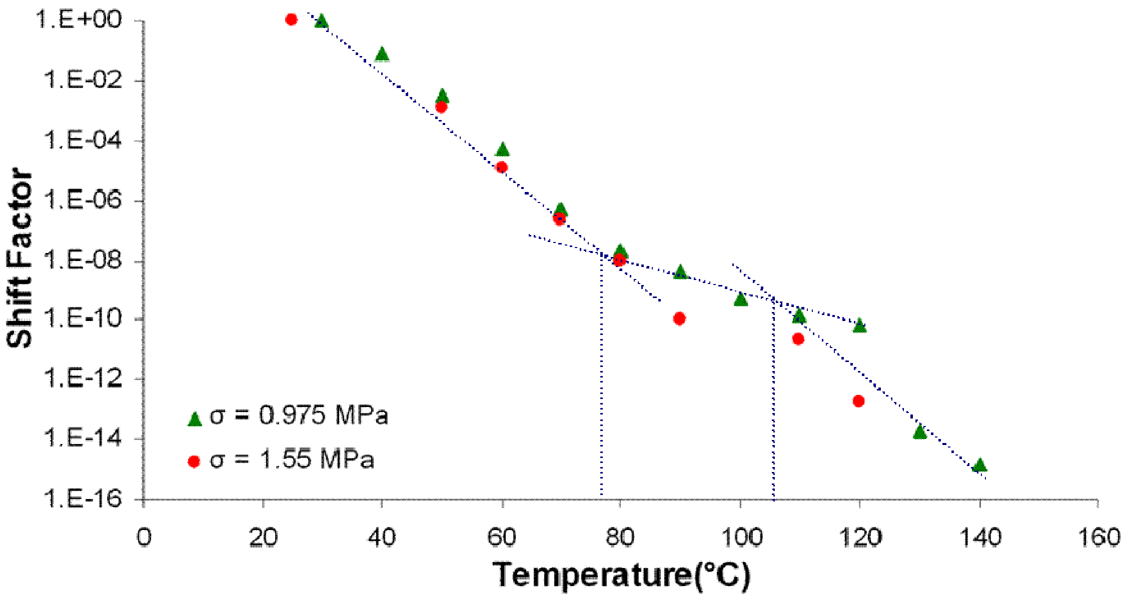

Figure 2-14 Shift factor plots for master curves of corresponding to curves found in Figure 2-11.

Looking at the evolution of the separate components of creep response with increasing temperature gives an idea of how temperature is affecting different molecular interactions. By comparing creep and creep recovery for runs with fixed creep time, a comparison can be made of the separate creep components (Figure 2-12). Extracting values for ε_e, ε_d, and ε_v (Figure 2-15), it is clear that the three components increase with temperature. A transition occurring between 50 and 70°C separates regions which give a fairly linear response when plotted on a semi-log plot.

Additionally, the curves for ε_d and ε_e cross around 40°C, suggesting that there is a transition at this point. Transitions are identified in DMA by plotting the ratio of storage to loss modulus (Tanδ) against temperature. Transitions are found to occur at peaks in Tanδ. Eisenberg and coworkers report a β transition around 20°C for dry Nafion[11].

Delayed elastic strain increases smoothly with temperature over the range shown. The slope decreases with temperature. ε_d, attributed to chain uncoiling, increases as attractive forces both within chains and between chains decreases with temperature.

Uncoiling occurs in the teflonic backbone as well as the short side chains. However, it is difficult to separate the contributions from the different portions of the molecules because of the intimacy and small size of the phase separated regions[11].

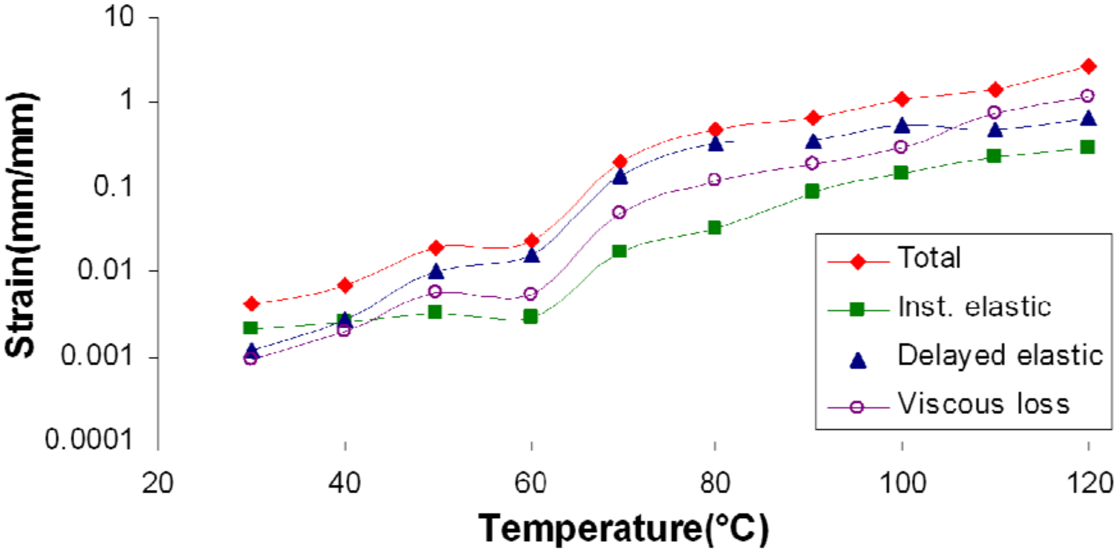

Figure 2-15 Creep components of dry Nafion with an applied stress of 0.975MPa.

2.5.2 Hydration effects on creep response

The previous section presented the results of tensile creep only for dry Nafion. This section presents the results of tensile creep on hydrated Nafion over a range of temperature with comparisons to the dry state.

Tensile creep curves for Nafion N1110 at 0.00, 0.08, and 0.65 water activity at 23, 40, 50, 60, 70, 80, 90, 100, and 108°C are given in Figure 2-17. Applied stress for all runs was 1.55MPa. Sample width before creep, at ambient temperature and humidity, was 0.500" and the initial gauge length was 1.00". Saturated LiBr and NaCl solutions were used to obtain the 0.08 and 0.65 water activity states, respectively.

At 23 and 40°C, we observe that the addition of water increases tensile creep response. At these temperatures and hydration levels, water acts to plasticize Nafion, causing creep strain to increase with water activity.

At 50°C, this trend of water increasing creep strain is no longer occurring. Surprisingly, increasing water activity from 0.00 to 0.08 at 50°C *decreases* creep strain. Increasing water activity further at 50°C from 0.08 to 0.65 again causes an increase in creep strain over both of the drier states. This result was found to be repeatable at other stress levels as well.

At 60°C, a trend of decreasing creep strain with hydration (relative to runs at the same temperature) is observed. At 60°C, creep response for both hydrated states is lower than the dry state. Creep strain at water activity of 0.65 is greater than that seen at 0.08. The same relative positions are seen for the curves at 70°C and 60°C.

Further increasing temperature to 90°C provides another shift in the relative positions of curves. At 90°C, the least amount of creep strain develops for the most hydrated state. Creep strain increases in order of decreasing hydration. This same trend occurs at 100 and 108°C.

Examining the entire series of plots shown in Figure 2-17, there is the general trend that the increase in total creep strain as temperature increases is greatest for the completely dry state and decreases with hydration. In other words, creep strain increases less with temperature as the level of hydration increases. The reason the order of curves is changing between the plots at different temperatures is that creep strain increases with hydration at room temperature while at the same time the rate of creep strain increase with temperature decreases with hydration.

Tensile creep was measured for Nafion N1110 at 120°C for water activities of 0.00 and 0.08 as shown in Figure 2-16. From this, we see that the trend seen up to 108°C in Figure 2-17 continues; creep strain increases for both the dry and hydrated states and the addition of water decreases creep strain below that of the dry state. A comparison of creep at 150°C and $a_w \sim 0.2$ is included[xi]. Tensile creep of the hydrated state at 150°C is substantially lower than the dry state at 120°C indicating that the trend of hydration increasing creep resistance over the dry state continues at least until 150°C.

Master curves for the three water activities compared in Figure 2-17 are shown in Figure 2-18. The curves have all been reduced to a temperature of 23°C. We see that, at this temperature, all three hydrations result in similarly shaped curves and that hydration increases creep strain. The reason why the master curves don't cross at any point within the range shown, even though the relative positions of the individual curves change in Figure 2-17, is that the master curves predict creep response at 23°C. If the curves were reduced to 50°C, the relative positions would be different, as occurs for the 50°C plot in Figure 2-17.

An additional series of tensile creep runs were conducted in order to further probe the effects of temperature and hydration on Nafion's mechanical properties (Figure 2-21-Figure 2-27). Measurements were expanded to include more hydration levels at 23, 50, 80, and 90°C. For all runs, samples were subjected to the desired creep stress for exactly 1 hr before recovery was initiated in order to permit comparison of strain components between samples. The applied stress was 4.19MPa for the 23°C runs and 2.096MPa for

---

[xi] Since the relative humidity sensors used for the creep experiments had an upper temperature limit of 124°C, the actual relative humidity for the creep run at 150°C was not measured. Hydration at this temperature was maintained by slowly injecting liquid water into the chamber with a syringe before and during the test. Assuming a total pressure of 1 bar attributed entirely to the pressure of water vapor, activity was calculated to be 0.21.

all other runs. Measurements were taken at the following water activities; 0.00, 0.01, 0.10, 0.35, 0.65, and 0.95. Humidity was supplied by the bubbler. Some temperatures include runs at additional water activities. Instantaneous elastic response from these runs is briefly mentioned since a more detailed discussion of instantaneous elastic response is given in the next section.

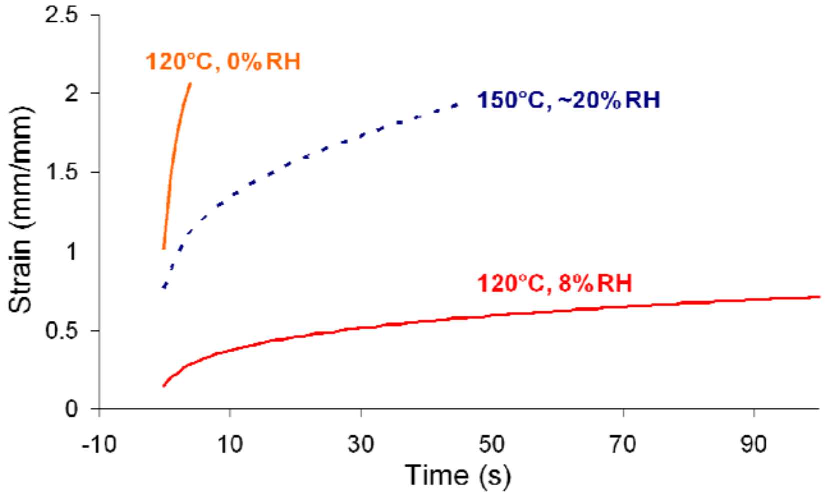

Figure 2-16: Tensile creep of Nafion 1110 at 120°C and 150°C. Applied stress is 1.55MPa.

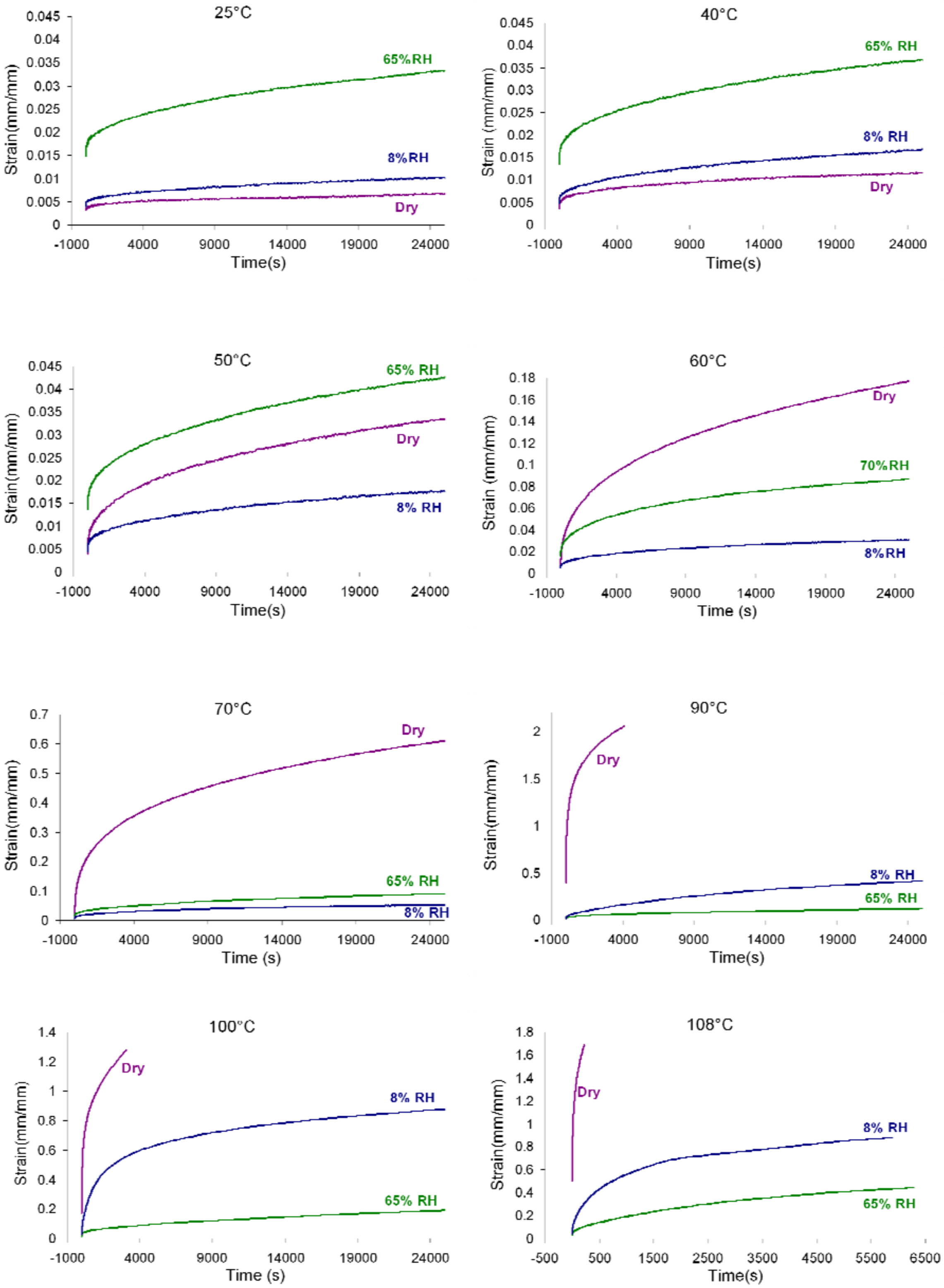

Figure 2-17: Tensile creep for Nafion 1110 from 23 – 108°C at 0, ~8, and ~65% RH. Applied stress is 1.55MPa.

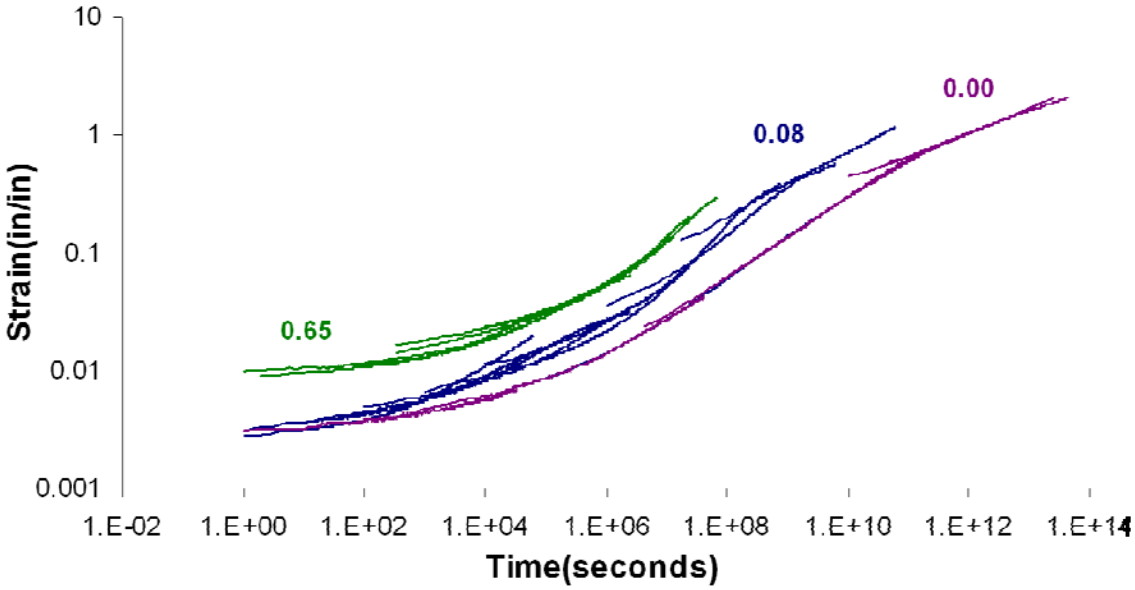

Figure 2-18 Master curves for Nafion N1110 at water activity of 0.00, 0.08, and 0.65 reduced to a temperature of 23°C. Applied stress for all runs is 1.55MPa. Individual curves correspond to data shown in Figure 2-17.

Referring to Figure 2-20 and Figure 2-21, we see that total creep strain increased with hydration from the dry state up to water activity of 0.99. We also notice that all of the separate components show an increase with hydration (Figure 2-21). Contributions from viscous loss and delayed elastic response are similar in magnitude (Figure 2-19). However, viscous loss underwent a sharp increase between water activity of 0.35 and 0.65. Delayed elastic strain increased more smoothly with activity.

At 50°C, there was again a large decrease in creep strain when going from the dry state to the first hydrated state shown (Figure 2-22 and Figure 2-23), as was already seen for the creep curves in Figure 2-17. For the hydrated states, the general trend was that all components increased with hydration. The exception was for the dip in total, delayed elastic, and viscous flow strain which occurred at water activity of 0.35. This deviation from what otherwise seems like a trend appears to be correct, based on repeating runs and the appearance of a similar trend at 80 and 90°C. Water uptake has a significant affect on creep response at 50°C with total strain increasing by a factor of 5 from 0.01 to 0.95 activity. The effect of the first waters on creep strain is also significant.

The jump in total creep strain between the dry state and lowest hydrated state is quite significant at 80°C – ε_t is almost a factor of four larger for the dry state than for the run at 0.01 activity. Comparing the different strain components for the dry state, we notice that a majority of the creep strain is the result of elastic strain (both delayed and instantaneous).

The trend for creep strain and the delayed elastic and viscous loss components is more complicated at 80°C. Maximum total creep strain for the hydrated states occurs at 0.09 activity. We also notice that viscous loss is about a factor of 1.5 times greater at 0.9 activity compared to 0.01 activity.

Total creep strain at 90°C, in general, decreased with hydration. A minimum in creep strain occurred at 0.34 activity. Reduction in creep strain from the dry to the hydrated states occurred more gradually with increasing water at 90°C than what was seen at 80°C. It is clearly seen at 90°C that the effects of hydration on viscoelastic response are complicated, resulting in mechanical response which undergoes a series of rising and falling with increasing hydration. It should be stressed that this behavior has not been previously reported. A possible explanation for this behavior, based on both changes in morphology/microstructure as well as bonding interactions, will be developed in the discussion section of this chapter.

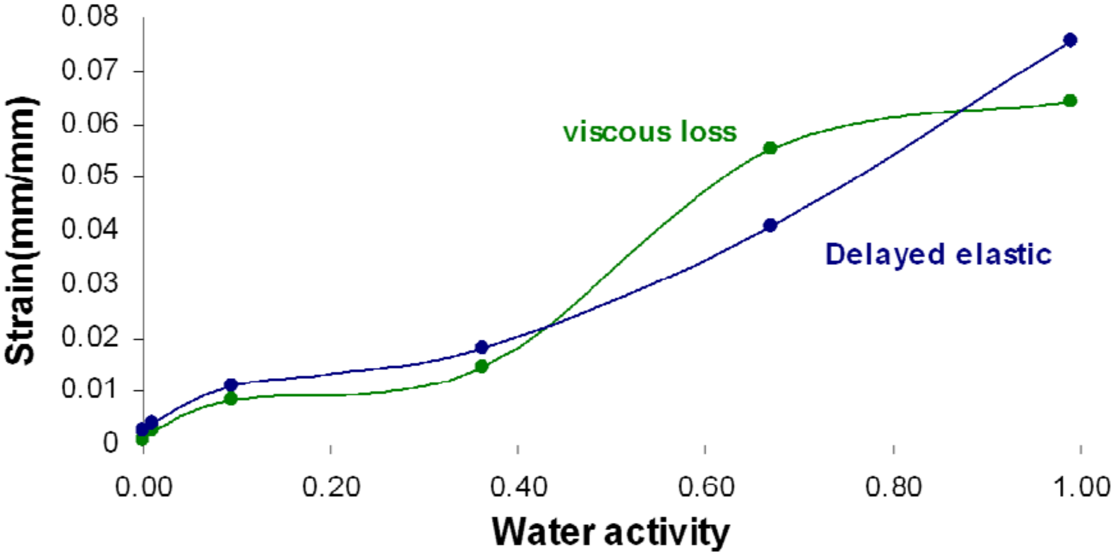

Figure 2-19 Components of viscous loss and delayed elastic strain at 23°C replotted from Figure 2-21 to show shape of curves.

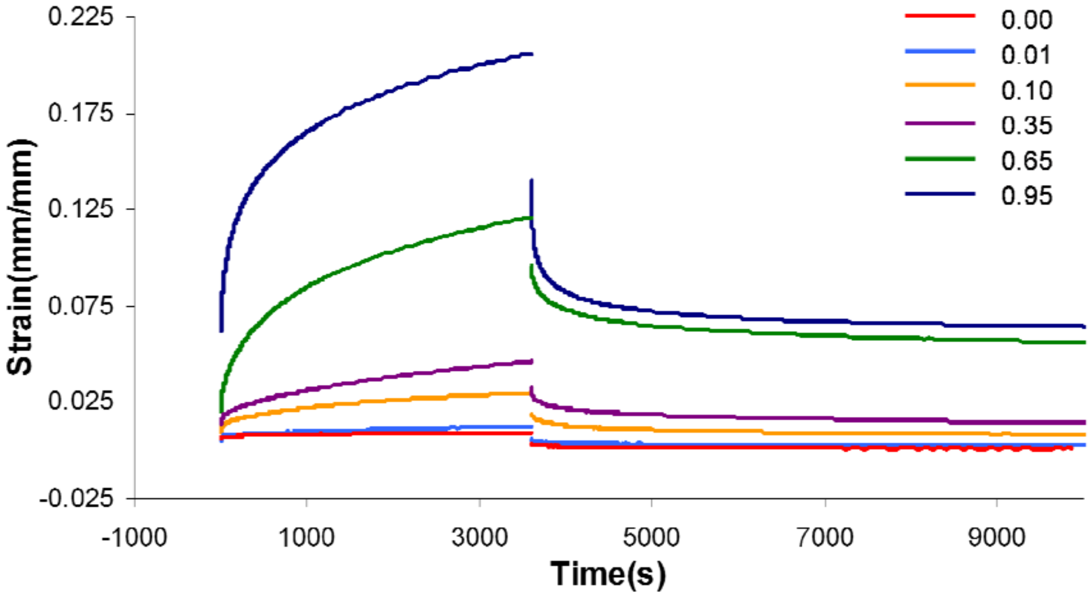

Figure 2-20 Tensile creep strain and recovery for Nafion N1110 at 23°C and the water activities indicated.

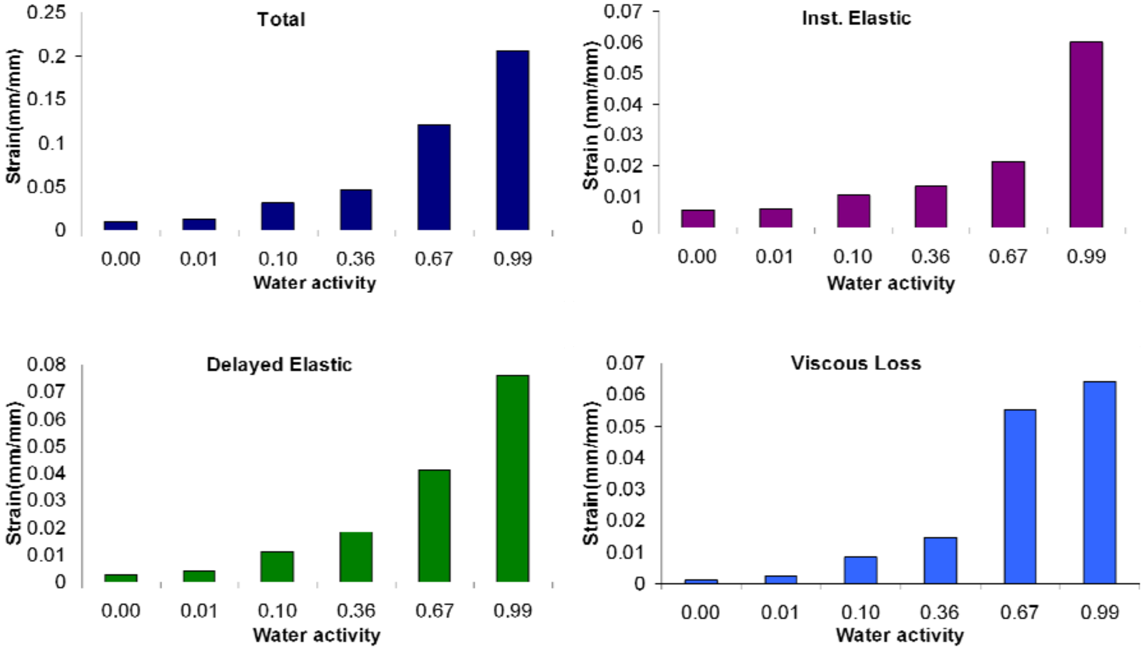

Figure 2-21 Creep strain and components at 23°C as a function of water activity. Values are associated with runs shown in Figure 2-20.

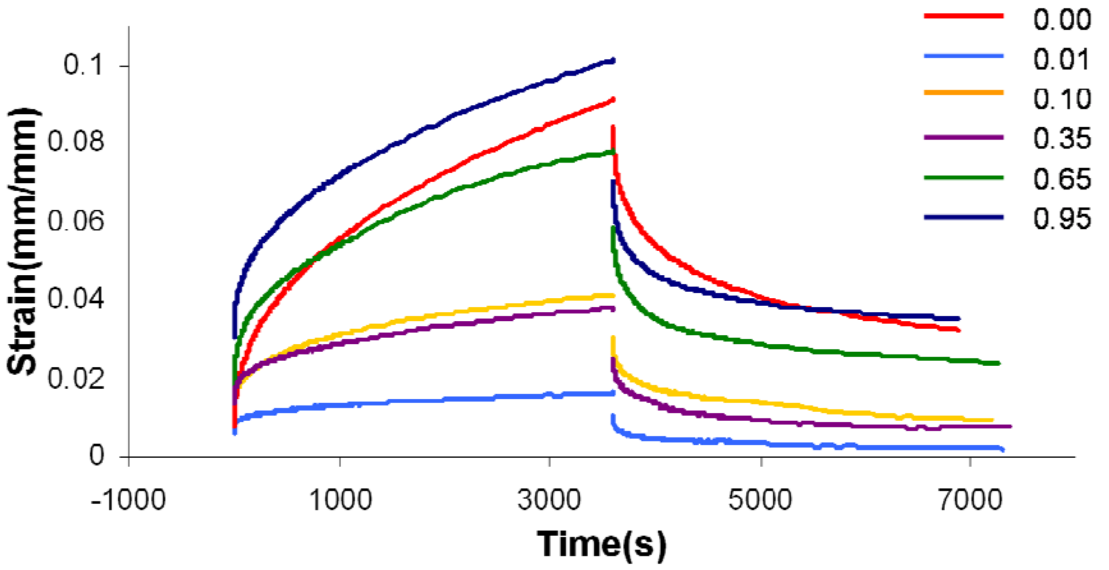

Figure 2-22 Tensile creep strain and recovery for Nafion N1110 at 50°C and the water activities indicated.

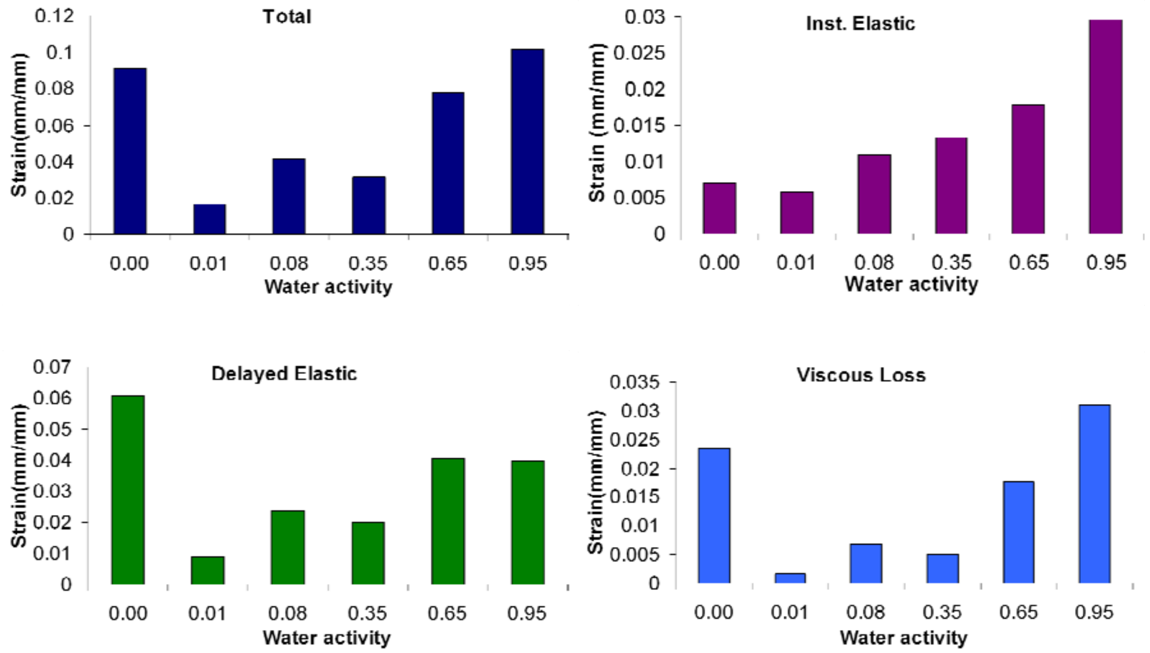

Figure 2-23 Creep strain and components at 50°C as a function of water activity. Values are associated with runs shown in Figure 2-22.

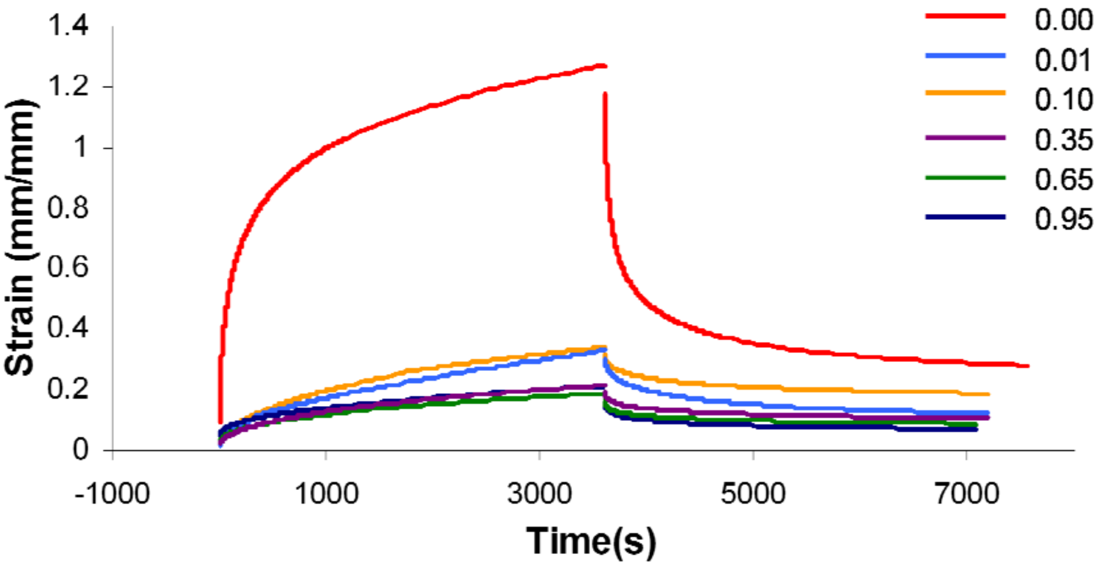

Figure 2-24 Tensile creep strain and recovery for Nafion N1110 at 80°C and the water activities indicated.

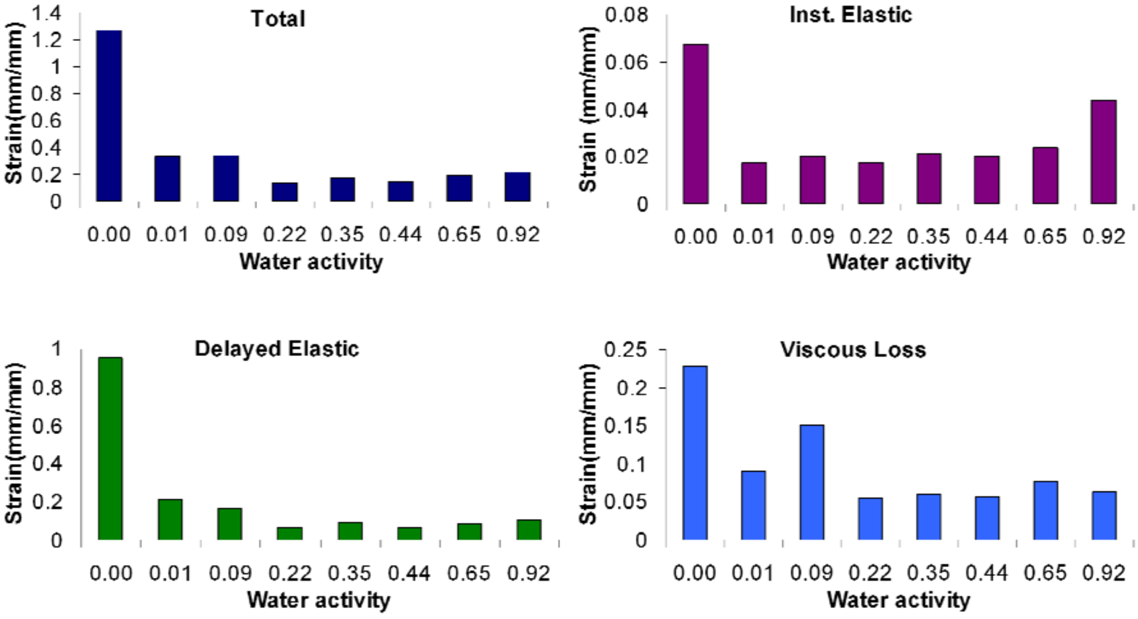

Figure 2-25 Creep strain and components at 80°C as a function of water activity. Values are associated with runs shown in Figure 2-21.

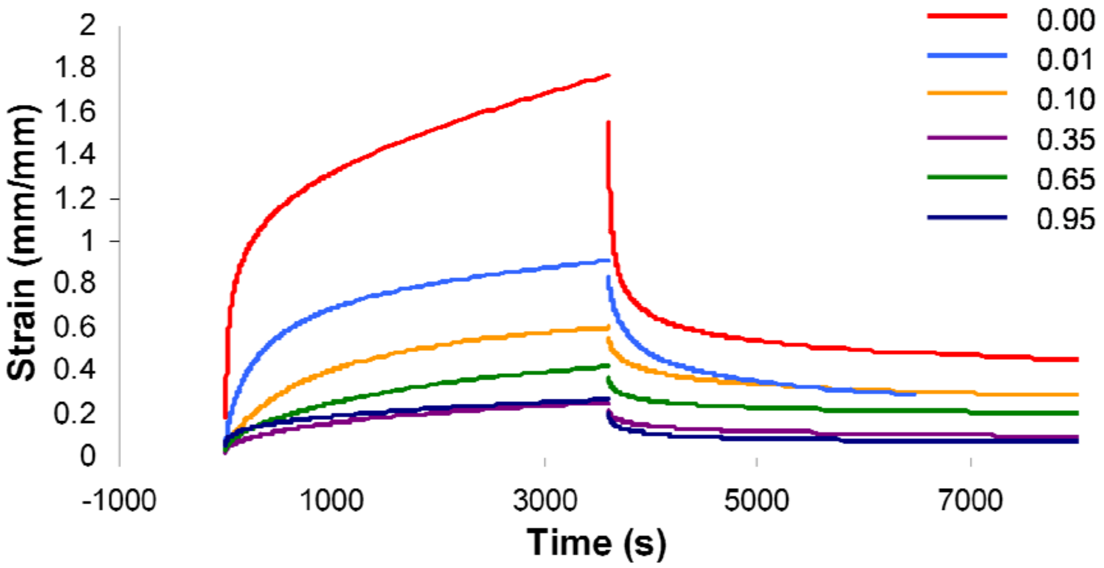

Figure 2-26 Tensile creep strain and recovery for Nafion N1110 at 90°C and the water activities indicated.

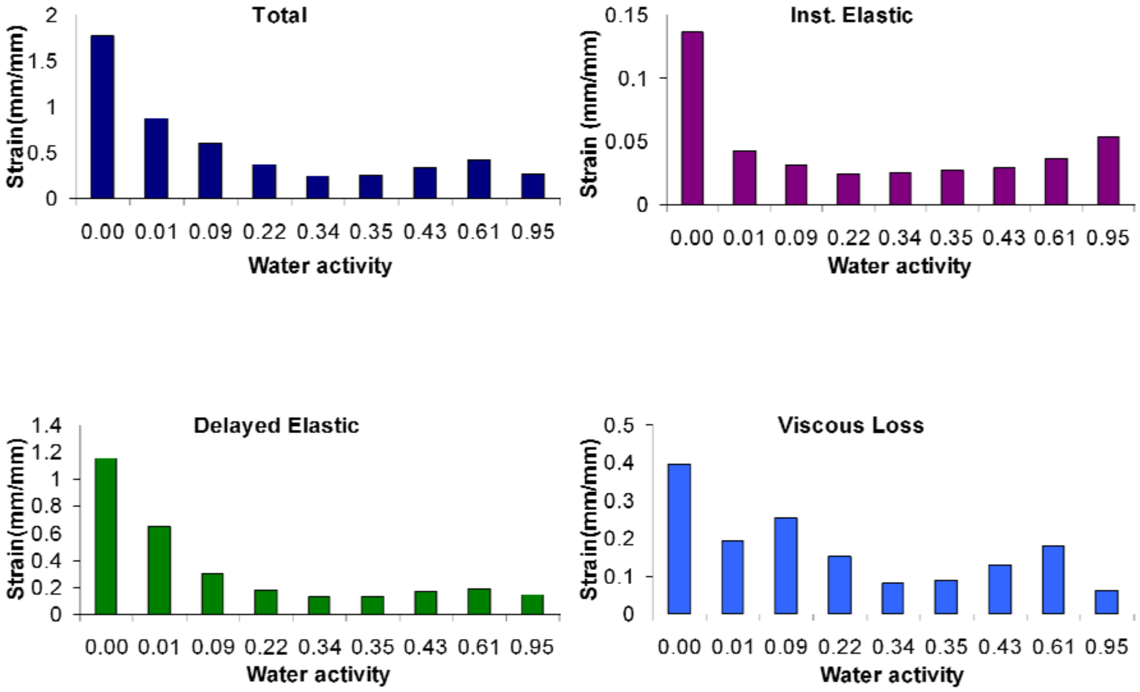

Figure 2-27 Creep strain and components at 90°C as a function of water activity. Values are associated with runs shown in Figure 2-26Figure 2-21.

2.5.3 Stress effects on tensile creep

As mentioned previously, the creep response for materials with linear viscoelastic response scales with applied stress. Creep compliance J is defined as ε/σ and does not vary with applied stress for materials with linear response. The general trend has been observed that Nafion does not respond linearly with changes in stress. In other words, for Nafion under different applied stresses (with all other conditions being constant), creep compliance is different. It has been observed that creep compliance decreases with increasing stress.

2.5.4 Instantaneous elastic response

This section presents values for the elastic modulus of Nafion N1110 as a function of hydration and temperature. The range of temperature and water activity over which values are reported is -5-120°C and 0.00 – 0.95, respectively. This data set dramatically increases available information on how the elastic modulus of Nafion changes with temperature and hydration. This study also reflects a major improvement in of control over water activity, relative to other investigations of Nafion's elastic modulus. During the course of data collection, great care was taken to ensure repeatable hydro-thermal history between different samples. Measurements were not taken until equilibrium in temperature and water activity existed between sample and surroundings. Additionally, temperature and water activity during data collection was precisely controlled.

The instantaneous elastic response for Nafion N1110 is shown from 23 – 90 °C as a function of water activity (Figure 2-28). The following observations are made based on these data:

1) Increasing temperature decreases the elastic modulus. For any given level of hydration (water activity), elastic modulus always decreases with temperature.
2) Water acts to plasticize Nafion in a predictable manner at 23 °C; elastic modulus decreases with hydration.
3) At 40 °C and above, increasing water activity from 0.00 to 0.01 ***increases elastic modulus.***
4) For the hydrated state (i.e., with water activity of 0.01 and above) elastic modulus decreases with water activity up to and including 70°C. Above 70°C, elastic modulus goes through a peak located somewhere above water activity 0.01. For the temperature range reported, the peak shifts to higher activity with temperature.
5) Above 70°C, all hydrated states investigated are stiffer than the dehydrated state.
6) Increasing water activity from 0.00 to 0.01 has a large affect at all temperatures.

The data presented in Figure 2-28 can also be represented by plotting constant water activity curves. This is shown in Figure 2-29 for water activities of 0.00, 0.01, 0.08, 0.60, and 0.95. The following observations can be added based on these curves:

1) The dry state of Nafion shows a transition occurring between 60 and 80°C.
2) The transition occurring in dry Nafion is present for hydration levels up to activity 0.1 and decreases in magnitude with hydration.
3) As hydration increases, elastic modulus varies less with temperature.
4) The crossing of curves indicates that, for some conditions, hydration actually stiffens Nafion.

The elastic response of dry Nafion over the temperature range of -5 – 120°C is presented in Figure 2-30. From this plot, the transition occurring between 50 and 80°C becomes more evident. Elastic modulus decreases nearly linearly between -5 to 50°C and 90 to 120°C.

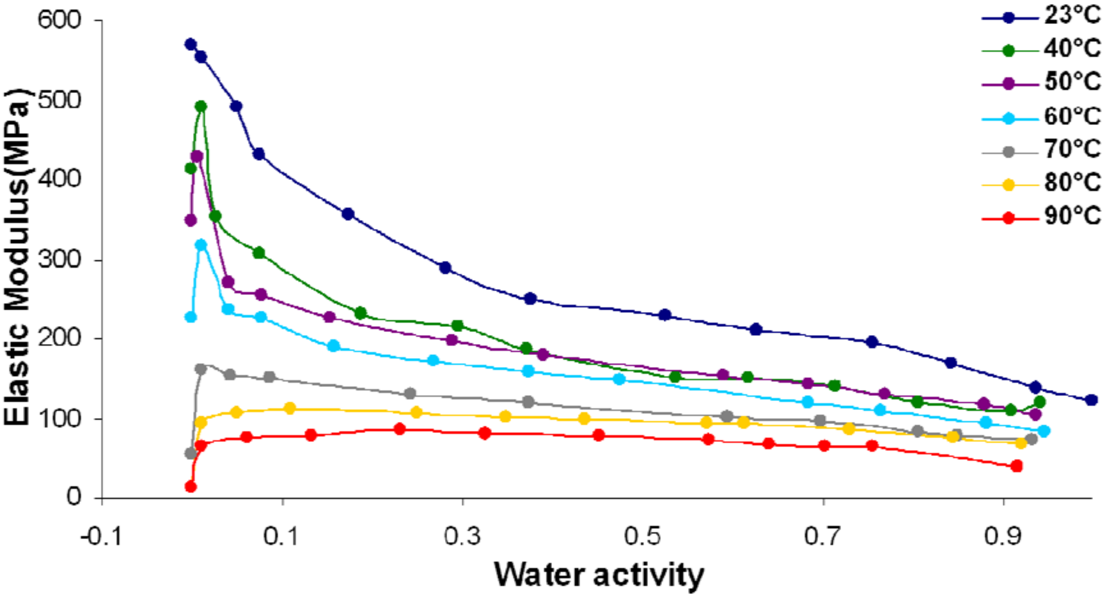

Figure 2-28 Instantaneous elastic response of Nafion N1110 as a function of water activity from 23 – 90°C.

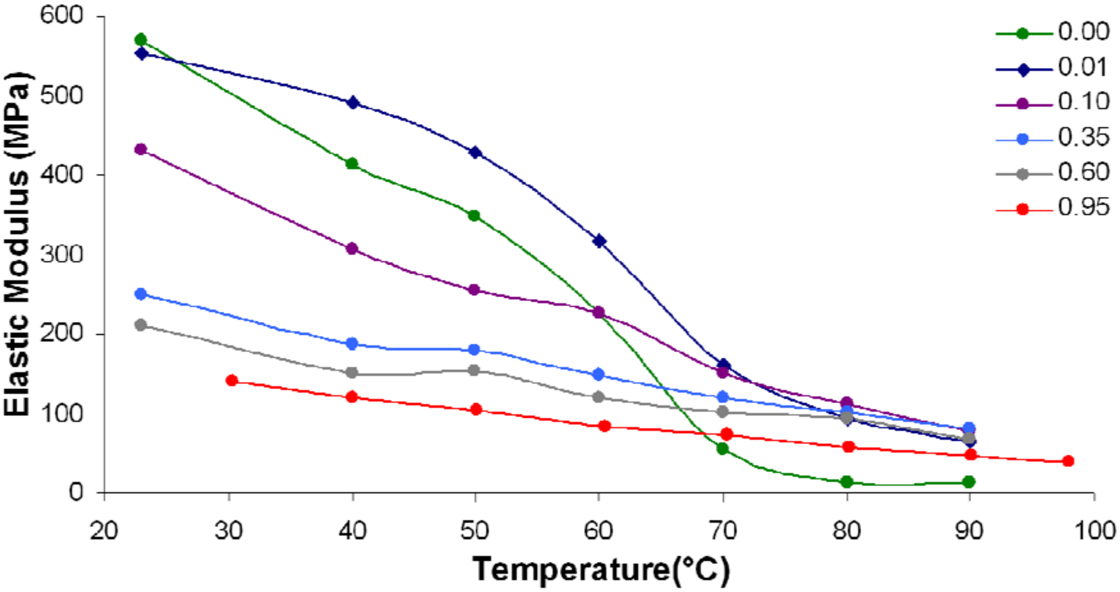

Figure 2-29 Instantaneous elastic response of Nafion N1110 as a function of temperature for films in equilibrium at constant water activities (activities indicated in legend). All points were replotted from Figure 2-28.

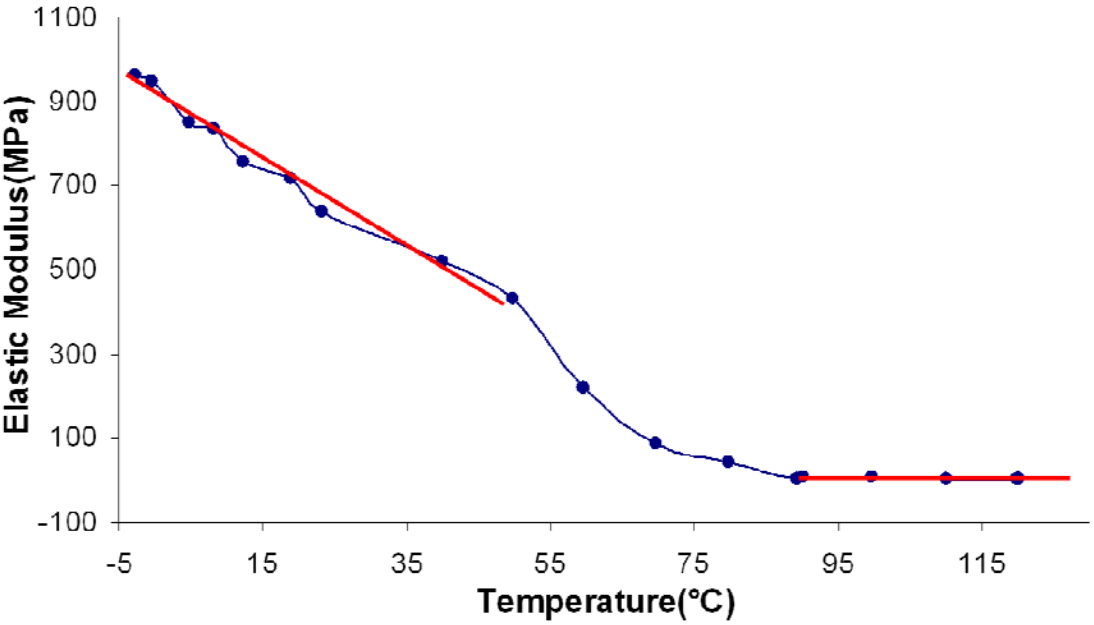

Figure 2-30 Instantaneous elastic response of Nafion N1110 from -5 – 120°C at 0.00 water activity. A transition is clearly visible between 50 and 80°C, separating nearly linear regions.

2.5.5 Thermal History Effects

Several tensile creep runs were carried out to probe the effects of thermal history on Nafion's mechanical properties—both to ensure consistency between creep experiments as well as to gain further understanding about the material's morphology. For these experiments, the effect of drying temperature on tensile creep response was investigated. The configuration of the creep instrument allowed for probing very dry states with *in situ* drying.

The standard drying temperature of 85°C is compared to drying at 150°C. Samples were dried at either 85°C for 6 hrs or 150°C for 2 hrs and cooled to the test temperature under a dry N_2 purge[xii]. Once at the test temperature, water was introduced (if desired) and creep response was measured after equilibration. Samples underwent

---

[xii] A longer drying time was prescribed for the 85°C drying temperature to ensure equilibration at this temperature. Unreported experiments indicated that complete drying occurs in approximately 2-3hrs at 85°C and that drying longer than this does not change mechanical properties appreciably. Drying for 2 hrs was assumed to be adequate for complete water removal based on results at 85°C.

creep for exactly 1 hr before undergoing creep recovery. This was done to permit comparison of the different creep components between runs.

The effect of drying temperature on viscoelastic creep was determined at 23 and 80°C for water activity of 0.00 and 0.65. Creep curves at these conditions are shown in Figure 2-30 and Figure 2-31. Table 2-4 summarizes the effect of the 150°C drying temperature on creep compared to drying at 85°C. In this table, total creep strain and creep strain components for 1 hr of creep are shown for the two drying temperatures at four separate conditions.

The largest effect due to drying temperature was seen for the dry 23°C run; a *10 fold increase* in total strain when dried at 150°C. Most of this strain increase is attributed to an increase in delayed elastic and viscous strain. Almost no change in instantaneous elastic response was seen. For the run dried at 85°C, delayed elastic and viscous strain contributions were very small, being 0.26 and 0.10% strain, respectively (out of a total0.92% total strain). The large increase in creep strain for dry Nafion at 23°C indicates that interactions occurring between sulfonic acid groups have been greatly reduced due to rearrangement occurring at the higher drying temperature. This can be inferred because the same thermal energy is available to both runs at 23°C for the bending of bonds, straightening of chains, and chain slippage.

Table 2-4 Summary comparing differences in creep strain due to thermal history effects. Values separated by a slash correspond to drying temperature of 85 and 150°C. Data corresponds to runs shown in Figure 2-31 and Figure 2-32.

Temp. (°C)	Water activity	Creep strain (mm/mm) (85°C/150°C)			
		Total	Inst. elastic	Delayed elastic	Viscous
23	0.00	0.0092/0.088	0.0073/0.0087	0.0026/0.030	0.0010/0.051
	0.65	0.12/0.08	0.021/0.018	0.041/0.030	0.055/0.033
80	0.00	0.43/0.83	0.079/0.17	0.29/0.36	0.10/0.19
	0.65	0.19/0.15	0.024/0.022	0.086/0.075	0.077/0.051

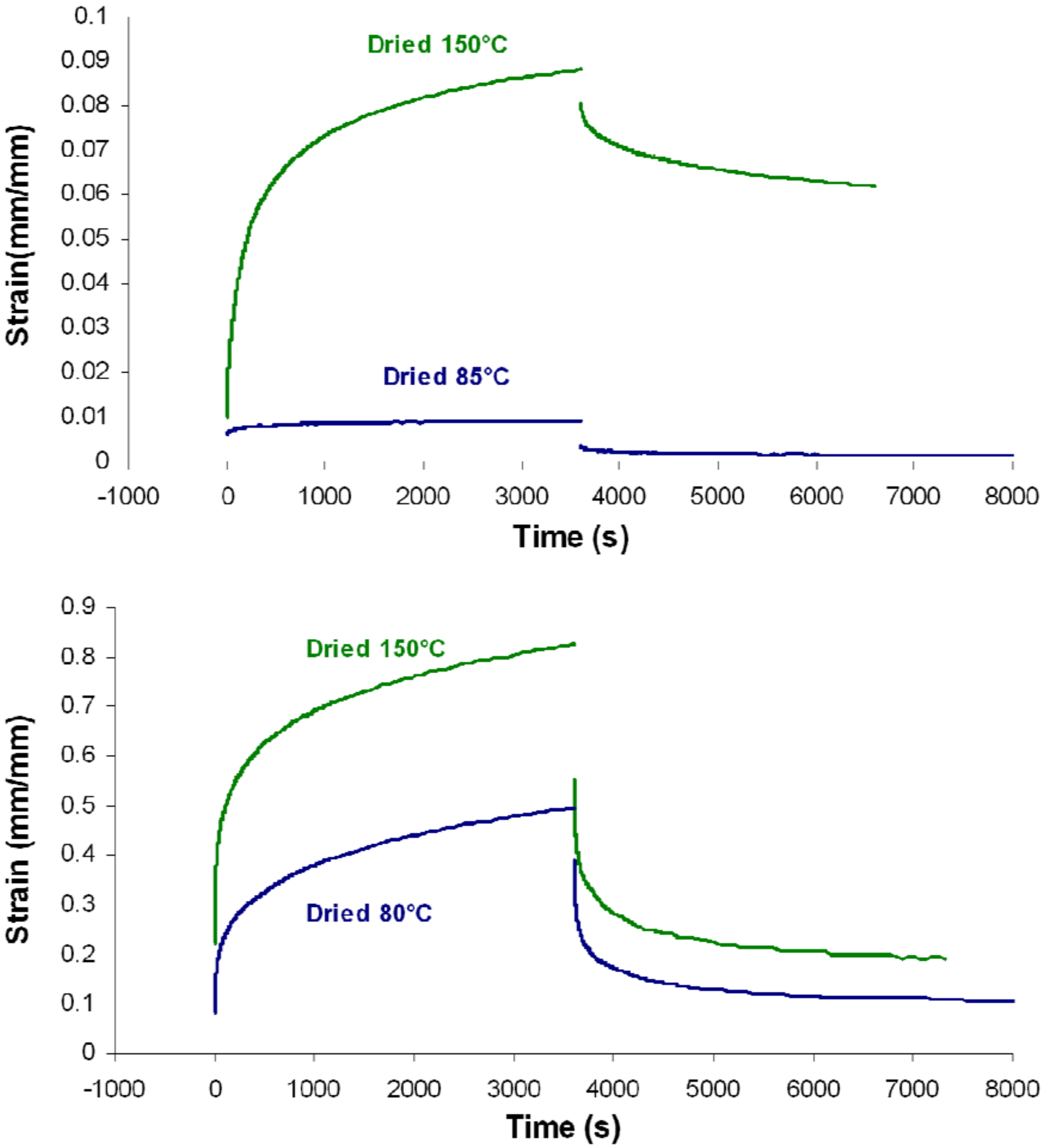

Figure 2-31 Tensile creep response of dry Nafion at 23°C (top) and 80°C (bottom) comparing effect of thermal history (i.e., drying temperature). The applied stress for the runs at 23 and 80°C is 4.19 and 0.97 MPa, respectively.

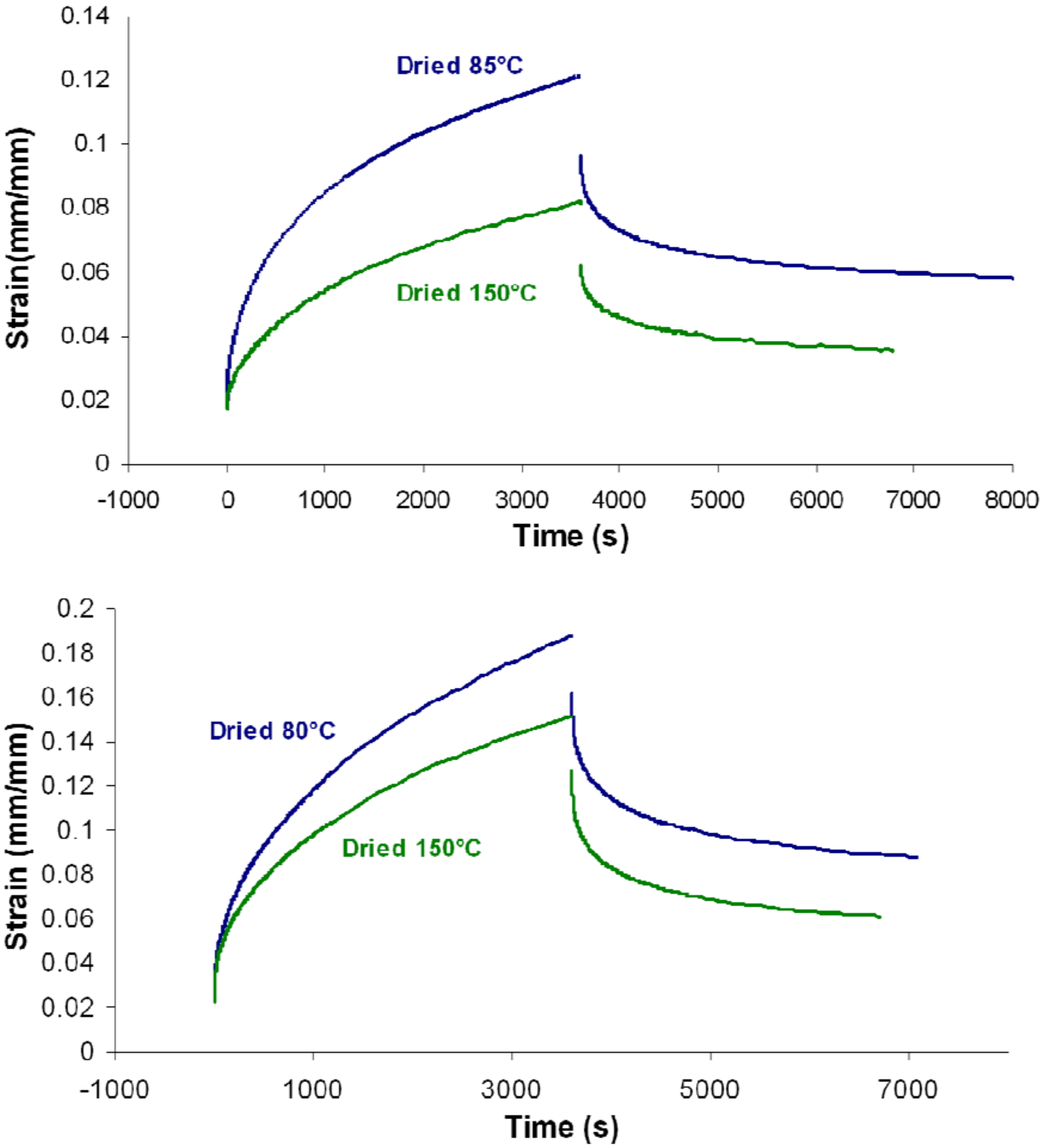

Figure 2-32 Tensile creep response of Nafion at 23°C (top) and 80°C (bottom) and 65%RH comparing effect of thermal history (i.e., drying temperature). The applied stress for the runs at 23 and 80°C is 4.2 and 2.1 MPa, respectively.

A change in morphology, caused by the high temperature treatment, could result in rearrangement of clusters into smaller and more divided regions, resulting in fewer cross-links between chains which normally give Nafion resistance to creep at 23°C in the absence of water.

At 80°C and an a_w of 0.00, the increase in creep strain brought about by high temperature drying was much greater in magnitude than what was seen at 23°C, but corresponded to a smaller fraction of the creep seen after normal drying conditions. Total strain increased by a factor of 1.9 with the largest contributions attributed to instantaneous elastic and viscous strain. The instantaneous elastic strain which occurred for the sample dried at 150°C was greater than the total strain after 1 hr of creep for the sample dried at 85°C.

For the hydrated runs, drying at 150°C resulted in less creep strain than samples dried at 80°C. This was opposite to what occurred with the dry runs. This trend was seen at both 23 and 80°C. The difference in creep response for the two thermal treatments was much less for the hydrated runs than for the dry runs.

For hydrated creep at 23°C, the total strain for the sample dried at 80°C was 1.5 times greater than that for the sample dried at 150°C. The increase was primarily due to viscous loss (increase of 1.7 times) and delayed elastic strain (increase of 1.4 times). For hydrated creep at 80°C, total strain for the sample dried at 80°C was 1.3 times greater than that for the sample dried at 150°C. This increase was due almost entirely to changes in the viscous loss component, an increase of a factor of 1.5.

It is difficult to determine why the high temperature drying treatment resulted in decreased creep strain for hydrated runs at both 23 and 80°C. Assuming smaller cluster sizes for the 150°C drying temperature, water uptake should be smaller at as a result. This can explain why creep strain is smaller at both 23 and 80°C for the high drying temperature. At 23°C, creep strain increased with hydration for the samples dried at 85°C. Thus, it is logical to assume that smaller water uptake due to smaller clusters could cause less creep strain. Indeed, liquid water uptake measured for Nafion dried at 105°C was reported to be lower than Nafion dried at 80°C[38]. It is reasonable to assume that uptake from water vapor would also be reduced with the higher drying temperature and that drying at 150°C would have an even greater effect than drying at 105°C. This should be carefully studied.

The effect of hydration on viscoelastic creep is more complicated at 80°C than at 23°C. Around water activity of 0.65, creep strain decreased with decreasing hydration (total creep strain was less at activity 0.44 than 0.65 (Figure 2-25)). This is consistent in explaining why creep strain decreased with high temperature drying for the hydrated run; smaller cluster size resulted in decreased water uptake and therefore decreased creep strain. Admittedly, the effect of microstructure on viscoelastic response is complicated. The assumption that smaller cluster size necessarily results in less viscous strain for hydrated conditions is overly simplistic.

Less of a relative increase in total strain is seen at 80°C compared to 23°C. The reason for this is that the cross-linking interactions between sulfonic acid groups are more easily broken (in the case of chain slippage) or stretched (in the case of instantaneous and delayed elastic) because of the higher thermal energy at 80°C. Therefore, one sees less of a contribution from the sulfonic acid groups and more from the teflonic matrix at 80°C in the absence of water.

Taking Nafion dried at 150°C and introducing water at lower temperatures, below 85°C for example, thermal history effects are still present. The actual effects are reduced for two reasons: one is that the addition of water allows for rearrangement of sulfonic acid groups so that some degree of cross-linking can be reestablished once water is added. The other reason is that cross-linking is made stronger in the presence of water (at 80°C, but not 23°C).

2.5.6 Solvent Effects

The tensile creep response of Nafion N1110 and other Nafion films was measured after exposure to several solvents. This was done to both directly measure the effect of the solvents on Nafion's mechanical properties and as a way to elucidate the interactions giving rise to mechanical properties. Separate creep strain curves for Nafion in equilibrium with five different solvents are shown in Figure 2-33.

Each solvent effected a different amount of swelling, relative to the dry state. Equilibrium swelling strain along the length of the sample (in the machine direction) is presented in Figure 2-34 for several solvents. The solvent activity in the vapor phase approached 1 for all runs. The alcohols induced the largest amount of swelling—about twice that of water. Acetonitrile caused swelling only slightly greater than that of water. Swelling due to solvent sorbtion by the polymer is caused by solvent interaction with both the ionic groups and, for some solvents, the matrix.

Solvent uptake by Nafion results in changes in the size, shape, and number density of clusters[39]. As a result, some degree of molecular rearrangement occurs, both of the pendant groups as well as the main chains. The final morphology is a function of solvent type, temperature, membrane history, and mass uptake of solvent. Solvent uptake is determined by the thermodynamics of mixing (both in the sulfonic acid clusters as well as the matrix), the work done to swell the polymer, and polymer reorganization (i.e., stress relaxation).

Water interacts with Nafion almost entirely through the acid clusters. Interaction is restricted to the clusters because water is highly polar, as are the acid groups, while the matrix is non-polar. SAXS studies have indicated that water molecules in hydrated Nafion are phase separated from the matrix with very sharp boundaries segregating the two phases[40, 41]. Water still has a large impact on the mechanical properties of Nafion, including relaxations of the matrix, because of the small cluster size and cross-linking of chains which occurs through the acid groups[11].

Solvent interaction with the matrix occurs if the solvent molecule is polar and possesses a hydrophobic tail group. The polar aspect allows the solvent to interact with the counterion[42], becoming sorbed by the polymer and inducing cluster formation which is similar to water-swollen membranes[36]. The non-polar or hydrophobic tail group can then interact with the teflonic matrix. Water, which doesn't possess a hydrophobic tail, is confined to the clusters. The alcohols, however, do have hydrophobic tails which can interact with the matrix.

Tensile creep curves for Nafion N1110 are shown in Figure 2-33 for the different solvents. 1 hr creep runs with recovery allow for comparison of strain components. All of the membranes were in the protonated form. In addition, a separate run was done with ethanol when the membrane was in the Na form. Total creep strain along with the strain components are presented in Figure 2-35 for the runs with different solvents.

For the membranes in the protonated form, total strain as well as the individual creep strain components, was significantly greater for the alcohols than for water or acetonitrile. All aspects of creep strain increased for the alcohols because of interaction of the non-polar groups with the matrix. The fact that the alcohols are polar allows them to penetrate the polymer, as stated above. Creep strain increased with the number of carbon atoms in the alcohols. It is assumed that this is due to increased interaction between solvent and matrix. The drop in viscous loss from isopropanol and ethanol to methanol supports this. Since methanol only has one CH_3 group, its interaction with the matrix is least. Viscous loss requires slipping of the main chains, which occurs due to varying levels of disruption of interactions between main chains as well as acid groups.

Acetonitrile is expected to effectively disrupt bonding between sulfonic acid groups. Comparing viscous loss for the alcohols to acetonitrile and water, cross-linking of sulfonic acid groups does a limited amount to prevent viscous loss. This is based on the observation that viscous loss is so low for acetonitrile and water which both interrupt cross-linking of the sulfonic acid groups to some degree (water results in new cross-linking bonds whereas acetonitrile is thought to eliminate cross-linking). At higher temperatures, secondary bonds in the matrix become less significant and viscous loss for acetonitrile and should increase much faster than for water since some degree of cross-linking between hydrated sulfonic acid groups would strengthen the polymer.

It is interesting to note that, among the alcohols, opposite trends for swelling and creep strain exists. Why should methanol cause the greatest amount of swelling while producing the least amount of creep? The decreased interaction of methanol with the matrix explains why it causes the least amount of creep strain, but shouldn’t it also cause significantly less swelling than the other alcohols? Measuring the swelling strain of Nafion N1110 in liquid methanol and ethanol revealed swelling strain that was slightly greater for ethanol than methanol at 23°C. After 48 hours, the total swelling strain for Nafion N1110 in was 42.2% in methanol and 46.8% in ethanol. Swelling strain in liquid water was measured as 19.7%. One possible reason why swelling strain due to solvent uptake from vapor was greater for methanol than ethanol could be that kinetics; swelling strain due to liquid uptake of ethanol and methanol was observed to take well over 10 hrs to reach equilibrium. On the other hand, Gebel and co workers[42] also report increased swelling strain from 2-propanol to ethanol to methanol for uptake from the vapor phase.

The Na form of Nafion shows reduced uptake of ethanol and creep strain. Reduced solvent uptake is the result of stronger interaction between sulfonate groups. In the Na form, strong dipole-dipole interactions within ionic aggregates[43]. Chain movement necessary for swelling is made more difficult as a result of the increased electrostatic interaction when the counterion is an alkali metal. The increased interaction also partially explains the decrease in creep strain; crosslinking interactions through the sulfonate groups (i.e., electrostatic dipole-dipole interactions within the ionic aggregates) stiffen the material, reducing molecular motion. Additionally, the reduced solvent uptake results in less disruption of secondary bonding (van der Waals interactions) in the matrix.

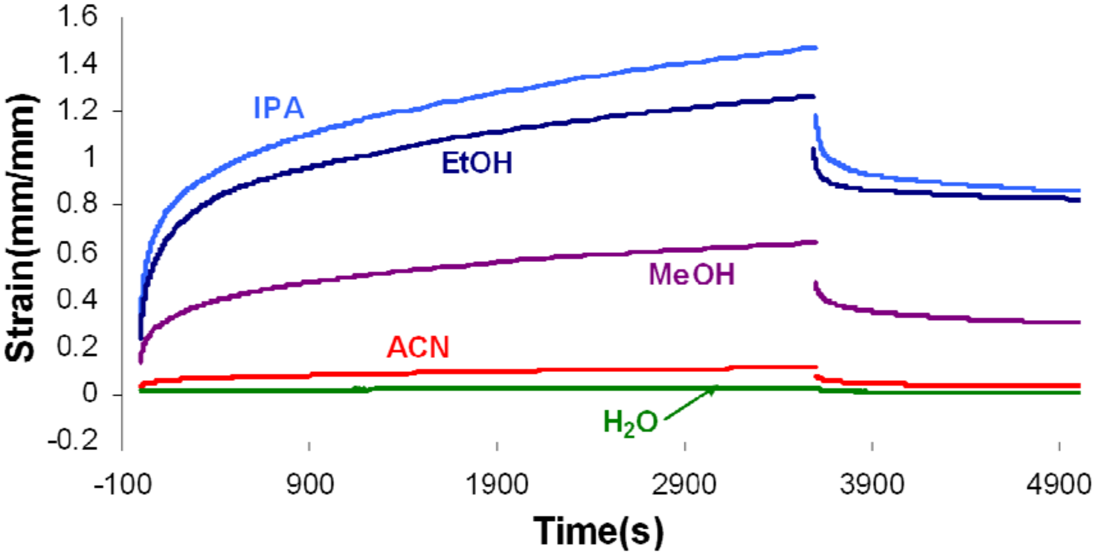

Figure 2-33 Tensile creep strain and recovery for Nafion N1110 at 23°C after absorbing different solvents from the vapor phase. Activity approaches 1 for all solvents. Applied stress for each run was 0.97MPa.

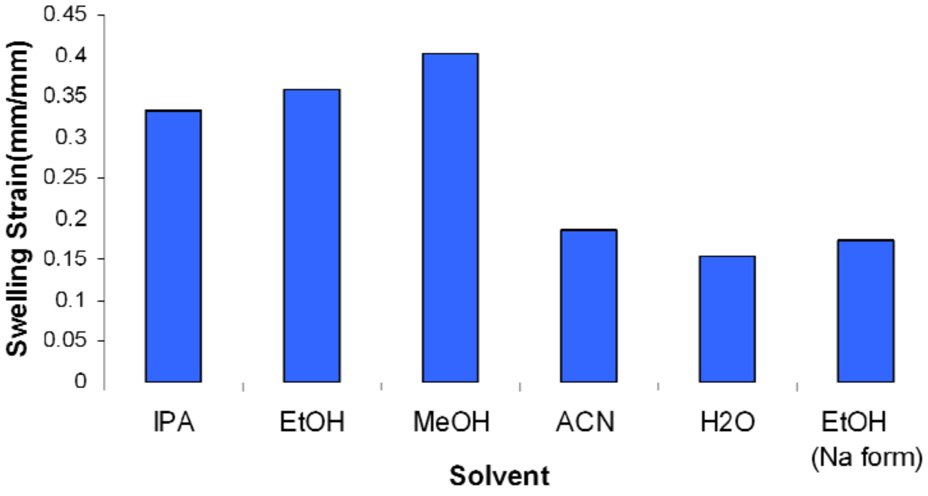

Figure 2-34 Swelling strain of Nafion N1110 at 23°C in equilibrium with the solvents indicated. Solvent activity in all cases approaches 1. All membranes are in the acid form except for one of the ethanol runs indicated which substituted Na form N1110 for the acid form.

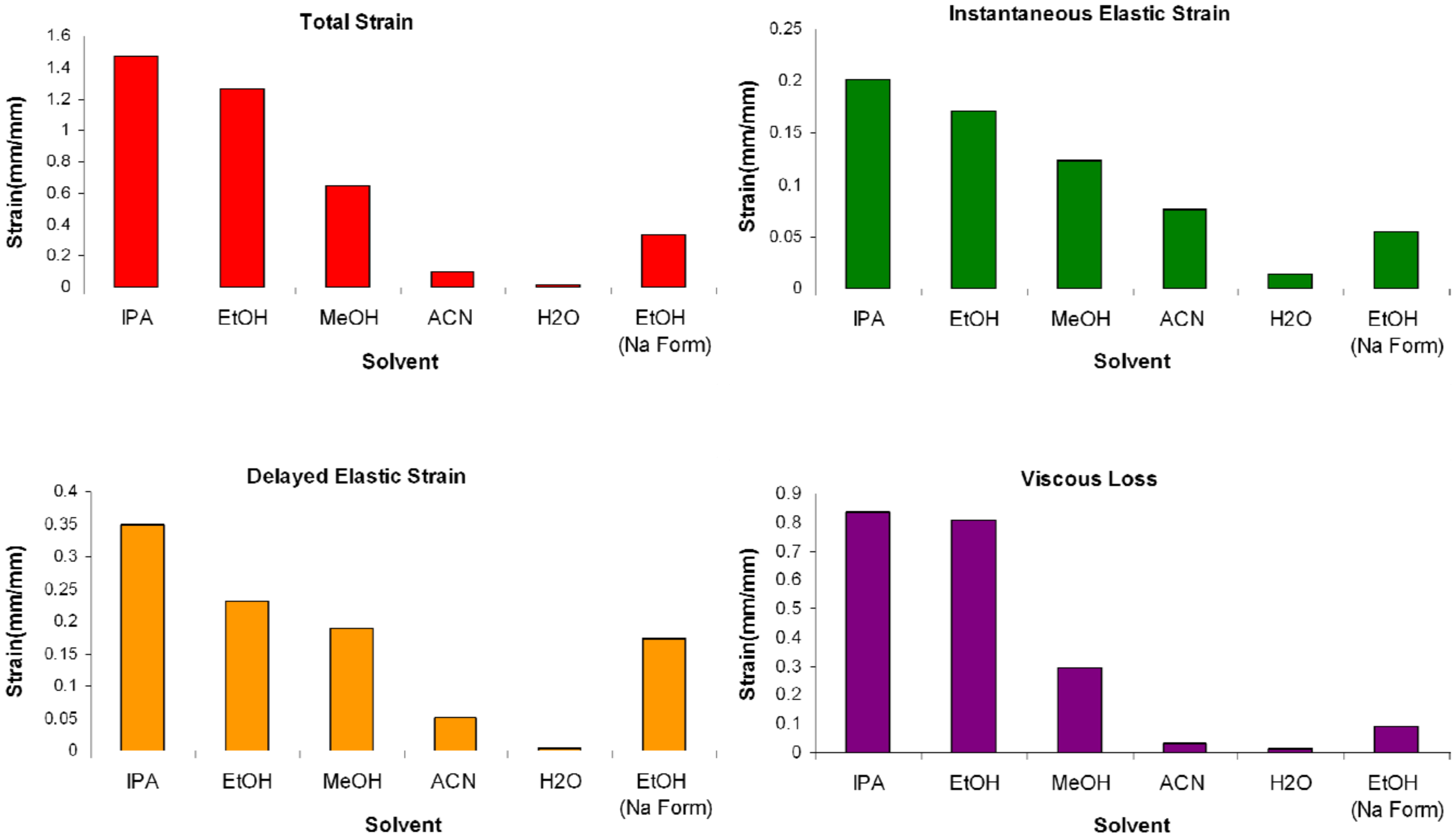

Figure 2-35: Total creep strain and creep strain components for Nafion N1110 at 23°C in equilibrium with the solvents indicated. Solvent activity in all cases approaches 1. All membranes are in the acid form except for one of the ethanol runs indicated which substituted Na form N1110 for the acid form.

2.5.7 Ion effects

A comparison was made between Nafion N1110 in the Na^+ and H^+ form (Figure 2-36). Creep strain was measured at 80°C with water activity of 0.00 and 0.65. The difference in creep response between the Na^+ and H^+ form of Nafion in the dry state is spectacular. There was essentially no creep strain seen in the dry Na^+ form film at 80°C while the dry H^+ form film showed significant creep strain in just a short period of time. The addition of water had opposite effects for the different ion forms. Water significantly reduced creep strain in the protonated film while it increased creep strain in the Na^+ exchanged sample. The difference in creep strain between samples was much less when hydrated than when dry.

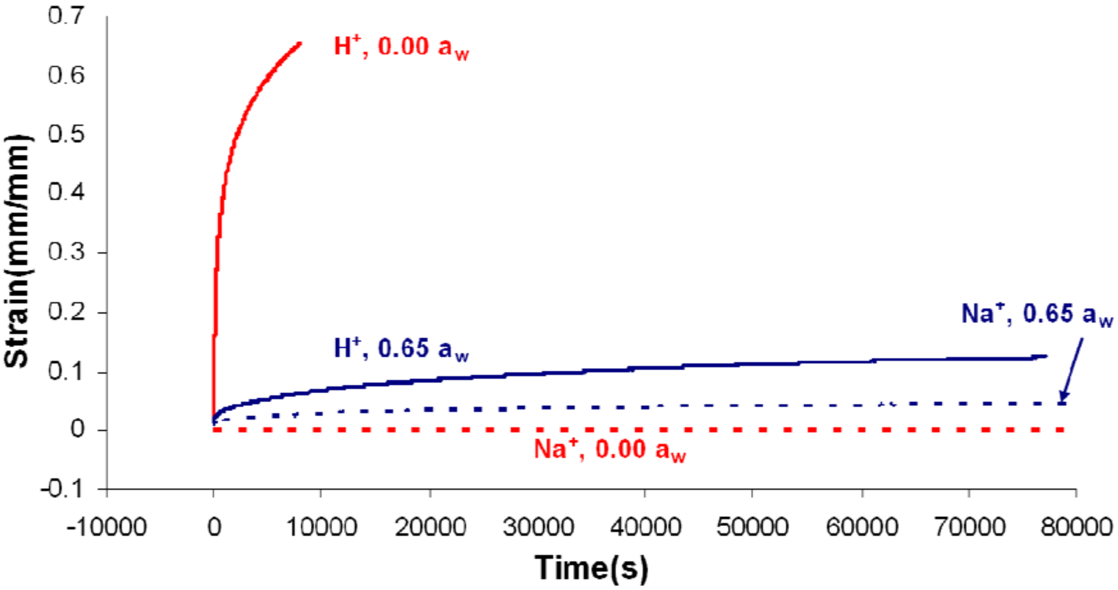

Figure 2-36 Creep strain comparison between Nafion N1110 at 80°C in the Na^+ and H^+ forms. Two hydration levels are shown (0% and 65% RH). Applied stress for all curves is 1.55MPa.

2.6 Discussion

2.6.1 Temperature and hydration effects

Information on the effect of temperature and hydration on the viscoelastic response of Nafion is present in both the tensile creep and instantaneous elastic modulus data. Together, these data give a picture as to how the mechanical properties of Nafion depend on temperature and hydration. Microstructure, crystallinity, and interaction between ionic aggregates are all affected by temperature and hydration and impact mechanical response. In this section, explanations are given for the unexpected and complex mechanical behavior of Nafion with changes in temperature and hydration.

To summarize, the main effects of temperature and hydration on the viscoelastic response of Nafion presented in the results section of this chapter:

1) Dry Nafion undergoes a transition between 50 and 80°C which is clearly seen in the instantaneous elastic response as well as the other components of creep strain.
2) At room temperature and slightly above, both tensile creep and instantaneous elastic response decrease with hydration (viz., water plasticizes Nafion).
3) At 40°C and above, small levels of hydration (i.e., 0.01 activity) increase elastic modulus/decrease creep strain above the dry state.
4) As temperature increases, the range of hydration which results in an increase in elastic modulus/decrease in creep strain above the dry state expands, shifting to higher hydration and having a larger effect.
5) The effect of hydration on the different components of creep strain at and above 50°C is complicated, with different components undergoing periods of increase and decrease with hydration.
6) In general, creep strain changes less with temperature as hydration increases.

The effect of temperature and hydration on microstructure and ionic interaction will be used to explain these observations.

Hydration strongly affects the viscoelastic response of Nafion. Introducing water to the ionic clusters 1) results in changes in the microstructure of the ionomer by changing cluster size and shape and 2) disrupts the bonding between sulfonate groups present in the absence of hydration. In some of the early work by Eisenberg and coworkers[11], it was proposed that water interaction was primarily with the clusters, but that, due to the intimacy of the phase separated regions in Nafion, water was also able to interact with side chains. The present state of understanding is that water interacts only with the ionic clusters and that sharp boundaries exist between phases[41]. First, a discussion of the changes in interactions which occur with the introduction of water.

It is a topic of debate whether Nafion dried at 85°C under dry N_2 contains residual water since the hydrophilic SO_3H groups have such a strong affinity for water. Laporta and coworkers[44] report that residual water always remains in Nafion and that decomposition of the polymer occurs before the last waters are removed, based on IR studies of water in Nafion. However, the reported procedure for drying Nafion and measuring its water content which includes "heating (it) in an oven at 433K (160°C) for two days and then leaving it in the infrared cell in the presence of P_2O_5" raises suspicions about optimal water removal and accidental water reintroduction. Specifically, water content of ambient air would give an estimated RH of 0.2% at the 160°C drying temperature. More importantly, transferring the sample from oven to IR cell would undoubtedly reintroduce water to the polymer which would then rely on removal at room temperature. Bunce *et al.*[45], through NMR studies, have shown that drying at room temperature under vacuum cannot bring water content below $\lambda = 1$. Zawodzinski *et al.*[46], however, suggest (without offering support) that complete water removal is achieved when drying Nafion over P_2O_5 at room temperature or at 105°C or under vacuum at 105°C. The large change in mechanical response which is seen with increasing relative humidity from 0% to 1% strongly suggests that significant changes in bonding are occurring and argues for complete water removal occurring when drying at 85°C is done.

Bauer *et al.*[2] report a hydration stiffening effect at 70°C and above, seen in the storage modulus of Nafion from DMA studies, which they attribute to stabilization of the hydrophilic clusters. They also report a sharp increase in *E'* for the addition of the first waters of hydration to dry Nafion. They suggest that "water could (also) stabilize the membrane by the formation of hydrogen bridge bonds and oligohydrates which act as cross-linkers linking the sulfonic acid groups"[2]. As a rough estimate, they compare the bond strengths of CF_2—CF_2 (400kJ/mol) and bridging hydrogen bonds in water (20kJ/mol), sighting an increase in *E'* of ~ 1/3 as being reasonable for a polymer assembled with a fluorinated matrix in parallel with a water phase.

For dry Nafion at room temperature, high stiffness and resistance to tensile creep is attributed mainly to cross-linking between ionic groups. However, these cross-linking bonds begin to be overcome by thermal kinetic energy ca. 50°C, giving rise to the transition in instantaneous elastic modulus between 50 and 80°C (Figure 2-30). Additionally, ε_t, ε_d, and ε_v show a strong transition between 60 and 70°C (Figure 2-15), presumably also due to thermal relaxation of the ionic groups. Being that all samples were dried at 85°C, there is probably little difference in morphology between dry samples from 23 – 90°C. Further discussion on thermal history effects on microstructure and mechanical response is contained later in this chapter. Once cross-linking between ionic groups is thermally deactivated, the viscoelastic response of the matrix is being measured.

I propose that nearly complete water removal from Nafion is achieved with drying at 85°C under a flow of dry N_2 for several hours. Cross-linking between sulfonic acid groups, as shown in Figure 2-37a, occurs in Nafion that has been completely dried.

With the first addition of water, which occurs when the surrounding water activity is 0.01, hydration of sulfonic acids occurs. Hydronium ions form a bridging hydrogen bonded structure, cross-linking sulfonic acid groups (Figure 2-37b). These bonds are generally stronger than the bridging bonds in dry Nafion. Increasing bond strength for the hydrated state is evidenced by the lack of thermal transition for the hydrated states (above 0.01 water activity) and the greater resistance to creep strain at temperatures above 50°C.

If stronger bonding occurs when hydrated then when dry, why does water seem to plasticize Nafion at room temperature? The explanation which I propose is one of free volume. Adding water to Nafion increases its free volume. Water filled clusters allow for increased mobility of side groups, which is supported by faster stress relaxation seen in stress relaxation of hydrated Nafion compared to dry, as reported by Satterfield[4, 22] and Eisenberg and coworkers[11]. Additionally, it is shown that the rate of swelling strain affected by water uptake at 40°C increases dramatically with hydration (Chapter 5). Swelling strain is partially controlled by molecular relaxations. The water phase has strong bonding, but bonds are also constantly being interchanged between neighboring water species. It is this ability to interchange bonds which allows for proton transport via the Grotthus mechanism.

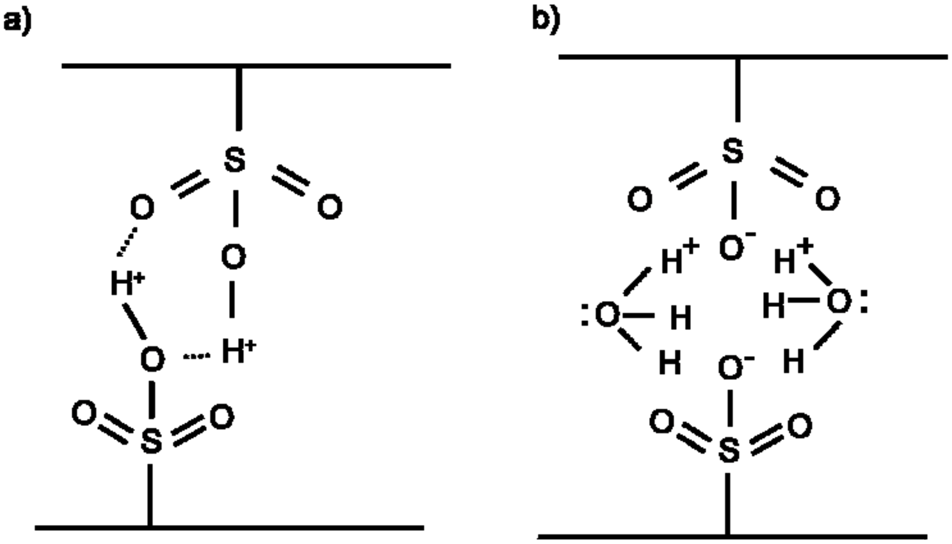

Figure 2-37 Bonding interaction between sulfonic acid groups in a) dry Nafion and b) hydrated Nafion.

As hydration increases, the water in clusters becomes more like bulk water than chemically bound water. Yet we see that, as temperature increases, maximum stiffness occurs at increasing levels of hydration. Additionally, there is evidence that the explanation for this observation is based on changes in microstructure which occur with hydration.

It is well known that diblock copolymer melts phase separate (self-assemble) into different ordered microstructural configurations due to immiscibility of different phases[47, 48]. Nafion is essentially a two phase polymer with the fluorinated backbone and side-chains constituting one phase and the sulfonic acid groups another. Water can be considered to become a part of the sulfonic acid phase when introduced to the polymer, maintaining a two phase material. The five phases normally encountered for diblock copolymer melts are shown in Figure 2-38 along with the corresponding phase diagram which shows the predicted structure based on volume fraction of components and the

Flory interaction parameter χ multiplied by the polymerization number N. Even if the exact structures shown in Figure 2-38 are not formed in Nafion with changes in hydration, it suggests that large morphological changes could exist which give rise to changes in mechanical properties.

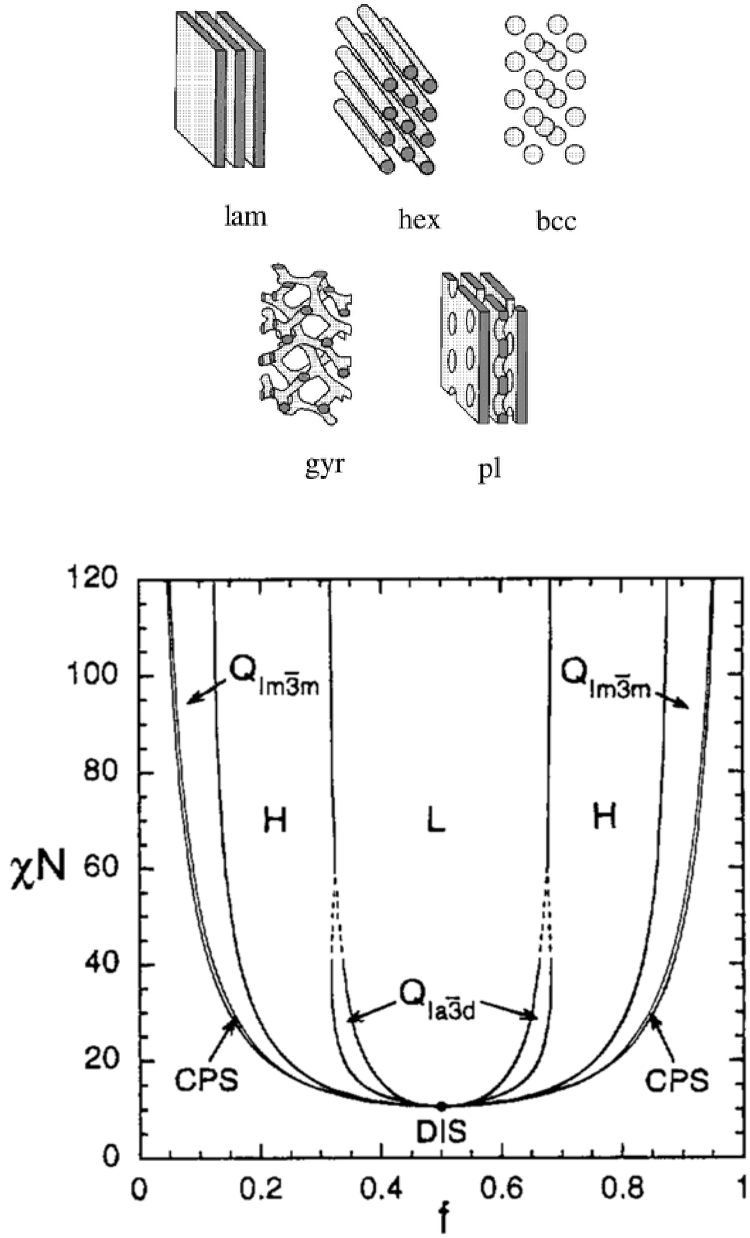

Figure 2-38 Phase diagram (bottom) of diblock copolymer melt showing five observed structures (top). Reprinted from reference 49 with permission from the ACS, © 1996.

For the case of ion exchanged Nafion, Eisenberg and coworkers have shown that exchanging H^+ for other ions significantly increase the glass transition temperature/stiffness of Nafion films in the "dry" state[11]. They attribute the increase in relaxation temperature to an increase in ionic interaction (i.e., increasing the strength of cross-links). SAXS studies suggest that the structure of Nafion in the acid and salt forms include phase separation of ionic groups[50-52]. Na^+, having greater electronegativity than H^+, will form stronger cross-links, leading to reduced creep strain. The addition of water to the Na^+ exchanged Nafion results in a decrease in ionic interaction and an increase in free volume, resulting in an increase in creep strain.

2.6.2 Thermal History Effects

It is well known that many of Nafion's physical properties are dependant on its history. Altering thermal, hydration, and mechanical pretreatment can have lasting effects on properties. For example, water uptake at 25°C is different for samples previously dried at 25, 80, and 105°C[38]. Pretreatment by submersion in boiling water and drying at lower temperatures results in greater water uptake than elevated drying temperature. It is thought that changes in microstructure are responsible for differences brought about by pretreatment[38, 51, 53-55]. Specifically, it has been proposed that high temperature drying (i.e., 105°C) results in pore (i.e., cluster) shrinkage which is increased at elevated temperature by increased mobility of side chains[38]. Elevated drying temperature results in "annealing" which brings about decreased free volume by denser packing of side and main chains and microstructure which is closer to the optimal equilibrium state of main and side chain packing[12]. Referring to the phase diagram for diblock copolymers (Figure 2-38), increasing temperature would decrease the product χN, possibly resulting in the transition from one phase to another which could be “frozen in” at lower temperatures.

A comparison was made between samples dried at 85 and 150°C. The large increase in creep strain at both 23 and 80°C and 0.00 water activity for samples dried at the elevated temperature is thought to be due to changes in microstructure, as speculated for water uptake in the previous paragraph. Elevated drying temperature brings about more efficient packing of side and main chains and also decreased cluster size. If we consider only the decrease in free volume of the matrix, we would expect a decrease in creep strain with increased drying temperature. This is commonly seen in polymers when crystallinity is increased (e.g., low density polyethylene vs. high density polyethylene[17]). However, the mechanical response of Nafion is intimately related to the cross-linking interactions occurring between acid groups. It is speculated that the elevated drying temperature produces a microstructure with smaller acid clusters[12, 38] and therefore less cross-linking. Since this microstructure after elevated drying temperature is presumed to be closer to the equilibrium structure, the structure undergoes little change when cooling to 80 or 23°C occurs. Reduced chain mobility at these lower temperatures would restrict further microstructural rearrangement, if it were thermodynamically favorable.

The large increase in creep strain at 23°C and 0.00 activity for the sample dried at 150°C strongly suggests that 1) a microstructure with significant acid cluster structures exists in “dry” Nafion if dried at 85°C (or less) and 2) the high resistance to creep strain for dry Nafion at 23°C is directly attributed to cross-linking through ionic domains. At 80°C and 0.00 activity, it can also be inferred that a cluster structure exists for the lower drying temperature. However, the contribution of cross-linking to mechanical strength is less significant at 80°C than it is at 23°C. This is based on the observation that the relative increase in creep strain at 80°C is less than what is seen at 23°C (i.e., creep strain increases by a factor of 10 at 23°C and a factor of 2 at 80°C). It is suggested that the electrostatic interactions between ionic groups in dry Nafion is very weak at 80°C relative to thermal energy, allowing small stress to overcome these interactions. The transition which appears between 50 and 80°C in the instantaneous elastic response of dry Nafion is attributed to this.

Thermal history effects were also seen for membranes which had hydration reintroduced. The effect of elevated drying temperature at both 23 and 80°C and 0.65 water activity was that creep strain decreased. This is attributed to changes in morphology, specifically that cluster size was reduced by the higher drying temperature. This is supported by the observation that Nafion dried at elevated temperature has lower water uptake (as reported by Hinatsu et al.[38]). The addition of water does result in changes in morphology from the dry state, as supported by microscopy studies, however, not all history effects are erased at this low temperature (viz., 23 and 80°C). Cluster size is still assumed to be smaller for the runs dried at 150°C. Smaller cluster size is thought to result in less water uptake. At both 23 and 80°C, decreasing water uptake slightly from the equilibrium level for normally dried membranes exposed to activity 0.65 results in decreased creep strain. Admittedly, other microstructural effects could also be contributing to the differences in viscoelastic response. For example, cluster shape could be significantly different, based on thermal history, affecting cross-linking.

The large change in mechanical response in dry Nafion brought about by elevated drying temperature should not be attributed to merely more complete water removal at the elevated temperature, though this may have a small contribution. Two pieces of evidence support this. The first is that, with normal drying, there does not appear to be a large jump in creep strain with the addition of small amounts of water at 23°C as there is at 80°C. This suggests that significant drying is achieved with drying at 85°C. The second and more compelling support suggesting that microstructural change is the main contribution is that effects of thermal history persist even after high levels of hydration are reintroduced to the polymer. Thus, even if more complete water removal occurs with the higher drying temperature, effects due to microstructural changes persist and result in differences in tensile creep response.

2.7 Conclusions

The viscoelastic response of Nafion has been measured using tensile creep over a wide range of temperature and hydration. It has been shown that water strongly affects the mechanical properties of Nafion giving rise to complicated behavior with changes in hydration and temperature. Water interacts with ionic clusters to change both microstructure and bonding interactions. At room temperature and slightly above, water plasticizes Nafion, decreasing resistance to tensile creep strain. As temperature increases, certain levels of hydration actually increase resistance to creep strain. The general trend is that resistance to creep strain occurs at higher hydration and over a larger range of water activity with increase in temperature.

In dry Nafion, interaction between ionic groups occurs through electrostatic attraction of S—H groups, resulting in polymer cross-linking. The strength of this bond is thermally deactivated between 50 and 80°C, resulting in a large decrease in creep strain resistance. The addition of water to the hydrophilic phase of Nafion produces bridging hydrogen bonds between sulfonate groups, cross-linking the polymer. These bridging bonds are stronger than the bonding occurring in dry Nafion, eliminating the transition seen between 50 and 80°C and producing mechanical response which varies much less with temperature from 23 – 120°C than dry Nafion. Reduced resistance to creep strain for hydrated Nafion at room temperature is attributed to increased free volume with hydration and thus increased freedom for side chain movement.

Changes in microstructure are thought to occur in Nafion as hydration changes. It is suggested that changes in microstructure impact mechanical properties. The exact morphology of Nafion is not fully understood and is an active area of research, but some general microstructural features, having wide acceptance, are thought to be linked to mechanical behavior.

The effects of several solvents on Nafion’s tensile creep response were investigated. It was proposed that creep strain increased for a given solvent due to the solvent’s ability to disrupt the cross-linking interaction between sulfonate groups and its ability to interact with the teflonic matrix. The alcohols investigated all gave the largest swelling strain and increase in creep strain. This was attributed the alcohols’ non-polar groups which were able to interact with the matrix.

Nafion’s mechanical properties are strongly dependant on its thermal history. It was shown that drying Nafion at 150°C produced a significant increase in creep response under dry and hydrated conditions at room temperature. The increase in creep response brought on by elevated drying temperature was attributed primarily to changes in microstructure. Specifically, it was proposed that higher drying temperature reduced aggregate size, thus reducing ionic interaction (i.e., cross-linking).

2.8 Acknowledgements

The work in this chapter would not have been undertaken without the keen insight of Prof. Jay Benziger. Prof. Benziger perceived the importance of measuring the mechanical properties of Nafion and Nafion/metal oxide composites while under a controlled environment of temperature and hydration. At the onset of this work, very little consideration had been given to the effects of hydration and temperature on the mechanical properties of Nafion, it being widely assumed that trends seen at room temperature continued at elevated temperature. Additionally, very little work was directed at measuring bulk properties under stresses relevant to PEM fuel cells or the viscoelastic response of Nafion.

Thanks also go to Dr. Barclay Satterfield for her initial efforts to measure the creep response of Nafion as a function of temperature and relative humidity. Her work provided an excellent starting point for the work done in this chapter, shaping its direction. Without her initial work, this chapter would likely have looked very different. Barclay's thorough survey of the literature, work measuring the stress relaxation of Nafion under humidified conditions, and willingness to discuss "all things Nafion" were extremely valuable to me.

Thanks go to Brent Kirby for generous assistance developing the Labview program for tensile creep data acquisition and, more importantly, for many helpful discussions concerning the analysis of creep data. Dr. Jonathan Mann provided some very helpful comments during the design of the creep instrument which are greatfully acknowledged. Christine Burgess engaged in many fruitful discussions of Nafion's microstructure and bonding interactions with me and answered my long stream of questions about various aspects of chemistry. Mr. Kenneth Andreas generously granted

me use of the chemistry machine shop and offered very helpful machining and design tips, all of which were critical in designing and building the creep instrument.

2.9 References

1. Tang, Y. L.; Karlsson, A. M.; Santare, M. H.; Gilbert, M.; Cleghorn, S.; Johnson, W. B., An experimental investigation of humidity and temperature effects on the mechanical properties of perfluorosulfonic acid membrane. *Materials Science and Engineering a-Structural Materials Properties Microstructure and Processing* **2006,** 425, (1-2), 297-304.
2. Bauer, F.; Denneler, S.; Willert-Porada, M., Influence of temperature and humidity on the mechanical properties of Nafion (R) 117 polymer electrolyte membrane. *Journal Of Polymer Science Part B-Polymer Physics* **2005,** 43, (7), 786-795.
3. Stanic, V. a. H. M., Mechanism of pinhole formation in membrane electrode assemblies for PEM fuel cells. In NASA Archive 2005.
4. Satterfield, M. B.; Majsztrik, P. W.; Ota, H.; Benziger, J. B.; Bocarsly, A. B., Mechanical Properties of Nafion and Titania/Nafion Composite Membranes for PEM Fuel Cells. *J. Polymer Science B: Polymer Physics* **2006,** 44, 2327-2345.
5. Majsztrik, P. W.; Satterfield, M. B.; Bocarsly, A. B.; Benziger, J. B., Water Sorption, Desorption and Transport in Nafion Membranes. *Journal of Membrane Science* **2007,** 301, (1-2), 93-106.
6. DuPont DuPont Fuel Cells: DuPont Nafion PFSA Membranes N-115, N-117, NE-1110. http://www.dupont.com/fuelcells/pdf/dfc101.pdf
7. Kawano, Y.; Wang, Y. Q.; Palmer, R. A.; Aubuchon, S. R., Stress-Strain Curves of Nafion Membranes in Acid and Salt Forms. *Polimeros* **2002,** 12, (2), 96-101.
8. Kundu, S.; Simon, L. C.; Fowler, M.; Grot, S., Mechanical properties of Nafion (TM) electrolyte membranes under hydrated conditions. *Polymer* **2005,** 46, (25), 11707-11715.
9. Werner, S.; Jorissen, L.; Heider, U., Conductivity and Mechanical Properties of Recast Nafion Films. *Ionics* **1996,** 2, (1), 19-23.
10. Kyriakides, S. A., Mechanical Behavior of Nafion and BPSH Membranes. *Journal of Undergraduate Materials Research* **2005,** 1, 11-14.
11. Kyu, T.; Eisenberg, A., Mechanical Relaxations in Perfluorosulfonate-Ionomer Membranes. *Acs Symposium Series* **1982,** 180, 79-110.
12. Mauritz, K. A.; Moore, R. B., State of Understanding of Nafion. *Chemical Reviews* **2004,** 104, (10), 4535-4585.
13. Uan-Zo-li, J. T. The Effects of Structure, Humidity and Aging on the Mechanical Properties of Polymeric Ionomers for Fuel Cell Applications. Master of Science, Virginia Polytechnic Institute and State University, Blacksburg, Virginia, 2001.
14. Tant, M. R.; Darst, K. P.; Lee, K. D.; Martin, C. W., Structure and Properties of Short-Side-Chain Perfluorosulfonate Ionomers. *Acs Symposium Series* **1989,** 395, 370-400.
15. Miura, Y.; Yoshida, H., Effects of Water and Alcohols on Molecular-Motion of Perfluorinated Ionomer Membranes. *Thermochimica Acta* **1990,** 163, 161-168.

16. Yeo, S. C.; Eisenberg, A., Physical-Properties and Supermolecular Structure of Perfluorinated Ion-Containing (Nafion) Polymers. *Journal of Applied Polymer Science* **1977,** 21, (4), 875-898.
17. Rosen, S. L., *Fundamental Principles of Polymeric Materials*. 2 ed.; John Wiley & Sons, Inc.: New York, 1993; p 407.
18. Zumdahl, S., *Chemical Principles*. 5th ed.; Houghton Mifflin Co.: Boston, 2005.
19. Atkins, L. J. a. P., *Chemical Princeiples; The Quest for Insight*. 2nd ed.; W. H. Freeman and Co.: New York, 2002.
20. Wang, J. Z.; Dillard, D. A.; Ward, T. C., Temperature and Stress Effects in the Creep of Armamid Fibers under Transient Moisture Conditions and Discussions on the Mechanisms. *Journal of Polymer Science Part B-Polymer Physics* **1992,** 30, (12), 1391-1400.
21. Menard, K. P., Ch. 4. In *Dynamic Mechanical Analysis; A Practical Introduction*, CRC Press: New York, 1999.
22. Satterfield, M. B. Mechanical and Water Sorption Properties of Nafion and Nafion/Titanium Dioxide Membranes for Polymer Electrolyte membrane Fuel Cells. Princeton University, Princeton, 2007.
23. Choi, P.; Jalani, N. H.; Thampan, T. M.; Datta, R., Consideration of thermodynamic, transport, and mechanical properties in the design of polymer electrolyte membranes for higher temperature fuel cell operation. *Journal of Polymer Science Part B-Polymer Physics* **2006,** 44, (16), 2183-2200.
24. Jalani, N. H.; Mizar, S. P.; Choi, P.; Furlong, C.; Datta, R., Optomechanical characterization of proton-exchange membrane fuel cells. *Proc. SPIE* **2004,** 5532, 316-325.
25. Jalani, N. H.; Choi, P.; Datta, R., TEOM: A novel technique for investigating sorption in proton-exchange membranes. *Journal Of Membrane Science* **2005,** 254, (1-2), 31-38.
26. DuPont Nafion PFSA Membrane Product Information. http://www.dupont.com/fuelcells/pdf/extrusion_cast.pdf
27. Fujimoto, C. H.; Hickner, M. A.; Cornelius, C. J.; Loy, D. A., Ionomeric poly(phenylene) prepared by diels-alder polymerization: Synthesis and physical properties of a novel polyelectrolyte. *Macromolecules* **2005,** 38, (12), 5010-5016.
28. Liu, D.; Kyriakides, S.; Case, S. W.; Lesko, J. J.; Li, Y. X.; McGrath, J. E., Tensile behavior of Nafion and sulfonated poly(arylene ether sulfone) copolymer membranes and its morphological correlations. *Journal of Polymer Science Part B-Polymer Physics* **2006,** 44, (10), 1453-1465.
29. Kawano, Y.; Wang, Y. Q.; Palmer, R. A.; Aubuchon, S. R., Stress-Strain Curves of Nafion Membranes in Acid and Salt Forms. *Polimeros: Ciencia e Technologia* **2002,** 12, (2), 96-101.
30. Kundu, S.; Simon, L. C.; Fowler, M.; Grot, S., Mechanical properties of Nafion$^{(TM)}$ electrolyte membranes under hydrated conditions. *Polymer* **2005,** 46, (25), 11707-11715.
31. Haddad, Y. M., *Viscoelasticity of Engineering Materials*. Chapman & Hall: 1995; p 33-35.
32. Liu, D.; Hickner, M. A.; Case, S. W.; Lesko, J. J., Relaxation of proton conductivity and stress in proton exchange membranes under strain. *Journal Of*

Engineering Materials And Technology-Transactions Of The Asme **2006,** 128, (4), 503-508.

33. Uan-Zo-li, J. T. Thesis: The Effects of Structure, Humidity and Aging on the Mechanical Properties of Polymeric Ionomers for Fuel Cell Applications. Master of Science, Virginia Polytechnic Institute and State University, Blacksburg, Virginia, 2001.

34. Majsztrik, J. B. B. a. P. W. Environmental control chamber for mechanical testing instrumentation accurately controlling temperature, relative humidity and pressure during mechanical tests. April 10, 2007, 2007.

35. Majsztrik P. W., B. A. B., and Benziger J. B., An instrument for environmental control of vapor pressure and temperature for tensile creep and other mechanical property measurements *Rev. Sci. Instrum.* **2007,** 78, 103904-103904-7.

36. Elliott, J. A.; Hanna, S.; Elliott, A. M. S.; Cooley, G. E., The swelling behaviour of perfluorinated ionomer membranes in ethanol/water mixtures. *Polymer* **2001,** 42, (5), 2251-2253.

37. Ferry, J. D., *Viscoelastic Properties of Polymers*. 2nd ed.; John Wiley & Sons, Inc.: New York, 1970; p 671.

38. Hinatsu, J. T.; Mizuhata, M.; Takenaka, H., Water-Uptake Of Perfluorosulfonic Acid Membranes From Liquid Water And Water-Vapor. *Journal Of The Electrochemical Society* **1994,** 141, (6), 1493-1498.

39. Hsu, W. Y.; Gierke, T. D., Ion-Transport and Clustering in Nafion Perfluorinated Membranes. *Journal of Membrane Science* **1983,** 13, (3), 307-326.

40. Gierke, T. D.; Munn, G. E.; Wilson, F. C., The Morphology in Nafion Perfluorinated Membrane Products, as Determined by Wide-Angle and Small-Angle X-Ray Studies. *Journal of Polymer Science Part B-Polymer Physics* **1981,** 19, (11), 1687-1704.

41. Roche, E. J.; Pineri, M.; Duplessix, R., Phase Separation in Perfluorsulfonate Ionomer Membranes. *Journal of Polymer Science* **1982,** 20, 107-116.

42. Gebel, G.; Aldebert, P.; Pineri, M., Swelling Study Of Perfluorosulphonated Ionomer Membranes. *Polymer* **1993,** 34, (2), 333-339.

43. Phillips, A. K.; Moore, R. B., Mechanical and transport property modifications of perfluorosulfonate ionomer membranes prepared with mixed organic and inorganic counterions. *Journal of Polymer Science Part B-Polymer Physics* **2006,** 44, (16), 2267-2277.

44. Laporta, M.; Pegoraro, M.; Zanderighi, L., Perfluorosulfonated membrane (Nafion): FT-IR study of the state of water with increasing humidity. *Physical Chemistry Chemical Physics* **1999,** 1, (19), 4619-4628.

45. Bunce, N. J.; Sondheimer, S. J.; Fyfe, C. A., Proton Nmr Method for the Quantitative-Determination of the Water-Content of the Polymeric Fluorosulfonic Acid Nafion-H. *Macromolecules* **1986,** 19, (2), 333-339.

46. Zawodzinski, T. A.; Derouin, C.; Radzinski, S.; Sherman, R. J.; Smith, V. T.; Springer, T. E.; Gottesfeld, S., Water-Uptake by and Transport through Nafion(R) 117 Membranes. *Journal of the Electrochemical Society* **1993,** 140, (4), 1041-1047.

47. Bates, F. S.; Schulz, M. F.; Khandpur, A. K.; Forster, S.; Rosedale, J. H.; Almdal, K.; Mortensen, K., Fluctuations, Conformational Asymmetry and Block-Copolymer Phase-Behavior. *Faraday Discussions* **1994**, 7-18.

48. Bates, F. S.; Fredrickson, G. H., Block Copolymer Thermodynamics - Theory and Experiment. *Annual Review of Physical Chemistry* **1990,** 41, 525-557.
49. Matsen, M. W.; Bates, F. S., Unifying weak- and strong-segregation block copolymer theories. *Macromolecules* **1996,** 29, (4), 1091-1098.
50. Yeo, S. C.; Eisenberg, A., Effect of Ion Placement and Structure on Properties of Plasticized Polyelectrolytes. *Journal of Macromolecular Science-Physics* **1977,** B13, (3), 441-484.
51. Duplessix R., E. M., Rodmacq B., Volino F., Roche E., Eisenberg A., Pineri M., , In *Water in Polymers*, P., R. S., Ed. American Chemical Society: Washington, DC, 1980; Vol. No. 127, p 469.
52. Gierke, T. D., The Morphology in Nafion Perfluorinated Membranes and Its Effect on Ion-Transport. *Bulletin of the American Physical Society* **1981,** 26, (3), 462-462.
53. Yeo R. S., a. Y. H. L., In *Modern Aspects of Electrochemistry*, Conway B. E., W. R. E., Bockris J. O'M., Ed. Plenum Press: New York, 1985; Vol. No. 16.
54. Zawodzinski, T. A.; Derouin, C.; Radzinski, S.; Sherman, R. J.; Smith, V. T.; Springer, T. E.; Gottesfeld, S., Water Uptake by and Transport Through Nafion 117 Membranes. *Journal of the Electrochemical Society* **1993,** 140, (4), 1041-1047.
55. Zawodzinski, T. A.; Springer, T. E.; Davey, J.; Jestel, R.; Lopez, C.; Valerio, J.; Gottesfeld, S., A Comparative-Study of Water-Uptake by and Transport through Ionomeric Fuel-Cell Membranes. *Journal of the Electrochemical Society* **1993,** 140, (7), 1981-1985.

3 Water Permeation through Nafion

3.1 Introduction

The uptake and transport of water in the membranes of PEM fuel cells is critically important to their operation[1-7], affecting both steady state and dynamic response. Membrane hydration is required for high proton conductivity. Water enters the membrane from anode or cathode feeds— either from humidified feeds or from product water generated at the cathode—and diffuses through the membrane from high concentration to low. Since Nafion has long been the most common membrane material used in PEM fuel cells, numerous investigators have studied water uptake and transport of the material [1, 2, 5, 7, 8]. The focus of these studies has been to determine values for the diffusion coefficient of water in Nafion. Values reported for the diffusivity of water in Nafion vary depending on experimental technique with values spanning over three orders of magnitude at a given temperature.

Three techniques are commonly used to study water transport in Nafion; mass uptake, NMR relaxation, and water permeation. Diffusivity values reported in the literature are summarized in Table 3-1[1]. The general findings are that diffusivity increases with temperature and water content. Diffusivity reported by NMR measurements gives the highest values of diffusivity ($\sim 10^{-6}$ cm^2/s) followed by permeation and water desorption ($\sim 10^{-7}$ cm^2/s) and water sorption ($\sim 10^{-8}$ cm^2/s).

The technique of NMR relaxation can be used to determine self diffusion of water in Nafion. It involves applying a pulsed electromagnetic gradient to water molecules in a Nafion membrane and monitoring relaxation times. This technique only considers the motion of water within the membrane and neglects the influence of a water activity gradient. It also neglects interfacial mass transport at the membrane interface. Additionally, measuring self diffusion with NMR does not consider the tortuosity of the material or the fact that the membrane has hydrophobic domains through which no transport can occur. As a result, values for *D* determined by NMR are high and need to be adjusted[9].

Mass uptake experiments involve monitoring the mass of a Nafion membrane or film as it either sorbs or desorbs water. For sorption experiments, a membrane with low water activity is introduced quickly to an environment of high water activity (vapor or liquid) and the mass of the sample recorded as a function of time until equilibrium is reached. For desorption experiments, the membrane has high water activity at the start and undergoes water loss to the lower water activity surroundings. Mass uptake involves interfacial mass transport at the membrane interface, water diffusion in the Nafion, a solvation reaction between sulfonic acid and water, as well as swelling and relaxation of the polymer network. The technique is dynamic, with properties changing as a function of time. As a result, mass uptake is very complicated and is not useful for determining diffusivity unless all aspects of transport are considered and carefully modeled[1, 7, 10]. Several investigators have wrongly assumed Fickian water sorption dynamics, leading to erroneous estimations of water diffusivity in Nafion[11-13].

This chapter focuses on measuring water permeation through Nafion. Permeation experiments closely approximate the transport of water into and through the membrane occurring in an operating fuel cell; mass transport at the membrane interfaces as well as diffusion through the membrane are present during steady state permeation. Experiments

Table 3-1 Summary of diffusivity values reported in the literature for water in Nafion[1].

Experimental technique	Diffusivity result (cm^2/s)	Diffusivity at 25°C (cm^2/s)	
Water sorption from vapor		2 x 10^{-8}	Takamatsu et al.[11]
Water sorption from vapor	6.3 x $10^{-3}e^{-24000/T}$	1.8 x 10^{-6}	Takamatsu et al.[11]
Desorption		1.1 x 10^{-7}	Takamatsu et al.[11]
NMR	6.3 x $10^{-3}e^{-24000/T}$	1.8 x 10^{-6}	Yeo and Eisenberg[8]
Water sorption	(0.1-1) x 10^{-7} increasing with λ		Morris and Sun[12]
Desorption	(0.25-4) x 10^{-7} increasing with λ		Morris and Sun[12]
Water sorption	10^{-8} to 10^{-7} to 10^{-9} goes through max with λ		Legras et al.[13]
NMR		2.5 x 10^{-6}	Zawodzinski et al. [14]
Streaming potential in liquid water	1.25 x 10^{-5} at 80 °C	6 x 10^{-6}	Okada et al.[15]
Permeation through an MEA	2.1 x 10^{-3} λ $e^{-2436/T}$	2.2 x 10^{-6} at $\lambda = 4$	Motupally et al.[16]
Water sorption from vapor	5 x 10^{-8} at 60°C		Gates and Newman[17]
NMR	10^{-7} at low λ, 10^{-6} at high λ, D increases with T		Gong et al.[18]
Water sorption	7.7 x 10^{-9} at 32°C		Rivin et al.[19]
Desorption	2.6 x 10^{-8} at 32°C		Rivin et al.[19]
Permeation	1.3 x 10^{-7} to 3.1 x 10^{-6} increasing with a_w		Rivin et al.[19]
Water sorption	$K_{sorption}$ = 0.03-0.04s^{-1} at λ = 2-3,23°C		Krtil et al.[20]
	$K_{sorption}$ = 0.01-0.02s^{-1} at λ = 8-10,23°C		Krtil et al.[20]
Desorption	$K_{desorption} = 5k_{sorption}$		Krtil et al.[20]
Desorption	5 x 10^{-7} at 40%RH, 2 x 10^{-6} at 10%RH		Damay and Klein[21]

were designed to measure water permeation from vapor feeds of different activity, as well as from liquid water, through Nafion and into vapor. Permeation was measured as a function of gas flow rate and temperature. Different membrane thicknesses were tested in order to separate interfacial mass transport resistance from diffusion resistance. Finally, the effect of an electrode at the surface of a Nafion membrane on water permeation was investigated.

3.2 **Experimental**

3.2.1 **Materials**

The following extruded Nafion films with 1,100 EW were purchased from Ion Power: N112, N115, and N1110. They were cleaned and protonated according to the procedure outlined in Chapter 2. Once cleaned, they were stored in liquid water at room temperature and installed in the permeation cell fully hydrated. Membranes without electrodes were installed without using a gasket since the Nafion made a good seal with the permeation cell.

Some of the permeation tests included an electrode. For these tests, a woven carbon cloth electrode purchased from E-TEK was used which had a gas diffusion/catalyst layer and was treated with PTFE wet proofing at the gas side (E-TEK A-6: ELAT, single sided and hand fabricated). The material was highly hydrophobic at the gas side due to PTFE treatment. A membrane electrode assembly (MEA) was made using Nafion N115 and the carbon cloth electrode. The electrode was only applied to one side of the Nafion with the other side being left bare. An electrode measuring 2.5cm x 2.5cm, oversized relative to the 1cm x 1cm flow channel, was hot pressed to the membrane at 135°C using a total force of 8,900N (average pressure of 1.53MPa over the entire MEA). A square silicone rubber gasket, 7.6 cm on a side with a hole in the center cut to receive the electrode, was applied to one side of the membrane. To increase the pressure transferred to the electrode during hot pressing, a 1/8” thick rubber sheet was placed over the MEA during this process. Hot pressing was done starting with fully hydrated Nafion. The MEA was in contact with the press during pre-heating with only a small amount of pressure applied. Pre-heating took ~13 minutes after which full pressure was applied for 90 seconds. Good adhesion between the electrode and Nafion was achieved only when the rubber sheet was used.

3.2.2 Permeation instrument

Water permeation was measured through Nafion membranes using a custom built permeation cell housed in an isothermal enclosure. The permeation cell was made with two separate halves which were machined from 1” thick polycarbonate (Figure 3-1). Each half of the cell had a square 1 cm^2 flow channel machined in the center which had an inlet and outlet through which vapor or gas could be flowed. The halves were designed to be bolted together with a membrane separating the two flow channels. A maximum operating temperature of ~100°C for the cell was based on the upper working temperature of the polycarbonate. The inlet and outlet for each cell half was connected to 1/8” PTFE tubing with a tube to female pipe adapter.

One of the permeation cell sides had 316 stainless steel electrodes on opposite sides of the flow channel. The electrodes were polished flush with the face of the cell half and were used to measure the proton conductivity along the length of the membrane. Each electrode had an electrical contact made from 1/8” diameter stainless steel rod attached with silver solder to the electrode and protruding out of the back of the cell half.

Proton conductivity was used as a rough measure of the average hydration level of the membrane during permeation experiments.

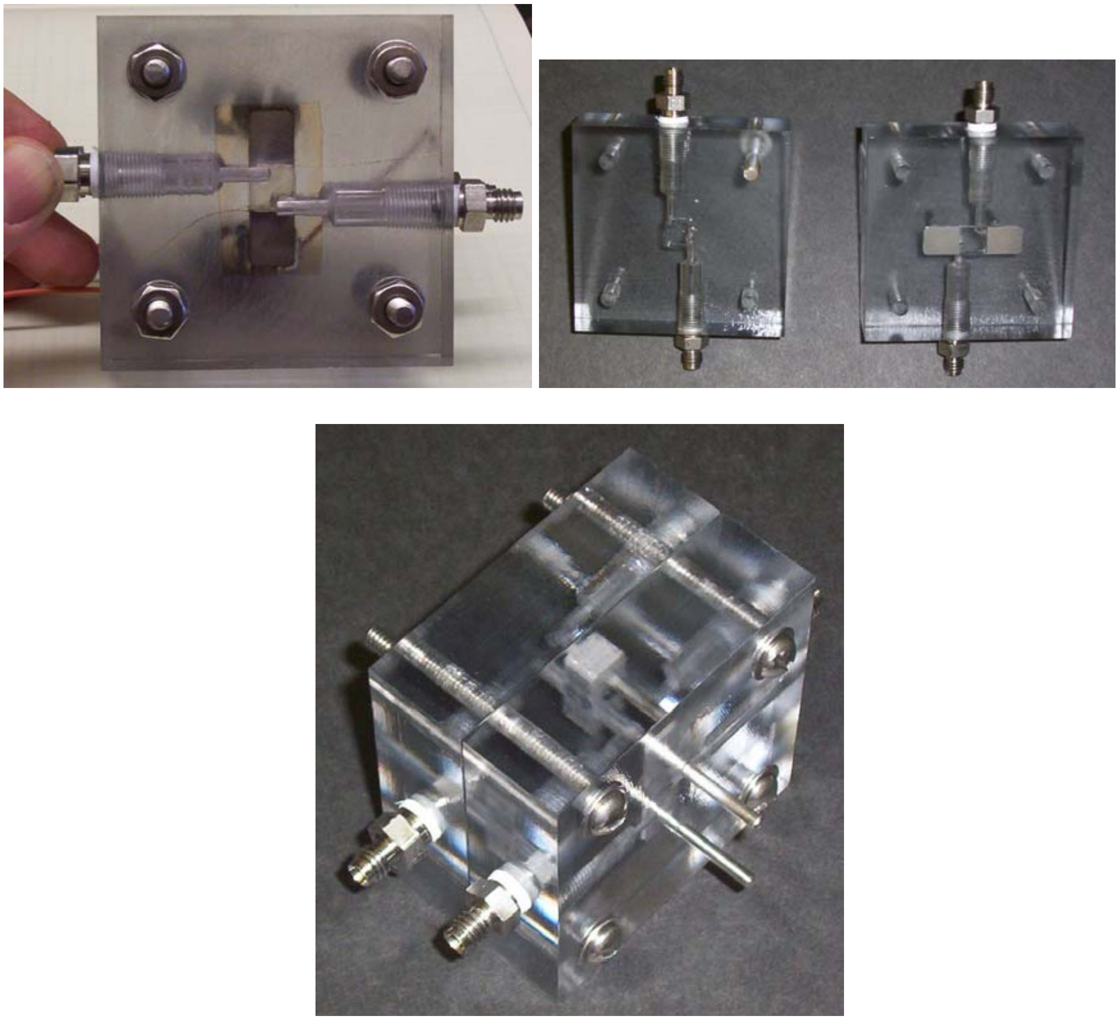

Figure 3-1 Photographs of the permeation cell from top left proceeding clockwise: 1) back of the fully assembled cell showing the outline of a membrane (brown translucent rectangle in cell center); 2) inside of disassembled cell halves showing square flow channels, stainless steel electrodes (right cell half), clearance holes for bolts, and pipe to tubing adapters; 3) isometric perspective of cell front showing the two electrode electrical contact rods protruding normal to the polycarbonate cell face.

Water activity was introduced to one flow channel by flowing either liquid water or humidified N_2 through it. Dry N_2 was caused to flow through the other flow channel, creating an activity gradient resulting in water transport through the membrane separating the two flow channels. Figure 3-2 shows a schematic representation of the permeation cell along with controls and instrumentation.

The average water activity of the N_2 streams exiting both sides of the cell were separately measured using commercially available relative humidity sensors (Sensirion model SHT75) mounted in custom built housings detailed in section 7.3 of the appendix. The temperature range of these sensors was -40-124 °C.

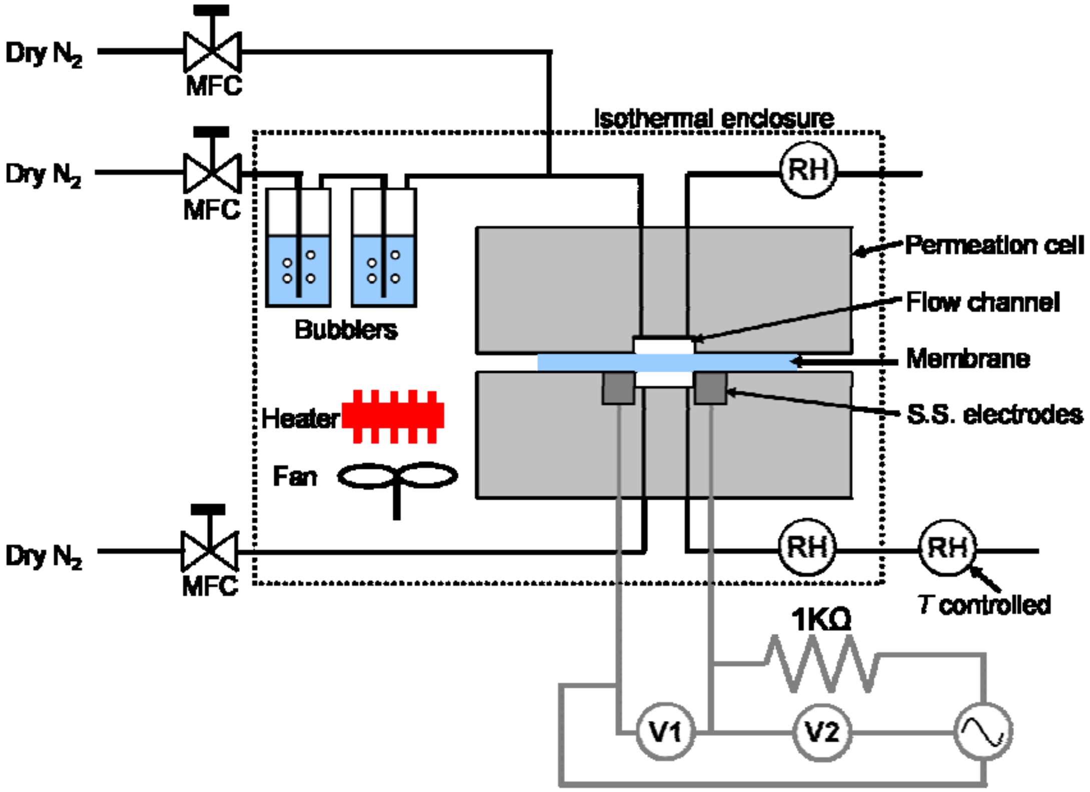

Figure 3-2 Schematic representation of permeation experiment. The bubblers, permeation cell, and relative humidity sensors were maintained in an isothermal enclosure (dashed line) during experiments. One relative humidity sensor, on the dry side exit, was located outside the isothermal enclosure with independent temperature control.

The operating range of the humidity sensors was 10-90% RH, above and below which the error in measurement increased linearly to ±10%RH at both extremes. In order to accurately measure water vapor content which fell below 10%RH at the temperature of the test, an additional relative humidity sensor was installed outside the heated enclosure and cooled to a point where the relative humidity of the gas on the feed side was above 10%RH. The sensor was also mounted in a custom-made housing similar to the one shown in section 7.3 of the appendix. Cooling was accomplished by either placing the sensor housing on ice or allowing the sensor to cool to room temperature. In some cases, heating tape was used to heat the housing and connecting tube above the ambient but below the test temperature.

A peristaltic pump was used to provide a constant flow of liquid water. The flow rate was kept low (~5mL/min) to prevent the pressure from increasing much above atmospheric pressure. Humidified N_2 was supplied to the feed side by mixing two N_2 streams, one which was passed through a series of two bubblers to establish a water activity of ~0.9. By mixing the dry and humidified nitrogen feeds, water activity between 0.00 and 0.9 was obtained. Rotameters were used to control the dry and humidified feeds on the feed side. The total flow rate of N_2 on the feed side was at least 1L/min and as high as 3 L/min. Such high flow rates were used to ensure that the drop in relative humidity between the gas entering and leaving the feed side flow channel was less than 2%. Relative humidity at the feed side exit was measured and compared with the flow of dry N_2 at the dry side set to 0 and 1L/min in order to determine this.

Dry N_2 flow on the dry side was controlled by either mass flow controllers or a rotameter. For flows between 5 and 50 sccm, an Alborg mass flow controller was used (model GFC 17). For flows between 75 and 1,000 sccm, an MKS mass flow controller was used (model 1179 A-13 CR-BV). A rotameter was used for flows greater than 1,000 sccm. Bubble meters were used to calibrate the mass flow controllers and rotameter.

The isothermal housing (Figure 3-3 and Figure 3-4) consists of an insulated base and a removable insulated top. The base houses a finned heater and has an aluminum mounting plate. The mounting plate has slots machined in it to allow for good transport of heat and rows of threaded holes as attachment points for hardware. Tubing and wires required for instrumentation etc. enter the base and can be accessed above the mounting plate. A fan (heating duct booster fan) provides forced convection to maintain an isothermal environment. A PID controller is used to control the temperature in the chamber. Coiled metal tubing segments (¼ ” diameter copper for N_2 and 1/8” diameter for liquid water) are included in the flow lines to bring the temperature of the incoming fluids to that of the chamber.

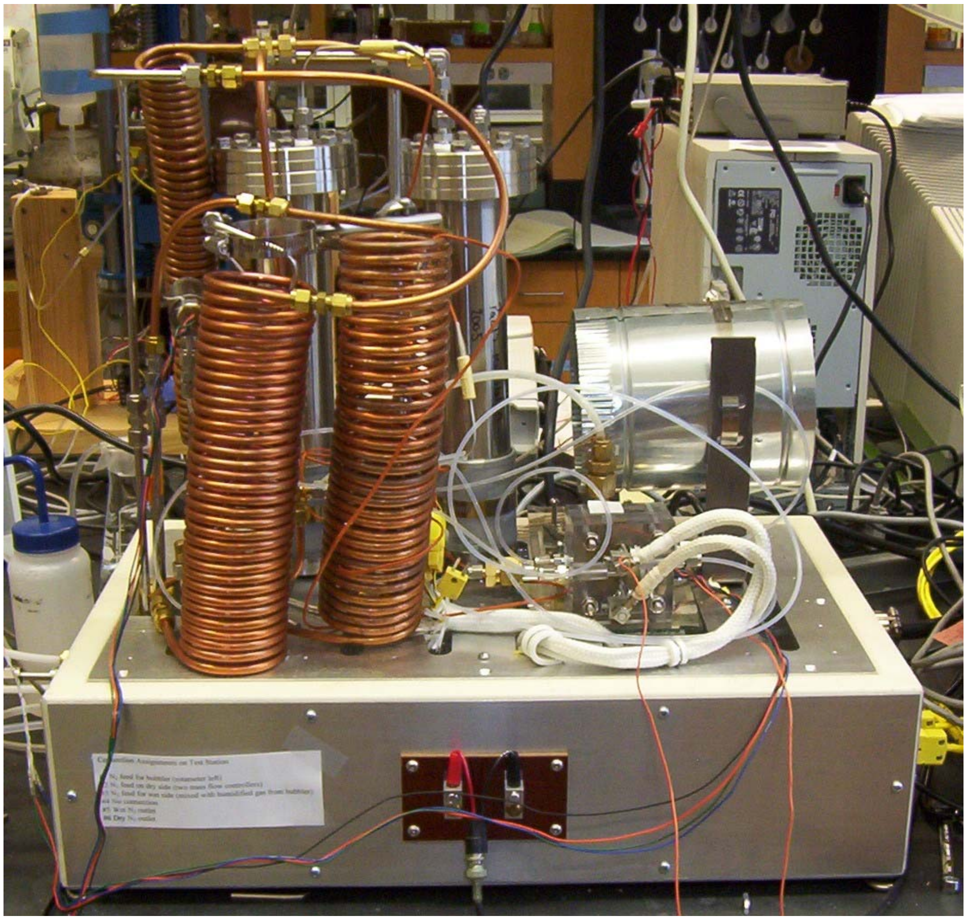

Figure 3-3 Photograph of permeation setup including the permeation cell, bubblers, heated base, and fan. Insulated top removed.

Figure 3-4 Photographs of instrumentation for controlled isothermal environment used for permeation experiments. Clockwise from top left: 1) base of instrument showing tubing bulkheads (front face) and aluminum base plate; 2) oven base with insulated top in place; 3) top view of oven base with base plate installed; and 4) top view of oven base with aluminum base plate removed to show finned heater and tubing.

Humidification bubblers were built from stainless steel tube/pipe and flanges. The bubblers had a total volume of ~ 1.5L which was partly filled with liquid water. N_2 was passed through a tube which entered at the bottom of the bubbler through a frit, creating bubbles which become humidified as they rose to the surface of the water, exiting at the top of the bubbler through a tube to pipe adapter. The bubblers were located inside the isothermal chamber, being heated to the temperature of the chamber and eliminating condensation that might otherwise arise from thermal gradients.

Proton conductivity was measured using ac impedance at a fixed frequency of 500Hz. To do this, a function generator supplied a sinusoidal voltage to the membrane which was one leg of a voltage divider. A 1 V_{rms}driving voltage was applied laterally across the membrane in series with a 1kΩ resistor (Figure 3-2). Two voltmeters were used to measure the voltage drop across both legs of the voltage divider. Previous experiments have shown that the resistance of Nafion membranes can be determined using fixed excitation frequencies above 2 Hz[22].

3.3 Water permeation experiments

3.3.1 Permeation measurements

Steady state water permeation was measured through Nafion membranes from either liquid water or water vapor into dry nitrogen. The activity of water on the feed side a_f (higher water activity) was controlled directly while the activity on the dry side a_d (lower water activity) was indirectly controlled by altering the flow rate of dry N_2 entering the flow cell. Water activity exiting both sides of the cell was measured, providing a measure of the thermodynamic driving force for water permeation through the membrane.

Because of the flow channel design, the composition within the flow channels was assumed to be nearly uniform and equal to the composition at the exit (Figure 3-5). Good mixing in the flow channels was assumed based on their dimensions and was approximated as a continuous stirred tank reactor (CSTR). Designing the flow channels this way greatly simplified our analysis of permeation, allowing us to assume 1D transport.

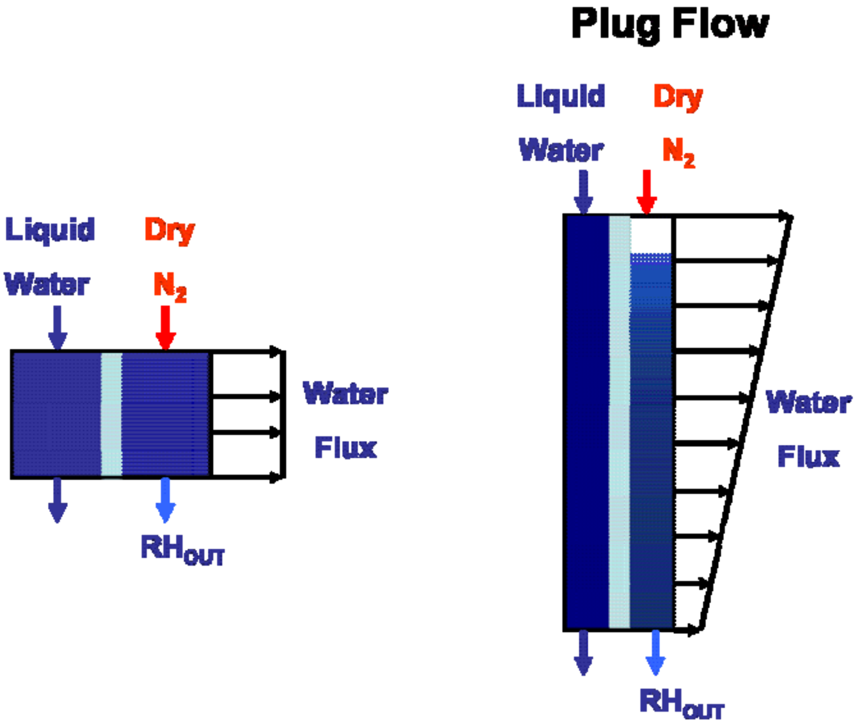

$$Permeation \propto \left(a_1 - \frac{RH_{OUT}}{100}\right) \qquad Permeation \propto \int_0^{RH_{OUT}} \left(a_1 - \frac{RH_{OUT}}{100}\right) dRH$$

Figure 3-5 Permeation of liquid water through a membrane into a flow of dry gas. Two flow channel designs are shown: left) continuous stirred tank reactor and right) plug flow reactor (serpentine flow channels).

This is in contrast to what would result if serpentine flow channels were employed, the flow pattern found in most fuel cells. As illustrated in Figure 3-5, serpentine flow channels result in water concentration which varies with position. This is because long, thin channels prevent mixing along the length of the channel, creating what is known as the plug flow reactor (PFR). Knowing only the exit concentration, one would need to integrate over relative humidity in order to estimate the permeation at each point based on driving gradient. Thus, with serpentine flow channels, transport is averaged spatially and temporally.

Steady-state water flux was measured at fixed temperature, feed side water activity, and dry side N_2 flow rate. To do this, relative humidity at the exit of the dry side was measured and monitored in real time until a steady state value was reached. A representative plot of dry side relative humidity vs. time is shown in Figure 3-6. Knowing temperature T, dry N_2 flow rate Q, and relative humidity ratio ω at the dry side, the water flux was calculated from the following expression,

$$Flux = \omega \dot{m}_g = \omega Q \rho_g \,, \qquad \text{Equation 3-1}$$

where $\dot{m}_g$ is the mass flow rate of dry N_2 at the dry side, Q is the volume flow rate of dry N_2 at the dry side, and ρ_g. ω is the mass ratio of water to air and is determined as follows;

$$\omega = \frac{m_V}{m_g} = \frac{M_V P_V}{M_g P_g} \,, \qquad \text{Equation 3-2}$$

where m_V is the mass of water vapor in a given volume of humid N_2, m_g is the mass of N_2 in that volume, M_V is the molecular weight of water, M_g is the molecular weight of N_2, p_V is the partial pressure of water vapor, and p_g is the partial pressure of the N_2. Knowing the temperature and relative humidity RH of the vapor mixture, p_V and p_g can be calculated from the following equations,

$$p_V = p_{sat} \frac{RH}{100} \qquad \text{Equation 3-3}$$

$$p_g = p_T - p_V = p_T - p_{sat} \frac{RH}{100} \,. \qquad \text{Equation 3-4}$$

Here, p_T is the total pressure of the water vapor/gas mixture (assumed to be 1 bar) and p_{sat} is the saturation vapor pressure of liquid water at the temperature at which the relative humidity was measured. Combining the above equations, we obtain an expression for the flux of the water through a membrane of area A_{mem},

$$Flux = \frac{Q\rho_g}{A_{mem}} \frac{M_V \frac{RH}{100} p_{sat}}{M_g \left(p_{tot} - \frac{RH}{100} p_{sat} \right)} \quad , \qquad \text{Equation 3-5}$$

The Goff-Gratch equation was used to calculate the saturation vapor pressure of water at temperature T (section 7.5 of the appendix).

By varying the flow rate of dry N_2 entering the dry side of the permeation cell, the steady state flux can be obtained as a function of the dry N_2 flow rate, as shown in Figure 3-7. In this plot, each point represents steady state permeation with dry N_2 flow rate, temperature, and feed side activity held fixed. We notice that flux increases with dry N_2 flow rate. There are two reasons for the increase:

1) As dry N_2 flow rate increases, the activity of water in the dry side flow channel decreases because it has a shorter residence time in the flow channel.

2) The component of interfacial transport resistance at the membrane vapor interface on the dry side k_d attributed to boundary layer thickness decreases with flow rate.

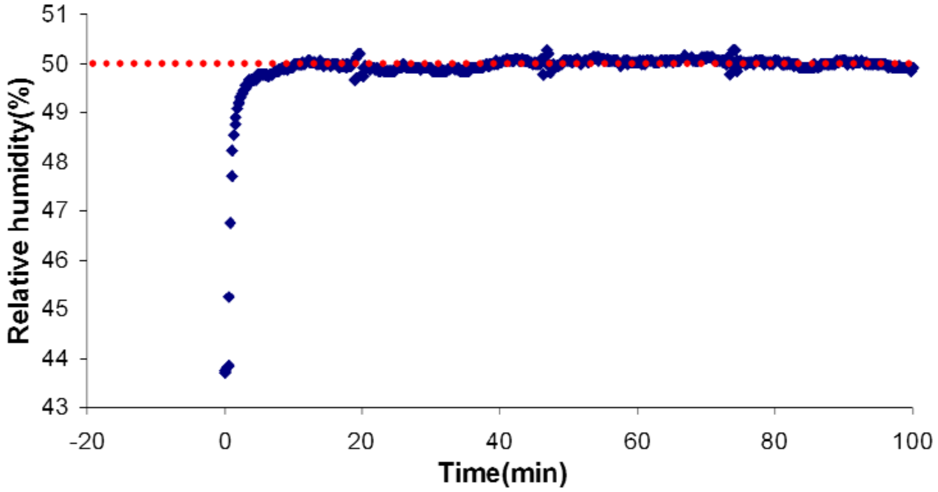

Figure 3-6 Raw permeation data showing the relative humidity of N_2 exiting the permeation cell at the dry side. The red dashed line indicates the average relative humidity at steady state. Relative humidity was measured at 80°C for a N1110 membrane with 80%RH vapor on the feed side and N_2 flow rate at the dry side of 10 mL/min.

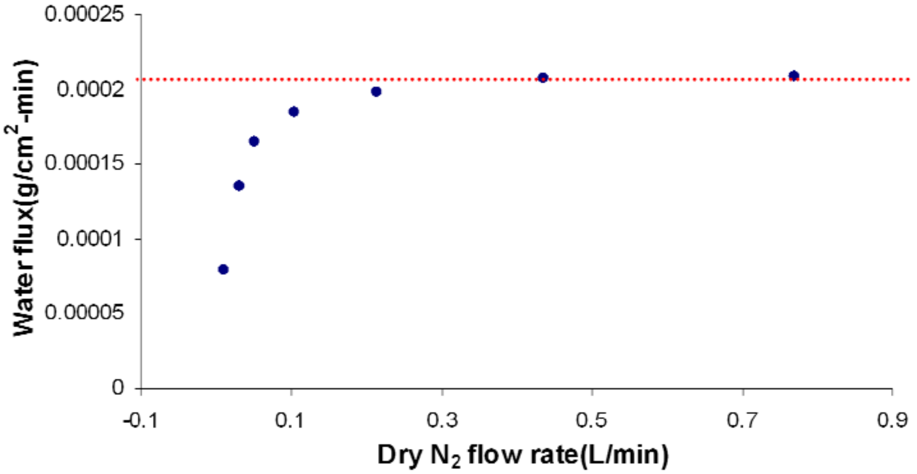

Figure 3-7 Representative plot of steady state permeation of water through Nafion at a fixed temperature and feed side water activity as a function of N_2 flow rate at the dry side. This plot is for permeation of water vapor with activity of 0.8 at the feed side through Nafion N1110 at 80°C.

3.3.2 1D permeation

Ideal 1D water permeation through a membrane from high to low water activity is shown in Figure 3-8. Water activity outside the membrane in the bulk vapor or water phases is fixed at a_f and a_d. At steady state, a water gradient across the thickness of the membrane is established based on the diffusivity *D* of the membrane. If *D* does not vary with water activity, the water activity profile is linear. If *D* depends on water activity, the profile is non-linear. The activities at the membrane's surfaces, $a_{m,f}$ and $a_{m,d}$, are not equal to the activities out in the bulk surrounding the membrane. The difference in activities between membrane surface and bulk is attributed to an interfacial mass transport coefficient *k*.

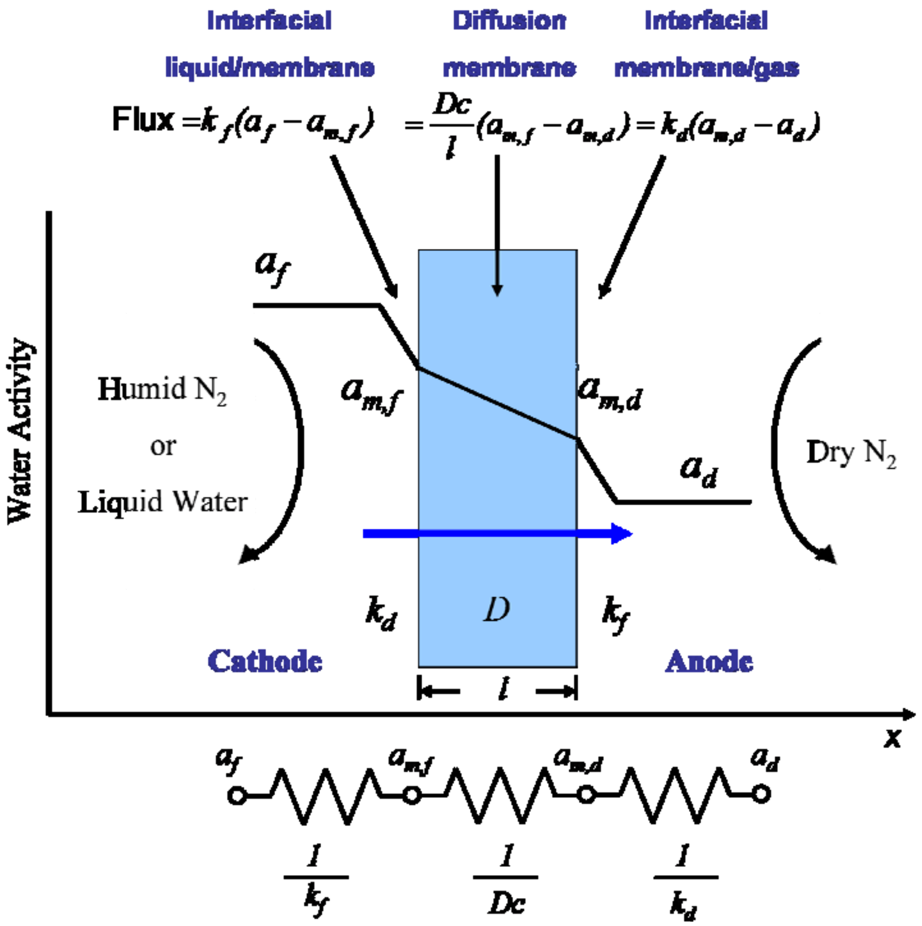

Figure 3-8 1D permeation of liquid water pr water vapor through a Nafion membrane into dryN_2 from high water activity to low activity. Activity profile is shown along with mass transport coefficients. Steady state permeation equations are shown at the top of the figure while the equivalent network of resistors describing mass transport resistances is shown at the bottom.

The interfacial mass transport coefficient *k* is attributed to both phase change as well the boundary layer occurring at the membrane interface. If we compare a water concentration profile outside and through the membrane to the water activity profile (Figure 3-9), we notice that there is a discontinuous jump between the bulk phase and the membrane. The discontinuity arises from the differences in concentration in the condensed phase of the membrane and that of water in the liquid or vapor phases. Water concentration is greater in liquid water and less in the vapor phase than in Nafion. At room temperature and atmospheric pressure, the concentration of water in the liquid phase is 55 x 10^{-3}mol/cm^3, 1.28 x 10^{-6}mol/cm^3 for saturated vapor, and 5.5 x 10^{-4} mol/cm^3 for Nafion with $\lambda = 12$[xiii].

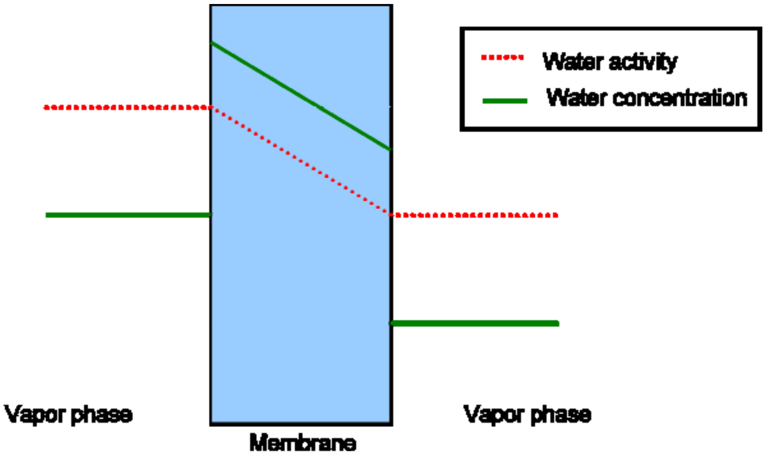

Figure 3-9 Water activity and concentration profiles across a Nafion membrane between surrounding water vapor with different chemical potential on each side of the membrane.

The boundary layer occurring at the membrane surface arises from a zero velocity boundary condition at the membrane/vapor interface which results in fluid phase velocity profile different from the bulk fluid (Figure 3-10). For mass transport into the vapor phase, diffusion through the boundary layer into the bulk must occur. For non-laminar flow conditions, convection as well as diffusion takes place. Boundary layer thickness decreases with fluid velocity (flow rate), increasing *k*. For a liquid water/membrane interface, interfacial mass transport resistance is assumed to be negligible[1]. This assumption is based on the high concentration of water available in liquid water at the interface (i.e., liquid water persists up to the membrane interface with activity of 1, but for vapor transport, a drop in activity from the bulk vapor to the membrane interface

---

[xiii] Calculated assuming a 10% volume expansion.

exists). It is further supported by the observation that water uptake by Nafion submerged in liquid water is very fast[5]. As will be discussed later, the nature of Nafion's surface when in contact with liquid water or water vapor will strongly impact interfacial transport.

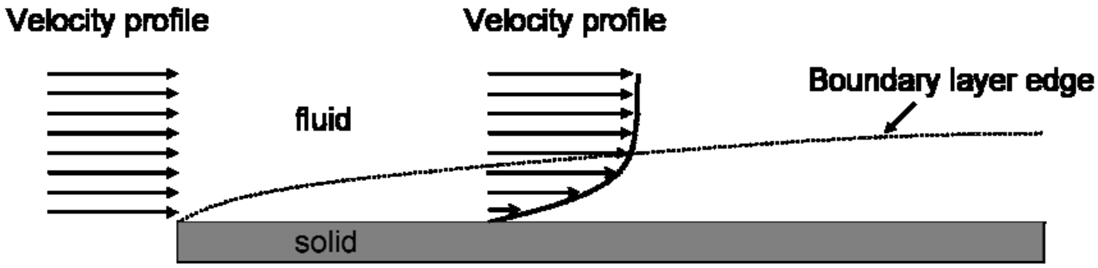

Figure 3-10 Development of a boundary layer in fluid (liquid or gas) flow over a solid surface. The boundary layer arises from a no slip boundary condition at the fluid/solid interface and results in a velocity profile which differs from the uniform free stream profile.

Water flux into the membrane can be calculated based on the interfacial transport coefficient k_l and the water activity in the bulk and in the membrane according to the following expression:

$$flux = k_f(a_f - a_{m,f}) . \qquad \text{Equation 3-6.}$$

A similar expression is obtained for water transport from the membrane into the vapor phase:

$$flux = k_d(a_{m,d} - a_d) . \qquad \text{Equation 3-7.}$$

Water flux through the membrane, based on diffusion, is given by

$$flux = \frac{Dc}{l}(a_{m,f} - a_{m,d}) , \qquad \text{Equation 3-8}$$

where c is the concentration of water in the membrane and l is the membrane thickness. The expression for flux through the membrane given by equation 3 was obtained by solving Fick's first law which describes steady state diffusion;

$$Flux = -D\frac{\partial c}{\partial x}, \qquad \text{Equation 3-9}$$

where c is the concentration of the diffusing species and x is position. D is assumed to be constant in this expression.

An overall mass transfer coefficient k_o or permeability can be defined based on diffusion and interfacial mass transport combined. Thus, flux can be related to only the water activities in the bulk surrounding the membrane;

$$flux = k_o(a_f - a_d). \qquad \text{Equation 3-10}$$

This expression is useful since there is no way to directly measure the water activities at the membrane surface while a_f and a_d can be measured.

The principle of conservation of mass dictates that, at steady state conditions, the flux into and out of the membrane is equal to the flux through the membrane. As such, equations 1-3 can be related to the overall flux;

$$flux = k_o(a_f - a_d) = k_f(a_f - a_{m,f}) = \frac{Dc}{l}(a_{m,f} - a_{m,d}) = k_d(a_{m,d} - a_d). \qquad \text{Equation 3-11}$$

Permeation through a membrane is shown in Figure 3-8 with mass transport resistances due to interfacial transport and diffusion included. Since these mass transport resistances are in series, the overall mass transport resistance R_o can be related to the individual components as follows:

$$R_o = \left(\frac{1}{k_o}\right) = \left(\frac{1}{k_f}\right) + \left(\frac{1}{k_d}\right) + \left(\frac{l}{Dc}\right). \qquad \text{Equation 3-12}$$

Thus, k_o can be written as

$$k_o = \frac{\frac{Dc}{l} k_d k_f}{\frac{Dc}{l} k_d + \frac{Dc}{l} k_f + k_d k_f}. \qquad \text{Equation 3-13}$$

If we neglect k_f, which is assumed to be negligible for a liquid interface or constant at fixed vapor activity, or lump all interfacial transport into k_d, we now can rewrite k_o as

$$k_o = \frac{\left(\frac{Dc}{l}\right) k_d}{\left(\frac{Dc}{l}\right) + k_d}. \qquad \text{Equation 3-14}$$

3.4 Results

Water permeation, from both liquid water and water vapor, through Nafion membranes into dry N_2 was measured at four temperatures. Three membrane thicknesses were compared. Some runs included a woven carbon cloth electrode on one face of the membrane, but most permeation measurements were made on plain Nafion membranes. For all runs, water flux was measured as a function of dry N_2 flow rate with temperature and feed side water activity held fixed. Table 3-2 gives a summary of the permeation runs which are presented in this chapter including membrane details, temperature, and feed side activity. The experimental results are presented and discussed based on effects of membrane hydration, temperature, membrane thickness, and electrode effects.

Table 3-2 Summary of permeation runs presented in this chapter. Note that feed side water activities of 0.3, 0.5, and 0.8 are for water vapor while 1 is for liquid water.

Membrane	Feed side activities	Temperatures (°C)
N112	0.3, 0.5, 0.8	30 and 80
N115 and N1110	0.3, 0.5, 0.8	30, 50, 70, 80
N112, N115, N1110	1	30, 80, 70, 80, 90
N115, feed side electrode	0.3, 0.5, 0.8, 1	30 and 80
N115, dry side electrode	0.3, 0.5, 0.8, 1	30 and 80

3.4.1 Liquid water permeation

Permeation of liquid water through Nafion is less complicated than vapor permeation. As will be shown, vapor permeation introduces an additional interfacial mass transport resistance at the membrane/vapor interface at the feed side. Vapor permeation depends strongly on feed side water activity, possibly a result of diffusivity increasing with membrane hydration. Liquid water permeation through Nafion will be presented first.

Comparing flux through membranes of different thickness allows one to separate interfacial mass transport resistance from diffusion. This is because membranes with different thickness have identical interfacial transport resistance but diffusional resistance which depends on thickness ($R_D = l/Dc$). This assumes that both k_{int} and Dc are independent of membrane hydration—good assumptions for permeation of liquid water through Nafion. If permeation scales with thickness, it suggests that it is limited by diffusion. Diffusivity can then be calculated based on permeation through the different membranes. However, if permeation does not scale with thickness, either 1) k changes with membrane hydration, 2) Dc changes with membrane hydration, or 3) interfacial mass transport resistance is significant. For liquid water permeation through Nafion, it is assumed that k_f and k_d are not dependant on membrane hydration.

Permeation of liquid water through Nafion membranes with three different thicknesses is shown at 30 and 80°C (Figure 3-11). Nafion N112, N115, and N1110 membranes with thicknesses of 54, 127, and 254 μm were compared. Flux does not scale with membrane thickness; permeation through the 54μm membrane is not 5x the permeation through the 254 μm membrane. In fact, there is very little change in permeation with thickness. Based on this, the conclusion is that interfacial mass transport at the membrane/vapor interface limits water permeation. In other words, for liquid water transport, diffusion is very fast compared to interfacial mass transport at the vapor interface. Interfacial mass transport resistance at the liquid/membrane interface is assumed to be negligible, as will be discussed in more detail later. The fact that flux is slightly higher through the 254 μm membrane than through the 127 μm is attributed to experimental error.

At 80°C (Figure 3-11), flux increased from 30°C for all membrane thicknesses. Again, water permeation through the three membranes is almost completely dominated by interfacial mass transport at the membrane/vapor interface, evident because flux does not vary appreciably with membrane thickness. Permeation of liquid water increases with temperature because interfacial mass transport at the membrane/vapor interface increases.

At 50 and 70°C (appendix section 7.4), liquid water permeation through Nafion N115 (127μm) and N1110 (254 μm) is essentially identical. Again, this indicates that interfacial transport resistance dominates and that Dc/l is very large compared to k_d.

At high gas flow rates on the dry side, interfacial mass transport is minimized due to decreasing boundary layer thickness. Additionally, the dry side activity approaches a water activity of 0 with increasing gas flow rate. Comparing permeation rates at high dry side gas flow rates for different membrane thickness can give a good idea of the effect of thickness on permeation. A summary of permeation of liquid water through Nafion at high dry N_2 flow rate is given in Table 3-3 over a range of temperature.

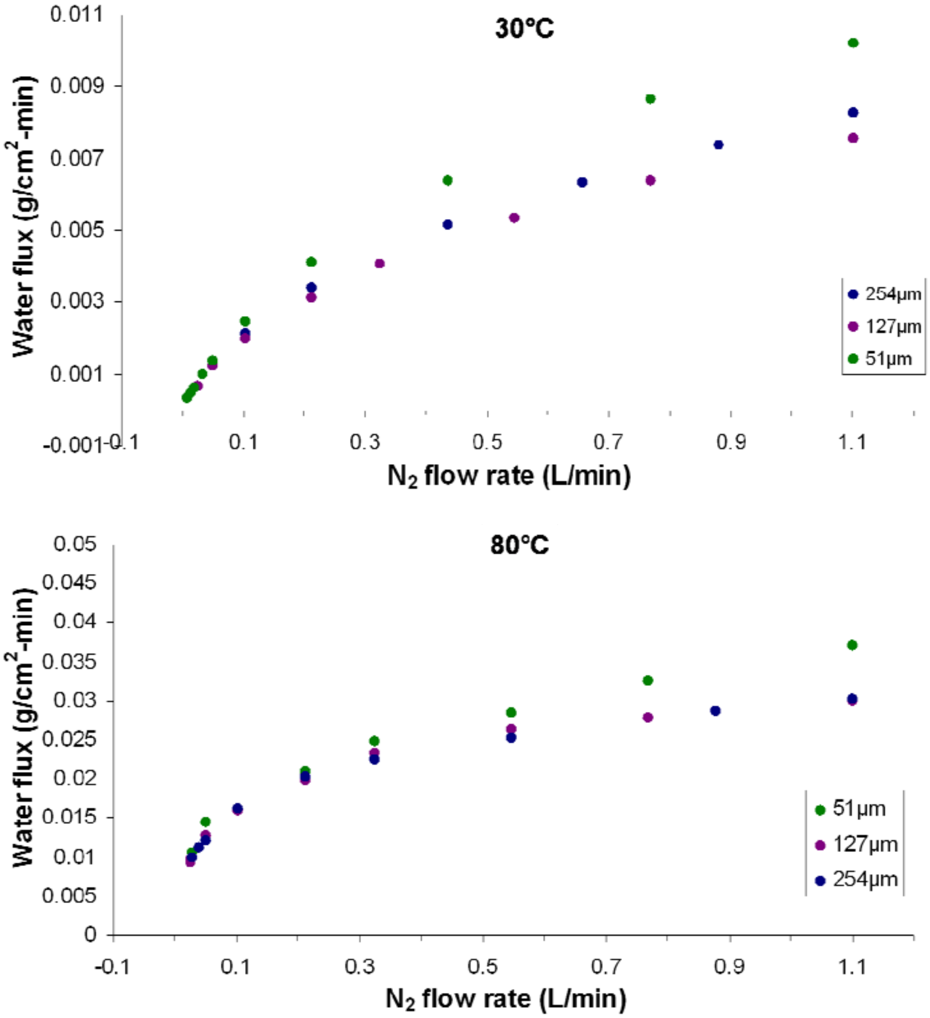

Figure 3-11 Comparison of membrane thickness for permeation of liquid water at 30 and 80°C.

Table 3-3 Summary of liquid water flux at 1.1L/min flow of dry N_2 at the dry side.

Membrane	Temperature (°C)	Flux at 1.1 L/min (g/cm^2-min)
N112	30	0.010
	50	0.023
	70	0.041
	80	0.037
N115	30	0.0076
	50	0.017
	70	0.027
	80	0.030
N1110	30	0.0083
	50	0.015
	70	0.024
	80	0.030

3.4.2 Vapor permeation

3.4.2.1 Feed side activity

Figure 3-12 shows permeation of vapor through Nafion N1110 at 30 and 80°C for three feed side water activities. Comparing the curves at fixed temperature, we notice that flux increases with feed side water activity, reaching a constant maximum value at high flow rate. For feed side activity of 0.8 at 30°C, the maximum flux is reached at a flow rate above 1.1 L/min (not shown). Flux increases with feed side activity because the driving gradient ($a_f - a_d$) and D increase. At high dry side flow rates, the dry side activity drops to zero, causing permeation rate to reach a maximum value which shows no further increases with flow rate.

Interfacial mass transport resistance for vapor transport exists at both membrane/gas interfaces. At high gas flow rates, interfacial mass transport resistance reaches a constant value, regardless of changes in activity at the feed side or dry side.

Thus, comparing flux at high flow rates between runs with only feed side activity varied allows for evaluation of how D changes with membrane hydration. It is assumed that interfacial mass transport resistance is the same between runs with different feed side vapor activities.

Flux does not scale with driving gradient for vapor permeation through N1110 at 30°C. At an N_2 flow rate of 1.1L/min on the dry side (essentially 0%RH), flux normalized by driving gradient ($Flux/(a_f - a_d)$) is 6.67×10^{-4}, 8.86×10^{-4}, and 2.66×10^{-3} g/cm^2-min for feed side activity of 0.3, 0.5, and 0.8, respectively. If k_o was independent of membrane activity, normalized flux wouldn't change with feed side activity. Instead, normalized flux increases significantly, suggesting that Dc increases with membrane activity.

Comparing permeation at 30 and 80°C (Figure 3-12) we notice that the curves are very similar, but that maximum flux increased with temperature. Additionally, at 80°C all of the curves reached their maximum value at N_2 flow rates well below 1.1L/min. Maximum flux increases with temperature because both D and k increase. p_{sat} also increases with temperature, giving rise to a lower water activity in the bulk vapor for a given water flux and dry N_2 flow rate. Additionally, more thermal energy is available to drive evaporation as temperature increases. At 80°C, normalized flux again increases with feed side activity. Normalized flux at 0.3, 0.5, and 0.8 feed side activity is 1.5×10^{-3}, 2.3×10^{-3}, and 5.5×10^{-3}, mol/cm^2-min, respectively. As seen at 30°C,Dc increased with membrane activity.

Table 2 gives a summary of flux at a dry side N_2 flow rate of 1.1L/min and extrapolated to 0.0 dry side activity for all water vapor permeation runs.

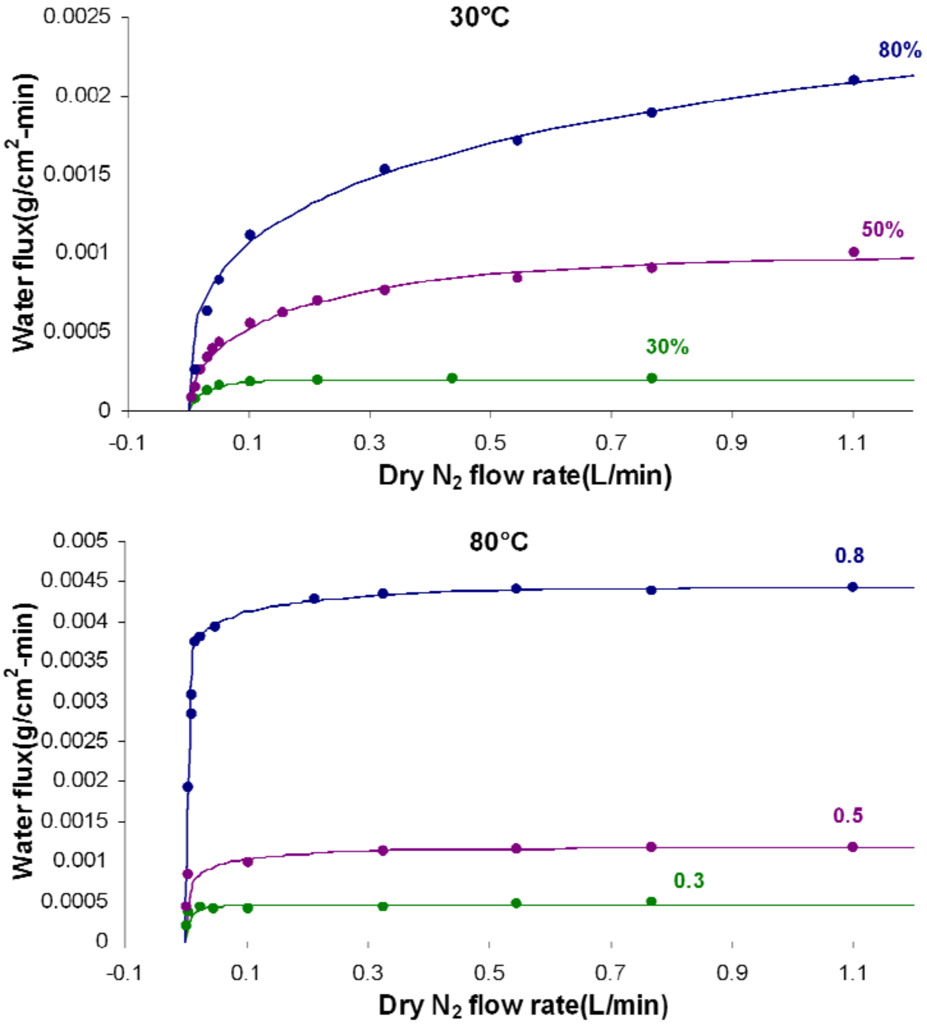

Figure 3-12 Permeation of water vapor through Nafion N1110 into dry N_2 at 30 and 80°C with the water activity at the feed side at the levels indicated.

Table 3-4 Summary of flux at 1.1L/min flow of dry N_2 at the dry side. Extrapolated values are included for flow rates resulting in 0%RH at the dry side.

Membrane	Temperature (°C)	Feed side Activity	Flux at 1.1 L/min	Flux at 0% RH
N112	30	0.3	0.00082	0.00084
		0.5	0.00165	0.00166
		0.8	0.00392	0.0042
	80	0.3	0.00208	0.00208
		0.5	0.00551	0.00551
		0.8	0.01497	0.01497
N115	30	0.3	0.000574	0.001003
		0.5	0.001053	0.00115
		0.8	0.002722	0.00287
	50	0.3	0.000787	0.001071
		0.5	0.00159	0.00159
		0.8	0.004346	0.0045
	70	0.3	0.001176	0.001596
		0.5	0.00264	0.00265
		0.8	0.00763	0.00763
	80	0.3	0.001138	0.001371
		0.5	0.00285	0.00285
		0.8	0.00988	0.00988
N1110	30	0.3	0.0002	0.0002
		0.5	0.000443	0.00098
		0.8	0.002129	0.002826
	50	0.3	0.000551	0.00057
		0.5	0.001327	0.00133
		0.8	0.003015	0.00303
	70	0.3	0.000609	0.00062
		0.5	0.001533	0.00159
		0.8	0.00366	0.004234
	80	0.3	0.00045	0.00045
		0.5	0.00117	0.00117
		0.8	0.004425	0.00443

3.4.2.2 Membrane thickness

As mentioned for permeation of liquid water, diffusional resistance can be separated from interfacial mass transport resistance by comparing flux through membranes of different thickness. For vapor transport from 30- 80°C, mass transport resistance due to diffusion is significant when compared to interfacial mass transport resistance.

Permeation of water vapor through Nafion N112, N115, and N1110 is shown in Figure 3-13. With feed side activity of 0.3, flux at 1.1L/min flow rate (see Table 3-4) was 0.0002, 0.000574, and 0.00082g/cm^2-min through Nafion N1110, N115, and N112, respectively. Normalizing by dividing all fluxes by the flux through the N1110 membrane gives a ratio of 1:2.9:4.1. If permeation through the different thickness membranes 1) was dominated by diffusion, 2) diffusivity was independent of membrane hydration, and 3) interfacial mass transport was the same between membranes, the flux ratio would be 1:2:5. Ratios smaller than this suggest that diffusion is not limiting (i.e., transport by diffusion is very fast). Ratios larger than this suggest that either diffusivity or interfacial mass transport decreased with membrane hydration since a thicker membrane would be less hydrated near the dry side interface due to increased transport resistance compared to a thinner membrane. We will make the assumption that the interfacial mass transport coefficient is unchanged between membranes of different thickness with identical feed side activity and that *D* increases with hydration. This assumption is reasonable since 1) the membrane/vapor interface at the feed side should be identical between membranes, 2) other investigators have reported an increase in water self diffusion with hydration in Nafion films[18]. Table 3-5 shows a summary of flux ratios for permeation through N1110, N115, and N1110 from vapor at 30 and 80°C. Three feed side activities are included for each temperature; 0.3, 0.5, and 0.8. The general trend observed at 30°C is that transport is diffusion limited for vapor transport and that diffusivity increases significantly with hydration. At feed side activity of 0.3 and 0.5, the flux increase from N1110 to N115 is greater than the decrease in thickness, suggesting a drop in *Dc* for the thicker and drier membrane. The ratios between N1110 and N112 are not consistent with this trend, perhaps because interfacial transport is now a more significant contributor to permeation resistance. With feed side activity of 0.8, the flux ratio is smaller than what diffusion dominated transport would give. From this, it is suggested that D increased significantly going from feed side activity of 0.5 to 0.8 and that interfacial transport is dominant.

Similar trends were observed at 30 and 80°C for vapor permeation through membranes of different thickness (Table 3-5). The main difference is that there is no clear occurrence of interfacial transport limitations at 80°C and 0.8 feed side activity.

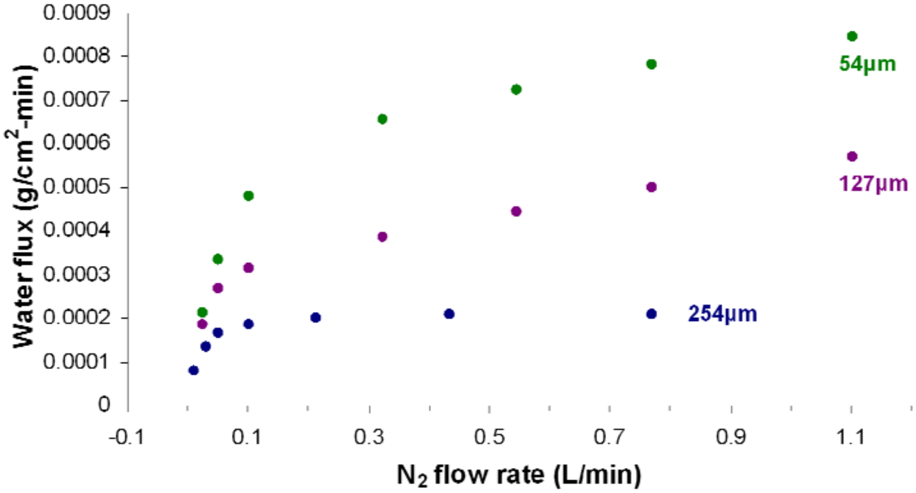

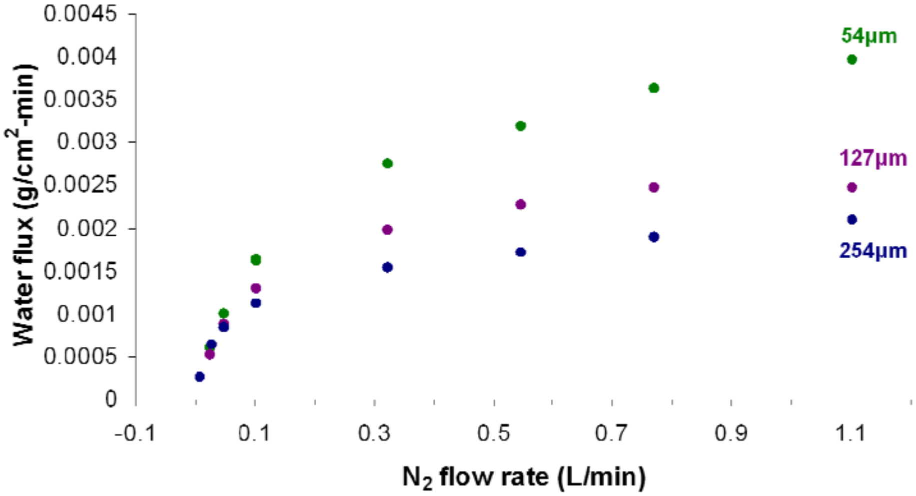

Figure 3-13 Comparison of membrane thickness for permeation of water vapor at 30°C with feed side activity of 0.3 (top) and 0.8 (bottom).

Table 3-5 Comparison of vapor and liquid flux through N112, N115, and N1110 membranes at 30, 50, 70, and 80°C at a dry side N_2 flow rate of 1.1 L/min. The ratios presented compare flux through N115 and N112 to the flux through N1110.

Temperature (°C)	Feed side a_w	Flux Ratio (N1110:N115)	Flux Ratio (N1110:N112)
30	0.3	1:2.9	1:4.1
	0.5	1:2.4	1:3.7
	0.8	1:1.3	1:1.8
	1.0	1:0.9	1:1.2
50	0.3	1:1.4	–
	0.5	1:1.2	–
	0.8	1:1.4	–
	1.0	1:1.1	1:1.5
70	0.3	1:1.9	–
	0.5	1:1.7	–
	0.8	1:2.1	–
	1.0	1:1.1	1:1.7
80	0.3	1:2.5	1:4.6
	0.5	1:2.4	1:4.7
	0.8	1:2.2	1:3.4
	1.0	1:1	1:1.2

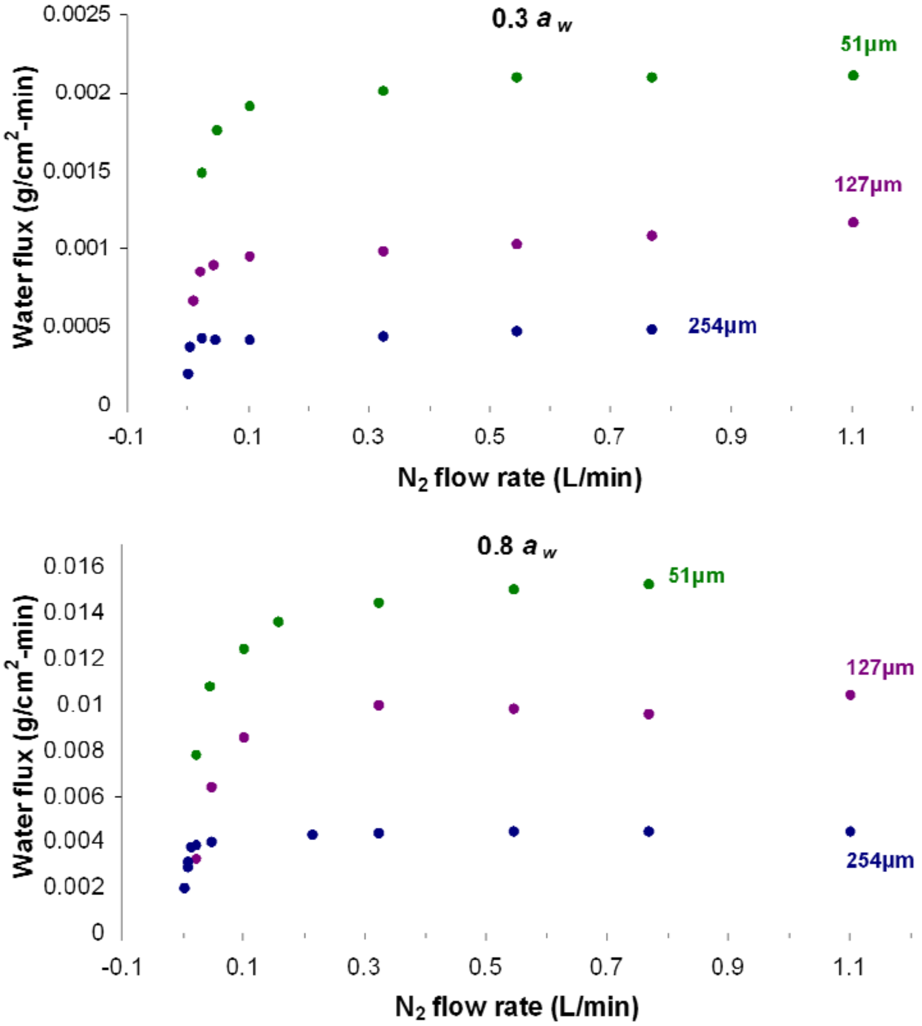

Figure 3-14 Comparison of membrane thickness for permeation of water vapor at 80°C with feed side activity of 0.3 and 0.8.

3.4.2.3 Normalized vapor permeation

Flux can be normalized by dividing it by driving gradient as a way to compare permeation at different driving potentials. Since permeation is equal to k_o times the driving gradient, normalized flux is equal to k_o:

$$Flux_{Normalized} = \frac{Flux}{(a_f - a_d)} = k_o \, . \qquad \text{Equation 3-15}$$

Thus, by plotting normalized flux against average membrane activity, the relationship between k_o and membrane water activity is more clearly seen. Assuming that k_f and k_d don't change with membrane hydration, normalized flux is proportional to D.

As an illustrative example of normalized permeation, Figure 3-15 shows a plot of normalized flux vs. average membrane water activity for Nafion N1110 at 70°C. Three feed side activities are included. The general trend is that normalized flux increases with membrane water activity. For each of the individual curves at fixed a_f, there is a small rise in normalized flux at the lowest membrane activity. This corresponds with high dry side gas flow rate. The increase in normalized flux occurs as k_d increases due to decreasing boundary layer thickness. The smooth curve formed by connecting points along the broad parts of the curves (neglecting high flow rate points) is proportional to D. For this curve, k_d and k_f are assumed to be fairly constant for the three activities at this temperature. The increase in normalized flux with average membrane water activity suggests that D increases significantly with hydration. Here we assume that $k_d >> Dc/l$ so that $k_o \sim Dc/l$.

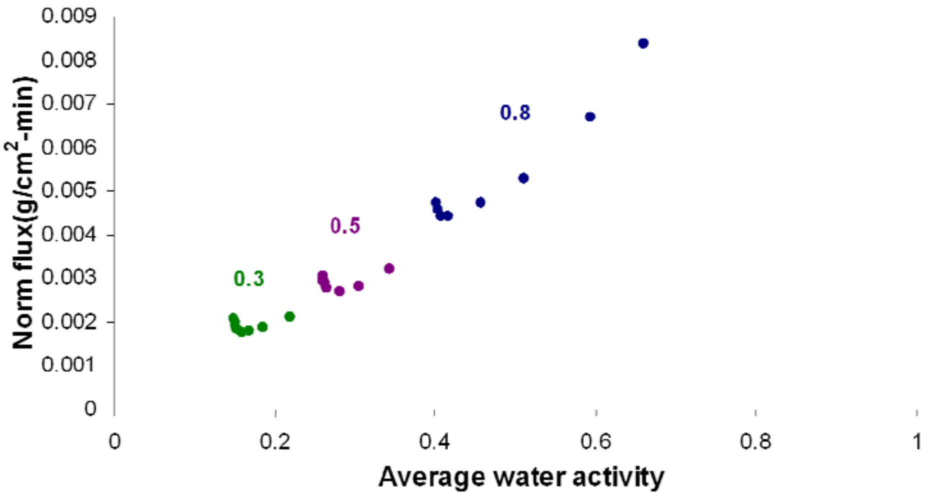

Figure 3-15 Normalized flux as a function of average membrane water activity for Nafion N1110 at 70°C. Feed side activities of 0.3, 0.5, and 0.8 are included.

Normalized flux plotted against average membrane water activity for permeation of vapor through membranes of three thicknesses at 30 and 80°C is shown in **Figure 3-16**. At 30°C, fitting lines through all points for a given membrane and forcing the line though zero doesn't give a very good fit. This suggests that permeation doesn't scale linearly with driving gradient at 30°C over the range of membrane hydration reported. The ratio between slopes of the fitted lines is 1:1.3 for N1110:N115 and 1: 1.8 for N1110:N112.

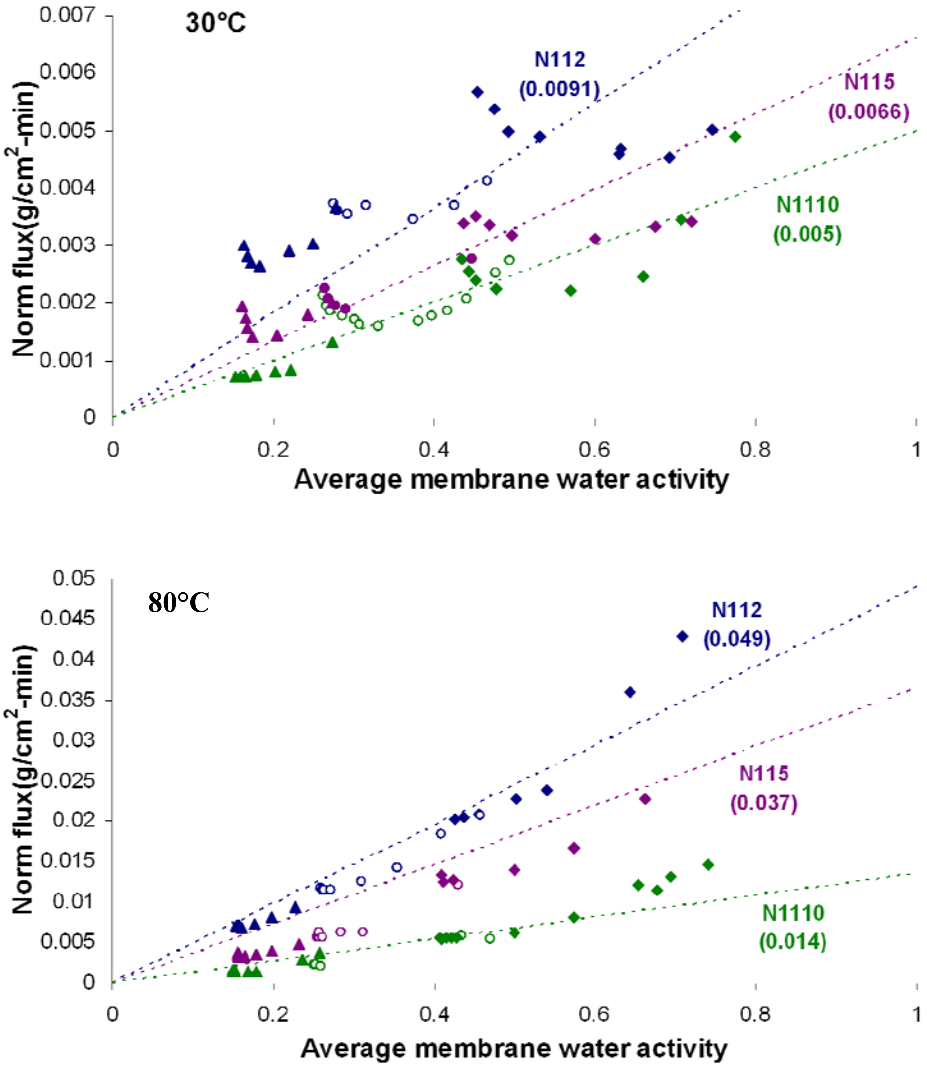

Figure 3-16 Normalized water flux as a function of average membrane water activity at 30 and 80°C for Nafion N112, N115, and N1110. Three feed side activities are shown for each membrane: solid triangle = 0.3, hollow circle = 0.5, and solid diamond = 0.8. Slopes of fitted lines are given in parentheses.

At 80°C, normalized permeation is closer to scaling with membrane hydration and thickness. The ratio between slopes of the fitted lines is 1:2.7 for N1110:N115 and 1: 3.6 for N1110:N112.

3.4.3 Comparison of vapor and liquid permeation

Does the phase of the feed side water affect permeation through Nafion into vapor? With respect to water activity, pure liquid water and saturated water vapor both have activity of 1. However, the concentration of water vapor and liquid water are very different. Additionally, a phase change is necessary for vapor, but not liquid, as water enters the condensed phase in the membrane. Thus, it is reasonable to anticipate that water permeation through Nafion form the liquid and vapor phases will be different, even if the membrane behaves equally in the presence of liquid and vapor. The results in this section compare permeation from liquid water and water vapor.

Figure 3-17 shows permeation through Nafion from both the vapor and liquid phases. As would be expected, flux increases with feed side activity from vapor to liquid. At 30°C, flux increases by a factor of four when going from water vapor activity of 0.8 to liquid water. At 80°C, there is a six fold increase in flux. These increases are far greater than what would be expected for just a difference in driving gradient from 0.8 to 1.0 (i.e., a factor of 1.25). Assuming a doubling of overall interfacial mass transport resistance (resistance at both membrane interfaces) when going from liquid to vapor would, at the most, result in a doubling in flux when going from vapor to liquid.

The increase in flux when going from vapor to liquid is partly due to decreased interfacial mass transport resistance for liquid transport—assuming that the interfacial mass transport resistance at the liquid/membrane boundary is negligible. Making k_f infinite would obviously increase flux by decreasing overall mass transport resistance.

The large increase flux when going from vapor to liquid transport is attributed mainly to changes in *Dc* with membrane hydration. As will be shown later, *Dc* increases with membrane hydration. Since there is no interfacial mass transport resistance at the liquid/membrane interface, membrane hydration is greater for liquid water transport. This increases Dc and thus overall water permeation for liquid water transport.

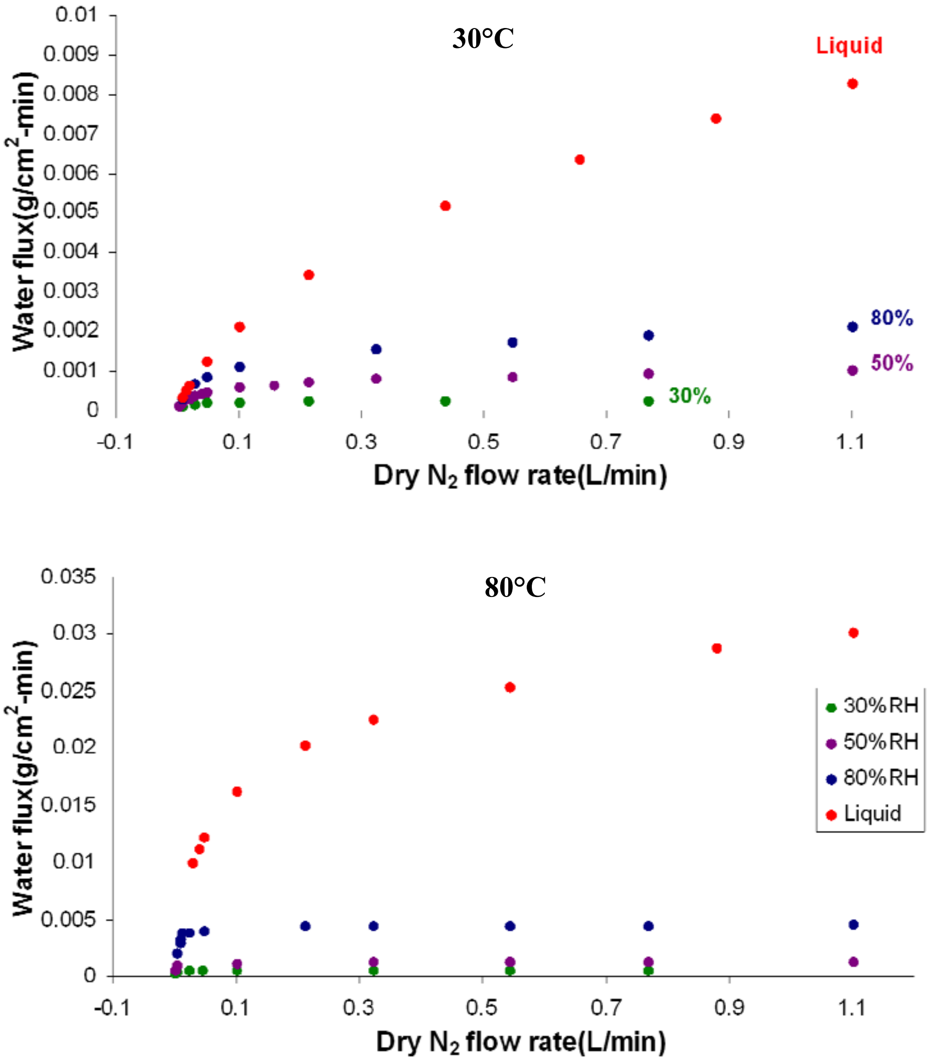

Figure 3-17 Permeation of water from liquid and vapor phase through Nafion N1110 at 30 and 80°C with feed side activities indicated.

As temperature was increased from 30 to 80°C, the gap between liquid water and vapor activity 0.8 also increased. This was due mainly to increasing k_d, which limits liquid water transport. For vapor transport, diffusional resistance dominates, so changes in k_d has less impact on flux.

Normalized flux vs. average membrane water activity for liquid and vapor phase feeds in shown in Figure 3-18 for Nafion N1110 at 30 and 80°C. It is evident that permeation is different for liquid and vapor phase feeds. The large increase in normalized flux for the liquid water curves is due to k_d dominating transport and increasing with dry N_2 flow rate. Since transport is dominated by D for vapor permeation, normalized flux reflects $D(c)$. For liquid permeation, membrane hydration likely changes very little with dry N_2 flow rate because $D >> k_d$. Therefore, it would probably be more accurate to shift all of the liquid permeation points to average membrane activity of 1.0.

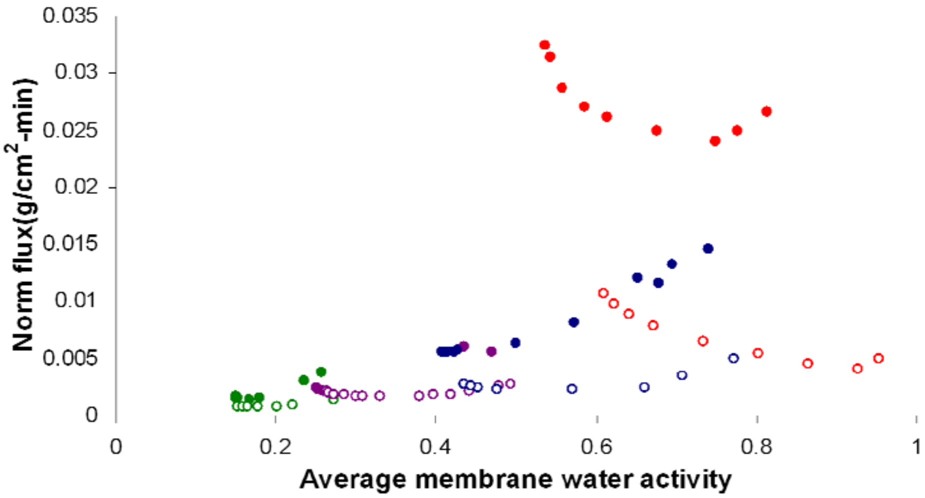

Figure 3-18 Normalized flux as a function of average membrane activity at 30°C (open circles) and 80°C (solid circles) for liquid and vapor phase feeds. The colors correspond to feed side water activity; green = 0.3, violet = 0.5, blue = 0.8, and red = 1.0.

3.4.3.1 Hydration and temperature effects

In Figure 3-19, the combined effects of hydration and temperature on permeation are shown for Nafion N1110. For liquid water and vapor feed of 0.8 activity, permeation increased with temperature from 30 to 80°C. However, for vapor feed activity of 0.5 and 0.3, flux at 80°C was lower than that at 50 or 70°C. This was an unexpected and important result and is most likely due to lower diffusivity as the membrane hydration decreased towards the dry side with increasing temperature. This is supported by the fact that this trend is present, but less pronounced, for N115 which is a thinner membrane (Figure 3-20). For the thinner membrane, hydration at the dry side would be greater because there is less mass transport resistance due to diffusion ($R_d = l / Dc$).

One possible reason for the drop in flux with increased temperature and feed side activity reported above for the thicker membranes at 80°C could be due to enhanced membrane drying at 80°C. The pore structure of Nafion is known to vary significantly with hydration. Membrane drying could increase significantly with temperature, resulting in changes in membrane structure which decrease water transport. Additionally, a stress gradient across the thickness of the membrane could be causing the drop in permeation. Since Nafion undergoes significant swelling with hydration, maintaining a hydration gradient across the membrane would result in a stress gradient. At the dry side, the membrane would be under tension while the hydrated side would be under compression. This could affect the structure of the membrane and thus water transport through it.

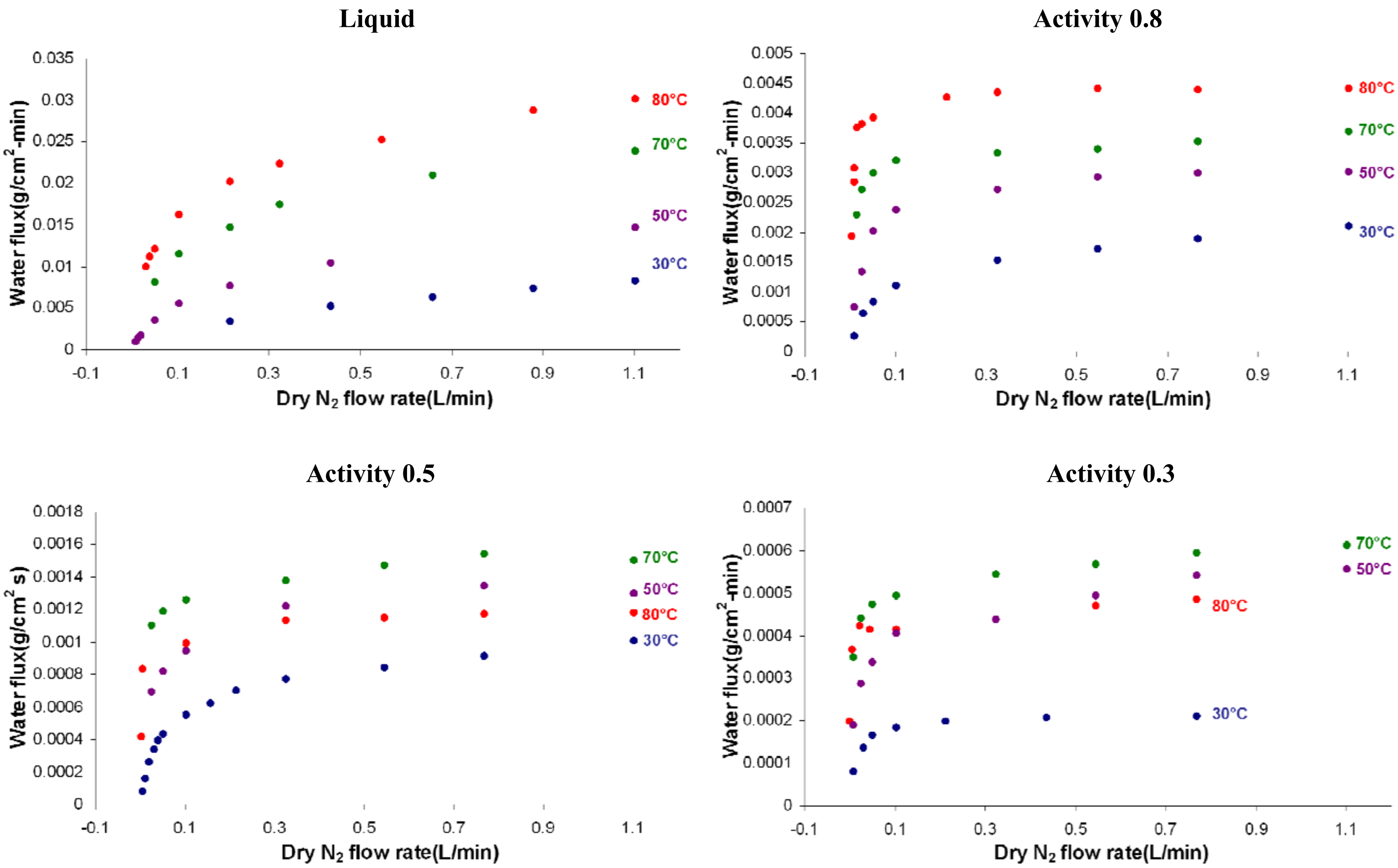

Figure 3-19 Permeation of water through Nafion N1110 with different feed side activity for each plot, as indicated. Flux is shown as a function of N_2 flow rate at the dry side for different temperatures.

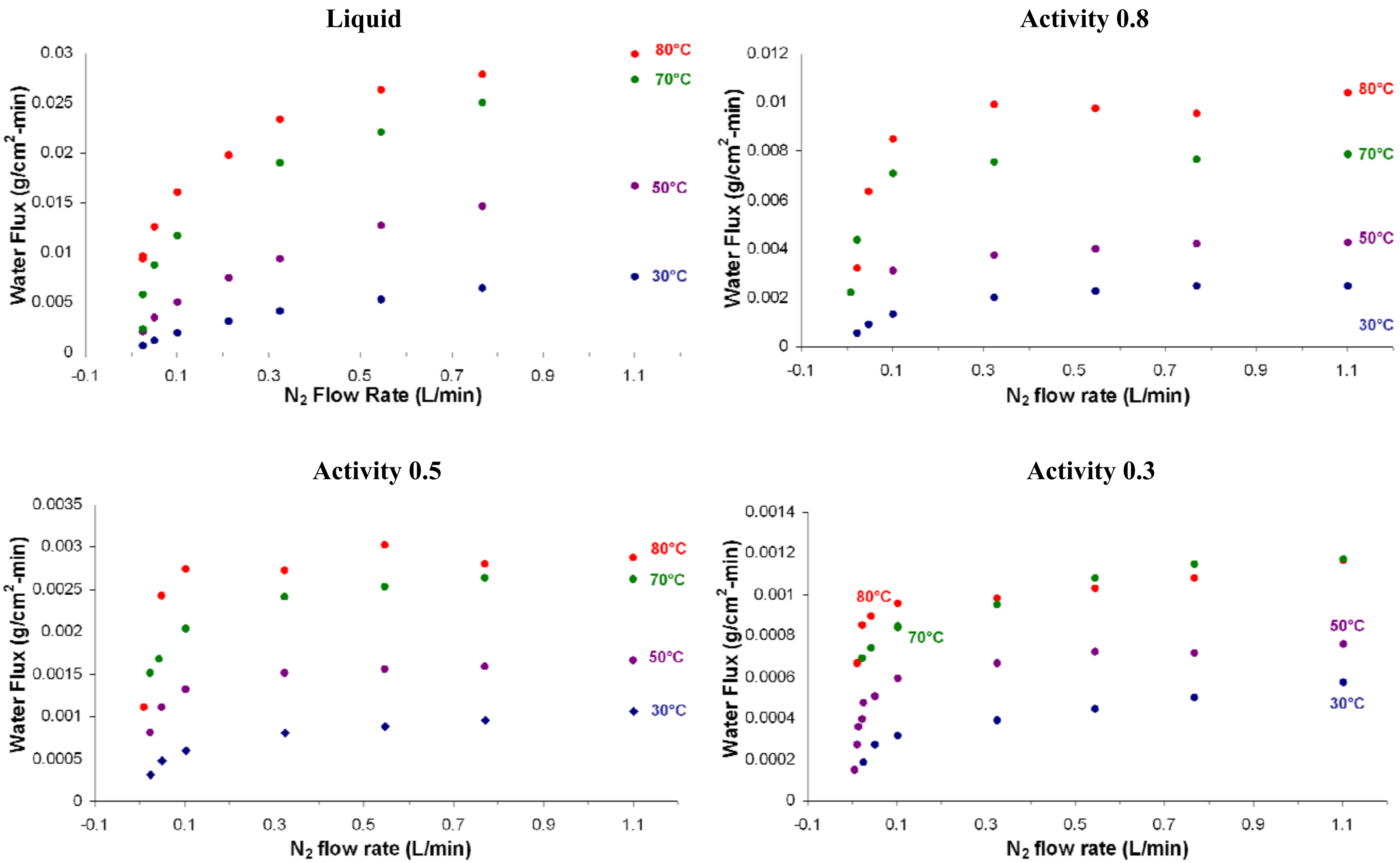

Figure 3-20 Permeation of water through Nafion N115 with different feed side activity for each plot, as indicated. Flux is shown as a function of N$_2$ flow rate at the dry side for different temperatures.

3.4.4 Diffusion coefficient estimation

Diffusion coefficients can be estimated by comparing permeation through membranes of different thickness. For liquid water transport, since D is so large compared to k_d, it is difficult to estimate D from permeation experiments. However, liquid permeation does provide a good estimate for k_g at the membrane/vapor interface.

It was observed that liquid water permeation through Nafion N115 and N1110 was essentially identical at a dry side N_2 flow rate of 1.1L/min from 30 - 80°C. As such, we can conclude that k_d is dominant and that $(Dc/l) >> k_d$ for liquid permeation and we see that $k_o = k_d$.

For vapor transport, it is reasonable to assume that $k_d = k_f$ when gas flow rate at the feed side and dry side is high. Thus, it is reasonable to estimate the total interfacial mass transport coefficient $k_{g,vapor} = \frac{1}{2}k_{g,liquid} = \frac{1}{2}k_{o,liquid}$. Solving equation 3.14 for Dc/l for vapor permeation, we obtain

$$\frac{Dc}{l} = -\frac{\frac{1}{2}k_{o,liquid}k_{o,vapor}}{k_{o,vapor} - \frac{1}{2}k_{o,liquid}}. \qquad \text{Equation 3-16}$$

A summary of interfacial mass transport and diffusion coefficients calculated based on these assumptions is presented in Table 3-6 for permeation of water vapor through Nafion N112, N115, and N1110. Figure 3-21 shows a plot of these values as a function of average membrane water activity for constant temperature curves.

Table 3-6 Summary of diffusion and interfacial mass transport coefficients for Nafion N112, N115, and N1110.

Temperature	Feed side	*Dc*(mol/cm-s x 10^8)				$k_g^\infty = k_{o,liquid}$
(°C)	Activity	N1110	N115	N112	average	(mol/cm^2-s x10^5)
30	0.3	0.14	0.21	0.12	0.16	0.91
	0.5	0.55	0.69	0.47	0.57	
	0.8	6.13	4.60	4.10	4.95	
50	0.3	0.40	0.28	-	0.34	1.83
	0.5	1.67	1.02	-	1.34	
	0.8	7.50	6.31	-	6.91	
70	0.3	0.43	0.42	-	0.43	2.82
	0.5	1.90	1.70	-	1.80	
	0.8	8.53	11.98	-	10.25	
80	0.3	0.32	0.41	0.31	0.35	2.98
	0.5	1.43	1.84	1.57	1.61	
	0.8	10.68	18.29	22.18	17.05	

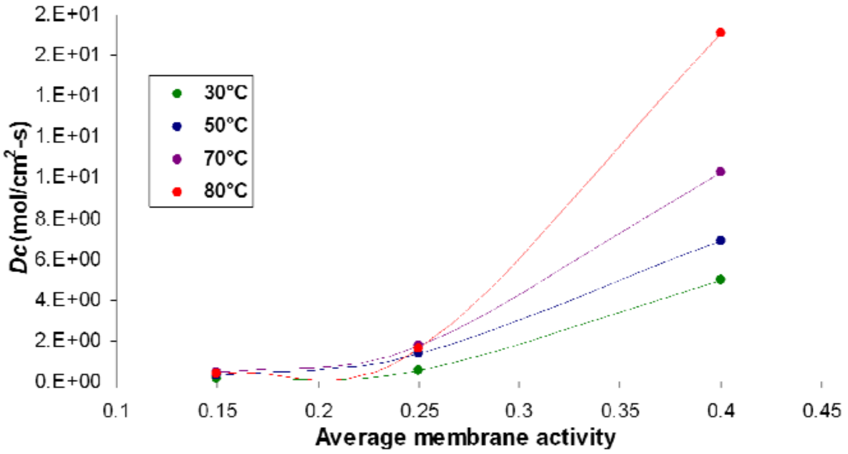

Figure 3-21 Average *Dc* from Table 3-6 plotted against average membrane water activity assuming a linear water concentration profile.

3.4.5 Permeation including gas diffusion layer

Water permeation through Nafion with a gas diffusion layer (GDL) on only one side was measured at 30 and 80°C. Flux was measured for vapor feeds with activity of 0.3, 0.5, and 0.8 as well as for liquid feeds. A comparison was made between having the

GDL on the feed side or the dry side. Plots summarizing these experiments can be found in section 7.4 of the Appendix.

Figure 3-22 shows steady state flux of liquid and vapor at 30°C through Nafion N115 with a GDL on one surface—comparing transport with the GDL on the feed side to the GDL on the dry side. For vapor transport, permeation is greater at a given feed side activity when the GDL is located on the dry side. When liquid water is present at the feed side, the opposite occurs; flux is greater when the GDL is on the dry side. At this point, since only a limited number of experiments have been done looking at permeation with a GDL in place, it is unclear whether this reversal in trend from liquid water to vapor is due to experimental error or is a real trend. Assuming that this observation is real, this result could be significant. Further investigation of the effect of the GDL on permeation is required.

A comparison of transport with and without the GDL at 30°C is shown in Figure 3-23. Permeation is significantly greater with the GDL removed for transport from both liquid and vapor due to increased interfacial transport resistance.

At 80°C, permeation through the membrane and GDL is greater when the GDL is located at the feed side for both liquid and vapor feeds. The largest effect is seen with feed side activity of 0.8; permeation is over 3 times larger when the GDL is located at the feed side than when the GDL is at the dry side. Table 3-7 gives a summary of permeation at dry N_2 flow rate (1.1L/min) for runs which included a GDL.

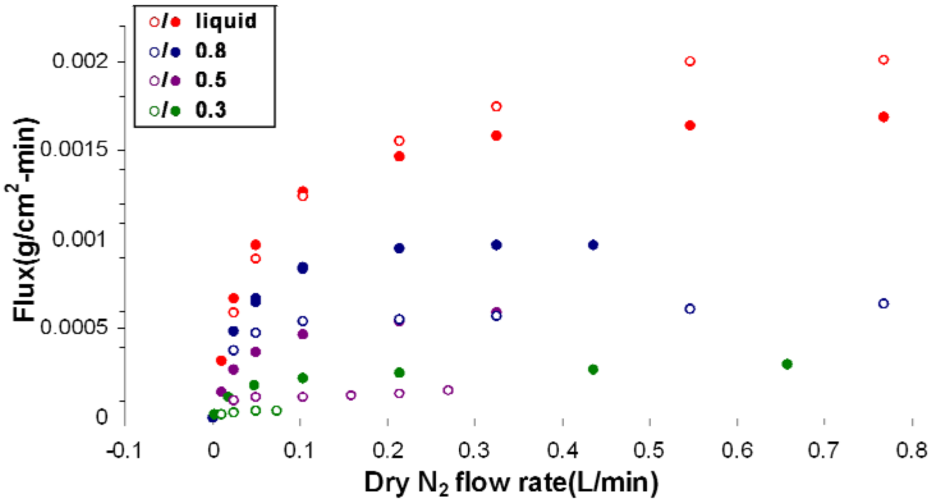

Figure 3-22 Water permeation through Nafion N115 at 30°C with a GDL on only the feed side (solid circles) or dry side (open circles) of the membrane.

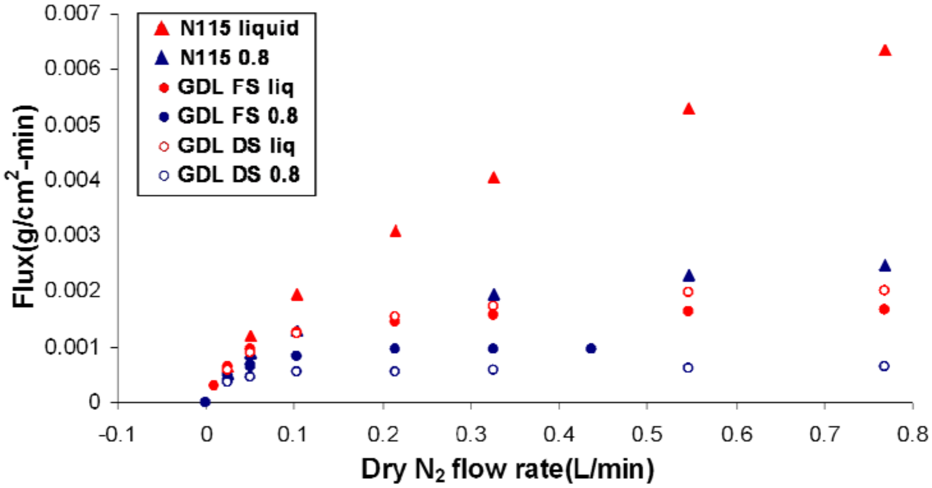

Figure 3-23 Permeation of liquid water and water vapor (activity 0.8) at 30°C through Nafion N115 with no GDL, and with a GDL layer at only the feed side (FS) or dry side (DS).

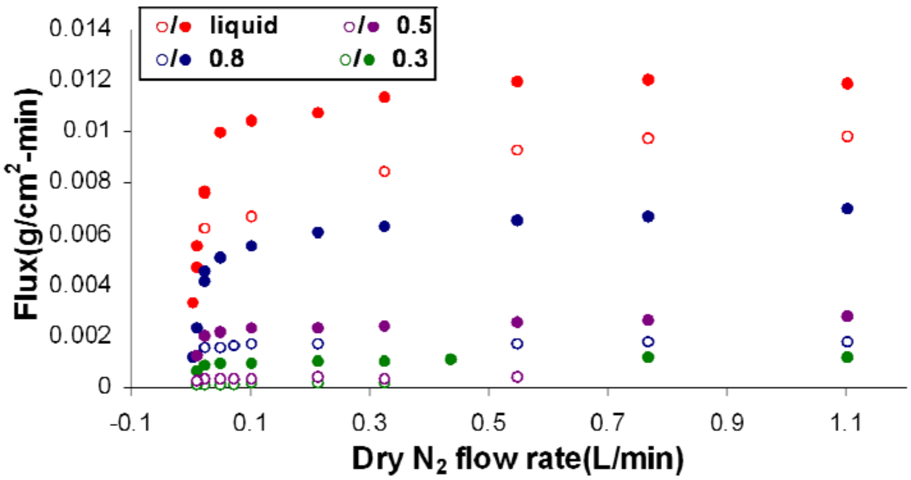

Figure 3-24 Water permeation through Nafion N115 at 80°C with a GDL on only the feed side (solid circles) or dry side (open circles) of the membrane.

Table 3-7 Summary of permeation through Nafion N115 with a carbon cloth electrode on either the feed side or dry side of the membrane. Flux is reported at a dry side N_2 flow rate of 1.1L/min.

GDL location	Temperature (°C)	Feed side activity	Flux at 1.1 L/min
Feed side	30	0.3	0.00030
		0.5	0.00061
		0.8	0.00097
		1	0.0017
	80	0.3	0.0012
		0.5	0.0028
		0.8	0.0070
		1	0.012
Dry side	30	0.3	0.00004
		0.5	0.00015
		0.8	0.00064
		1	0.0020
	80	0.3	.00014
		0.5	0.00040
		0.8	0.0018
		1	0.010

3.4.6 Oscillations

At low dry side N_2 flow rates, for both liquid and vapor feeds, oscillation in permeation was observed after steady state was reached. Oscillations were seen at all temperatures investigated—from room temperature to 90°C. They were also seen with a GDL on the feed side of the membrane with both liquid and vapor feeds, but were not seen when the GDL was on the dry side of the membrane.

Sample oscillations are shown Figure 3-25 - Figure 3-27. In general, the period and amplitude of the oscillations were very regular. The following summary of observations concerning oscillations were made:

1) Oscillations only occur when the dry side water activity is high/N_2 flow rate is low.
2) As temperature is increased, the range of flow rate over which oscillations occur decreases (due to an increase in p_{sat}).
3) Oscillation duration and frequency decreases with flow rate.
4) During oscillations, the feed side activity always increases above the expected steady state permeation/dry side activity and dry side activity has been observed to exceed feed side activity for vapor feeds.
5) Oscillations vary in shape, being similar to either a square wave or saw tooth function.

Figure 3-25 shows oscillations in permeation through plain Nafion N115 and N1110 membranes. For vapor permeation through N115 at 80°C, it is interesting to note that water activity at the dry side reaches 0.95 during oscillations even though feed side water activity is set to 0.8. This suggests that there might be liquid water present at the membrane surface. Since the relative humidity sensor did not show a drop in temperature, cooling at the feed side is ruled out. If there were cooling at the dry side, relative humidity at the dry side RH sensor would be lower (this is assuming that flux drops as a result of cooling). Indeed, if cooling at the membrane surface did occur, oscillations where flux decreased would arise. Thus, it is unlikely that liquid water is forming at the dry side surface of the membrane due to thermal condensation. Nor is it likely that condensation would occur at the feed side surface of the membrane due to a thermal gradient. It is also interesting to note that peak water activity during oscillations for liquid water permeation through Nafion N1110 at the same temperature and dry side flow rate is lower, with oscillations having a longer period.

Comparing permeation of liquid water through Nafion N1110 at 80°C and two different dry side N_2 flow rates (Figure 3-25), it is evident that oscillation frequency and period is strongly dependant on temperature. Increasing dry side N_2 flow rate to 10mL/min at 80°C (not shown) eliminates oscillations. At 50°C, however, oscillations are seen at this higher flow rate.

When a GDL is added to the feed side surface of Nafion N115 (Figure 3-26), oscillations in vapor transport still arise (Figure 3-26). In fact, the amplitude of oscillations actually increases and occurs at higher dry side flow rates than for plain Nafion. At 80°C, dry side activity varies from 0.4 to 0.9! We also observe that the frequency of oscillations increases while the period decreases with the addition of the GDL. Since the GDL used for these experiments was hydrophobic, it is unlikely that liquid water could reach the membrane at the feed side unless condensation was occurring at the GDL/membrane interface. Oscillations at 80°C with a GDL on Nafion N115 were observed with feed side activity as low as 0.7 (not shown), so it seems unlikely that condensation due to thermal gradients would be occurring at the feed side since a very large thermal gradient would be needed. Additionally, we can also rule out condensation at the dry side membrane surface since water activity before oscillation is around 0.4.

Oscillations are also seen for membrane with GDL at the feed side when liquid water is present (Figure 3-27). The baseline dry side activity is significantly higher with liquid water than for water vapor. Also, oscillations were observed over a larger range of dry side N_2 flow rates when vapor was present. At 80°C, flow rates up to 25mL/min induced oscillations with a vapor feed while the maximum flow rate observed to induce oscillations for the liquid feed was 10mL/min.

The phenomenon of permeation oscillations is not fully understood. The obvious explanation—that temperature fluctuations due to evaporative cooling are causing condensation of liquid water at the membrane surface which brings about a sudden spike in dry side activity—seems to have been sufficiently ruled out on account of oscillations occurring with fairly low activity at both sides of the membrane. It's also interesting and not fully understood that oscillations persist when a GDL is included at the feed side. It is also not clear why oscillations were not observed when the GDL was at the dry side; if condensation were to occur at the feed side, oscillations should still arise.

Nafion's surface interaction with liquid water/water vapor, its pore structure, and swelling with hydration might possibly be used to explain oscillations. There is also the possibility that the oscillations are specific the experimental setup used for the experiments or arise from basic physics of evaporative cooling.

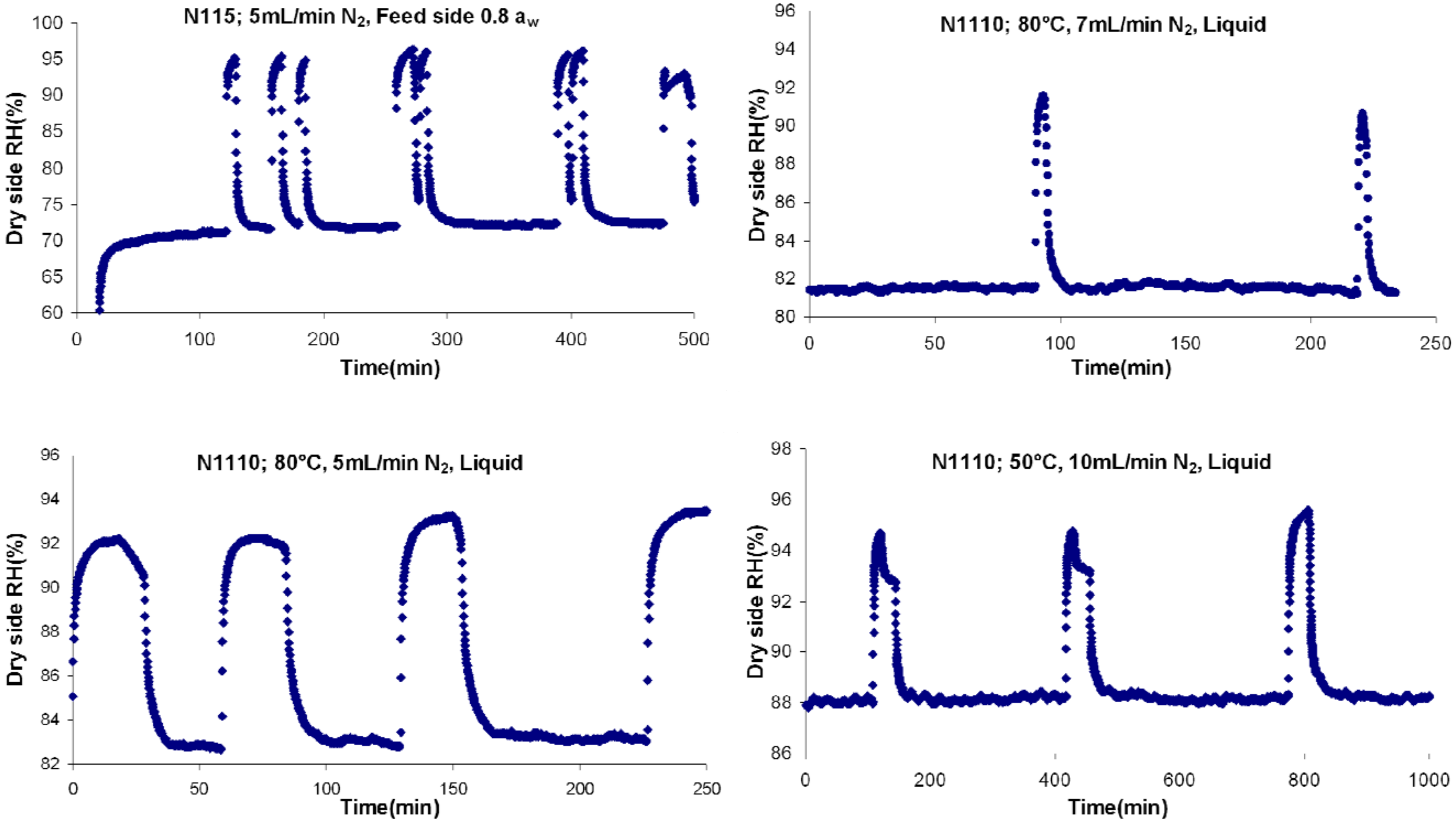

Figure 3-25 Oscillations in permeation through Nafion from liquid water and vapor feeds. Temperature, membrane, feed side phase, and dry side N_2 flow rate indicated.

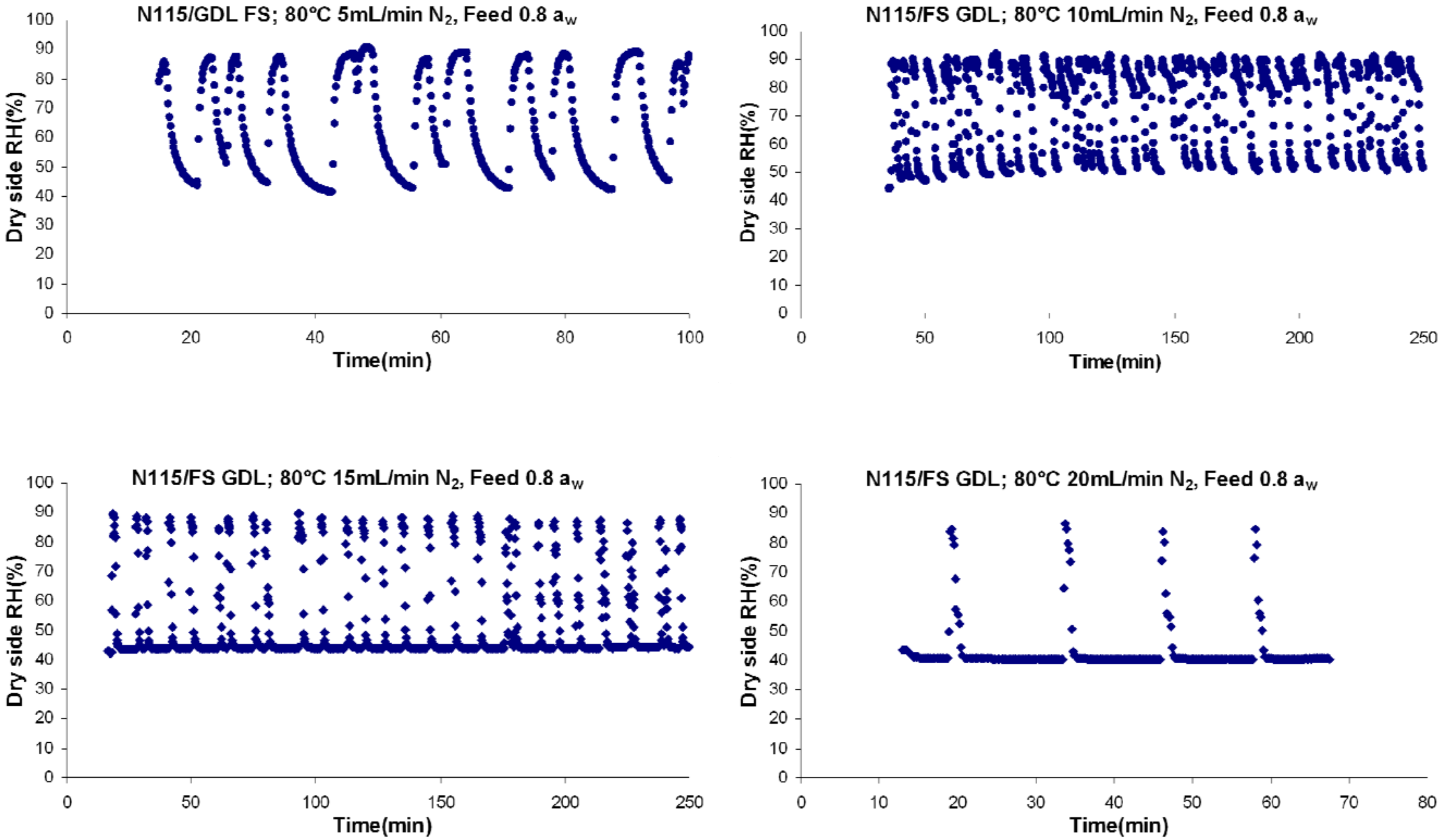

Figure 3-26 Oscillations in permeation of water vapor through Nafion with a GDL on the feed side surface. Permeation is at 80°C with feed side activity of 0.8 and dry side N_2 flow rates indicated.

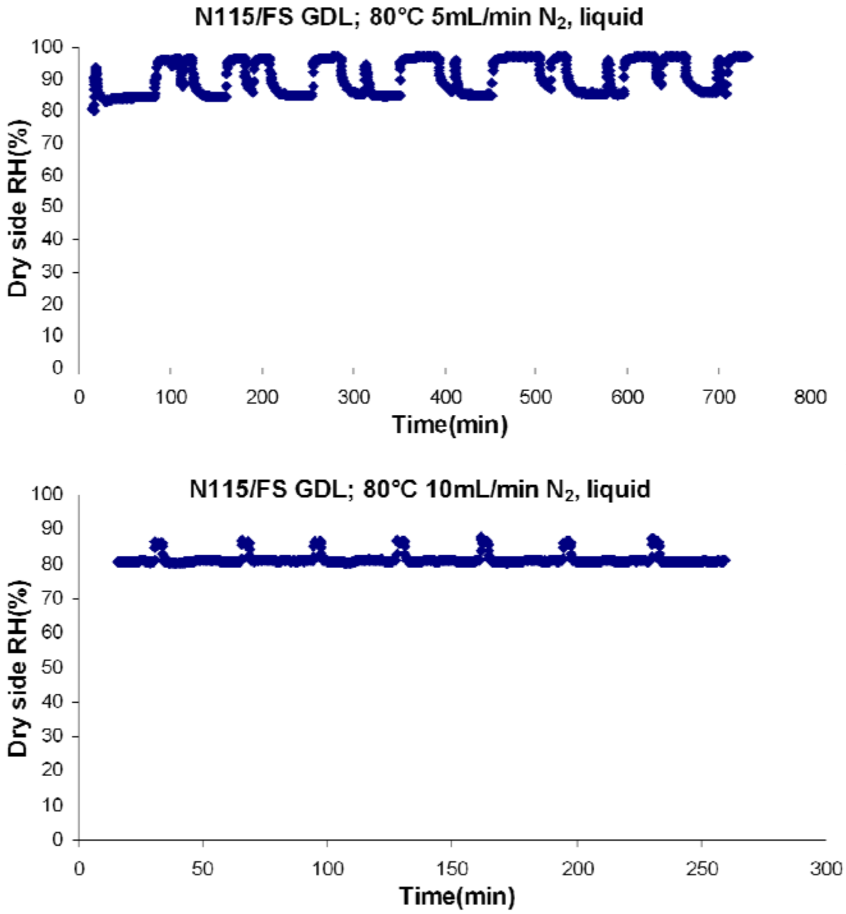

Figure 3-27 Oscillations in permeation of liquid water through Nafion with a GDL on the feed side surface. Permeation is at 80°C with and dry side N_2 flow rates indicated.

3.5 Discussion

3.5.1 Permeation summary

The main results of the water permeation experiments can be summarized as follows:

1) Water diffusivity is strongly dependant on membrane hydration, increasing nearly exponentially with hydration.

2) Liquid water permeation is limited by interfacial transport resistance at the vapor/membrane interface for the temperatures and membrane thicknesses investigated.

3) Permeation of water vapor through Nafion is dominated by diffusion.
4) The presence of a GDL on Nafion's surface adds a significant interfacial mass transport resistance for transport from vapor and liquid phases.

Permeation of water through Nafion involves not only diffusion, but also interfacial mass transport at the membrane/gas interface. Interfacial transport is significant for water leaving and entering Nafion to/from the vapor phase because of Nafion's hydrophobic surface which acts as a barrier to water transport. As suggested by the Geirke model[23] (and other models), Nafion undergoes phase separation. When exposed to vapor, the hydrophobic chains become oriented towards the surface in order to create an interface which minimizes interfacial energy. When exposed to liquid water, the presence of clusters increases[1]. Fairly recently, AFM studies[24] of Nafion's surface at different hydration levels indicate that Nafion has a surface which is rich in Teflon when exposed to vapor. Such a surface would present a high interfacial mass transport resistance to water from the vapor phase. This is analogous to placing a thin film of oil on the surface of liquid water; the hydrophobic layer greatly reduces evaporation from the liquid water surface. In contrast, the hydrophilic, sulfonate rich surface of Nafion when exposed to liquid water would render negligible interfacial mass transport resistance for liquid water.

Figure 3-28 shows a more complete representation of the mass transport resistances for water permeation through Nafion, from liquid to gas. Included in this figure are 1) negligible interfacial mass transport resistance at the membrane/liquid interface, 2) non-linear water activity profile due to D increasing with hydration, 3) a thin teflonic region at the membrane/gas interface increasing interfacial mass transport, 4) a discontinuous drop in water activity from the membrane surface to the gas phase due to phase change, and 5) interfacial mass transport resistance contribution from boundary layer thickness at the membrane/gas interface.

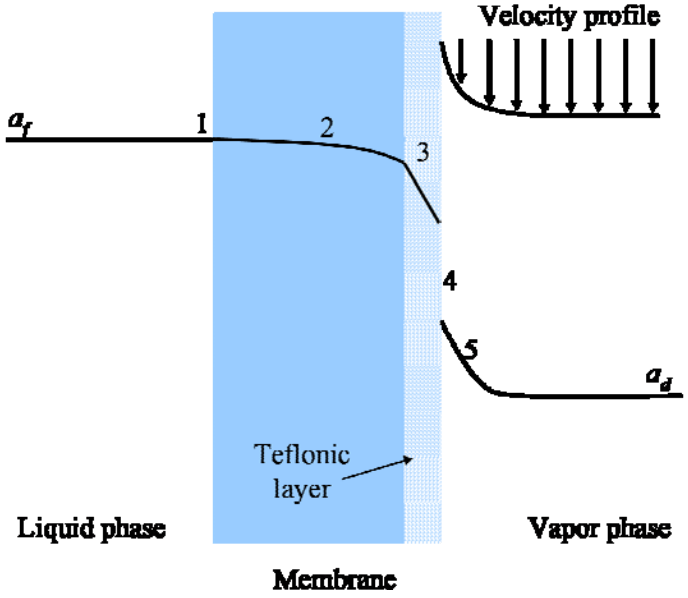

Figure 3-28 Water activity profile for water permeation through Nafion from liquid (activity a_f) into gas (activity a_d). The following mass transport resistances are included: 1) negligible interfacial mass transport resistance at the membrane/liquid interface, 2) non-linear water activity profile due to *D* increasing with hydration, 3) a thin teflonic region at the membrane/gas interface increasing interfacial mass transport, 4) a discontinuous drop in water activity from the membrane surface to the gas phase due to phase change, and 5) interfacial mass transport resistance contribution from boundary layer thickness at the membrane/gas interface.

Permeation increases significantly with membrane hydration and is attributed to diffusivity increasing with hydration. It is logical that diffusivity increase with membrane hydration because of swelling which occurs with water uptake. Swelling increases acid cluster size, increasing effective permeation cross sectional area and decreasing tortuosity. NMR studies of self diffusion of water in Nafion also reflect an increase in diffusivity with membrane hydration[18]. Looking at mass uptake and swelling strain as a function of water activity, there is a rapid rise in water uptake above water activity of ~0.75. Greatly increasing cluster volume fraction when going from activity of

0.8 to 1 due to increased water uptake explains why there is such a large increase in water permeation when going from vapor with activity 0.8 to liquid water.

Permeation of liquid water with activity of 1.0 through Nafion is thought to be greater than vapor with activity of 1.0 for two reasons—increased *D* and decreased *k* at the liquid membrane interface. As mentioned earlier, Nafion is expected to assume a hydrophilic surface when exposed to liquid water. Coupling this with the high concentration of water in the liquid phase makes interfacial mass transport resistance at the liquid/membrane interface negligible. Even with vapor of activity 1.0, the vapor/membrane interface will have significant interfacial mass transport resistance. This will lower the concentration of water in the membrane below that obtained when liquid water is present. Since *D* increases with concentration, *D* will be lower when exposed to water vapor under steady state permeation conditions. It is not clear what will occur at equilibrium (i.e., permeation rate of zero) since *k* is no longer important but surface hydrophobicity is expected to differ between the two conditions.

For permeation of liquid water through Nafion, k_d at the vapor/membrane interface dominated for all membrane thicknesses tested from 30 – 80°C. This is concluded based on the observation that permeation through membranes of different thickness was identical. For liquid water permeation, *D* is assumed to be significantly larger than k_d. As mentioned previously, *D* is also thought to be larger for transport from liquid than for transport from vapor.

For permeation of water vapor though Nafion, *D* is thought to dominate. This conclusion is based on the observation that permeation scaled roughly with thickness, at a given level of membrane hydration. That permeation did not scale perfectly with membrane thickness is attributed to the dependence of D on c—as membrane thickness increased, water concentration profile varied more significantly across the membrane, resulting in changes in the effective D between membranes with the same feed side and dry side water activities.

For all cases, permeation increased temperature, though permeation is more strongly dependant on hydration than temperature. The increase in permeation of liquid water with temperature is attributed almost entirely to the interfacial mass transport coefficient at the membrane/vapor interface increasing. For vapor transport, both D and k_{int} increase significantly, but the increase in D is dominant.

Introducing a GDL to one or both surfaces of Nafion significantly reduces permeation, both from vapor and liquid phase water. If the GDL is hydrophobic from PTFE treatment, liquid water never contacts the membrane. This is supported by the observation that permeation of liquid water through Nafion with a GDL on only the feed side is comparable to permeation from vapor at activity 0.8. With the GDL on the dry side, the membrane can become fully hydrated, but permeation is still low because of the large increase in k_d due to the presence of the GDL through which water vapor must now diffuse.

Permeation of water vapor through Nafion is also reduced by the presence of a GDL. Having the GDL at the feed side causes a larger reduction in permeation than what is seen with the GDL at the dry side because of the increase in diffusion resistance caused by lower hydration levels in the membrane.

3.5.2 Error analysis

Error in calculating water flux through Nafion with the method outlined in this chapter arises mainly due to uncertainty of the relative humidity sensors in measuring temperate and relative humidity. Another source of error includes uncertainty of dry side N_2 flow rate, but this is less significant. The sensors used in these experiments, Sensirion SHT75, have accuracy for temperature and relative humidity shown in Figure 3-29. Error in relative humidity increases significantly below 10% and above 90% RH, rising linearly in these regions. Note that the error of the sensor is given in %RH (e.g., error at 5%RH is 5 ±2.75%RH, or 5%RH ±55%). This makes error increasingly more significant at low RH. As an illustration of this, Figure 3-30 is a plot showing percent error from 0 to 100%RH.

Error analysis was performed on a typical permeation run to show what the upper and lower bounds on error was. The permeation run selected for the analysis is vapor permeation with feed side activity of 0.8 for Nafion N115 at 80°C. For this run, two sensors were used to record the relative humidity at the dry side; one located in the isothermal environment at the temperature of the test and one external to the test chamber with temperature control. The raw data are shown in Table 3-8.

Flux calculated using relative humidity values from the externally located sensor is shown in Figure 3-32 along with error limits for flux calculated using both sensors. To calculate the error limits for the internal sensor, the relative humidity at the test temperature was calculated using the relative humidity measured with the external sensor (Table 3-8). It is obvious that error for the internal sensor increases significantly with N_2 flow rate. This is because water activity at the test temperature drops to very low values. The error in flux using the internal sensor is unacceptably large, surpassing 100% for the data shown. Comparing flux calculated using the lower limit of relative humidity for the internal sensor (Figure 3-32) to the flux calculated using the internal sensor without taking into account error limits (Figure 3-31) it is obvious that using the internal sensor can produce large errors in the range of interest.

Equipping the permeation setup with a second relative humidity sensor on the dry side whose temperature can be controlled to maintain the relative humidity above at least 10% greatly improves the accuracy of flux calculations. Figure 3-32 includes error limits for flux calculated using such a design (labeled “Ext. sensor”). Error in calculating flux using relative humidity measured by the external sensor is significantly lower than for the internal sensor. Error can be much lower for calculating flux using the external sensor data because sensor error can be reduced by cooling the vapor at the point of measurement to increase sensor accuracy. Table 3-9 illustrates error in flux calculated for a sample of humid air measured at two temperatures.

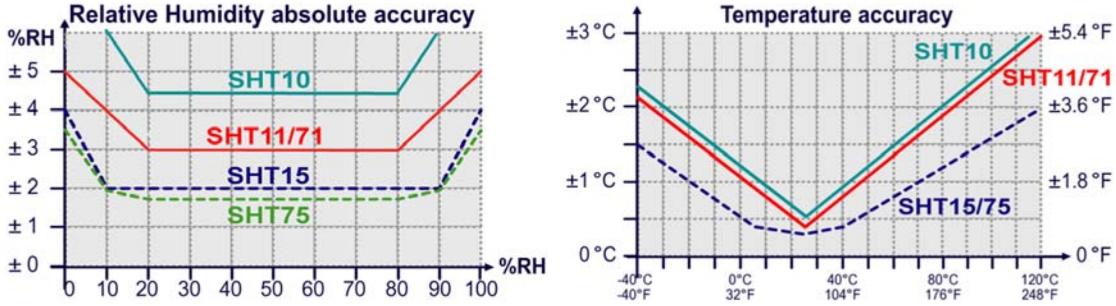

Figure 3-29 Relative humidity and temperature accuracy of Sensirion dual relative humidity/temperature sensors[25]. Plots reprinted from reference 25.

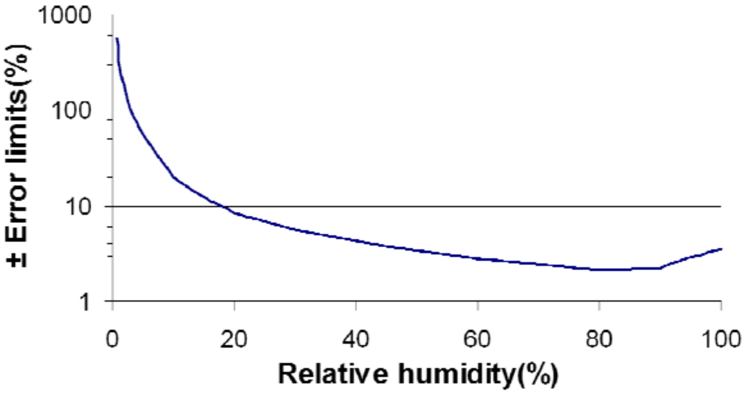

Figure 3-30 Upper and lower error limits for humidity measured by Sensirion SHT75 relative humidity sensor. Error is reported as a percent of the actual reading.

Table 3-8 Raw data from permeation of water vapor through Nafion N115 at 80°C with feed side activity of 0.8. Two relative humidity sensors were used to measure the dry side flow, located internally and externally.

	Feed side		Dry side (internal)		Dry side (external)		
N_2 flow rate (L/min)	T (°C)	RH (%)	T (°C)	RH (%)	T (°C)	RH (%)	RH at T_{int} (%)
1.102	80.56	79.46	80.84	0	39.72	16.21	2.41
0.769	80.52	79.2	80.88	0	36.64	25.13	3.16
0.547	80.56	80.43	81.08	1.21	50.16	17.73	4.47
0.325	80.56	80.34	8.84	4.56	65.36	14.69	7.63
0.102	80.52	80.4	80.44	18.83	68.52	32.5	19.71
0.050	80.48	80.53	80.36	34.25	70.84	42.98	28.91
0.025	80.52	80.63	80.44	51.96	71.88	41.38	29.00
0.010	80.31	80.22	80.25	68.60	-	-	-

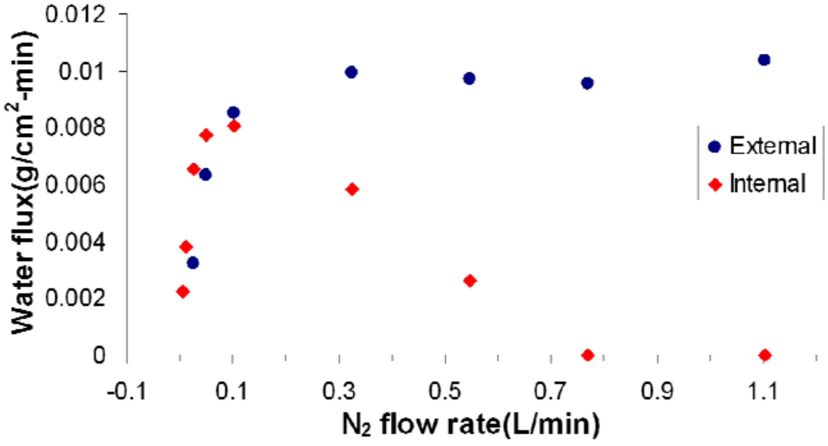

Figure 3-31 Water flux calculated from data shown in Table 3-8 comparing internally and externally housed relative humidity sensors.

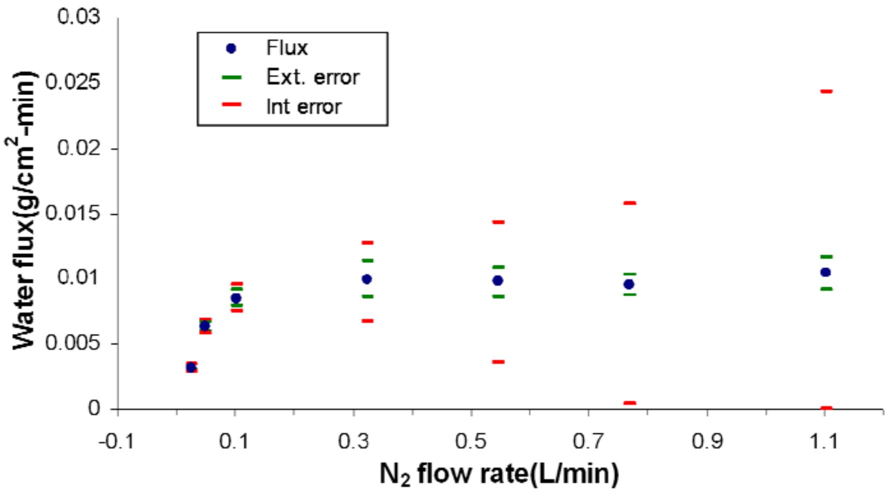

Figure 3-32 Water vapor flux through Nafion N115 at 80°C with error limits shown for using a relative humidity sensor at the temperature of the experiment (internal) and with adjustable temperature (external).

Table 3-9 Flux calculated from two sensors measuring the same vapor sample at different temperatures including error analysis.

			Flux			
Sensor location	Temperature (°C)	RH (%)	Calculated (g/cm^2-min)	Upper limit (g/cm^2-min)	Lower limit (g/cm^2-min)	Error (%)
Internal	80±1.2	30±1.7	0.0101	0.0109	0.0093	7.65
External	23±0.3	1.79±3.23	0.0101	0.0302	0	299

3.5.3 Evaporative cooling

A phase change occurs when water in the vapor phase enters Nafion or when water in Nafion evaporates entering the vapor phase. This phase change is accompanied by a change in internal energy or enthalpy ΔH_{lg}, even if temperature is held fixed. Evaporation of water from Nafion into the vapor phase requires energy input, resulting in cooling, while condensation from the vapor phase liberates an equal amount of energy.

In order to determine the extent of evaporative cooling during permeation, a thermocouple was placed in the dry side flow channel and the temperature of the gas monitored and recorded at steady state permeation. This was done for liquid water permeation through Nafion N115 at 23 and 80°C (Figure 3-33). From this plot, it cane be seen that evaporative cooling is more significant at 80°C than 30°C. The explanation for this observation is that flux is greater at the higher temperature and therefore lowers the temperature of the incoming gas more. Evaporative cooling goes through a maximum at 80°C due to thermal mass of the incoming N_2 and permeation both increasing with flow rate, but at different rates. A maximum at 23°C is expected to occur at a flow rate higher than 1.1 L/min.

Evaporative cooling was not measured for vapor permeation, but is expected to be much less significant than for the case of liquid water. This is based on the observation that permeation rates are significantly lower for vapor transport. Additionally, thermal conductivity seems to be a minor contributor to the thermal balance of the dry side gas based on the observation that a maximum occurs in evaporative cooling at 80°C.

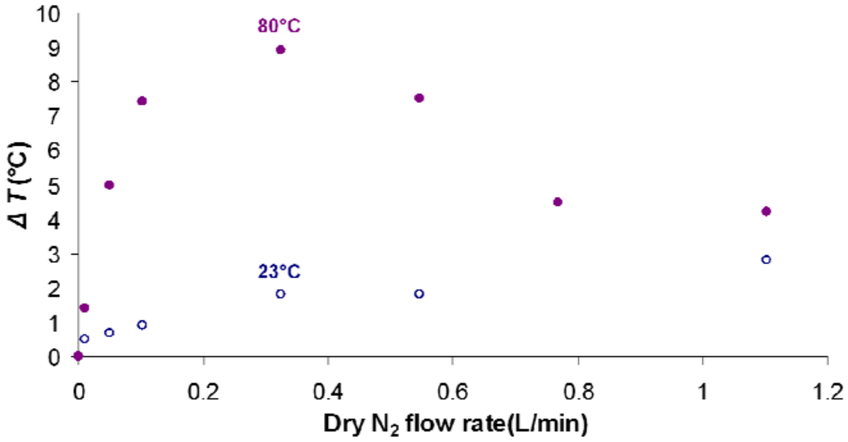

Figure 3-33 Evaporative cooling in dry side flow channel measured for liquid water permeation through Nafion N115 at 23 and 80°C. ΔT is the difference in temperature without and with permeation with all points representing cooling.

3.6 Conclusion

Permeation of liquid and vapor phase water through Nafion membranes of several thicknesses into dry N_2 was directly measured from 30 – 80°C. Permeation from liquid water was much greater than from vapor due to the negligible interfacial mass transport coefficient at the liquid/membrane interface and the increase of diffusivity with hydration. Permeation of liquid water through the membrane was dominated by vapor side interfacial mass transport. Permeation of water vapor through Nafion was dominated by diffusion and thus scaled roughly with membrane thickness.

For water vapor transport, permeation increased significantly with hydration, an observation attributed to diffusivity increasing significantly with hydration. Permeation increased with temperature, though less significantly than with hydration.

The phase of Nafion which segregates to the membrane/fluid interface, based on arguments of minimizing interfacial energy, is thought to differ in the presence of vapor and liquid water. For liquid water, a hydrophilic surface forms which results in enhanced interfacial mass transport. For water vapor, a hydrophobic surface with increased transport resistance impedes vapor transport into and out of Nafion.

The addition of a GDL significantly reduced permeation through Nafion for both liquid and vapor phase water. This decrease is attributed to the increase in interfacial mass transport resistance added by the GDL. Most GDLs used in fuel cells are hydrophobic, preventing liquid water from contacting the membrane surface.

3.7 Acknowledgements

Thanks go to Prof. Jay Benziger for his insight into water uptake and transport through Nafion films. I am indebted to Jay's patience and the time he spent with me in analyzing permeation results. Dr. M. Barclay Satterfield conducted water uptake experiments with Nafion concomitant with my permeation experiments. Many fruitful conversation about transport occurred with Barclay which shaped my thinking.

Brent Kirby's help in setting up a Lab View program to acquire data for the permeation setup is gratefully acknowledged. Brent also engaged in many helpful discussions on transport with me.

3.8 References

1. Majsztrik, P. W.; Satterfield, M. B.; Bocarsly, A. B.; Benziger, J. B., Water Sorption, Desorption and Transport in Nafion Membranes. *Journal of Membrane Science* **2007,** 301, (1-2), 93-106.
2. Ge, S. H.; Li, X. G.; Yi, B. L.; Hsing, I. M., Absorption, desorption, and transport of water in polymer electrolyte membranes for fuel cells. *Journal Of The Electrochemical Society* **2005,** 152, (6), A1149-A1157.
3. Thampan, T.; Malhotra, S.; Tang, H.; Datta, R., Modeling of Conductive Transport in Proton-Exchange Membranes for Fuel Cells. *Journal of The Electrochemical Society* **2000,** 147, (0), 3242-3250.
4. Weber, A. Z.; Newman, J., A theoretical study of membrane constraint in polymer-electrolyte fuel cells. *Aiche Journal* **2004,** 50, (12), 3215-3226.
5. Zawodzinski, T. A.; Derouin, C.; Radzinski, S.; Sherman, R. J.; Smith, V. T.; Springer, T. E.; Gottesfeld, S., Water-Uptake by and Transport through Nafion(R) 117 Membranes. *Journal of the Electrochemical Society* **1993,** 140, (4), 1041-1047.
6. Doyle, M., and Rajendran, G., Perfluorinated Membranes (Ch. 30). In *Handbook of Fuel Cells-Fundamentals, Technology, and Applications*, W. Vielstich, H. G., A Lamm, Ed. 2003; Vol. 3, p 377.
7. Satterfield, M. B. Mechanical and Water Sorption Properties of Nafion and Nafion/Titanium Dioxide Membranes for Polymer Electrolyte membrane Fuel Cells. Princeton University, Princeton, 2007.
8. Yeo, S. C.; Eisenberg, A., Physical-Properties and Supermolecular Structure of Perfluorinated Ion-Containing (Nafion) Polymers. *Journal of Applied Polymer Science* **1977,** 21, (4), 875-898.
9. Benziger, J., Conversation on calculating diffusivity from self diffusion determined by NMR. In Majsztrik, P., Ed. Princeton, 2007.
10. Satterfield, M. B.; Benziger, J. B., NonFickian Water Sorption Dynamic by Nafion Membranes. **2007,** forthcoming.
11. Takamatsu, T.; Hashiyama, M.; Eisenberg, A., Sorption Phenomena in Nafion Membranes. *Journal of Applied Polymer Science* **1979,** 24, (11), 2199-2220.
12. Morris, D. R.; Sun, X. D., Water-Sorption and Transport-Properties of Nafion-117-H. *Journal of Applied Polymer Science* **1993,** 50, (8), 1445-1452.
13. Legras, M.; Hirata, Y.; Nguyen, Q. T.; Langevin, D.; Metayer, M., Sorption and diffusion behaviors of water in Nafion 117 membranes with different counter ions. *Desalination* **2002,** 147, (1-3), 351-357.
14. Zawodzinski, T. A.; Neeman, M.; Sillerud, L. O.; Gottesfeld, S., Determination of Water Diffusion-Coefficients in Perfluorosulfonate Ionomeric Membranes. *Journal of Physical Chemistry* **1991,** 95, (15), 6040-6044.

15. Okada, T., Modeling polymer electrolyte membrane fuel cell performances. *Journal of New Materials for Electrochemical Systems* **2001,** 4, (4), 209-220.

16. Motupally, S.; Becker, A. J.; Weidner, J. W., Diffusion of water in Nafion 115 membranes. *Journal Of The Electrochemical Society* **2000,** 147, (9), 3171-3177.

17. Gates, C. M.; Newman, J., Equilibrium and Diffusion of Methanol and Water in a Nafion 117 Membrane. *AIChE Journal* **2000,** 46, (10), 2076-2085.

18. Gong, X.; Bandis, A.; Tao, A.; Meresi, G.; Wang, Y.; Inglefield, P. T.; Jones, A. A.; Wen, W. Y., Self-diffusion of water, ethanol and decafluropentane in perfluorosulfonate ionomer by pulse field gradient NMR. *Polymer* **2001,** 42, (15), 6485-6492.

19. Rivin, D.; Kendrick, C. E.; Gibson, P. W.; Schneider, N. S., Solubility and transport behavior of water and alcohols in Nafion (TM). *Polymer* **2001,** 42, (2), 623-635.

20. Krtil, P.; Trojanek, A.; Samec, Z., Kinetics of Water Sorption in Nafion Thin Films -- Quartz Crystal Microbalance Study. *Journal of Physical Chemistry B* **2001,** 105, 7979-7983.

21. Damay, F.; Klein, L. C., Transport properties of Nafion (TM) composite membranes for proton-exchange membranes fuel cells. *Solid State Ionics* **2003,** 162, 261-267.

22. Satterfield, M. B.; Majsztrik, P. W.; Ota, H.; Benziger, J. B.; Bocarsly, A. B., Mechanical Properties of Nafion and Titania/Nafion Composite Membranes for PEM Fuel Cells. *J. Polymer Science B: Polymer Physics* **2006,** 44, 2327-2345.

23. Gierke, T. D.; Munn, G. E.; Wilson, F. C., Morphology of Perfluorosulfonated Membrane Products - Wide-Angle and Small-Angle X-Ray Studies. *Acs Symposium Series* **1982,** 180, 195-216.

24. McLean, R. S.; Doyle, M.; Sauer, B. B., High-resolution imaging of ionic domains and crystal morphology in ionomers using AFM techniques. *Macromolecules* **2000,** 33, (17), 6541-6550.

25. Sensirion Data sheet humidity sensor SHT1x/SHT7x. http://www.sensirion.com/en/pdf/product_information/Data_Sheet_humidity_sensor_SHT1x_SHT7x_E.pdf (10/26/2007),

4 Nafion TiO_2 Composite Membrane Development

4.1 Introduction

Operating conditions of PEM fuel cells are limited, in part, by the dependence of certain membrane properties on temperature and hydration. Polymer electrolytes such as Nafion have an upper operating temperature of ~80°C, above which long-term performance sharply declines. Further, proton conductivity is dependant on membrane water content and maintaining high levels of hydration is often a challenge. Improving the mechanical properties and proton conductivity of membrane materials at elevated temperature and reduced relative humidity would improve the operation of PEM fuel cells.

Several investigators have taken the approach of forming composites with ionomers such as Nafion in order to improve its performance under elevated temperatures and reduced water activity[1-21]. Two approaches have been taken. One is to add inorganic additives that are known to have high acidity (proton conductivity) and hydrophilicity (for retaining hydration) such as heteropolyacids (HPA) or zirconium phosphate ($Zr(HPO_4)_2$). The other approach is to add metal oxides (e.g., SiO_2, TiO_2, ZrO_2, etc.) which are thought to either crosslink ionomers through their ionic groups and/or enhance water absorption and proton transport due to surface acidity, improving their mechanical properties and water retention at elevated temperatures and reduced relative humidity.

The Bocarsly and Benziger labs have investigated both approaches with moderate success[1-4, 22-27]. Much work has been done to characterize composite membranes and test them in working fuel cells in this lab. My specific contribution to the area of composite Nafion/metal oxide membranes was to improve the procedure for recasting membranes while adding to the understanding of the interaction occurring between the metal oxide particles and the polymer[28]. My focus was specifically on recast TiO_2 membranes, but the approaches and principles can be applied to other metal oxide systems.

4.1.1 Literature review of Nafion/metal oxide composites

The first composite Nafion/ metal oxide membranes were made by Mauritz and coworkers by the sol-gel method[18-21]. In this early work, Mauritz et al. used Nafion to template the formation of SiO_2 by *in situ* sol-gel reaction of tetraethoxysilane (TEOS) acid catalyzed by the sulfonic acid groups of the polymer. The formula for the silica was reported to be $SiO_{2(1-0.25x)}OH_x$. They found, through SAXS studies, that there was a gradient of SiO_2 through the cross section membranes as a result of diffusion and sol-gel reaction rates. They also reported increased mechanical strength (tensile modulus) which increased with weight loading up to a point. Scattering and spectroscopic studies revealed that an inorganic phase formed throughout the material with the morphology of Nafion acting to template the formation of silica.

Chalkova and co workers[29] recently reported on their work with Nafion/TiO_2 composites produced by recasting. Membranes with 0, 10 and 20 wt% TiO_2 were investigated. They attribute increased fuel cell performance at 120°C and reduced RH to increased water absorption by the hydrophilic titania particles. No increase in water uptake was seen at high relative humidity, but was significant in the 25 – 50% RH range. High water retention at lower water activity was attributed to the electrostatic attraction of the electrical double layer (EDL) at the TiO_2 surface.

Interaction of metal oxide particles in recast Nafion composites was investigated by Arico and co workers[17]. Specifically, they examined the influence of the acid-base characteristics of several inorganic fillers on direct methanol fuel cell performance at high temperature. Membranes were prepared with SiO_2, SiO_2-PWA, Al_2O_3, and ZrO_2 particles. These particles were selected to give a range of surface pH values which were measured for slurries of each of the particles. It was reported that water retention and conductivity increased with surface acidity and this was attributed to the electronegitivity of the metals making up the metal oxides. Si, which has the highest electronegativity of the metal oxides tested, gave the highest surface acidity and the best elevated temperature fuel cell performance. They attribute the improved performance to improved conductivity/water retention brought about by coordination of water on the particle surface.

Adjemian, et al.[3, 27, 30, 31] reported on the performance and characterization of several metal oxide composites recast with Nafion. Membranes were made using SiO_2, TiO_2, Al_2O_3, and ZrO_2. Both SiO_2 and TiO_2 produced improved fuel cell performance at elevated temperature and reduced humidity. The authors attributed the improvement in performance to a specific chemical interaction between the metal oxide particles and the the sulfonate groups in Nafion[31]. TG-MS and fluorescence experiments, along with physicochemical measurements, were cited as compelling evidence for a chemical interaction in the membranes contributing to improved fuel cell performance. They also reported an increase in conductivity for the TiO_2 and SiO_2 composites.

Higher water uptake and conductivity at elevated temperature and low RH was also reported by Datta et al.[12] for ZrO_2 membranes produced by both recasting and sol-gel methods. They report that particle size strongly influenced water uptake and conductivity of membranes, and thus fuel cell performance. The smallest particles/largest effect were seen for *in situ* ZrO_2 membranes.

Additional work by Datta and coworkers[9] was reported for composite Nafion membranes prepared containing ZrO_2, SiO_2, and TiO_2 particles via *in situ* sol-gel synthesis . They report improved water uptake for all membranes at 90 and 120°C. In their study, only ZrO_2 showed increased conductivity over plain Nafion (a 10% increase at 40% RH at the two temperatures investigated). They attribute this increase in conductivity to surface acidity which was obtained from a decrease in EW for the ZrO_2 membrane, relative to the Si and Ti counterparts. They also infer improved thermo-mechanical properties for all composites based on TGA and DMA studies.

In the work of Baglio et al.[10], surface area of filler particles is reported to be the dominant parameter affecting membrane properties. For this study, TiO_2 particles produced from sol-gel synthesis *ex situ* were calcined over a range of temperature as a way to obtain different size particles[xiv]. Membranes were then recast using these particles. The main conclusions reached in this study were that particle surface area and functional groups determined membrane water uptake and that proton transport occurring on the surface of particles enhanced fuel cell performance. Water retention on the filler surface was attributed to absorption on acidic sites.

Alberti and Casciola[16], in a review of composite membranes, reported that recast 3 wt% silica membranes increase water uptake from 18 to 41 wt% compared to plain Nafion. They attribute this increase in water uptake to changes in morphology of the membrane brought about by inclusion of silica particles. It should be pointed out that the

---

[xiv] Calcining temperature of 500 and 650°C produced anatase particles while 800°C produced rutile. Particle size increased with temperature from 12 to 22 to 39nm.

silica membranes were impregnated with Pt which was found to reduce crossover in H_2/O_2 cells, and the authors state that this is an unrealistic membrane treatment due to cost. Without the Pt impregnation, the authors report that there is poor fuel cell performance of silica membranes when dry feeds are used, citing the work of Watanabe, et al[5].

4.2 Composite Membrane Preparation

Composite Nafion/metal oxide membranes are prepared by two distinct methods; *in situ*/sol-gel and recast. The sol-gel method starts with a standard Nafion film which has been annealed. The membrane is then swollen with reactants which undergo a sol-gel reaction in the membrane to produce an amorphous metal oxide phase inside the membrane. The two-phase microstructure of the membrane serves as a template for the formation of the metal oxide particles. Precursors for the sol-gel reaction are hydrophilic and infiltrate the sulfonic acid clusters where they remain to form metal oxide nanoparticles. The teflonic matrix of the Nafion is largely free from the metal oxide particles. In their final form, the metal oxide particles are amorphous and nanoscale, resulting in transparent membranes.

The recast method begins with a Nafion dispersion in a mixture of solvents and involves creating a suspension of metal oxide particles in the Nafion solution. The solvents are removed by evaporation, leaving behind a uniform membrane of polymer and inorganic particles. Membranes prepared by this method are opaque above a certain loading, suggesting agglomeration. Since metal oxide particles in the recast membranes are made *ex situ*, they can be made by a number of processes including the sol–gel method and flame sprayed pyrolysis (FSP). Particles can also be calcined over a range of temperature which are beyond the degradation temperature of Nafion, leading to increased control over particle size and crystal structure. The greater processing flexibility for metal oxide particles prepared outside the membrane leads to an increase in available particle morphology, size, and shape. There is compelling evidence that particle size, shape, and morphology strongly impact interaction with Nafion and the overall properties of the composite membrane.

4.2.1 Materials

Nafion solutions are commercially available from Ion Power with different equivalent weights (1,000 and 1,100 g Nafion/mol SO^{-}_3) and solvent to polymer ratios (5 and 15 wt%). Composition ratio varies between the 5 and 15 wt% solutions according to Table 4-1. Several similar methods[32-35] are described in the literature for creating perfluosulfinated ionomer dispersions by dissolving the solid ionomer in a water/alcohol mixture at high temperature and pressure which are likely similar to the process used by Ion Power.

Investigations of Nafion solutions by light and neutron scattering have indicated that in water and ethanol solutions form colloidal suspensions[36, 37]. The Nafion "particles" assemble into micelles with PTFE like crystalline interiors and hydrophilic exteriors. Electrostatic repulsion between micelles maintains uniform spacing with a 3D cubic array being most likely. The colloidal aggregates are non-spherical with dimensions over15nm. Though Nafion dispersions are not actually true solutions, settling does not seem to be a problem [38].

Titanium dioxide nanoparticles spanning a range of dimensions were purchased from various suppliers. A list of the particles, dimensions, distributors, as well as crystal structure can be found in Table 4-2. SEM micrographs of 5nm and 10nm particles are shown in Figure 4-1.

Table 4-1 Composition of Liquion-1100® and Liquion-1000 Nafion solutions produced by Ion Power[39].

Component	5wt% Liquion	15wt% Liquion
Nafion	4.95-5.05 wt%	14.9-15.1wt%
Water	20 wt%	45 wt%
Isopropanol	75 wt%	40 wt%
1-propanol, methanol, methyl propyl ether, propyl ether.	< 1%	<1%

Table 4-2 Summary of TiO_2 nanoparticles used in the study of composite Nafion membranes presented in this chapter. Suppliers of particles: a = Nanostructured & Amorphous Materials, Inc.; b = Sigma-Aldrich; c = Degussa-Huls; d = Alfa Aesar.

Particle Size (nm)	Surface area (m^2/g)	Crystallinity (anatase/rutile)	Supplier	Comment
5	210	99/0	a	Spherical particles
10	120	99/0	a	Spherical particles
15	190-290	100/0	b	
21	50	70/30	c	FSP => ~1µm agglomerates
30-40	20-25	0/100	b	“35 nm”
10 x 40	130-190	0/100	b	Needle like
1,000		0/100	d	

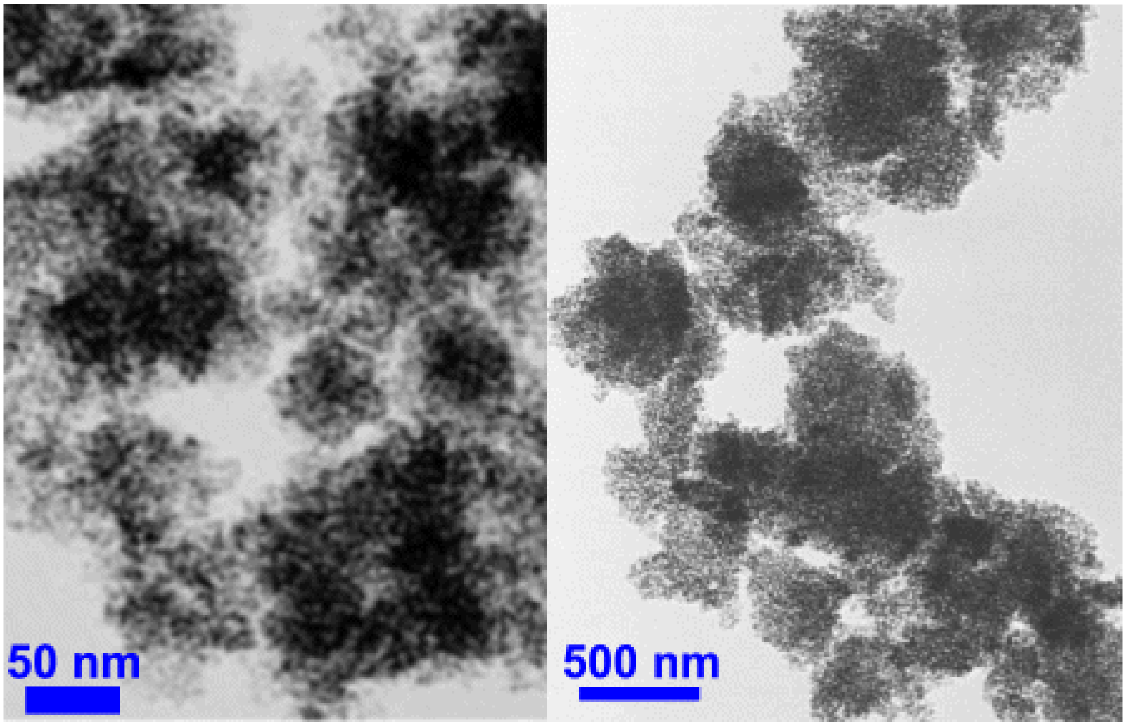

Figure 4-1 SEM micrograph of 5nm (left) and 10nm(right) TiO_2 particles purchased from Nanostructured & Amorphous Materials, Inc. SEM micrograph courtesy of Dr. Hitoshi Ota.

4.2.2 Composite Membrane Recasting Procedure

What follows is a reliable procedure for producing composite TiO_2 (or other metal oxide) membranes by the recasting method. Membranes ranging in thickness from 25.4 – 254µm and with TiO_2 weight loading up to 20%[xv] were successfully produced by this method. Uniform, mechanically robust membranes over this range of thickness and weight loading were achieved. Following the procedure, an explanation of the various factors impacting membrane quality and properties will be discussed.

Recasting a composite membrane requires mixing together solubolized Nafion, metal oxide particles, and (usually) a solvent in addition to what is already part of the Nafion solution. To achieve good dispersion of particles in a colloidal suspension, metal oxide particles are first mixed with the *solvent alone* and sonicated for at least an hour.

[xv] Weight loadings are based on weight of TiO_2 particles to weight of dry Nafion.

12 mL glass vials (or 25 mL Erlenmeyer flasks for larger membranes) work well for this. To the suspension of particles in solvent, add the Nafion solution and sonicate[xvi] until well-mixed. Because the Nafion solutions are viscous, mixing with the solvent suspension is slow and can be encouraged by shaking by hand (avoid excessive formation of air bubbles which may appear in the finished membrane). The ratio of solvent added to the Nafion dispersion is an important factor in producing a good membrane. Both solvent type and Nafion solution weight percentage influence what ratio to use. The proportions needed for a 127μm thick membrane with 3wt% loading of metal oxide particles is shown in Table 4-3.

The colloidal suspension of metal oxide particles in Nafion solution is then cast on a flat glass plate[xvii]. A glass cylinder about 1 – 2" high and the diameter of the finished membrane (membranes were always 2.5" diameter for the research presented in this chapter) is placed on the glass plate to act as a mold for the membrane[xviii]. Solvents are removed in an oven at 50 – 80°C. Solvent removal takes approximately 12 hrs, depending on membrane thickness, solvent volume and type, and oven temperature. Once solvents are completely removed, anneal the membrane for 1 hr at 160°C. Failure to completely remove recasting solvents before annealing will result in a membrane with a blistered surface.

[xvi] Fisher Scientific ultrasonic cleaner model FS20 was used for all experiments.

[xvii] Using a glass mirror instead of plain glass makes it easier to detect smudges on the surface which should be cleaned.

[xviii] The Nafion solution will leak between the ground edge of the cylinder and the glass plate unless an old Bocarsly lab trick is followed. Before pouring the Nafion solution into the cylinder, place the cylinder on the glass in the final desired location, wetting the cylinder/plate interface with excess IPA or ethanol. Place in the solvent removal oven at the solvent evaporation temperature and allow all of the solvent to evaporate. The cylinder is now "sealed" to the plate just enough to prevent leaking of the recasting solution, so don't move it. Perhaps some residual Nafion on the ground edge of the ring forms the seal after the alcohol swells it.

Table 4-3: Quantities of metal oxide particles, Nafion solution (15wt% from Ion Power) and ethanol *or* isopropanol to be used in making a 3wt% membrane 127μm thick membrane and 6.35cm diameter.

Membrane Thickness (μm)	Particle loading (wt%)	Metal oxide (mg)	Ethanol or (IPA)(g)	Nafion solution (15wt%)
127	3	27	16 (8)	6g

4.3 Recasting Considerations

The exact phenomena occurring during the recasting process of plain or composite membranes is not fully understood. However, there are a number of parameters which influence membrane quality and characteristics. This section presents several relevant recasting parameters, observations gained from experience recasting membranes, and proposed explanations for observed effects.

4.3.1 Solvent

Solvents used in recasting composite membranes interact both with the metal oxide particles as well as the Nafion suspension. Differences in morphology as well as particle dispersion are attributed to the solvents used in recasting. The exact interaction between solvents and the Nafion dispersion/particle suspension is complicated and not completely understood. However, some general interactions are likely to exist which affect composite membrane morphology.

Nafion dispersions are thought to form rod-like micelle structures, based on light scattering experiments[40]. In polar solvents, such as water and alcohols, the hydrophilic end groups orient towards the outside while the hydrophobic backbone segments are in the center. Upon solvent removal, orientation of micelle structures (and thus morphology) should depend on solvent composition. Increasing solvent polarity should increase the interaction between sulfonic groups. Protic solvents should also interact more strongly with the dispersion. Solvents which have a non-polar segment, such as IPA and ethanol, should increase chain mobility during transition from dispersion to polymer, affecting morphology. The presence of multiple solvents, such as Ethanol and water, should have synergistic effects on morphology (similar to the swelling seen in Nafion by ethanol/water mixtures[41]).

It is unclear exactly how the solvent/Nafion/metal oxide interaction develops during solvent removal. It is likely that bonding/interaction between particles and Nafion, through sulfonic groups, occur in solution and remain in the final membrane, impacting morphology.

Early work suggested that only high boiling points would result in high mechanical strength films when recasting and that low boiling point solvents (e.g., ethanol) produced brittle membranes[32, 35]. However, it was found, through trial and error, that by carefully selecting solvent ratios and solvent removal temperature, high quality recast membranes with properties similar to commercially available Nafion can be produced by recasting without using high boiling point solvents. High quality membranes have been produced by the recasting method using the following alcohols added to Liquion solutions; ethanol, IPA, IBA, and DMSO. Solvent recasting with DMSO requires the use of a vacuum oven for solvent removal due to DMSO's high boiling point. Additionally, high-quality membranes were also made by recasting Nafion in pure ethanol after the other solvents in the Ion Power solution were removed.

It should be noted that sonicating TiO_2 particles in DMSO produces a strong sulfurous odor. It is likely that this odor is caused by the presence of dimethyl sulfide[xix][42]

[xix] Dimethyl sulfide (DMS) commonly occurs in nature and is one of the main chemicals responsible for giving the sea its distinctive odor.

(DMS) and is the result of catalytic interaction of DMSO with TiO_2. It is assumed that no modification of the titania surface occurs due to sonication in DMSO or the generation of DMS, though no experiments were done to investigate this.

4.3.2 Annealing temperature

Before the annealing process, bonding between polymer chains in Nafion are not completely formed and the microstructure of the membrane is not fully formed, being partially like the aggregates found in the dispersion. This results in a mechanically weak membrane. The membrane can easily be redissolved in IPA, ethanol, or even water at room temperature before the annealing step is complete. After annealing, these alcohols only swell the membrane. Annealing temperature should be great enough to permit unhindered chain movement for a time that allows for relaxation to reach equilibrium (around an hour). With chains free to move at high temperature, the polymer assumes a morphology which is thermodynamically stable. This may not be the same morphology that the polymer would assume at lower temperatures, but at low temperatures polymer chains are not as free to move. Cooling the membrane below the annealing temperature where chains are less free to move partially locks in the annealing morphology. Boiling the membrane in liquid water at 100°C alters the morphology somewhat, but does not provide the same critical change in morphology that annealing does.

Through trial and error, it was found that membranes recast from DMSO were mechanically weak after being annealed at 130°C for 15 minutes, the annealing procedure developed for composites recast with IPA. It is possible that residual DMSO which remained in the membrane after solvent removal under vacuum at 80°C interfered with annealing at the lower time and temperature. Increasing annealing temperature and time 160°C and 1 hr, respectively, produced membranes with excellent mechanical properties. Nafion does not undergo significant rapid thermal degradation until temperature exceeds at least 280°C, and heat sealing of Nafion is performed at 300°C[43]. A range of temperatures are reported to give good annealing of Nafion, depending on the history of sample treatment, including recasting solvent and counterion type. Gebel and coworkers investigated recasting Nafion solutions using several different solvents[44]. They found that an annealing temperature of 200°C gave optimum results for plain recast Nafion. Therefore, annealing at 160°C for 1 hr was adopted for all recast membranes, regardless of recasting solvents.

4.3.3 Particle Dispersion

Particle dispersion in the recasting solution strongly impacts the final morphology of the recast membrane. If particles are agglomerated during solvent evaporation, the resulting membrane are less mechanically robust than if good dispersion is achieved. Agglomerated particles have less ability to stay in suspension, due to an increase in settling forces relative to Brownian motion, electrostatic repulsion, and buoyancy/viscous forces which keep particles in suspension. Membranes recast from poorly dispersed particles can have visible non-uniformities resulting from large scale phase separation (on the order of mm). For very poorly dispersed suspensions, settling of particles during recasting results in membranes with an exposed layer of particles on the bottom side of the membrane.

Particle dispersion can be increased by sonication of the suspension prior to recasting. It is especially useful to sonicate particles first in the solvent alone (i.e., before adding Nafion solution) in order to have good dispersion. Sonication serves to break up particle agglomerates, resulting in smaller agglomerates and perhaps even individual particles. Sonication results in membranes which are visibly more uniform and of higher mechanical strength compared to those obtained using mechanical stirring with a magnetic stir bar to achieve particle dispersion. Additionally, TGA scans of composite membranes comparing the dispersion methods of stirring and sonication indicate that greater interaction between TiO_2 particles and sulfonic acid groups occurs for sonication. A TEM micrograph of a composite membrane produced by stirring is shown in Figure 4-2. Note the large agglomerates formed in the membrane.

Particle flocculation can be reduced by increasing electrostatic repulsion between particles by adjusting the pH/ionic content of the solution by the addition of an acid or salt. Since ions can interact with Nafion's sulfonic acid groups, the affect of ions on the Nafion suspension as well as particles must be considered.

Solvent interaction with particles also affects the quality of the colloidal dispersion. Increased viscosity reduces particle settling while polarity affects electrostatic interaction with particles.

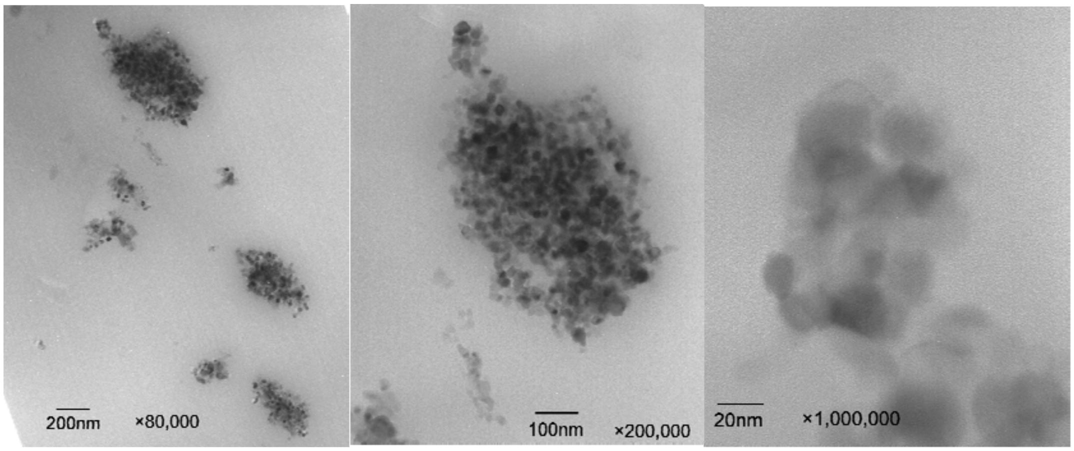

Figure 4-2 TEM micrograph of a 3%, 21nm TiO_2 composite membrane (0.005" nominal thickness) recast using IPA and dispersed using only stirring. Dark regions are particle agglomerations appearing throughout the membrane. Image courtesy of Dr. Hitoshi Ota and Mitsubishi inc.

4.3.4 Solvent Removal Temperature

The temperature at which the recasting solvents are removed is determined by membrane thickness as well as the recasting solvents being used. An upper limit for the temperature at which solvent is removed is generally considered to be around 80°C[44]. Evaporation should occur quickly enough to avoid as much particle settling as possible, yet slow enough to prevent the appearance of non-uniformities, such as blistering. To increase the rate of evaporation for high boiling point solvents (e.g., Dimethylsulfoxide (DMSO)), solvents should be removed in a vacuum oven at elevated temperature. Low boiling point solvents such as ethanol can easily be removed at atmospheric pressure. Generally, solvent removal for thicker membranes should be done at lower temperature than thinner membranes. This is because the solvents must diffuse through more polymer as thickness increases. If evaporation temperature is too high, blistering and other imperfections will result. Differential expansion, due to solvent gradients, can result in stresses that lead to cracking.

For multi-component solvent systems, solvent composition changes with time and is temperature dependant. Lower boiling point solvents evaporate first, leaving behind the higher boiling point solvents. For example, recasting with DMSO added to 15 wt% Ion Power solution gives a mixture of primarily DMSO, water, and IPA. Since DMSO has such a high boiling point compared to the other solvents, a point will arrive during solvent removal when all of the water and IPA have been removed, leaving only DMSO and polymer. Since solvent type impacts the final morphology of the membrane, evaporation temperature can affect morphology. If solvents with similar boiling points are used, evaporation temperature has more of an impact on the composition of the recasting solution.

Solvent composition is also strongly dependant on the starting solvent ratios, of course. Through trial and error, it was determined that different amounts of ethanol and IPA needed to be added to the Ion Power Nafion solution when recasting. For a 0.005" thick membrane cast in a 2.50" diameter cylinder, 6g of N115 15wt% Ion Power solution mixed with 8g of IPA produced uniform composite membranes at 75°C. Substituting the same weight fraction of ethanol for IPA, however, produced cracked membranes under the same conditions. Increasing the amount of Ethanol to 12g from 8g and keeping all other variables constant produced uniform composite membranes. Using 12g of IPA resulted in poor quality (cracked and phase-separated) membranes.

As membranes become thicker (greater than 0.005"), producing a uniform membrane without defects becomes increasingly difficult. The reason for the difficulty is that solvent evaporation occurs from the recasting surface and creates a concentration gradient in the recasting solution which can lead to the formation of a polymer skin on the surface of the solution. Reducing the solvent removal temperature decreases the concentration gradient. A similar situation arises when applying paints and other polymer finishes to surfaces. Thick coats of finish tend to blister and have other defects as a result of the finish “skinning over”. Just as thick coats of paint can be built up from multiple applications of thin coats, thick Nafion membranes can be made by recasting smaller amounts of polymer solution at a time, allowing solvent evaporation to occur between “coats”. Since Nafion is easily solubolized by the recasting solutions as long as annealing has not been done, layers created by separate “coats” will blend seamlessly together. A similar affect is seen for paints and other polymer coatings if only a short time elapses between coats; chemical bonds between coats will form to create a polymer coating which is a single, uniform layer. If too much time elapses between applications for polymer coatings, chemical bonds at the coating’s surface completely react, necessitating mechanical roughening of the surface to allow for adhesion of the subsequent coat.

Besides affecting solvent evaporation rate and thus solvent/polymer concentration gradients, temperature should have a direct affect on morphology. This is because the polymer aggregates of the colloidal dispersion become more free to undergo rearrangement as temperature increases, increasing interaction between aggregates. The presence of solvents increases aggregate mobility. Polar protic solvents which have a non-polar group (e.g., ethanol) are especially effective at disrupting inter-chain bonding and thus facilitating chain rearrangement.

4.3.5 Recasting Surface

The wetting angle of the recasting substrate should impact membrane morphology. Hydrophilic surfaces (i.e., glass) interact with the sulfonic acid groups which are oriented to the outside of the Nafion micelles, causing the dispersion to wet the glass. A hydrophobic surface would tend to repel the Nafion micelles. The final solvent free polymer likely shows some small degree of history dependence on casting substrate. Additionally, solvent interaction with the substrate impacts wetting.

The casting surface should be reasonably level to ensure uniform thickness over the entire membrane. However, it is neither practical nor necessary to maintain levelness on the order of the desired membrane thickness tolerance (~ 0.0005” of thickness per 1” of length) since surface wetting/tension acts as a natural control for membrane thickness and uniformity. Experience has shown that membranes 0.010 ±0.00025” thick can be produced with repeatability by casting on a surface leveled with a bubble level to ~0.002” per linear inch. Hydrophilic recasting surfaces should provide better thickness control through surface wetting than do hydrophobic surfaces, though no experiments were done in this area by the author.

4.4 Interaction of TiO_2 Particles with Nafion

4.4.1 Introduction

The interaction between Nafion and TiO_2 nanoparticles in recast composite membranes was investigated. Both TGA and TG-MS were used as tools. The impact of particle size/surface area, particle loading, and membrane preparation method were investigated. Mechanisms for the thermal decomposition mechanism of Nafion and composite Nafion/TiO_2 are suggested. This investigation was the result of a collaboration with Dr. Hitoshi Ota, a research scientist at the Mitsubishi Chemical Group

Science and Technology Research Center, Inc. Dr. Ota held a postdoctoral position under Prof. Andrew Bocarsly at Princeton University during the time that this project was being done. Dr. Ota conducted the initial analysis on the thermal decomposition of composite Nafion/TiO_2 using TG-MS.

4.4.2 Experimental

Nafion composite TiO_2 membranes were prepared by recasting using a 5% by weight Nafion solution (Ion Power) mixed with a solvent (either isopropanol (IPA) or dimethyl sulfoxide (DMSO)) and TiO_2 particles. Details about the particles used in the investigation are listed in Table 4-2. The particles were suspended in a mixture of DMSO or IPA and Liquion by sonication, cast on a flat glass surface, and the solvent was removed at ~80 °C in a vacuum oven (for DMSO) or at 75 °C without vacuum (for IPA). The membranes were then annealed, cleaned, and acid exchanged.

Analysis of the interaction of the TiO_2 particles with Nafion was performed using Thermogravimetric-Mass Spectrometry (TG-MS) analysis ((TG)(Seiko EXSTAR6000), (MS) (Agilent 6890N)) and Thermogravimetric Analysis (TGA) (Perkin Elmer TGA 7). For the TGA scans, a heating rate of 1 °C/min was used and samples were held at 100 °C for 60 minutes to allow for water removal. All TGA runs were performed under Argon. The TG-MS scans were performed on samples dried at 70 °C in a vacuum oven and a scan rate of 10°C/min was used. The TGA scans were performed by the author while the TG-MS runs were conducted Dr. Hitoshi Ota.

The thermogravimetry-mass spectrometry (TG-MS) and temperature programmed desorption or decomposition (TPD-MS) analyses of Nafion/Inorganic composite membrane were performed with the TG-MS system by coupling TG-DTA (Seiko

EXSTAR6000) with GC/MS (Agilent 6890N) and the TPD-MS system by coupling the pyrolyzer with GC/MS (Agilent 5973N). The pyrolysis temperature was programmed to increase from 25 to 500°C at a rate of 10°C/min under helium flowing at 60 ml/min. The gaseous decomposition products were introduced directly into the MS unit via a gas transfer tube with a deactivated fused silica capillary. The transfer lines were maintained at 200°C. The MS interface temperature was set at 250°C. The MS system was maintained at about 1×10^{-6} torr.

4.4.3 Results of TG-MS investigation

TG-MS data for the thermal decomposition of extruded Nafion and Nafion composite TiO_2 (21 nm particles) membranes are presented in Figure 4-3and Figure 4-4, respectively. From these data, we propose that plain Nafion decomposes in two steps while the Nafion TiO_2 composite decomposes in three steps, as indicated in the figures.

For both plain and TiO_2 membranes, free water is the first to be removed. The sulfonate group is removed next, concomitant with the removal of water bound to the sulfonate. The sharpening and shifting to lower temperature of the water and SO_2 peaks (MS plots) with the addition of TiO_2 indicates that there is likely a chemical interaction between the acid groups in Nafion and the surface of the TiO_2 particles and that TiO_2 catalyses the reaction. We propose that there are coordinately unsaturated sites on the surface of the TiO_2 which bond to an O on the sulfonate. This proposed interaction is illustrated in Figure 4-5.

Along with the loss of H_2O and SO_2 is CFO from the ether linkages. This is visible as a small peak in the MS plot for the TiO_2 membrane, but is not visible for the plain Nafion since the loss of the sulfonate group occurs over a broader temperature range and is thus, present in concentrations beyond the sensitivity of the instrument. Further support for this is seen in TG-MS scans showing the appearance of CF_2 and C_2F_4 along with H_2O and SO_2.

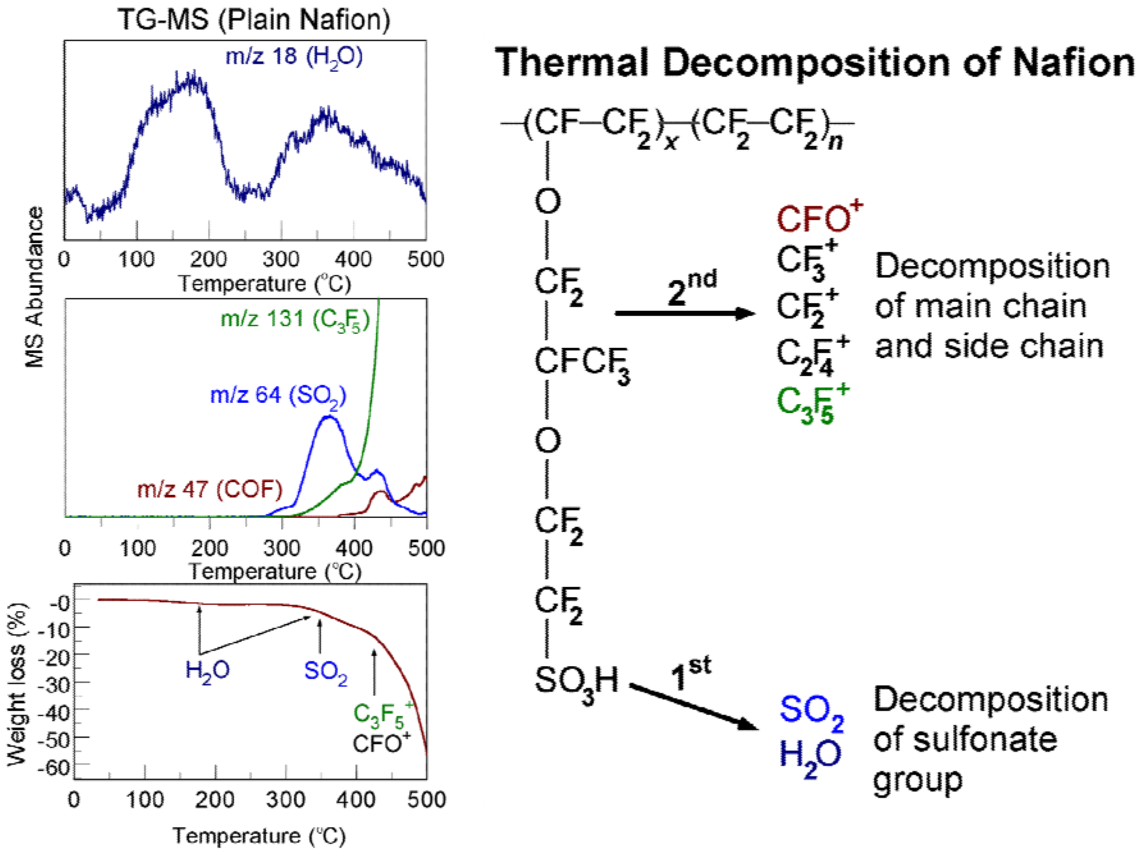

Figure 4-3 TG-MS of plain Nafion (N115) in the acid form with the appearance of different species indicated (left). Thermal decomposition order of plain Nafion (determined from TG-MS plots at left) including probable sources for the different species detected. Data collected by and provided with the kind permission of Dr. Hitoshi Ota[28].

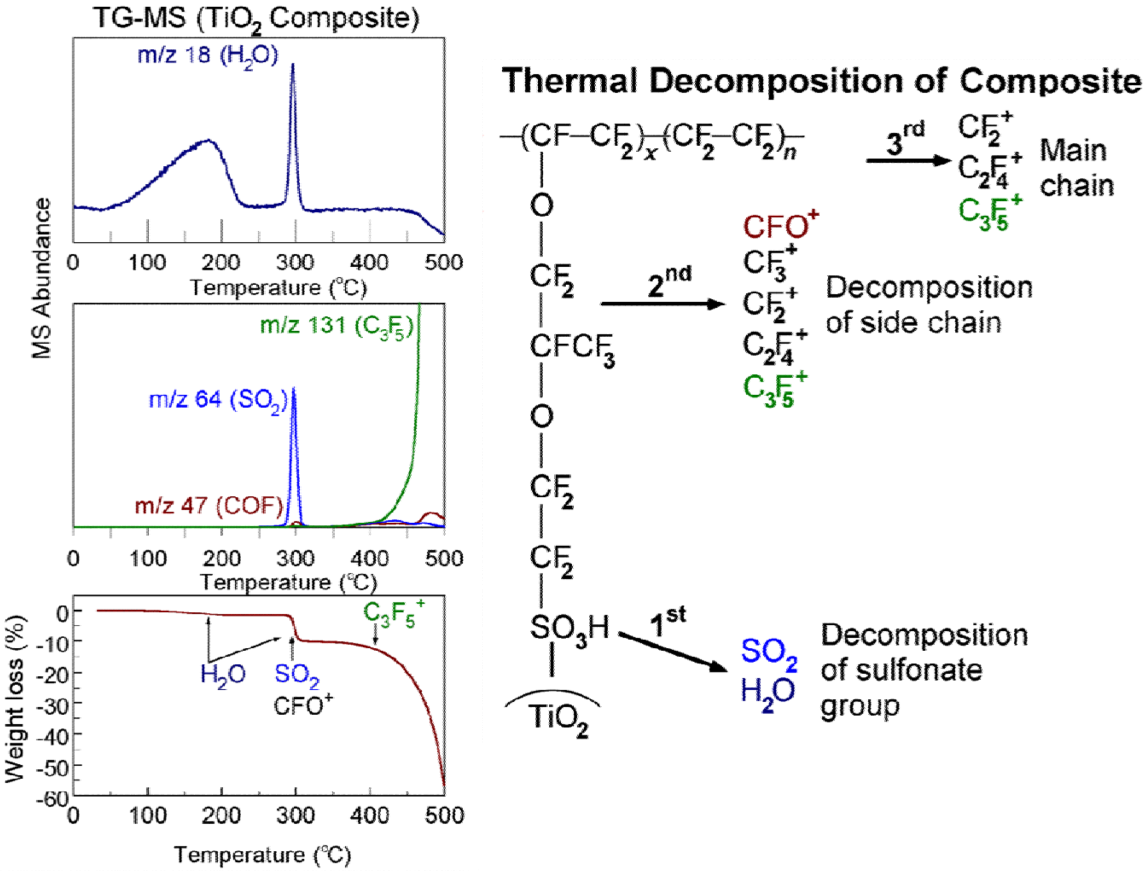

Figure 4-4 TG-MS of a 3 wt % composite Nafion/TiO_2 film in the acid form with the appearance of different species indicated (left). Thermal decomposition order the composite (determined from TG-MS plots at left) including probable sources for the different species detected. Data collected by and provided with the kind permission of Dr. Hitoshi Ota[28].

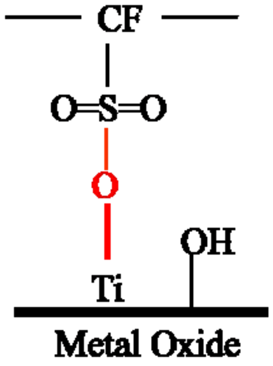

Figure 4-5 Proposed interaction between TiO_2 particles and Nafion in composite membranes. TiO_2 particles are thought to crosslink Nafion through interaction of unsaturated sites on the surface of titania with oxygen as shown in red.

4.4.4 Results of TGA Investigation

Knowing the differences in thermal decomposition between plain Nafion and Nafion/TiO_2 composites based on the TG-MS results presented in the preceding section, TGA can be used to further investigate the interaction of TiO_2 with Nafion. A comparison of the thermal decomposition of Nafion composites prepared with different size/types of TiO_2 (Error! Reference source not found.) suggests that the different TiO_2 particles interact differently with Nafion. The addition of 5, 10, 21 and 35 nm TiO_2 particles all result in the bound water and SO_2 loss shifting to lower temperature and occurring over a smaller temperature range. The 21, 10, and 5 nm particles give the largest slope in the water and SO_2 loss region (ca. 230°C). This indicates that these particles have the strongest interaction with the sulfonate group.

Perhaps the most interesting result shown here is the comparison of the thermal decomposition of plain Nafion to the Alfa Aesar TiO_2 composite. It was previously reported that membranes prepared with Alfa Aesar TiO_2 filler showed no improvement over plain Nafion when tested at elevated temperature[4]. The TGA curves for plain Nafion and the Alfa Aesar composite are identical (up to 300°C), indicating that no chemical interaction is occurring between the particles and Nafion. This strongly suggests that it is the chemical interaction between metal oxide particles and Nafion which improves the performance of Nafion.

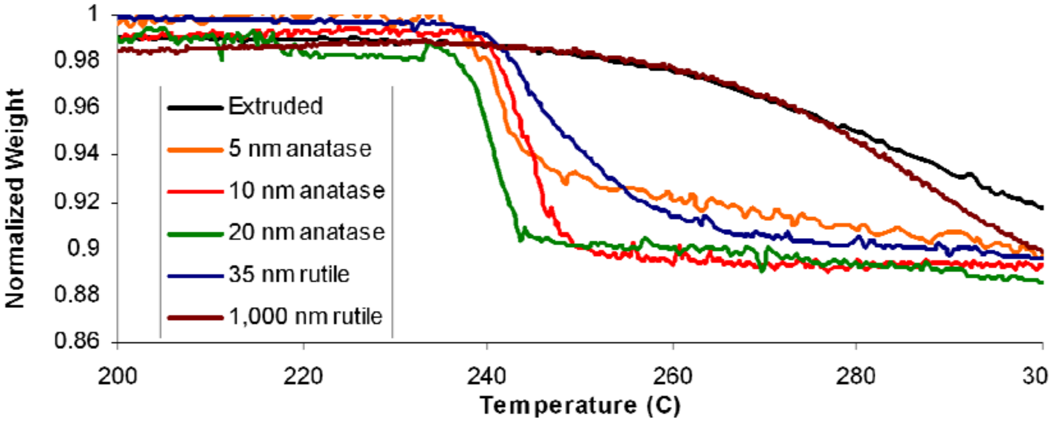

Figure 4-6 TGA scan of different Nafion TiO_2 composites. All are 0.005" thick, recast from ethanol based solutions and are 3wt% TiO_2. Scan shows the affect of particle size on the thermal decomposition in the temperature range associated with the decomposition of the sulfonic acid groups. From reference [28].

Looking at the effect of particle surface area for both rutile and anatase particles (Figure 4-7) we notice that particle interaction roughly increases with surface area. The deviation from this trend can be seen when comparing the 21 nm particles to the 5 nm particles. Surface area for the 21 nm particles is much lower than that of the 5 nm particles, yet the interaction appears greater for the 21 nm particles (shift in steep slope region to lower temperature). One possible explanation for this trend is that the 5 nm particles undergo more agglomeration since it is more difficult to get a good dispersion for particles this small. Thus the effective area of the 5 nm agglomerates is smaller than that of the 21 nm particles.

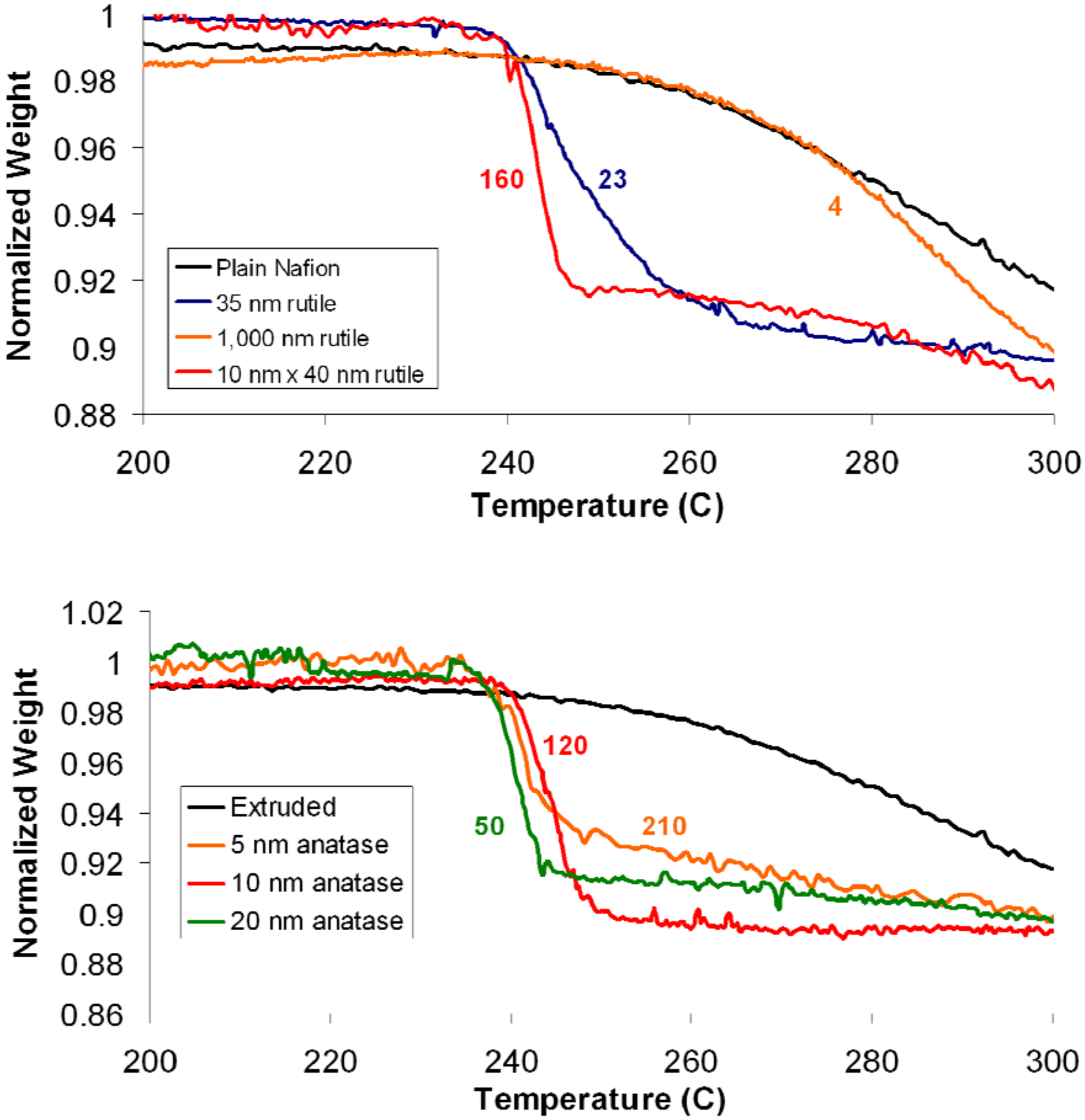

Figure 4-7 TGA scan of different Nafion TiO_2 composites made with rutile particles to show the affect of particle surface area on thermal decomposition. All are 0.005" thick, recast from ethanol based solutions and are 3wt% TiO_2. The top plot is for rutile particles while the bottom plot is for anatase particles[28].

Comparing the rutile particles, particle interaction with sulfonic acid groups increases with surface area for the particles tested. The needle like particles give the highest level of interaction, having the highest surface area. As mentioned previously, the 1,000 nm particles give almost no measurable interaction with the Nafion, having very low surface area. The particles are large enough that suspension during recasting could be a significant issue.

Looking at the effect of particle loading on interaction by making a series of membranes varying only in weight loading of particles (Figure 4-8) we notice that there is a strong dependence on interaction. As would be expected, the level of interaction between sulfonic acid groups and TiO_2 particles increases with loading. This is seen by slope increasing in the temperature region of interest with increasing particle weight loading. This trend is seen for the range of 0 – 6% weight loading. Increasing loading from 6 to 20%, however, results in a large decrease in particle/polymer interaction. An explanation for this observation is that particle agglomeration occurs at 20 wt% TiO_2, greatly reducing effective particle surface area and reducing interaction. If this is indeed true, it reflects the importance of proper particle dispersion.

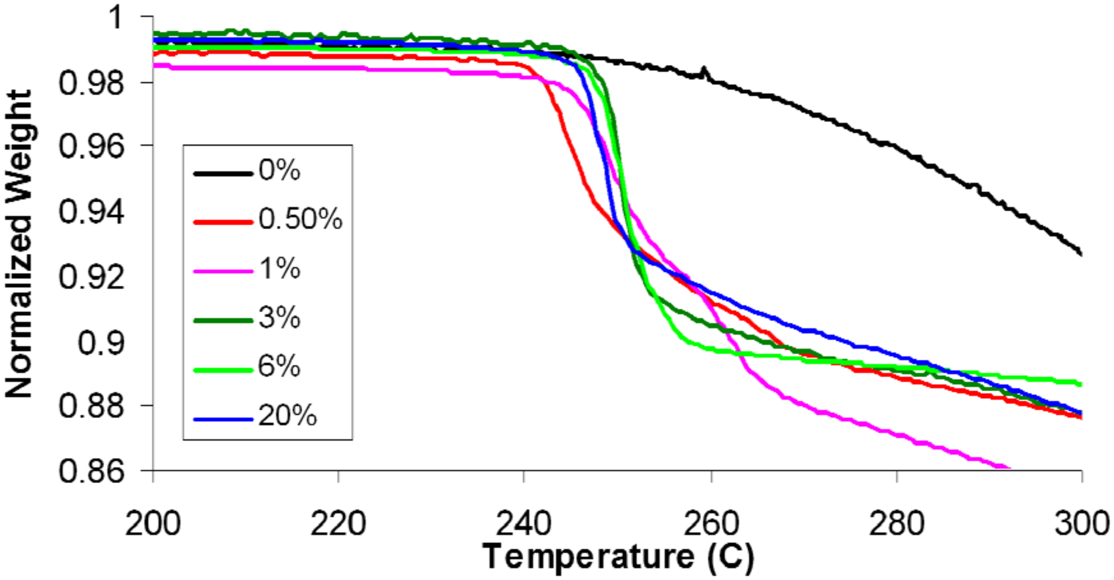

Figure 4-8 TGA scans of composite Nafion TiO_2 films. All are 0.005" thick, recast from ethanol based solutions and use 21 nm Degussa Hul TiO_2. Curves show the affect of weight loading on thermal decomposition[28].

Further evidence of the importance of proper particle dispersion was obtained by comparing different membrane preparation techniques. Specifically, a comparison was made between membranes prepared by the methods of sonication and stirring to suspend particles ( ). Comparing the TGA curves for the different preparation techniques gives strong evidence that particle dispersion directly affects particle/polymer interaction. It is assumed that sonication acts only to better disperse particles and that no alterations in surface chemistry are occurring between the two techniques.

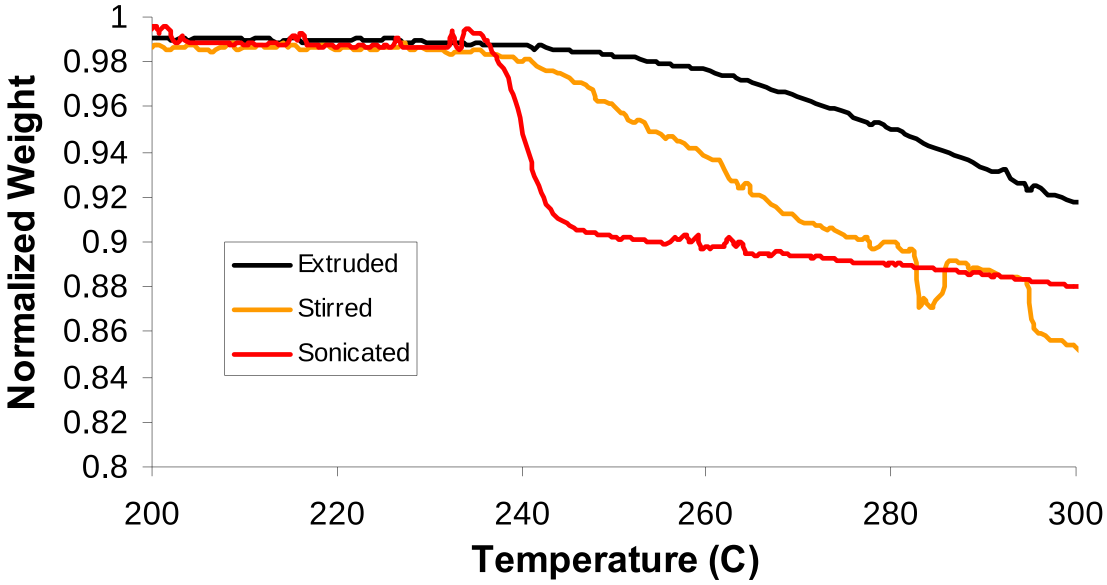

Figure 4-9 TGA scans of composite Nafion TiO_2 films comparing the affect of particle dispersion method on thermal decomposition. All are 0.005" thick, recast from ethanol based solutions and use 21 nm Degussa Hul TiO_2[28].

Interaction between particles and polymer appears to be linked to the improvement seen in fuel cell performance for composite membranes. Comparing fuel cell performance data for different composite membranes with corresponding TGA scans at 120°C (Figure 4-10) suggests that fuel cell performance increases with the degree of interaction. Note that the TGA scan compares composite membranes to extruded Nafion while the fuel cell curve shows a comparison to plain recast Nafion. There was no detectable difference in the TGA scans of plain extruded and recast Nafion for the two materials. However, morphological differences between recast and extruded Nafion results in differences in fuel cell performance. Comparing recast composites to plain recast instead of extruded Nafion for the fuel cell tests gives a better comparison of the effect of particles on fuel cell performance.

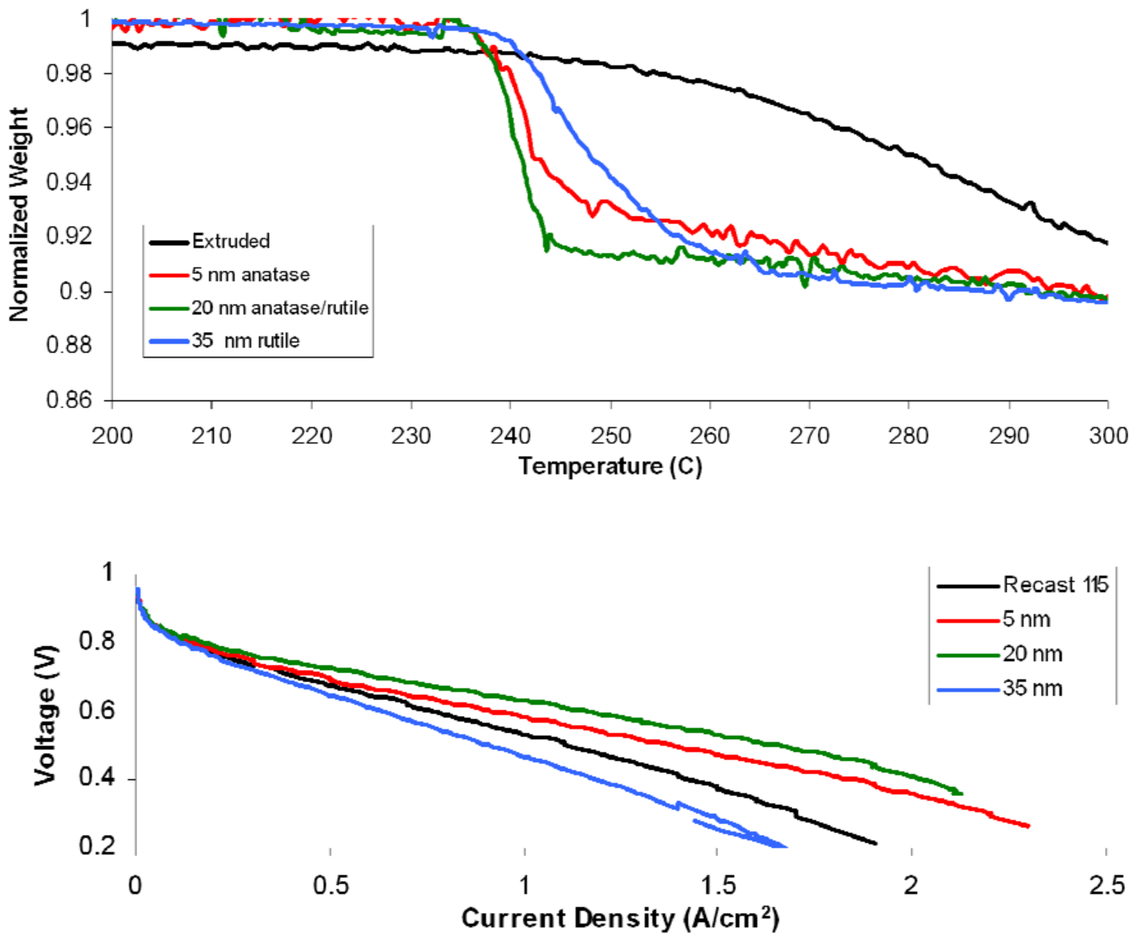

Figure 4-10 TGA scans (top) and current-voltage curves for Nafion N115 and Nafion/TiO_2 composite membranes. TGA scans for membranes made with these particles are show at bottom. Fuel cell curves were taken at 120°C and ca. 90%RH by Dr. Hitoshi Ota and used with his permission.

4.5 Membrane Characterization

A brief summary of experiments done by the author to identify differences in mechanical response between Nafion and Nafion/TiO_2 composites is presented here. The study is by no means complete, but adds to our understanding of how TiO_2 nanoparticles interact with Nafion. A more complete study of the mechanical properties of Nafion/TiO_2 composites has been presented by my colleague, Barclay Satterfield, and includes tensile strain, stress relaxation, and water swelling experiments[45, 46].

4.5.1 Tensile creep and elastic modulus

The tensile creep response of Nafion and Nafion/TiO_2 composites is shown in Figures 11- 14. A description of tensile creep procedures is given in Chapter 2 while membrane preparation techniques are described earlier in this chapter. Comparing tensile creep response of extruded Nafion N1110 to recast Nafion/TiO_2 composite with 3wt% Degussa Hul TiO_2, we notice that there is little difference between the composite and plain membrane at the conditions tested. In some cases, the composite has more resistance to creep strain while in others the plain material is superior. The differences between the membranes are slight, attributed largely to errors in measurement (membrane dimensions, etc.) and should probably be repeated to for a more accurate comparison.

When weight loading of TiO_2 is increased to 20%, however, a difference in mechanical response between plain Nafion and the composite is clearly seen (Figure 4-12 and Figure 4-14). At 23 and 80°C and water activity of ~0.1, the 20wt% membrane has significantly more resistance to tensile creep strain than plain Nafion or the 3wt% composite. Qualitatively, it has been observed that the 20wt% composite undergoes less compressive creep when clamped in the jaws of the tensile creep instrument at elevated temperature.

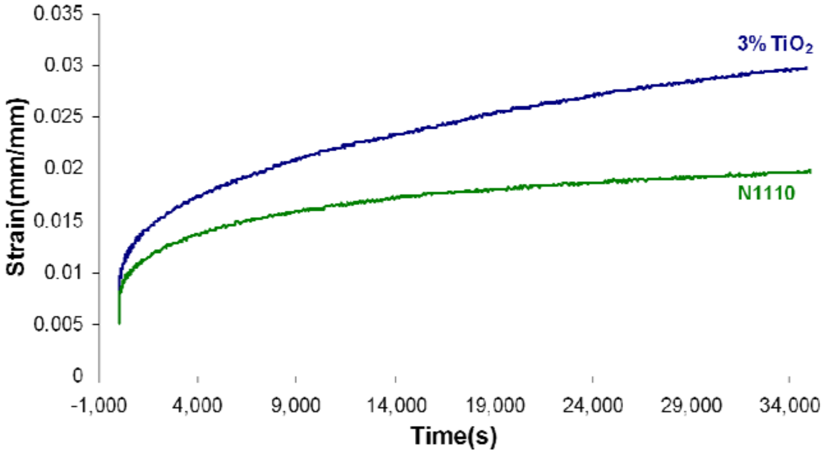

Figure 4-11 Tensile creep strain for Nafion N1110 and a 3wt% Nafion/TiO_2 (Degussa Hul) composite at 23°C and 0.00 water activity. Applied stress was 4.2 MPa.

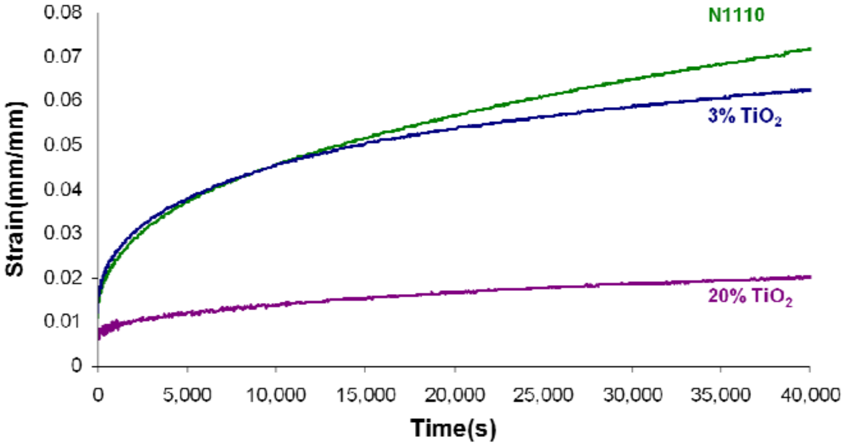

Figure 4-12 Tensile creep strain for Nafion N1110 and Nafion/TiO_2 (Degussa Hul) composites at 23°C and ~ 0.1 water activity. Applied stress was 4.2 MPa. Composite membranes were recast with the loadings indicated.

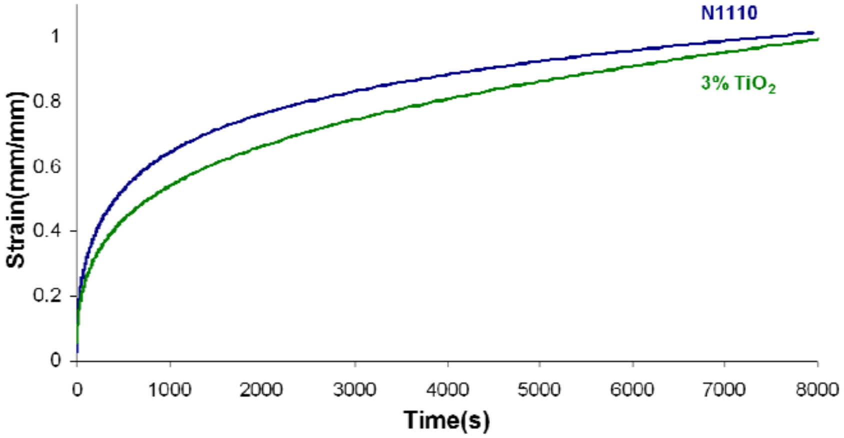

Figure 4-13 Tensile creep strain for Nafion N1110 and a 3wt% Nafion/TiO_2 (Degussa Hul) composite at 80°C and 0.00 water activity. Applied stress was 1.55 MPa.

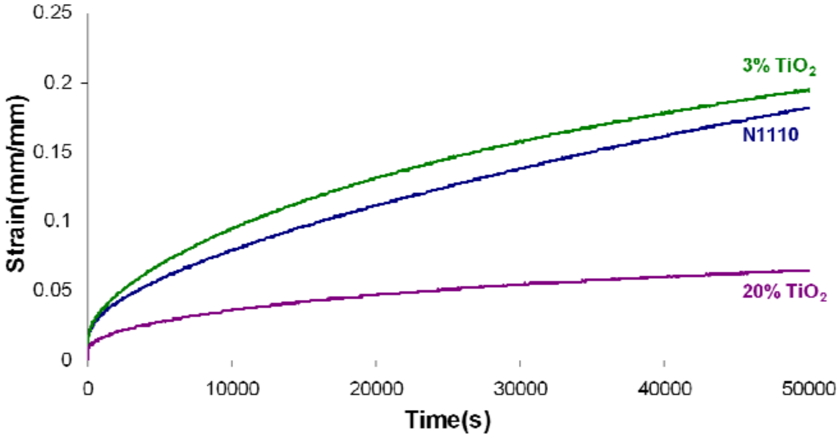

Figure 4-14 Tensile creep strain for Nafion N1110 and Nafion/TiO_2 composites at 80°C and ~ 0.1 water activity. Applied stress was 1.55 MPa. Composite membranes were recast with the loading of Degussa Hul's 21nm particles indicated.

Improved mechanical properties are also seen when comparing the instantaneous elastic response of plain Nafion and the 20 wt% composite (Figure 4-15). Instantaneous elastic modulus is greater for the composite membrane than for plain recast or extruded Nafion. However, the greatest difference between plain and composite is seen at low water activity. At 0.00 activity, there is a nearly 10 fold increase in elastic modulus. With water activity of 0.01, elastic modulus of both plain and composite increases, with the composite being over 2 times stiffer. As hydration increases further, elastic modulus of both the composite and plain Nafion decreases, with the difference between the two membranes also decreasing.

In addition to measuring the mechanical response of composite Nafion, swelling strain due to water uptake was also measured. Chapter 5 describes the procedure for measuring equilibrium swelling strain. Figure 4-16 shows a comparison of swelling strain for uptake of water at 80°C between Nafion N1110 and recast Nafion/TiO_2 composite made with 20wt% Degussa Hul TiO_2 particles. This data suggests that there is no difference in swelling strain between composite and plain Nafion, even at 20wt%

loading. Note that some variation existed between runs, with changes existing depending on history. The data shown represents data with identical sample treatment histories.

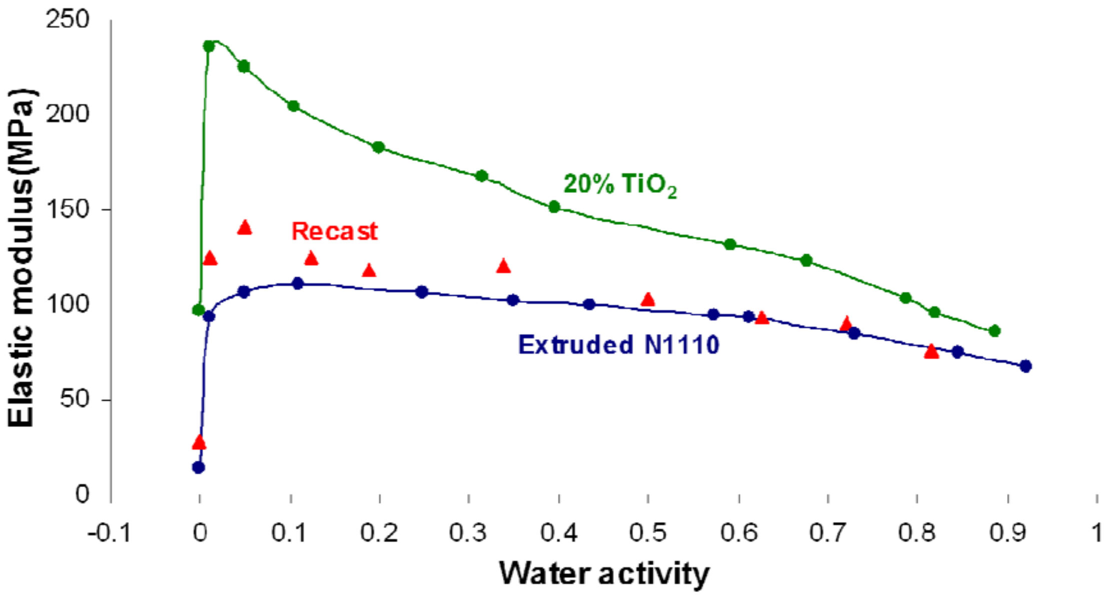

Figure 4-15 Elastic modulus as a function of water activity for Nafion N1110, recast 1,100 EW Nafion (~200µm thick), and recast composite Nafion/TiO_2 (20wt% loading, ~200µm thick). All measurements were taken at 80°C.

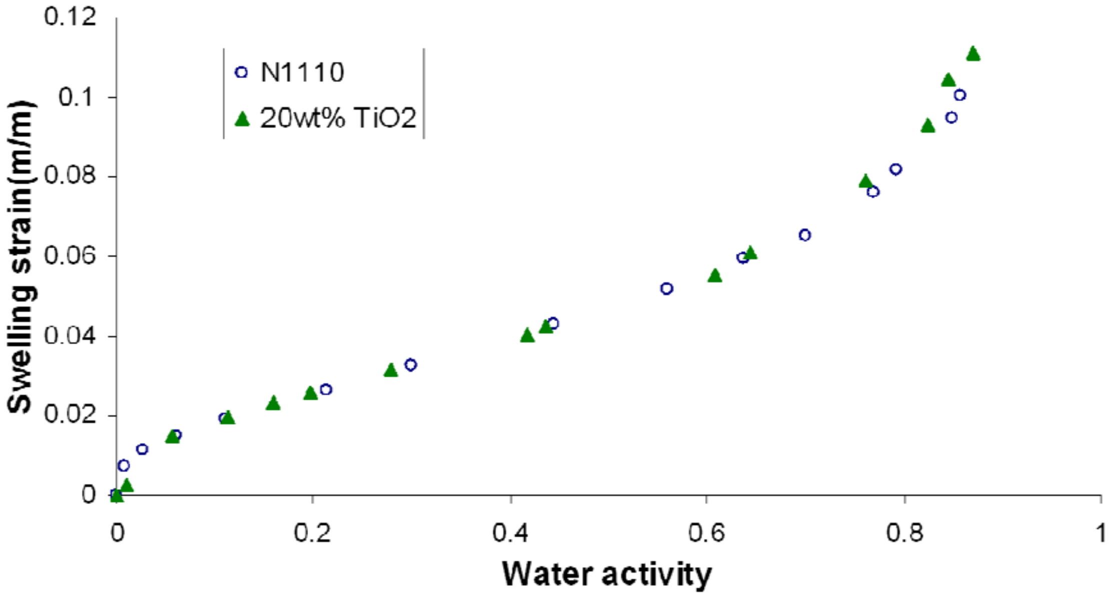

Figure 4-16 Swelling strain due to uptake of water vapor by Nafion N1110 and Nafion/TiO_2 composite (20wt% Degussa Hul) at 80°C.

At high TiO_2 loading, there appears to be crosslinking occurring between Nafion and TiO_2—presumably through the sulfonic acid groups—which increases stiffness/ resistance to tensile creep. Additionally, it appears that the addition of water disrupts this crosslinking interaction. It is somewhat puzzling that mechanical properties are increased for the composite while swelling strain is unaffected; intuitively, crosslinking should increase both. It is also not clear what role water plays in the interaction between sulfonic acid groups and TiO_2 particles. Additional experiments over a range of temperature, hydration, and particle loading are required to further elucidate the effect of TiO_2 particles on the mechanical properties of Nafion.

4.6 Conclusions

Uniform and mechanically robust composite Nafion/metal oxide membranes can be recast from Nafion dispersions using ethanol, IPA, DMSO, and other solvents. Recasting temperature, solvent amount and type, and annealing temperature all impact membrane morphology and quality. Further work needs to be done to determine the effects of the different recasting parameters on morphology and material properties.

From TG-MS scans of plain Nafion and Nafion/tiO_2 composites, decomposition steps are suggested for both materials. The presence of TiO_2 in Nafion membranes catalysis the decomposition of the sulfonic acid group and ether linkage. Because of this, it is proposed that the TiO_2 particles are interacting with sulfonate groups through unsaturated sites on the TiO_2 surface. This interaction, which results in an overall crosslinking of the polymer through sulfonate groups, is used to explain the increase in mechanical strength seen in the Nafion/TiO_2 composites.

Based on these assumptions, TGA scans were used to compare the interaction occurring between different TiO_2 particles and Nafion. It was concluded that increasing effective particle surface area by 1) changing the size/shape of particles and 2) promoting good particle dispersion during recasting increases the interaction between particles and polymer. Particle loading affects the level of interaction in a similar manner. It was also proposed that the level of interaction between particles and polymer is a direct indication of fuel cell performance.

4.7 Future Work

Based on the work presented in this chapter as well as the work of others both within and outside this group, further work should be done to characterize the influence of particle size, shape, and surface acidity on fuel cell performance and physicochemical properties. Specifically, the effect of temperature and water activity on mechanical properties, swelling due to water uptake, mass uptake, and conductivity should be further investigated. Additional studies should be made to determine the interaction between filler particles and Nafion to determine what influences crosslinking, particle surface conductivity/water retention, and morphological alterations have on these properties and performance.

A personal area of interest includes a series of studies which examine tailoring the shape of metal oxide particles. This includes adding metal oxide nanotubes to Nafion as well as having Nafion infiltrate organized metal oxide structures. It would be interesting to see how surface acidity and/or the influence of shape on morphology affect membrane properties and fuel cell performance.

4.8 Acknowledgements

I am grateful to Dr. Hitoshi Ota for the collaborative work which occurred on the analysis of the composite membranes and for allowing me to use the TG-MS scans which he obtained at Mitsubishi Chemical Group Science and Technology Research Center, Inc. Thanks also go to Hitoshi for the use of the fuel cell data and SEM/TEM images of TiO_2 particles and composite membranes.

4.9 References

1. Yang, C.; Costamagna, P.; Srinivasan, S.; Benziger, J.; Bocarsly, A. B., Approaches and technical challenges to high temperature operation of proton exchange membrane fuel cells. *Journal of Power Sources* **2001,** 103, (1), 1-9.
2. Yang, C.; Srinivasan, S.; Arico, A. S.; Creti, P.; Baglio, V.; Antonucci, V., Composition Nafion/zirconium phosphate membranes for direct methanol fuel cell operation at high temperature. *Electrochemical and Solid State Letters* **2001,** 4, (4), A31-A34.
3. Adjemian, K. T.; Dominey, R.; Krishnan, L.; Ota, H.; Majsztrik, P.; Zhang, T.; Mann, J.; Kirby, B.; Gatto, L.; Velo-Simpson, M.; Leahy, J.; Srinivasant, S.; Benziger, J. B.; Bocarsly, A. B., Function and characterization of metal oxide-naflon composite membranes for elevated-temperature H-2/O-2 PEM fuel cells. *Chemistry of Materials* **2006,** 18, (9), 2238-2248.
4. Yang, C.; Srinivasan, S.; Bocarsly, A. B.; Tulyani, S.; Benziger, J. B., A comparison of physical properties and fuel cell performance of Nafion and zirconium phosphate/Nafion composite membranes. *Journal of Membrane Science* **2004,** 237, (1-2), 145-161.
5. Watanabe, M.; Uchida, H.; Seki, Y.; Emori, M.; Stonehart, P., Self-humidifying polymer electrolyte membranes for fuel cells. *Journal of the Electrochemical Society* **1996,** 143, (12), 3847-3852.
6. Si, Y. C.; Kunz, H. R.; Fenton, J. M., Nafion-Teflon-Zr(HPO4)(2) composite membranes for high-temperature PEMFCs. *Journal of the Electrochemical Society* **2004,** 151, (4), A623-A631.
7. Park, Y. I.; Kim, J. D.; Nagai, M., Increase of proton conductivity in amorphous phosphate-Nafion membranes. *Journal of Materials Science Letters* **2000,** 19, (18), 1621-1623.
8. Ramani, V.; Kunz, H. R.; Fenton, J. M., Investigation of Nafion (R)/HPA composite membranes for high temperature/low relative humidity PEMFC operation. *Journal of Membrane Science* **2004,** 232, (1-2), 31-44.
9. Jalani, N. H.; Dunn, K.; Datta, R., Synthesis and characterization of Nafion (R)-MO2 (M = Zr, Si, Ti) nanocomposite membranes for higher temperature PEM fuel cells. *Electrochimica Acta* **2005,** 51, (3), 553-560.
10. Baglio, V.; Arico, A. S.; Di Blasi, A.; Antonucci, V.; Antonucci, P. L.; Licoccia, S.; Traversa, E.; Fiory, F. S., Nafion-TiO2 composite DMFC membranes: physico-

chemical properties of the filler versus electrochemical performance. *Electrochimica Acta* **2005,** 50, (5), 1241-1246.

11. Baglio, V.; Di Blasi, A.; Arico, A. S.; Antonucci, V.; Antonucci, P. L.; Fiory, F. S.; Licoccia, S.; Traversa, E., Influence of TiO2 nanometric filler on the behaviour of a composite membrane for applications in Direct Methanol Fuel Cells. *Journal of New Materials for Electrochemical Systems* **2004,** 7, (4), 275-280.
12. Thampan, T. M.; Jalani, N. H.; Choi, P.; Datta, R., Systematic approach to design higher temperature composite PEMs. *Journal Of The Electrochemical Society* **2005,** 152, (2), A316-A325.
13. Yuan, S.; Hu, S. S., Characterization and electrochemical studies of Nafion/nano-TiO2 film modified electrodes. *Electrochimica Acta* **2004,** 49, (25), 4287-4293.
14. Klein, L. C.; Daiko, Y.; Aparicio, M.; Damay, F., Methods for modifying proton exchange membranes using the sol-gel process. *Polymer* **2005,** 46, (12), 4504-4509.
15. Mauritz, K. A.; Stefanithis, I. D.; Huang, H. H., Microstructural Evolution of a Silicon-Oxide Phase in Nafion Membranes by an Insitu Sol-Gel Reaction. *Abstracts of Papers of the American Chemical Society* **1991,** 202, 285-POLY.
16. Alberti, G.; Casciola, M., Composite membranes for medium-temperature PEM fuel cells. *Annual Review of Materials Research* **2003,** 33, 129-154.
17. Arico, A. S.; Baglio, V.; Di Blasi, A.; Creti, P.; Antonucci, P. L.; Antonucci, V., Influence of the acid-base characteristics of inorganic fillers on the high temperature performance of composite membranes in direct methanol fuel cells. *Solid State Ionics* **2003,** 161, (3-4), 251-265.
18. Mauritz, K. A., Storey, R.F., amd Jones, C. K., Multiphase Polymer Materials: Blends, Ionomers, and Interpenetrating Networks. In *ACS Symp. Ser. no. 395*, American Chemical Society: Washington, DC, 1989.
19. Mauritz, K. A.; Warren, R. M., Microstructural Evolution of a Silicon-Oxide Phase in a Perfluorosulfonic Acid Ionomer by an Insitu Sol-Gel Reaction .1. Infrared Spectroscopic Studies. *Macromolecules* **1989,** 22, (4), 1730-1734.
20. Mauritz, K. A.; Stefanithis, I. D., Microstructural Evolution of a Silicon-Oxide Phase in a Perfluorosulfonic Acid Ionomer by an Insitu Sol-Gel Reaction .2. Dielectric-Relaxation Studies. *Macromolecules* **1990,** 23, (5), 1380-1388.
21. Stefanithis, I. D.; Mauritz, K. A., Microstructural Evolution of a Silicon-Oxide Phase in a Perfluorosulfonic Acid Ionomer by an Insitu Sol-Gel Reaction .3. Thermal-Analysis Studies. *Macromolecules* **1990,** 23, (8), 2397-2402.
22. Yang, C. Composite Nafion/Zirconium Phosphate Fuel Cell Membranes: Operation at Elevated Temperature and Reduced Relative Humidity. Doctoral, Princeton University, Princeton, New Jersey, 2003.
23. Adjemian, K., T. Investigation of High Temperature Operation of Proton Exchange Membrane Fuel Cells. Ph.D., Princeton University, Princeton, 2003.
24. Krishnan, L. Composite Membranes for High Temperature and Low Relative Humidity Operation in Proton Exchange Membrane Fuel Cells. Ph.D., Princeton University, Princeton, 2005.
25. Zhang, T. Composite Polymer Membranes for Proton Exchange Membrane Fuel Cells Operating at Elevated Temperatures

and Reduced Humidities. Princeton University, 2006.

26. Satterfield, M. B. Mechanical and Water Sorption Properties of Nafion and Composite Nafion/Titanium Dioxide Membranes for Polymer Electrolyte Membrane Fuel Cells. Ph.D., Princeton University, Princeton, 2007.

27. Adjemian, K. T.; Lee, S. J.; Srinivasan, S.; Benziger, J.; Bocarsly, A. B., Silicon oxide Nafion composite membranes for proton-exchange membrane fuel cell operation at 80-140 degrees C. *Journal of the Electrochemical Society* **2002,** 149, (3), A256-A261.

28. Majsztrik, P.; Ota, H.; Bocarsly, A. B., Interaction between TiO2 nanoparticles and Nafion((R)) in Nafion composite membranes for PEM fuel cell applications. *Abstracts of Papers of the American Chemical Society* **2005,** 230, U1676-U1676.

29. Chalkova, E.; Pague, M. B.; Fedkin, M. V.; Wesolowski, D. J.; Lvov, S. N., Nafion/TiO2 proton conductive composite membranes for PEMFCs operating at elevated temperature and reduced relative humidity. *Journal Of The Electrochemical Society* **2005,** 152, (6), A1035-A1040.

30. Adjemian, K. T.; Srinivasan, S.; Benziger, J.; Bocarsly, A. B., Investigation of PEMFC operation above 100^oC employing perfluorosulfonic acid silicon oxide composite membranes. *Journal of Power Sources* **2002,** 109, (2), 356-364.

31. Adjemian, K. T.; Dominey, R.; Krishnan, L.; Ota, H.; Majsztrik, P.; Zhang, T.; Mann, J.; Kirby, B.; Gatto, L.; Velo-Simpson, M.; Leahy, J.; Srinivasan, S.; Benziger, J. B.; Bocarsly, A. B., Function and characterization of metal oxide-naflon composite membranes for elevated-temperature H_2/O_2 PEM fuel cells. *Chemistry of Materials* **2006,** 18, (9), 2238-2248.

32. Martin, C. R.; Rhoades, T. A.; Ferguson, J. A., Dissolution of Perfluorinated Ion Containing Polymers. *Analytical Chemistry* **1982,** 54, (9), 1639-1641.

33. Silva, R. F.; De Francesco, M.; Pozio, A., Solution-cast Nafion (R) ionomer membranes: preparation and characterization. *Electrochimica Acta* **2004,** 49, (19), 3211-3219.

34. Laporta, M.; Pegoraro, M.; Zanderighi, L., Recast Nafion-117 thin film from water solution. *Macromolecular Materials and Engineering* **2000,** 282, (9), 22-29.

35. Moore, R. B.; Martin, C. R., Procedure for Preparing Solution-Cast Perfluorosulfonate Ionomer Films and Membranes. *Analytical Chemistry* **1986,** 58, (12), 2569-2570.

36. Aldebert, P.; Dreyfus, B.; Pineri, M., Small-Angle Neutron-Scattering of Perfluorosulfonated Ionomers in Solution. *Macromolecules* **1986,** 19, (10), 2651-2653.

37. Aldebert, P.; Dreyfus, B.; Gebel, G.; Nakamura, N.; Pineri, M.; Volino, F., Rod Like Micellar Structures in Perfluorinated Ionomer Solutions. *Journal De Physique* **1988,** 49, (12), 2101-2109.

38. Technician, I. P., Technician at Ion Power explained that Nafion dispersions show no signs of settling even after extensive centrifuging. In 2005.

39. Ion Power, I. Liquion MSDS http://www.ion-power.com/res/liquion.html

40. Gebel, G., Structural evolution of water swollen perfluorosulfonated ionomers from dry membrane to solution. *Polymer* **2000,** 41, (15), 5829-5838.

41. Elliott, J. A.; Hanna, S.; Elliott, A. M. S.; Cooley, G. E., The swelling behaviour of perfluorinated ionomer membranes in ethanol/water mixtures. *Polymer* **2001,** 42, (5), 2251-2253.

42. Todd, J. D.; Rogers, R.; Li, Y. G.; Wexler, M.; Bond, P. L.; Sun, L.; Curson, A. R. J.; Malin, G.; Steinke, M.; Johnston, A. W. B., Structural and regulatory genes required to make the gas dimethyl sulfide in bacteria. *Science* **2007,** 315, (5812), 666-669.

43. DuPont Safe Handling and Use of Perfluorosulfonic Acid Products. http://www.dupont.com/fuelcells/pdf/dfc301.pdf

44. Gebel, G.; Aldebert, P.; Pineri, M., Structure and Related Properties of Solution-Cast Perfluorosulfonated Ionomer Films. *Macromolecules* **1987,** 20, (6), 1425-1428.

45. Satterfield, M. B. Mechanical and Water Sorption Properties of Nafion and Nafion/Titanium Dioxide Membranes for Polymer Electrolyte membrane Fuel Cells. Princeton University, Princeton, 2007.

46. Satterfield, M. B.; Majsztrik, P. W.; Ota, H.; Benziger, J. B.; Bocarsly, A. B., Mechanical Properties of Nafion and Titania/Nafion Composite Membranes for PEM Fuel Cells. *J. Polymer Science B: Polymer Physics* **2006,** 44, 2327-2345.

5 Hydration induced swelling strain of Nafion

5.1 Introduction

Exposing Nafion to water vapor results in uptake of water by the polymer. Equilibrium mass uptake is a strong function of the activity of the surrounding water vapor. Uptake also depends weakly on temperature. Equilibrium water uptake by Nafion is important because proton conductivity is dependant on water activity[1]. Mass uptake is accompanied by dimensional swelling, necessary for the polymer to accommodate the solvent. Swelling strain of membrane materials in PEM fuel cells is critically important because the membrane is constrained (both by clamping pressure of flow plates and by contact with electrode), so swelling due to water uptake creates stresses in the membrane. Equilibrium mass uptake for Nafion in the H^+ form has been widely reported in the literature[1-6]. Despite this, little work has focused on measuring the swelling strain of Nafion as a function of water activity.

The dynamics of mass uptake by Nafion is also important to the operation of PEM fuel cells. Mass uptake dynamics determine fuel cell response to changes in hydration at startup and due to changing operating conditions. Mass uptake has also been used by some to determine diffusivity of water in Nafion[xx][7-9] and several studies report on mass uptake of Nafion[10-14]. In these studies, dry Nafion is exposed to an environment of high water activity and the mass of the sample is monitored over time as the polymer sorbs water. A similar procedure is followed for water sorption; fully hydrated Nafion is quickly exposed to a very low water activity environment.

[xx] It has been recently shown by the work of Satterfield and co workers that, for mass uptake of water by Nafion, interfacial mass transport as well as diffusion are important.

In this chapter, results are reported for the equilibrium swelling strain of Nafion films at several temperatures after being exposed to varying water activities. Results are compared to equilibrium mass uptake. Additionally, the swelling strain dynamics are reported for a range of water activity and temperature. The studies are incomplete—lacking detailed analysis and a full array of conditions. Despite this, they offer valuable insight into the behavior of Nafion which has not been reported by others[15].

5.2 Experimental

Both equilibrium and dynamic swelling strain experiments were performed using the tensile creep instrument described in Chapter 2.

5.2.1 Equilibrium swelling strain

Equilibrium swelling strain of Nafion due to water uptake from vapor was measured using the creep instrument with environmental chamber. Extruded Nafion N1110 film was cleaned, air dried and cut into a 0.635cm wide strip. It was then clamped in the jaws of the instrument to give a gauge length of approximately 2.54cm. The film was then dried *in situ* at 85°C for over 2 hrs in a purge of dry N_2. Only a small force applied (enough to pull the film taught, but not enough to induce measurable creep – approximately 0.1N). A step change in temperature and/or water activity was introduced and the length of the sample was monitored while the temperature and water activity of the environmental chamber was held fixed. The final length was recorded when a steady state length was reached. Depending on the temperature and relative humidity, time to reach steady state took anywhere from under 10 minutes to over 24 hrs. Equilibrium strain was measured at 30, 40, 50, 80, and 98°C from 0 to ~ 95%RH at intervals of ~

10%RH. Swelling strain was calculated with reference to dry Nafion at 23°C. Swelling strain is reported from low to high water activity.

5.2.2 Swelling strain dynamics

Swelling strain dynamics of Nafion sorbing and desorbing water vapor was measured using a procedure similar to that outlined for equilibrium swelling strain. Sample preparation was identical for both equilibrium and dynamic measurements, including cleaning, cutting, and drying procedures. Swelling dynamics were measured by making a step-change in water vapor activity and monitoring swelling strain with temperature held fixed. Again, only a small force (~0.1N) was applied to the sample. An equilibrium state of water activity was established between Nafion and the surrounding vapor. Next, by using a humidified feed from the bubbler, the water activity in the environmental chamber was quickly changed. The time required to establish a new water activity level in the environmental chamber was less than 200 seconds and was limited by the volume of the humidity chamber and the flow of humidified gas. For most conditions tested, the time to establish a change in water activity was an order of magnitude faster than water sorption and desorption. Sample length was recorded over time and strain was calculated relative to the equilibrium sample length at the starting condition.

5.3 Results

5.3.1 Equilibrium swelling strain

Equilibrium swelling strain for Nafion N1110 at 80°C as a function of water activity is shown in Figure 5-1. As would be expected, swelling strain increases with water activity due to increased water uptake.

Comparing swelling strain at different temperatures (Figure 5-2), we notice that temperature has little effect on swelling strain. In fact, within the error limits of the experiment, there are no discernable temperature effects. For all curves, strain was measured at equilibrium starting at low water activity and increasing to high water activity. This was to prevent hysterisis /history effects.

A point showing swelling strain for uptake of liquid water at 23°C is included for comparison in Figure 5-2. Extrapolating the trend for strain due to vapor uptake at 80°C to activity of 1, we see that swelling strain for the uptake of liquid water falls in line with what is expected for uptake of vapor with activity 1.

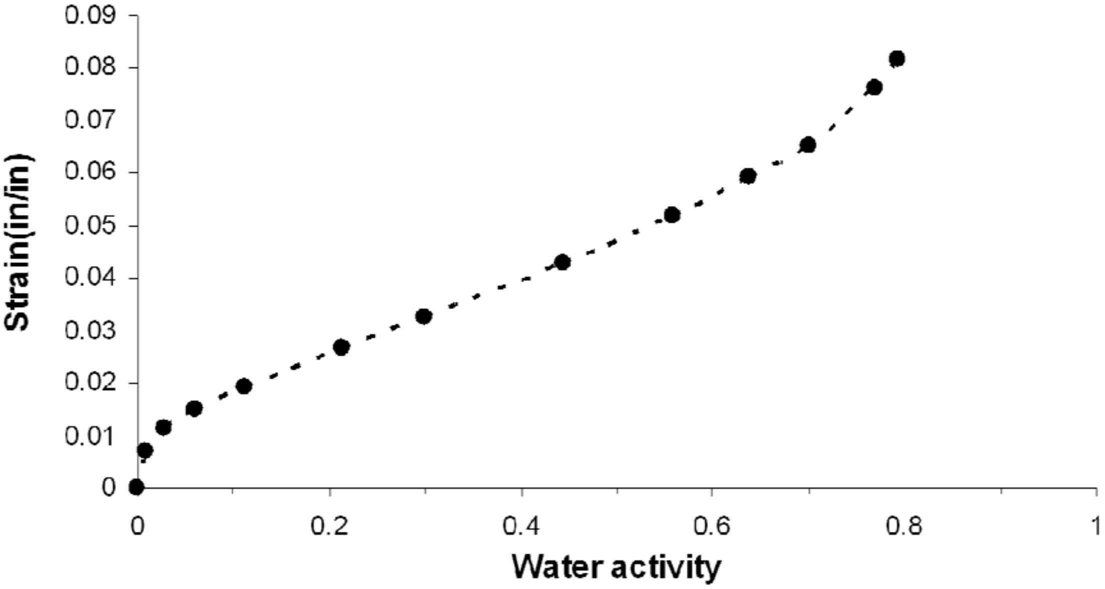

Figure 5-1 Equilibrium swelling strain of Nafion N1110 at 80°C as a function of water vapor uptake[15].

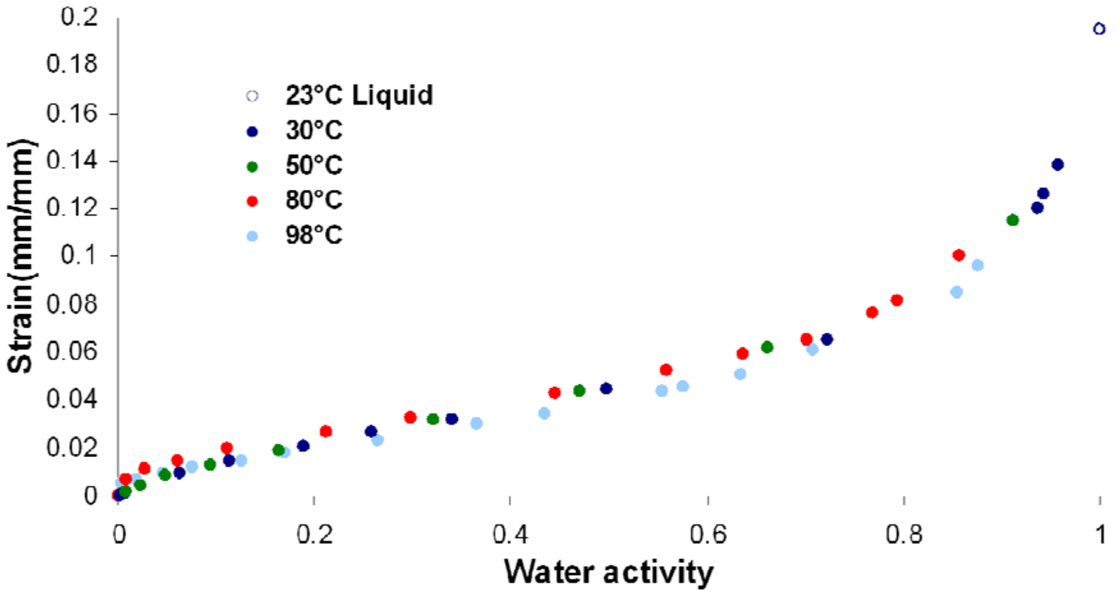

Figure 5-2 Equilibrium swelling strain for Nafion N1110 at 30, 50, 80, and 98°C as a function of water activity of surrounding water vapor. A point showing liquid water swelling strain at 23°C is added for comparison.

5.3.2 Swelling strain dynamics

The dynamics of swelling, as monitored by strain, are shown in Figure 5-3 for Nafion N1110 as it sorbs water. In this plot, sample strain is monitored as a function of time as a dry sample is exposed to water vapor. Four runs reflect water uptake for dry membranes exposed to different levels of water vapor. Again, equilibrium swelling strain increased with water activity. Comparing the swelling strain curves at 0.25 and 0.75 activity, we notice that both have similar initial slopes (differences are attributed mainly to the amount of time it takes to change the water activity level in the humidity chamber). This is likely due to interfacial mass transport resistance being the limiting step to water uptake. This is based on the observation that interfacial mass transport limits mass uptake for dry Nafion exposed to water vapor with activity approaching 1.0[7-9]. The slopes of strain for activity 0.01 and 0.05 are significantly smaller than the slopes at higher activity. In other words, time for swelling strain to reach equilibrium increases significantly at low water activity. This is more clearly seen when strain is normalized by

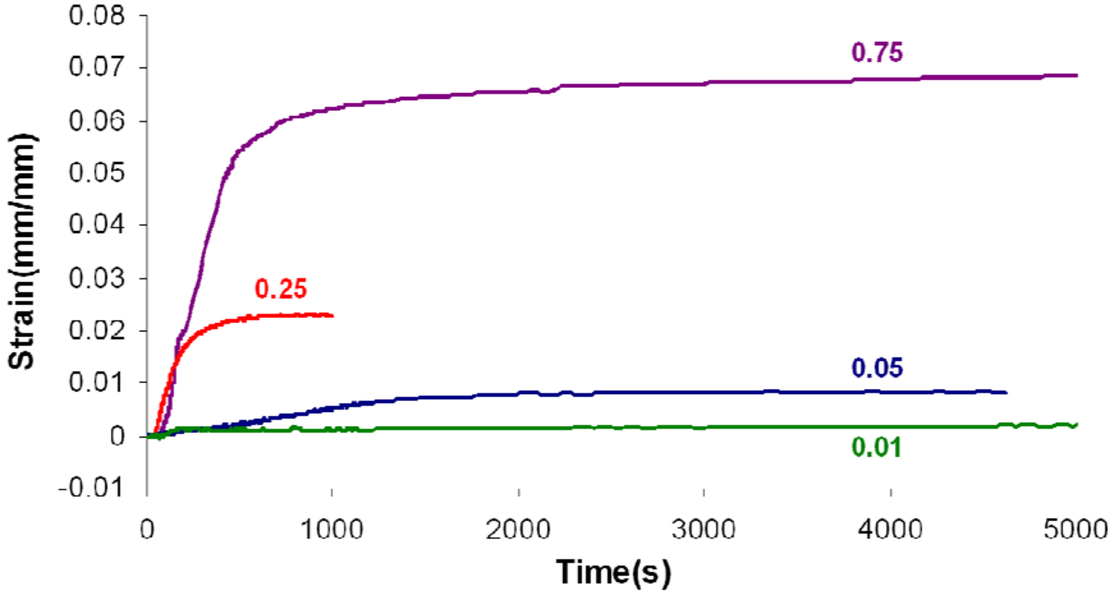

Figure 5-3 Swelling strain dynamics due to water sorption for Nafion N1110 at 50°C. A step-change in water activity surrounding the sample was made from 0.00 to activity indicated next to curves.

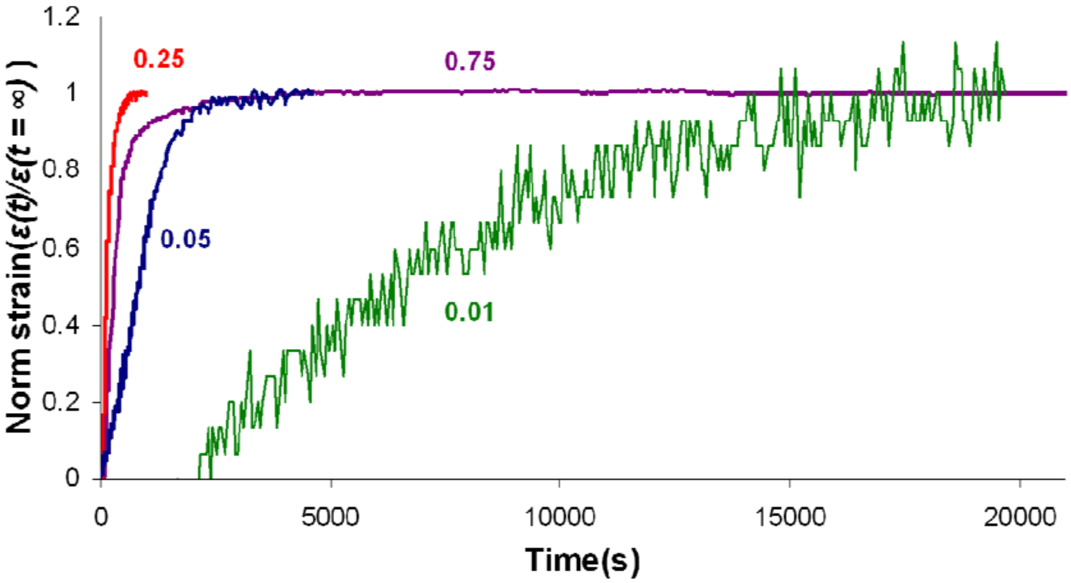

Figure 5-4 Normalized swelling strain dynamics due to water sorption for Nafion N1110 at 50°C. A step-change in water activity surrounding the sample was made from 0.00 to activity indicated next to curves[15].

dividing it by total strain at t = ∞. Equilibration takes less than 1,000 seconds for activity of 0.25 and 0.75. However, equilibration time increases to ~2,500 and 20,000 seconds when activity is reduced to 0.05 and 0.01, respectively. At low water activity, diffusion limits water transport in Nafion.

Swelling strain of dry Nafion exposed to water vapor of activity 0.01 at four temperatures is shown in Figure 5-5. Strain dynamics at 23 and 50°C appear to be identical. At 60°C, strain rate and total strain increases significantly. A large increase in strain rate and total strain is also seen when increasing temperature from 60 to 80°C. It is interesting to note that total strain appears to increase significantly with temperature at water activity of 0.01. This is not what was seen at higher water activity (Figure 5-2).

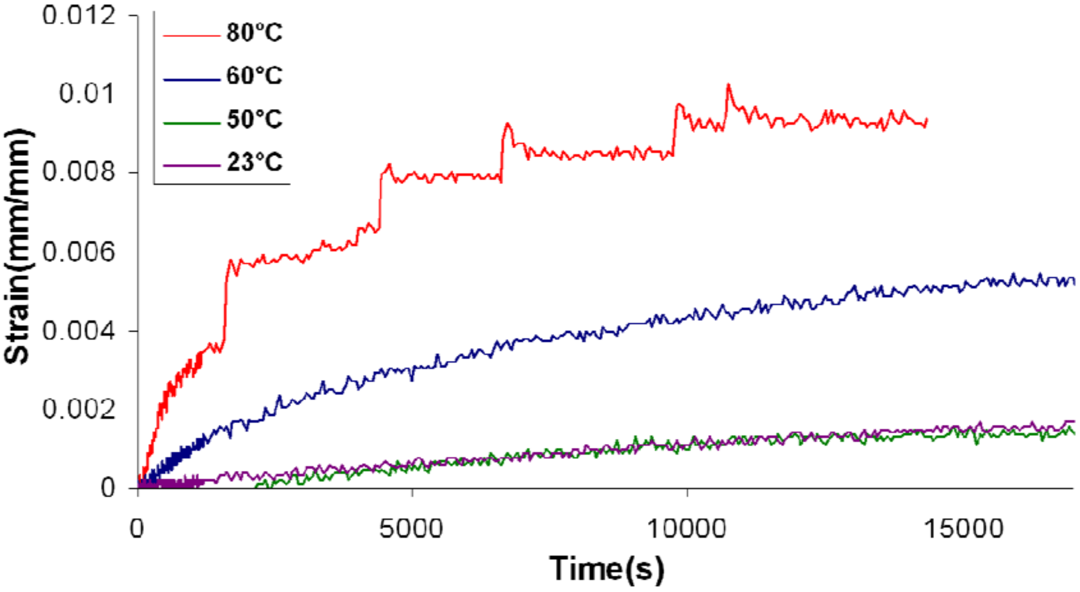

Figure 5-5 Swelling strain dynamics due to water vapor sorption for Nafion N1110 at temperatures indicated. A step-change in water activity surrounding the sample was made from 0.00 to activity 0.01.

Due to the size of the humidity chamber (0.5L) and the maximum flow rate of humidified vapor or dry N_2 (1L/min for humidified feeds and ~ 5L/min for dry feeds) approximately 60 seconds are required for a step change in water activity to be completed. A typical adsorption run, showing the relative humidity monitored in the chamber as well as swelling strain, is shown in Figure 5-6.

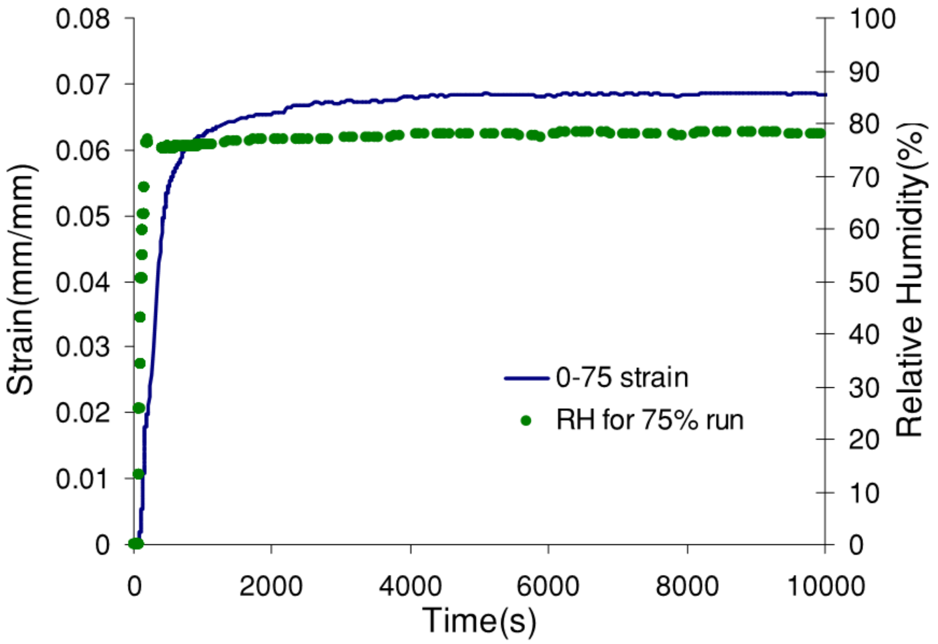

Figure 5-6 Water activity and swelling strain for Nafion exposed to a step change in water activity at time t = 0. Relative humidity was changed from 0 to ~75%, requiring approximately 30 seconds to reach equilibrium.

5.3.3 Water desorption

The dynamics of desorption, as monitored by strain, are shown for Nafion N1110 at 50°C in Figure 5-7. In this figure, Nafion equilibrated to various levels of water activity was quickly exposed to dry N_2 resulting in sample shrinkage as water evaporated from the polymer surface. Initial slope increases with hydration. This occurs because the difference in activity between sample and surrounding gas increases membrane hydration. As a result, initial flux increases with initial membrane hydration. As membrane hydration decreases, due to lower initial hydration level and as drying occurs, driving gradient decreases and transport becomes limited by diffusion[7-9]. Water removal becomes very slow as the membrane activity decreases. This is due to decreasing diffusivity and driving gradient with decreasing membrane water activity. As the membrane becomes very dry, diffusivity becomes very small and dominates.

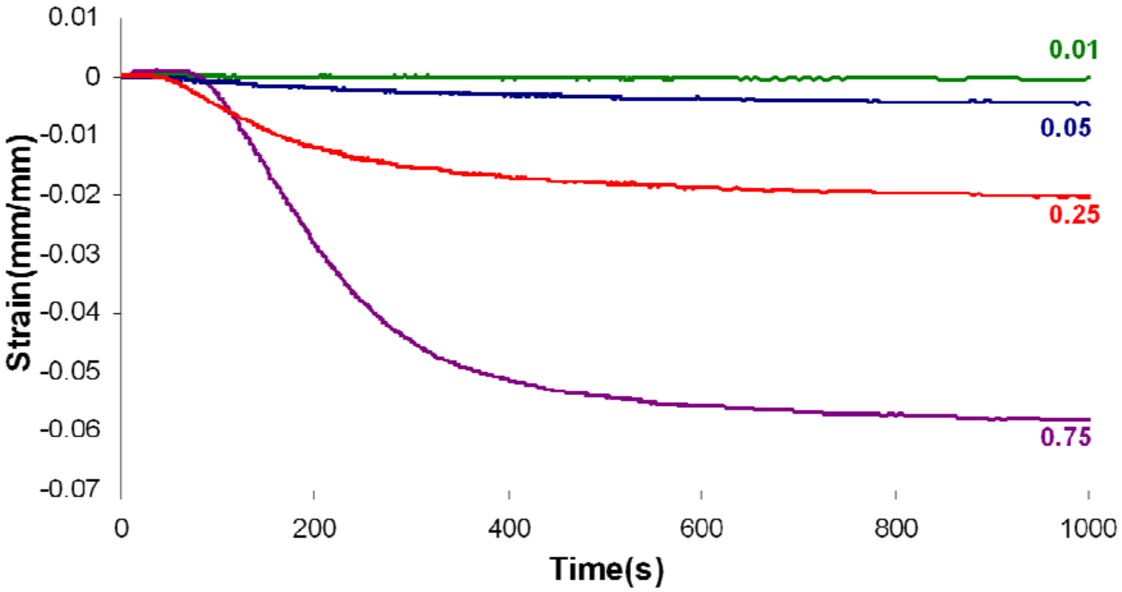

Figure 5-7 Dynamic swelling strain due to water desorption from Nafion N1110 at 50°C. A step-change in water activity surrounding the sample to 0.00 was made for membranes equilibrated to the different water activities indicated.

5.4 Discussion

5.4.1 Equilibrium swelling strain

Figure 5-8 shows a comparison of mass uptake and swelling strain for 1,100 EW Nafion exposed to water vapor[xxi] at 80°C. The mass uptake data was furnished by Dr. Chris Yang for a Nafion N115 membrane[1, 16] and is close agreement with mass uptake measured by other investigators[5]. The curves were normalized by uptake at water activity ~1 to allow comparison. We notice that the curves have very similar shape. The deviation between the two curves could be caused by an offset which is attributed to error in measurement or differences in sample history.

The curves appear to posses three separate regions; 1) a region at small water activity (0.0-0.1) in which strain increases significantly with water activity from the dry state, 2) a region at intermediate activity (0.10-0.75) with moderate linear increase in strain, and 3) a rapid growth region at water activity above this region.

[xxi] The 1.0 water activity point for swelling strain is for liquid water uptake at 23°C.

In the first region, it is speculated that solvation of protons occurs. Solvation of the highly hydrophilic acid groups occurs easily due to thermodynamic favorability. The strong bonding occurring between the water and acid groups is the reason why it is difficult to fully dry Nafion films. Dissociation of the sulfonate groups is speculated to occur with the addition of the first water molecules, as shown by the FT-IR studies of Laprota and coworkers[17].

In the second region, marked by modest uptake of water, solvation has already occurred and additional water serves to form hydronium clusters[17]. Eventually, the water in Nafion appears as bulk water at high activity. It is speculated that the large increase in mass uptake/swelling strain is associated with rearrangement of water clusters.

According to Zawadzinski and co workers[18], two regions are seen in the mass uptake curve which are attributed to 1) proton solvation from water activity of 0.14 – 0.75 and a region of water uptake which is significantly greater (0.75 – 1.0). The first region, they suggest, corresponds to proton solvation while the second region corresponds to “water involved in proton swelling”. Since swelling strain occurs concomitant with mass uptake and is little affected by temperature change, it is unlikely that polymer swelling resistance has much affect on water uptake. In other words, the elastic modulus of Nafion changes significantly with temperature and hydration, yet we see little change in mass uptake/swelling strain to suggest that elastic modulus is dominant. Instead, it is suggested that the size and shape of the hydrophilic regions dictates equilibrium water uptake. Swelling strain is the result of polymer reorganization as water content changes.

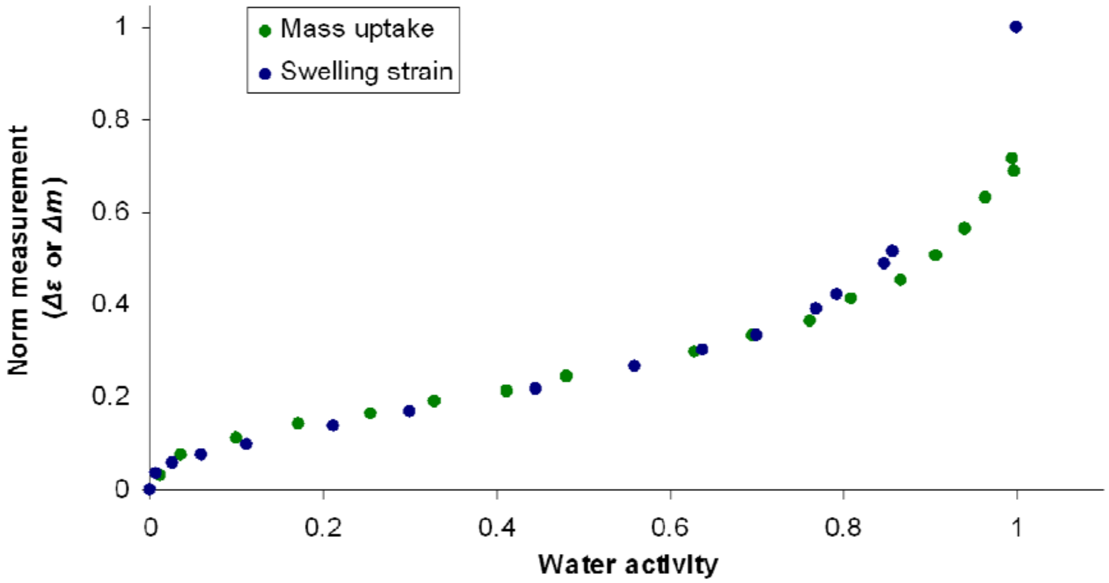

Figure 5-8 A comparison of mass uptake and swelling of Nafion exposed to water vapor. Both mass uptake and swelling strain have been normalized to swelling strain at activity 0.55. Mass uptake data was collected by Dr. Chris Yang [16].

Several investigators have noted that water uptake of Nafion is different for exposure to vapor and liquid at the same activity[5, 10, 11, 18-20]. From the data presented here on swelling strain, it does not appear that there is a difference between equilibrium values of water uptake from vapor and liquid near room temperature. There are three probable reasons why others have measured higher water uptake from liquid than vapor: 1) at room temperature, ~ ten hours are needed to reach equilibrium uptake from water vapor, 2) it is difficult to accurately establish/measure water activity of 1.0, 3) there is a rapid rise in mass uptake/swelling strain as activity approaches 1.0, so errors in activity measurement at high activity can have a large effect, and 4) history effects can strongly impact water uptake.

5.4.2 Dynamics

Swelling strain of Nafion due to water uptake was observed to be significantly slower at low water activity than what was seen at high water activity. Slow swelling strain at low water activity can be attributed to either 1) slow diffusion of water through the polymer or 2) slow relaxation of the polymer chains as rearrangement occurs due to the change in water activity. With the data presented in this chapter, it is difficult to conclude which factor is dominant. Additional measurements of diffusivity at low water activity (with NMR) and/or of proton conductivity during water uptake could shed light on the mechanism of uptake dynamics at low water activity. Additionally, monitoring mass uptake dynamics at low water activity would also provide information about diffusivity.

5.5 Conclusions

Equilibrium and dynamic swelling strain of Nafion for uptake of water vapor was reported. The equilibrium uptake measurements indicate that swelling strain is closely related to mass uptake. There appears to be little effect of temperature on equilibrium swelling strain, suggesting that elastic modulus has only a small effect mass uptake/swelling strain. No significant difference in swelling strain was seen between water uptake from liquid and vapor. This suggests that Schroeder’s paradox in Nafion may be an experimental artifact.

The rate of swelling strain was observed to increase significantly with hydration and temperature. For very low levels of hydration, time to reach equilibrium strain was significant, requiring over 24 hrs in some cases. It is not clear if swelling strain is controlled by diffusion or polymer relaxation at very low water activity levels.

5.6 References

1. Yang, C.; Srinivasan, S.; Bocarsly, A. B.; Tulyani, S.; Benziger, J. B., A comparison of physical properties and fuel cell performance of Nafion and zirconium phosphate/Nafion composite membranes. *Journal of Membrane Science* **2004,** 237, (1-2), 145-161.

2. Duplessix, R.; Escoubez, M.; Rodmacq, B.; Volino, F.; Roche, E.; Eisenberg, A.; Pineri, M., Water-Absorption in Acid Nafion Membranes. *Abstracts of Papers of the American Chemical Society* **1979**, (SEP), 19-19.
3. Zawodzinski, T. A.; Neeman, M.; Sillerud, L. O.; Gottesfeld, S., Determination of Water Diffusion-Coefficients in Perfluorosulfonate Ionomeric Membranes. *Journal of Physical Chemistry* **1991,** 95, (15), 6040-6044.
4. Zawodzinski, T. A.; Springer, T. E.; Davey, J.; Jestel, R.; Lopez, C.; Valerio, J.; Gottesfeld, S., A Comparative-Study of Water-Uptake by and Transport through Ionomeric Fuel-Cell Membranes. *Journal of the Electrochemical Society* **1993,** 140, (7), 1981-1985.
5. Hinatsu, J. T.; Mizuhata, M.; Takenaka, H., Water-Uptake Of Perfluorosulfonic Acid Membranes From Liquid Water And Water-Vapor. *Journal Of The Electrochemical Society* **1994,** 141, (6), 1493-1498.
6. Futerko, P.; Hsing, I. M., Thermodynamics of water vapor uptake in perfluorosulfonic acid membranes. *Journal of the Electrochemical Society* **1999,** 146, (6), 2049-2053.
7. Satterfield, M. B. Mechanical and Water Sorption Properties of Nafion and Nafion/Titanium Dioxide Membranes for Polymer Electrolyte membrane Fuel Cells. Princeton University, Princeton, 2007.
8. Satterfield, M. B.; Benziger, J. B., NonFickian Water Sorption Dynamic by Nafion Membranes. **2007,** forthcoming.
9. Majsztrik, P. W.; Satterfield, M. B.; Bocarsly, A. B.; Benziger, J. B., Water Sorption, Desorption and Transport in Nafion Membranes. *Journal of Membrane Science* **2007,** 301, (1-2), 93-106.
10. Takamatsu, T.; Hashiyama, M.; Eisenberg, A., Sorption Phenomena in Nafion Membranes. *Journal of Applied Polymer Science* **1979,** 24, (11), 2199-2220.
11. Morris, D. R.; Sun, X. D., Water-Sorption and Transport-Properties of Nafion-117-H. *Journal of Applied Polymer Science* **1993,** 50, (8), 1445-1452.
12. Rivin, D.; Kendrick, C. E.; Gibson, P. W.; Schneider, N. S., Solubility and transport behavior of water and alcohols in Nafion (TM). *Polymer* **2001,** 42, (2), 623-635.
13. Krtil, P.; Trojanek, A.; Samec, Z., Kinetics of Water Sorption in Nafion Thin Films -- Quartz Crystal Microbalance Study. *Journal of Physical Chemistry B* **2001,** 105, 7979-7983.
14. Damay, F.; Klein, L. C., Transport properties of Nafion (TM) composite membranes for proton-exchange membranes fuel cells. *Solid State Ionics* **2003,** 162, 261-267.
15. Majsztrik P. W., B. A. B., and Benziger J. B., An instrument for environmental control of vapor pressure and temperature for tensile creep and other mechanical property measurements *Rev. Sci. Instrum.* **2007,** 78, 103904-103904-7.
16. Yang, C. Composite Nafion/Zirconium Phosphate Fuel Cell Membranes: Operation at Elevated Temperature and Reduced Relative Humidity. Doctoral, Princeton University, Princeton, New Jersey, 2003.
17. Laporta, M.; Pegoraro, M.; Zanderighi, L., Perfluorosulfonated membrane (Nafion): FT-IR study of the state of water with increasing humidity. *Physical Chemistry Chemical Physics* **1999,** 1, (19), 4619-4628.

18. Zawodzinski, T. A.; Derouin, C.; Radzinski, S.; Sherman, R. J.; Smith, V. T.; Springer, T. E.; Gottesfeld, S., Water-Uptake by and Transport through Nafion(R) 117 Membranes. *Journal of the Electrochemical Society* **1993,** 140, (4), 1041-1047.

19. Pushpa, K. K.; Nandan, D.; Iyer, R. M., Thermodynamics of Water Sorption by Perfluorosulfonate (Nafion-117) And Polystyrene-Divinylbenzene Sulfonate (Dowex 50w) Ion-Exchange Resins At 298 +/- 1-K. *Journal Of The Chemical Society-Faraday Transactions I* **1988,** 84, 2047-2056.

20. Legras, M.; Hirata, Y.; Nguyen, Q. T.; Langevin, D.; Metayer, M., Sorption and diffusion behaviors of water in Nafion 117 membranes with different counter ions. *Desalination* **2002,** 147, (1-3), 351-357.

6 Conclusions and future work

This work has explored several aspects of the mechanical and transport properties of Nafion. Additionally, the synthesis and characterization of composite Nafion/metal oxide membranes has been briefly presented. As a result of this body of work, a greater understanding of the effects of temperature and hydration on mechanical properties of Nafion has been obtained and linked to microstructure and molecular level interactions. Water transport through Nafion was measured directly with permeation experiments to determine the importance the interfacial mass transport, diffusion, temperature, membrane hydration, and the phase of water at the membrane interface on transport.

The viscoelastic creep response of Nafion was measured over a wide range of temperature and hydration, from very dry states to water activities approaching 1.0. A custom tensile creep instrument with environmental control was designed, built and used for these experiments. Elastic modulus is also reported for Nafion over this wide range of temperature and hydration, obtained from the instantaneous elastic response during tensile creep experiments.

The viscoelastic response of Nafion as temperature and hydration are changed is very complicated. Around room temperature, increasing hydration always results in decreasing elastic modulus and tensile creep response (i.e., water plasticizes Nafion). This has been widely reported for Nafion and assumed to apply at all levels of hydration and temperature by almost all investigators. At temperatures ca. 50°C and above, greater elastic modulus/resistance to tensile creep was seen with increasing hydration for certain levels of hydration. In particular, the dry state showed a very sharp drop in elastic modulus/creep resistance ca. 50°C. In general, increasing hydration of Nafion results in less dependence of viscoelastic response on temperature. This results in the crossing of curves having fixed hydration levels as temperature changes. It appears that hydration actually stabilizes the viscoelastic response of Nafion, as also reported by Satterfield[1] and Bauer and coworkers[2]. It also appears that changes in morphology with hydration, similar in nature to what is seen with diblock copolymer melts with varying compositions, might partially explain changes in mechanical properties with hydration.

There remains much additional work to be done with probing the effects of temperature and hydration on Nafion and other ionomers. The high sensitivity of certain mechanical measurement techniques allows detecting changes in morphology which spectroscopy techniques (e.g., X-ray and neutron scattering) cannot detect. The effects of hydration/thermal history on Nafion's mechanical properties/morphology are very significant and should be further explored. Tensile creep was only measured at fixed levels of hydration, yet hydration levels change frequently during PEMFC operation. Since investigations of materials other than Nafion show significantly different creep response under transient moisture conditions[3], it is likely that Nafion too will behave differently under transient conditions. It would also be useful to expand the conditions over which creep of Nafion was measured, including different levels of temperature and hydration, effects of solvents other than water on tensile creep (this was only briefly touched on in this dissertation), and the effects of EW and counter-ion on tensile creep. Additionally, the viscoelastic response of Nafion/metal oxide composites should be further explored since preliminary experiments have indicated that the composites show improved creep resistance and elastic modulus which is strongly dependant on hydration level metal oxide loading. There are manifold opportunities to perform investigations on materials other than Nafion with the environmentally controlled tensile creep instrument.

Swelling dynamics of Nafion during water uptake have not been fully investigated. It would be useful to probe the effects of temperature, hydration, and history on swelling strain and determine if mass uptake and swelling dynamics are identical. There is also the open question of whether polymer relaxation or water diffusion controls water uptake. Modifying the tensile creep instrument to measure the resistance of Nafion with AC impedance during water uptake could allow for a comparison of mass uptake and swelling strain. Additionally, monitoring conductivity could possibly give some indication of microstructure.

Permeation of liquid water and water vapor through Nafion membranes into vapor was measured over a range of temperature and feed side water activity. It was discovered that interfacial mass transport at the membrane/gas interface is very significant and dominates for liquid water transport. Permeation rates for liquid water were significantly higher than water vapor. This was attributed to negligible interfacial transport at the membrane/liquid interface and increased diffusivity with water activity. For water vapor transport, diffusion dominated for the membrane thicknesses and temperatures investigated. Diffusion increased significantly with membrane hydration. For the combined conditions of thick membranes, elevated temperature, and high vapor activity feeds, it appears that stress across the membrane due to activity gradients resulted in permeation rates falling below expected levels. Including a GDL at the surface of the membrane resulted in a significant decrease in permeation rate with the GDL at either the feed side or dry side.

Future areas to explore with the permeation of water through Nafion include looking at the effects of history on permeation, more carefully measuring proton conductivity of the membrane in situ during permeation, measuring permeation for feed side vapor with activity approaching 1.0, and more carefully measuring the effects of carbon cloth electrodes and other electrode materials on permeation. Additionally, measuring permeation of solvents other than water, such as ethanol and methanol, would be useful.

SDG

6.1 References

1. Satterfield, M. B. Mechanical and Water Sorption Properties of Nafion and Nafion/Titanium Dioxide Membranes for Polymer Electrolyte membrane Fuel Cells. Princeton University, Princeton, 2007.
2. Bauer, F.; Denneler, S.; Willert-Porada, M., Influence of temperature and humidity on the mechanical properties of Nafion (R) 117 polymer electrolyte membrane. *Journal Of Polymer Science Part B-Polymer Physics* **2005,** 43, (7), 786-795.
3. Wang, J. Z.; Dillard, D. A.; Ward, T. C., Temperature and Stress Effects in the Creep of Armamid Fibers under Transient Moisture Conditions and Discussions on the Mechanisms. *Journal of Polymer Science Part B-Polymer Physics* **1992,** 30, (12), 1391-1400.

7 Appendix

7.1 Estimating clamping pressure from bolt torque

Calculating bolt tension precisely from a known applied torque is a complicated affair which depends on thread dimensions, bolt and nut material, bearing surface (washers or otherwise) and thread lubrication. When a bolt is first tightened, some of the torque goes into twisting the bolt. Over time, the bolt relaxes (untwists) and the tension on the bolt decreases. Also, bolt tension decreases over time as creeping of the clamped material occurs (for our fuel cells, Nafion and silicone gaskets will creep/flow over time, reducing bolt tension from the initial value). Greater changes in bolt tension are seen with more rigid bolts/clamped members since less elongation is present when the bolt is initially tightened. Thermal cycling can also act to reduce bolt tension over time.

A torque wrench can be used to tighten a bolt within ± 30% or if special care is taken to ± 15%. Since the magnitude of static friction and kinetic friction differ, tightening without continuous motion (when near the desired bolt torque) will give a false bolt tension. Thus a bolt should be tightened with a smooth and continuous motion to get the most accurate and repeatable results.

Other methods used for determining bolt tension are:

1) bolts equipped with strain gauges (an axial hole in the middle of the bolt holds the strain gauge)
2) measuring the length of the bolt before and after tightening with a micrometer (this requires that both ends of the bolts are exposed when in use and also require knowledge of bolt dimensions and elastic modulus to calculate the tension from strain)

3) ultrasonic equipment to measure the length of the bolt before and after tightening
4) turning a bolt a set number of degrees past finger tight.

If a bolt is tightened with a known torque T, the tension of the bolt can be estimated using the following equation,

$$T = 0.2F_i d \text{ ,} \qquad \text{Equation 7-1}$$

where T is the applied torque, F_i is the tension in a given bolt and d is the nominal major diameter of the thread (#10 = 0.19”, #12 = 0.216”, ¼” = 0.25” for coarse threaded bolts). Using this equation, and assuming that eight ¼” bolts are tightened to 10 newton meters (88.5 inch lbs), the total bolt tension would be

$$F = 8(bolts) \times \frac{88.5(inch \cdot lbs)}{0.2 \times 0.25''} = 14{,}000 lbs \text{ .} \qquad \text{Equation 7-2}$$

The total pressure exerted by bolts is additive; doubling the number of bolts tightened to a certain tension will double the total pressure exerted by the bolts.

It is not a simple matter to convert bolt tension, even if it were accurately known, to pressure on the membrane. The difficulty arises from the fact that 1) the thickness of an MEA is not uniform across its length (Figure 7-1) and 2) an MEA is not homogeneous. Since pressure is defined as force per area, one might be tempted to say that the pressure exerted on a Nafion membrane sandwiched between two plates is equal to the total bolt tension divided by the active area of the membrane (or the total area of Nafion or the area of the MEA). None of these assumptions would be correct. Furthermore, one couldn’t say that the apparent area to be used in calculating pressure is equal the area of the graphite block touching the MEA (that is, the apparent area is the area of the MEA minus the area of the flow channels). This assumption would only be correct if the MEA were 1) uniform in thickness across its entire area and 2) homogeneous throughout. The reason for this is that the actual pressure applied to each section of the membrane depends on the elastic modulus E and the strain ε at each point. Areas with thicker cross section and stiffer materials would have a higher pressure than thinner areas or areas with softer material. Using the apparent area to calculate pressure would give the *average* pressure on the MEA.

For an axially loaded member, which is a simple case illustrating the relationship between deformation, pressure, and elastic modulus, the following relationships hold,

$$\sigma = \frac{F}{A} \text{ and } \delta = \frac{FL}{AE}, \qquad \text{Equation 7-3}$$

which can be rearranged to give

$$\varepsilon E = \sigma, \qquad \text{Equation 7-4}$$

where σ is stress (pressure), δ is the change in length of the material, A is the cross sectional area, L is the initial length, and E is Young's Modulus.

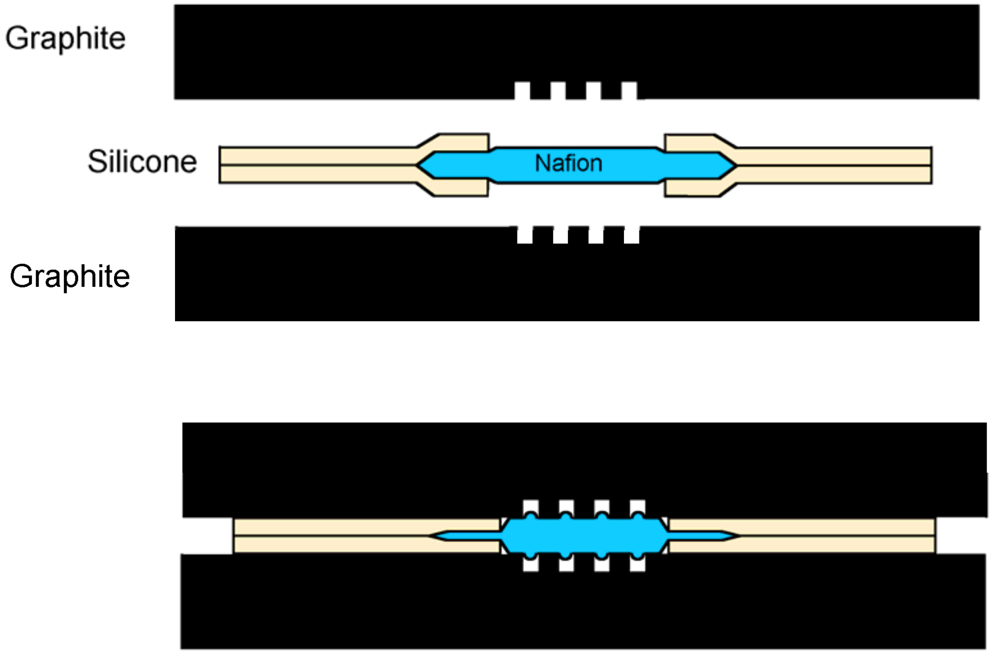

Figure 7-1 A cross sectional schematic diagram of an MEA before (top) and after (bottom) compression between graphite fuel cell blocks (electrodes omitted for clarity).

Another way to look at the compression of dissimilar materials is to think of springs instead of the material being compressed. Figure 7-2 shows springs of two different lengths and spring constants being compressed to the same final length by force transferred through a clamping member. The compressive force in a given spring after compression is given as

$$F_{spring} = K\delta , \qquad \text{Equation 7-5}$$

where K is the spring constant and δ is the change in length of the spring. From this analogy it is clear that the pressure in different regions of a heterogeneous material will be unequal and will depend on the degree of strain and elastic modulus. Since clamping pressure is important in fuel cell operation, it should be reproducible from test to test.

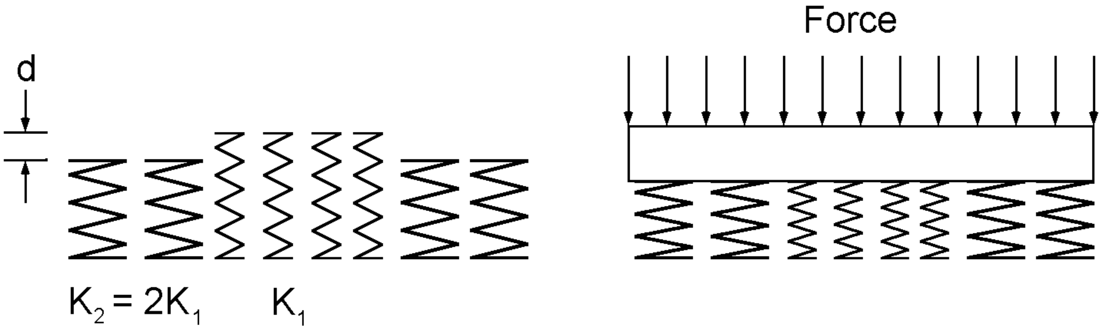

Figure 7-2 Representation of compressed material (MEA) as springs of different length and spring constant K.

7.2 Press instrument; water uptake of constrained membrane

In a typical PEM fuel cell, the MEA is pressed between the flow field plates with enough pressure to form a good seal between the plates and gaskets. Besides preventing gas leaks, good electrical contact must also be made between the current collection plates and the electrodes. Depending on gasket, electrode, and membrane thickness and material properties, part of the compressive stress is carried by the gasket while the remainder is transferred to the electrodes and membrane. Furthermore, water uptake by the membrane cases dimensional swelling which, in turn, affects the amount of stress on the membrane. It has been proposed by Prof. Jay Benziger (Satterfield, Majsztrik *et al.* and elsewhere) that constraining the membrane, as occurs in the fuel cell environment, limits the dynamics and equilibrium amount of water uptake by the membrane. Limiting water uptake by confinement the affects proton transport and thus affects fuel cell performance.

As a way to probe the effects of compressive stress on water uptake and proton conduction in PEMFC membranes, the apparatus show in Figure 7-3 was designed and built by Professor Jay Benziger and the author. A description of an earlier version of this apparatus can be found in Satterfield et al. With this apparatus, stress is applied to a membrane sample under controlled amounts of compressive stress while the proton conductivity is measured with AC impedance spectroscopy. Water is introduced to the membrane while under compression by means of a single flow channel in the center of the membrane.

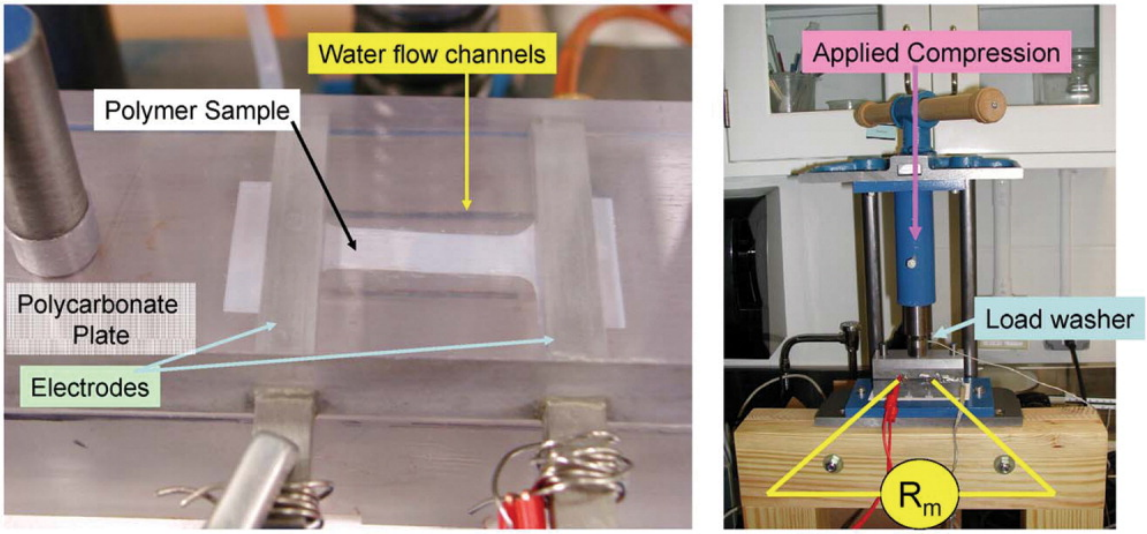

Figure 7-3 Photograph of (right) press instrument for measuring proton conductivity of Nafion under compression and (left) close up view of membrane sample being compressed by polycarbonate plates with stainless steel electrodes[33].

A rectangular membrane is placed between two flat non-conducting plates through which compression is applied. The top plate has two 0.635cm wide stainless steel electrodes flush mounted to the surface and polished. It is between these electrodes that the proton conductivity of the membrane sample is measured. The bottom plate has a single 0.3175cm wide flow channel machined along its center. The flow channel is longer than the length between the electrodes (2.54cm) to give uniform hydration in portion of the membrane sample being monitored for conductivity. In order to prevent a portion of the membrane being unconstrained and interfering with conductivity measurements, the membrane is cut away in the center. Before this step was taken, the part of the membrane over the flow channels would expand into the flow channel and create a strip of high conductivity membrane overwhelming measurement of the conductivity of the constrained portions. Either liquid water or humidified gas can be flowed through the channel.

Compressive pressure is supplied to the membrane sample through the polycarbonate plates by means of a modified woodworking vise. The vise is mounted vertically for ergonomic reasons. At the top plate of the vise, a cylinder holds a solid steel piston and a large stiff spring used to apply force a constant force to the sample. The spring ensures that the applied force is nearly constant since small changes in spring length don't change the applied force by much. Springs of different stiffness expand the range over which sensitive measurements can be made. A load cell is placed between the end of the piston and a hardened steel plate which acts to uniformly distribute load to the flexible polycarbonate plates. Without the hardened steel plate, the polycarbonate would flex and not provide uniform pressure to the sample. The end of the piston is machined to accept the end of the load cell, providing alignment over the center of the sample.

Heating of the sample is accomplished by having copper plates above and below the polycarbonate plates. The copper blocks are heated with cartridge heaters and controlled with a thermocouple and PID controller. High thermal conductivity in the copper reduces heat gradients. Since the polycarbonate has such low thermal conductivity, the temperature of the sample is not equal to the temperature of the copper blocks, even after steady state is reached. Because of this, temperature in the polycarbonate very near the sample is monitored with a small thermocouple. The bottom copper carries water into and out of the flow channel in the polycarbonate block. NPT to tube adapters connect to channels in the back of the block while holes in the top, sealed with O-rings recessed in the surface of the copper, form a good seal between the copper and the polycarbonate once pressure is applied. 1/8" PTFE tube is used to align the plates. Thermal insulation between the heated copper blocks and the vice is accomplished by 0.3175cm thick G-11 spacers at both copper blocks. Alignment of all plates (copper blocks, G-11 insulation, polycarbonate plates, and the hardened steel plate) is accomplished with the two vertical guide pins welded to a plate attached to the bottom of the vice.

7.3 High pressure humidity sensor housing

The permeation experiments described in this dissertation required measuring the temperature and relative humidity of a gas which was flowing through a tube. To the best of the author's knowledge, at the time of this writing there was no commercially available sensor which was prepackaged to allow off-the-shelf connection of a humidity sensor to monitor flow in a tube/pipe. Sensors that were available at that time were merely mounted on a printed circuit board with four pins to be connected to a controller. The most robust and accurate sensors which operated over the widest temperature range were found to be Sensorion dual temperature/RH sensors. Of these, SHT75 offered a temperature range of -40 – 123°C and greatest accuracy within this range.

In order to adapt this sensor to measure the relative humidity and temperature of gas flowing in a tube, the sensor was mounted directly in the gas flow by means of the custom made fitting shown in Figure 7-4. Positioning the sensor directly in the flow as shown gives an excellent response time and accurate measurement of humidity and temperature. The main body of the fitting was made from a rod of either brass or stainless steel by drilling a cavity into which the RH sensor was placed. Flow into and out of the fitting passed through ¼" straight tube soldered to the fitting. Compression fittings were used to make a leak-free connection to tubing at both inlet and outlet. The sensor was mounted at the end of a lab-made feed thru which allowed the sensor to be removed from the fitting for easy replacement. The feed thru was made from a male 1/2" NPT plug (stainless steel or brass) which formed a good seal with the fitting and had four leads passing through which were soldered to the sensor pins. To form a seal between the wires and the NPT plug, a high temperature metal filled epoxy (JB Weld) was used. Holes were drilled to allow the wires to pass through the plug while a larger blind hole allowed space for the epoxy. The plug's threads were protected with electrical tape during gluing and were removed once the epoxy cured. Since JB Weld s quite viscous at room temperature, a heat gun was used to get it to flow into the spaces between wires.

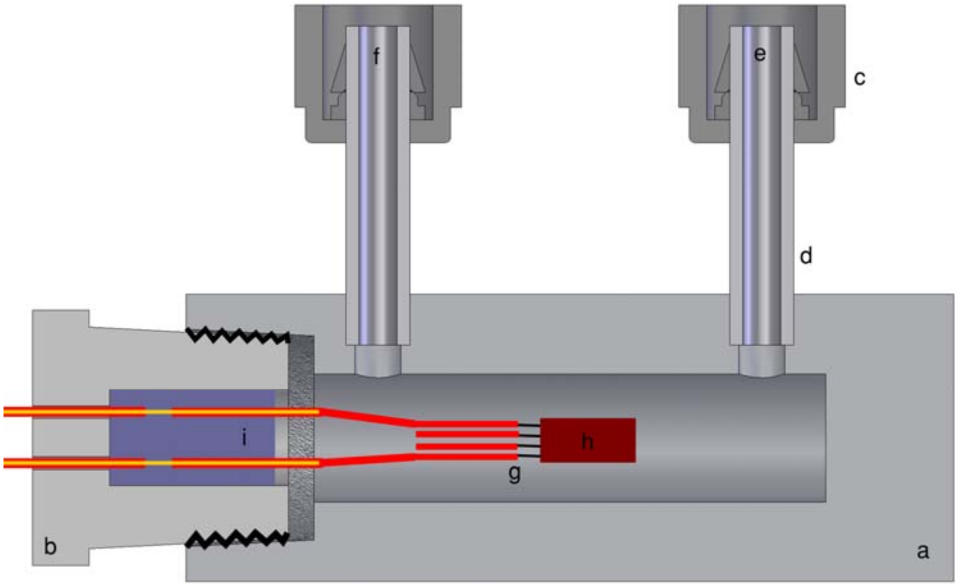

Figure 7-4 Cross-section of a fitting designed to house a combination humidity and temperature sensor to measure these properties of a gas flowing through a tube at pressure. Positioning the sensor directly in the flow gives an excellent response time and accurate measurement. The components are: (a) SS cylinder body, (b) ½" NPT hex plug, (c) compression fitting assembly for ¼" tube (nut and ferrule), (d) ¼" SS tube (soldered to cylinder), (e) gas inlet, (f) gas outlet, (g) wires soldered to leads on sensor, (h) dual relative humidity and temperature sensor, and (i) metal filled epoxy sealant. Note that a small band of wire insulation has been removed in an area covered by epoxy to ensure a pressure-tight seal. Wires exiting the hex plug are connected to an RJ-45 terminated cable.

Also, if a leak-free, high pressure fitting was needed, it was necessary to remove a small band of insulation from each wire in an area that was completely covered by epoxy.

Failure to do so often resulted in leaking between the metal core of the wire and insulation. Best results were achieved with solid wire.

The controller provided with the sensor included an electrical lead with a four prong connector which plugged directly into the sensor. Since this connection could not be easily adapted to the design show in Figure 7-4, the lead and connector was replaced with a standard RJ-45 terminated cable (standard 8 conductor Ethernet connection). The wires corresponding to the correct pins were connected to the wires on the outside of the NPT feed thru. Note that only four of the pins are needed to operate the sensor.

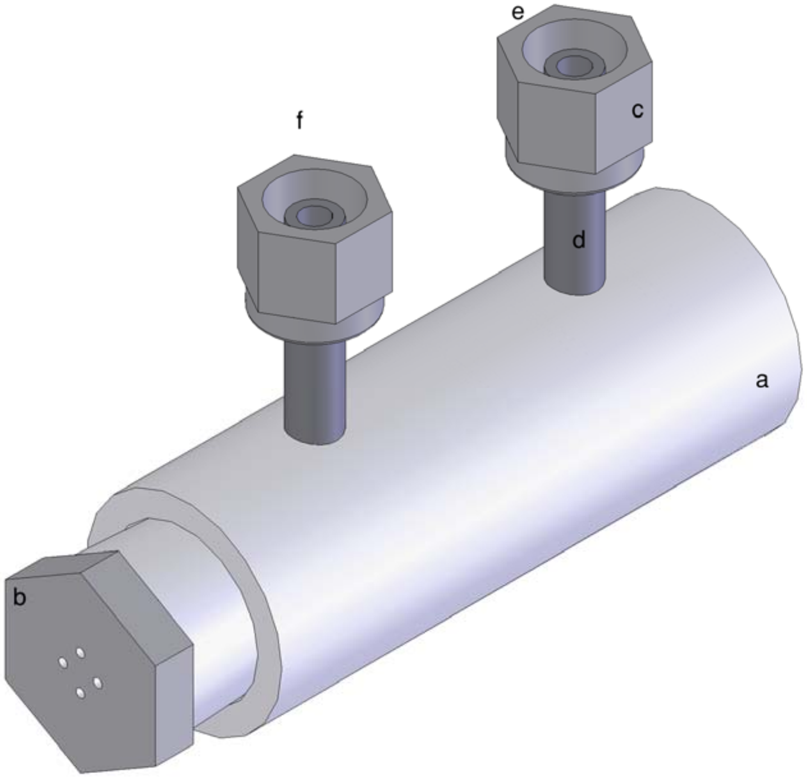

Figure 7-5 Isometric view of CAD drawing of fitting shown in Figure 7-4. See Figure 7-4 for label key. Note that wires passing through hex plug (b) have been omitted from this schematic.

7.4 Supplemental permeation data

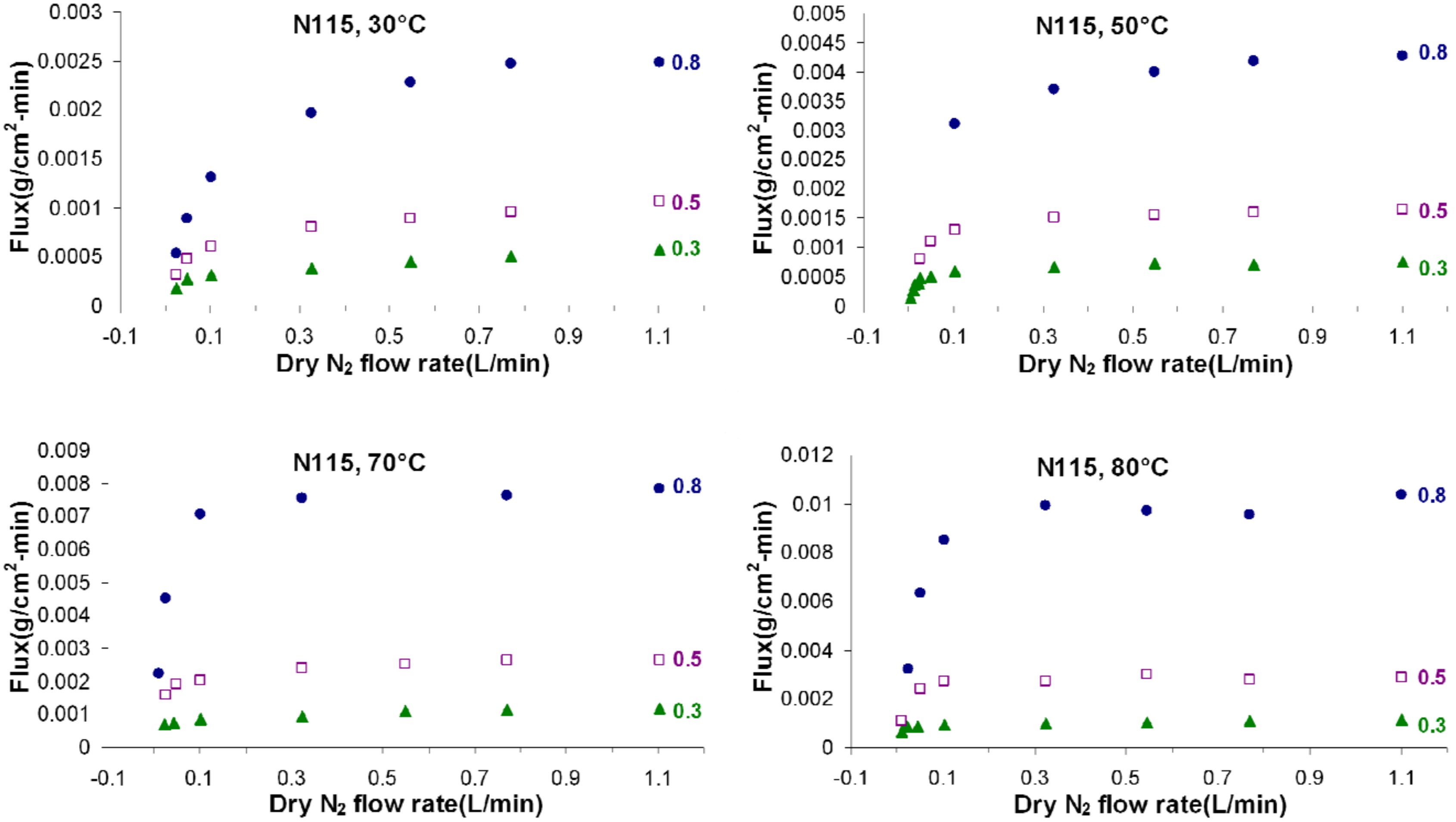

Figure 7-6 Water vapor flux through Nafion N115 at 30, 50, 70, and 80°C for feed side activity of 0.3, 0.8, and 0.8 as a function of N$_2$ flow rate at the dry side.

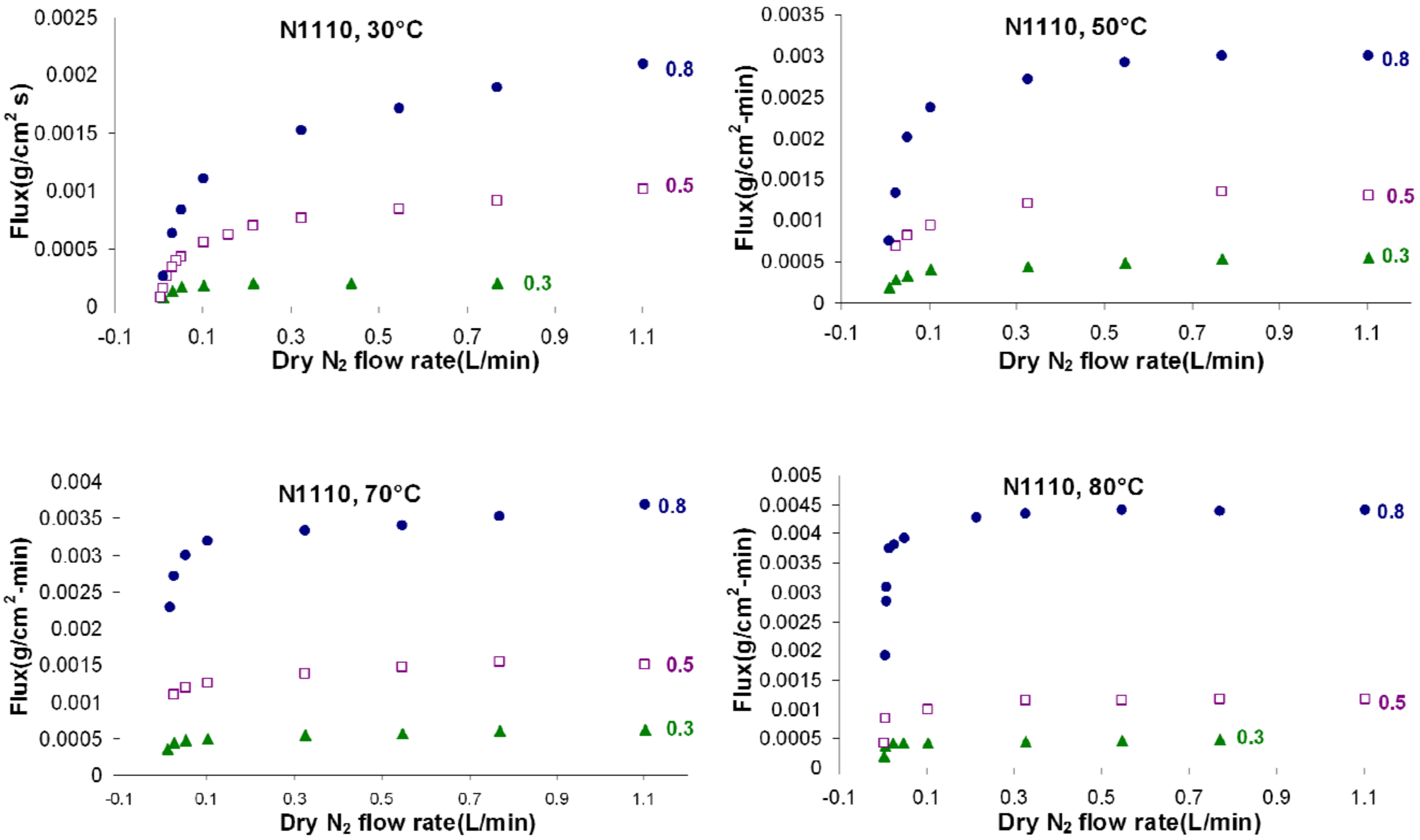

Figure 7-7 **Water vapor flux through Nafion N1110 at 30, 50, 70, and 80°C for feed side activity of 0.3, 0.8, and 0.8 as a function of N$_2$ flow rate at the dry side.**

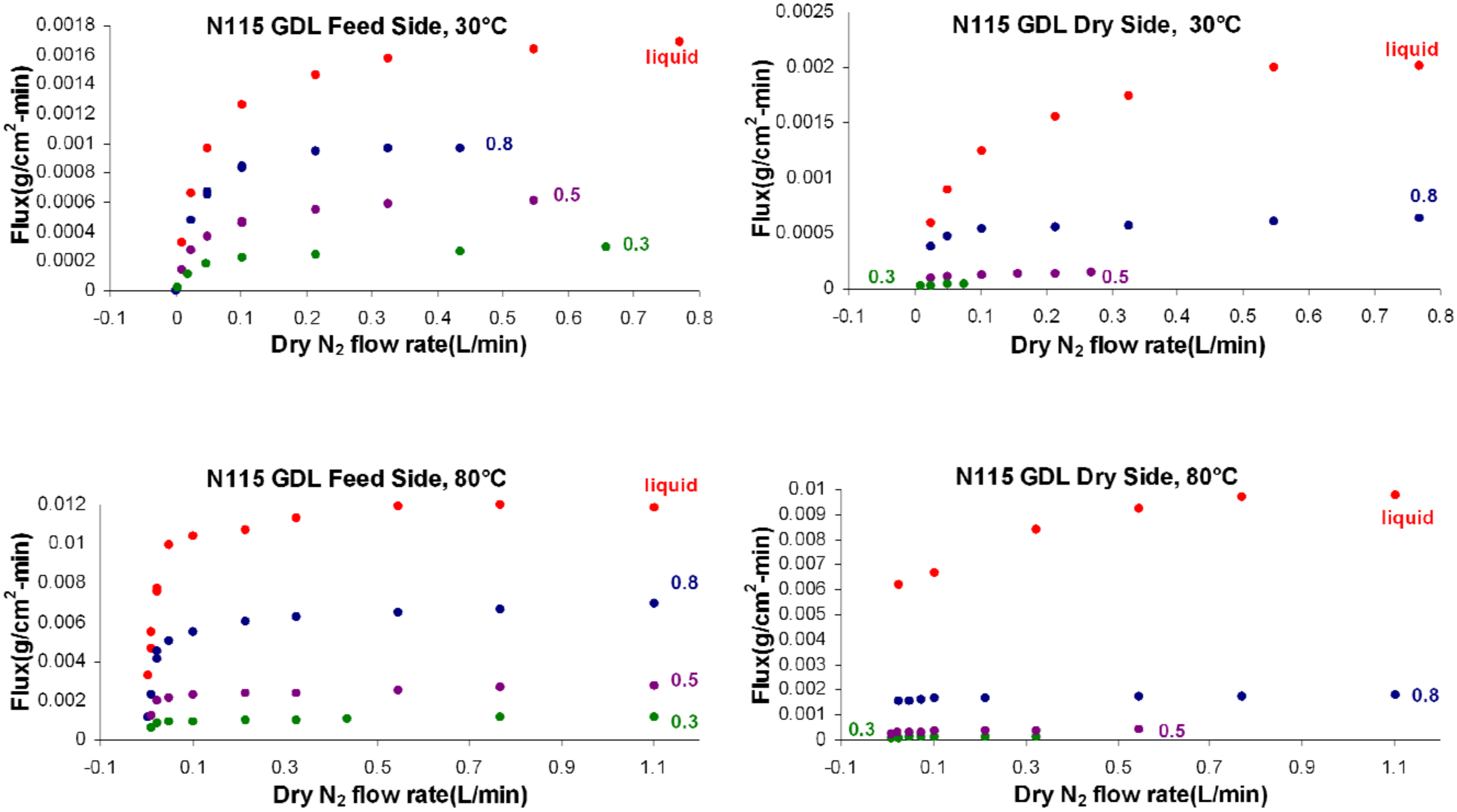

Figure 7-8 Liquid and vapor transport through Nafion N115 with a gas diffusion layer on either the feed side or dry side at 30 and 80°C.

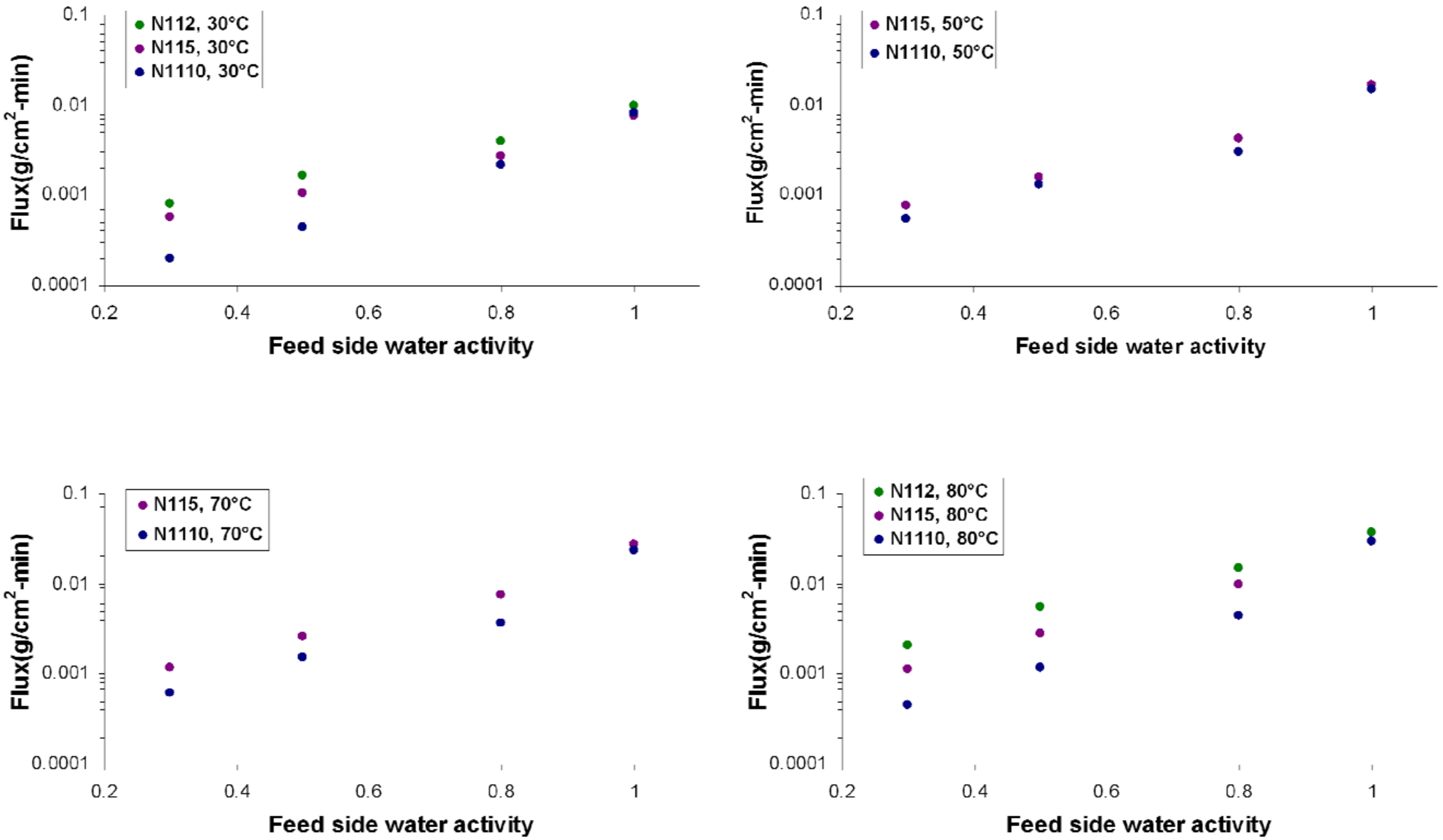

Figure 7-9 Water permeation through Nafion as a function of water activity at the feed side. Flux is for a dry side N_2 flow rate of 1.1L/min. Permeation through Nafion N112, N115, and 1110 is shown at the temperatures indicated.

7.5 Goff-Gratch equation for vapor pressure

The Goff-Gratch equation approximates the equilibrium vapor pressure above liquid water and was used in calculating saturation vapor pressure to calculate water permeation. Saturation vapor pressure p_{sat} is given as

$$p_{sat} = e_{st} 10^{Z}, \qquad \text{Equation 7-6}$$

where

$$Z = a\left(\frac{T_s}{T} - 1\right) + b\log_{10}\left(\frac{T_s}{T}\right) + c\left(10^{d\left(1-\frac{T_S}{T}\right)} - 1\right) + f\left(10^{h\left(1-\frac{T_S}{T}\right)} - 1\right) \qquad \text{Equation 7-7}$$

and T is the temperature, in Kelvin, at which vapor pressure is being calculated.

Table 7-1 Constants for the Goff-Gratch equation. Using these constants gives p_{sat} in units of millibar.

Constants	Value
a	-7.90298
b	5.02808
c	-1.3816×10^{-7}
d	11.344
f	8.1328×10^{-3}
e_{st}	1013.246 mb
h	-3.49149
T_s	373.16 K

Vita

Paul Majsztrik was born in New Jersey in 1976 to Andrew and Virginia as one of four children. He spent his years leading up to college tinkering, being inquisitive, and avoiding school assignments. In 2000, he earned B.S. degrees in physics and mechanical engineering from The Richard Stockton College of New Jersey and Rutgers University, respectively. Paul received the degree of M.S. in mechanical engineering at Vanderbilt University in Nashville, Tennessee in 2002. At Vanderbilt, he conducted his thesis work under the direction of Timothy S. Fisher on developing energy conversion technologies using diamond-based solar-thermionic emission. From 2003-2007, he was a Ph.D. candidate in chemistry and materials at Princeton University. At Princeton, he worked under the joint direction of Andrew Bocarsly and Jay Benziger measuring the mechanical and transport properties of Nafion, a membrane material for PEM fuel cells. After graduating from Princeton, Paul will join the start-up company RSI Silicon, founded by Steven Amendola. There he will be part of a team working to develop a new procedure for producing high-purity silicon at low cost for the solar cell industry. Paul is deeply committed to using his knowledge of engineering and chemistry to develop renewable energy technologies.